PHD THESIS

CONCEPTUALIZATION OF FIRE BARRIERS : FUNDAMENTALS AND EXPERIMENTAL APPROACH

Presented and defended at the
UNIVERSITY OF LILLE
Doctoral School for Materials, Radiation and Environmental Sciences (EDSMRE)
Materials and Transformations Unit (UMET), UMR CNRS 8207, ENSCL

for the degree of
DOCTOR OF PHILOSOPHY
Specialty : Materials chemistry

by
Tatenda NYAZIKA

PhD thesis supervised by
Prof. Serge BOURBIGOT and Dr. Fabienne SAMYN

Defended on the 7th of October 2019 before the following PhD committee:

Prof. Maude JIMENEZ	University of Lille, France	President
Prof. Patrick VAN HEES	Lund University, Sweden	Reviewer
Prof. Baljinder KANDOLA	University of Bolton, UK	Reviewer
Prof. Sylvain BROHEZ	University of Mons, Belgium	Examiner
Prof. Serge BOURBIGOT	ENSCL, France	Supervisor
Dr. Fabienne SAMYN	ENSCL, France	Co-supervisor

THÈSE DE DOCTORAT

CONCEPTUALISATION PHYSIQUE DE BARRIÈRES DE PROTECTION AU FEU : APPROCHE NUMÉRIQUE ET EXPÉRIMENTALE

Présentée et soutenue publiquement à
L'UNIVERSITÉ DE LILLE
École Doctorale Sciences de la Matière, du Rayonnement at de l'Environnement
Unité de Matériaux et Transformation, UMR CNRS 8207, ENSCL

pour obtenir le grade de
DOCTEUR
Spécialité : Chimie des matériaux

par
Tatenda NYAZIKA

Thèse dirigée par
Prof. Serge BOURBIGOT et Dr. Fabienne SAMYN

Soutenue le 07 octobre 2019 devant la Commission d'Examen composée de :

Prof. Maude JIMENEZ	Université de Lille, France	Présidente du jury
Prof. Patrick VAN HEES	Université de Lund, Suède	Rapporteur
Prof. Baljinder KANDOLA	Université de Bolton, Royaume-Uni	Rapporteur
Prof. Sylvain BROHEZ	Université de Mons, Belgique	Examinateur
Prof. Serge BOURBIGOT	ENSCL, France	Directeur
Dr. Fabienne SAMYN	ENSCL, France	Co-encadrante

"Remember that all models are wrong; the practical question is how wrong do they have to be to not be useful." - Box and Draper

"Any model is only ever a model—experiments are the truth!"- Covell

To my late parents.

ACKNOWLEDGEMENTS

Firstly, I would like to thank Prof. Alexandre Legris the former head of the UMET laboratory as well as Prof. Patrice Woisel, the current head of the UMET laboratory for giving me the opportunity to join and work in the laboratory.

I would like to thank my supervisors, Serge, Fabienne and Maude who gave me the opportunity to work with them on this project. Working with them was a great pleasure and they provided me with valuable scientific support throughout the whole duration of my PhD.

I am very grateful to Prof. Patrick Van Hees, Prof. Baljinder Kandola and Prof. Sylvain Brohez who accepted to take their time to review this manuscript and be part of the jury.

I would also like to thank the European Research Council (ERC) for funding the FIREBAR Concept project (ERC Advanced Grant Agreement no. 670747) as well as the project team members for their contributions and valuable feedback during our monthly meetings. Special thanks to Pauline for the trainings on the measuring equipment and discussions on numerical modeling, and Johan for helping me out in setting up my experiments especially at the beginning.

Furthermore, I would like to thank all the current and former members of the R_2Fire team for the favorable working conditions. Thanks to all the lab's permanent members and engineers/ technicians: Gaëlle, Sophie, Serge, Fabienne, Mathilde, Maude, Charaf', Fanny, Severine, Tsila, Pierre, Ben, Johan.

I also sincerely thank my office mates; Adi, Maman Soso, Lolo, Manon and Charlotte for supporting me especially during the preparation of this manuscript and for the convivial moments shared. Props to Adi for the valuable scientific discussions at any given moment even during the mini-breaks.

Thanks also to the other PhDs/PostDocs (former and current): Roro (fréro), Anne-lise, Alexandre, Elodie Angeline, Fei, Bertrand, Ninit, Maryem, Agnes, Chi, Hirak, Kai, Gizem as well as the interns I met during my PhD.

Finally, I would like to thank all my friends especially Ben, Admire, Levi, Mushunje and Mabika ('vana Mustapha'), Harmony, Bongani, James and Jessica for their continued support. Not forgetting my family members and a special mention to my brother Tafadzwa.

TABLE OF CONTENTS

LIST OF ABBREVIATIONS

ALE	Arbitrary Lagrangian Eulerian
ASTM	American Society for Testing and Materials
ATH	Aluminum tri-hydroxide
BLEVE	Boiling Liquid Expanding Vapor Explosion
calsil	Calcium silicate
CC	Cone Calorimeter
CF	Closed-cell mullite foam/ Ceramic foam
CFD	Computer Fluid Dynamics
DAE	Differential Algebraic Equation
DSC	Differential scanning calorimetry
DTG	Derivative thermogravimetric
EG	Expandable Graphite
EMT	Effective Medium Theory
EN	European Standards
EPS	Expanded polystyrene
ERC	European Research Council
ETICS	External Thermal Insulation Composite Systems
EU	European Union
EVA	Ethylene-vinyl acetate copolymer
FDS	Fire Dynamic Simulator
FEM	Finite-Element method
FPA	Fire Propagation Apparatus
FR	Fire retardant
FSCABC	Fitness Scaled Chaotic Artificial Bee Colony algorithm
FTIR	Fourier Transform Infrared
GA	Genetic Algorithm
GF	Glass Fibers
GUI	Graphical User Interface
GWP	Global Warming Potential

HAM	Heat, air and moisture
HDPE	High-density polyethylene
HGA	Hybrid Genetic Algorithm
HGM	Hollow Glass Microspheres
HIPS	High-impact polystyrene
HRR	Heat Release Rate
IR	Infrared
ISO	International Organization for Standardization
LFA	Laser Flash Analysis
LHS	Left-hand side
LP	Lignophenolic
LTE	Local Thermal Equilibrium
MCC	Microscale Combustion Calorimetry
MCMC	Markov Chain Monte Carlo
MDF	Medium Density Fiberboard
MLR	Mass Loss Rate
NC	Nanoclay
NFPA	National Fire Protection Association
NIST	National Institute of Standards and Technology
ODE	Ordinary Differential Equation
ODP	Ozone Depletion Potential
PA66	Polyamide 6,6
PBD	Perfomance-based design
PBT	Poly (butylene terephthalate)
PC	Polycarbonate
PDE	Partial differential equation
PE	Polyethylene
PET	Polyethylene terephthalate
PF	Phenolic Foam
PIR	Polyisocyanurate foam
PMLR	Peak Mass Loss Rate

PMMA	Poly(methylmethacrylate),
POM	Polyoxymethylene
PP	Polypropylene
PSO	Particle Swarm optimization
PUR/PU	Polyurethane foam
PVC	Polyvinylchloride
RHS	Right-hand side
RPSO	Repulsive particle swarm optimization
RTE	Radiative heat transfer equation
SA	Sensitivity Analysis
SBIC	Silicone-based intumescent coating
SCE	Shuffled Complex Evolution
SFPE	Society of Fire Protection Engineers
SHC	Stochastic hill-climber
SPH	Smoothed Particle Hydrodynamics
SQP	Sequential quadratic programming
SSE	Sum of squared errors
STA	Simultaneous Thermal Analysis
TACOT	Theoretical Ablative Composite for Open Testing
TC1	Thermocouple at the first position
TC2	Thermocouple at the second position
TC3	Thermocouple at the third position
TGA	Thermogravimetric Analysis
TPS	Transient Plane Source
US	United States
XPS	Extruded polystyrene

NOMENCLATURE

Roman letters

q_{ext}	External radiant heat flux [kWm^{-2}]
A_s	Surface area [m^{2}]
Q	Heat of decomposition [kJkg^{-1}]
T	Temperature [K]
t	Time [s]
q_{net}	Net heat flux [kWm^{-2}]
h_h	Convective heat transfer coefficient on a horizontal surface [Wm^{-2} K^{-1}]
h_v	Convective heat transfer coefficient on a vertical sides [Wm^{-2} K^{-1}]
T_{amb}	Ambient temperature [K]
L	Thickness [m]
T_P	Pyrolysis temperature [K]
t_p	Time when pyrolysis starts [s]
q_f	Flame heat flux [kWm^{-2}]
k	Thermal conductivity [Wm^{-1} K^{-1}]
$\dot{m}''$	Volatile mass flux [kgm^{-2}s^{-1}]
C_p	Specific heat capacity [Jkg^{-1}K^{-1}]
m	Mass [kg]
E	Activation energy [kJmol^{-1}]
R	Ideal gas constant [Jmol^{-1}K^{-1}]
A	Pre-exponential factor [s^{-1}]
P	Pressure [Pa]
u	Superficial gas velocity [ms^{-1}]
h_g	Enthalpy of gases [kJkg^{-1}]
h_s	Enthalpy of solid [kJkg^{-1}]
h_T	Total convective heat transfer coefficient [Wm^{-2}K^{-1}]
q'	Energy flux density [kgs^{-3}]
n	Reaction order

M_n	Molecular mass [kgmol^{-1}]
F	View factor
T_r	Temperature of the cone heater [K]
n1	Refractive index
a1	Longitudinal pore size [m]
b1	Transverse pore size [m]
f_s	Fraction of solid materials in foam
K_w	Cell wall extinction coefficient
d	Pore diameter or dimension [m]
$\dot{m}$	Mass loss rate [kgs^{-1}]
x	x-coordinate
y	y-coordinate
T_f	Failure temperature [K]
abl	Surface recession rate [ms^{-1}]
$swell$	Expansion rate [ms^{-1}]

Greek symbols

α	Thermal diffusivity [m^{2}s^{-1}]
σ	Stefan Boltzmann constant [Wm^{-2}K^{-4}]
ε	Emissivity
δ_x	Thermal penetration depth [m]
δ_c	Depth of char layer or pyrolysed material [m]
δ_p	Distance of the front surface from the initial position after pyrolysis [m]
δ	Porosity [-]
μ	Viscosity of volatile gases [Pa.s]
Γ	Permeability [m^2]
β	Inertial term of the non-linear darcy equation or misalignment angle
γ	local concentration ratio of char to unreacted solid
$\alpha 1$	Conversion degree
ν	Volume fraction

ω	Geometrical factor
ρ	Density [kgm^{-3}]
$\sigma_{e,R}$	Rosseland mean extincition coefficient
$\beta 1$	Heating rate [Kmin^{-1}] or [°Cmin^{-1}]
δ_{back}	Error when thermocouple is placed from the backside of sample [m]
δ_{side}	Error when thermocouple is placed from the side of sample [m]
λ	Wavelength [m]

Subscripts and superscripts

v	Virgin layer
c	Char layer
g	Gas
s	Solid
rad	Radiation
eff	Effective
pyro	Pyroceram
max	Maximum
*	Scaling factor
cs	Calcium silicate
st	Steel
co	Copper
a	Apparent

GENERAL INTRODUCTION

Fire causes injuries, the loss of lives and property. In 2016, in the United States (US) alone, 475 500 structure fires were recorded and contributed to 2 950 civilian fire deaths, 12 775 civilian fire injuries and $7.9 billion in property damage [1]. In the case of a fire in an enclosed system such as buildings, naval ships or aircraft, the fire should be compartmentalized and restricted from spreading from one point to another in order to save lives and property as well as give people enough time to evacuate. Normally these enclosed systems can be constructed from materials such as steel, wood or composites.

Different types of fire protection systems exist for example active and passive fire protection methods. Passive fire protection methods such as fire barriers based on thermal insulation systems are often used to prevent the transfer of heat from the fire to the substrate materials. Fire barriers are generally cementitious products (e.g. calcium silicate insulation), cellular foams (e.g. rigid polyisocyanurate foam, phenolic foam) or even intumescent coatings [2]. In the European Union (EU), wool minerals such as stone wool and cellular foams such as polyurethane (PUR) foam are often used as materials for building insulation because of their good thermal properties. In the context of improving the energy efficiency of buildings, the use of cellular foam insulation is expected to increase by 2027 [3]. The problem with these cellular foams is that they are combustible and they exhibit low fire resistance properties due to their low thermal inertia consequently causing their surface to ignite quickly when subjected to an external heat flux [4]. Intumescent coatings are also widely used for insulation as well as fire protection of substrates (e.g. steel) and their application is one of the oldest and one of the most efficient ways to protect materials from fire [5]. When exposed to heat, they begin to swell and expand to form an insulative char layer which limits mass and heat transfers between the flame and the substrate [6]. Even though the overall fire performance of these traditional insulation materials has improved over the years, most of the materials may only be efficient for a specific fire scenario. There is therefore need to develop innovative fire safe materials with high performances adapted for different fire scenarios. Innovative materials such has high reflective nano-coatings, aerogels, advanced insulation foams, nanocellular foams, aerogels, etc are currently under development as reported by Pavel and Blagoeva [3]. This study will contribute to the development of innovative fire safe materials by highlighting the fundamental rules on how to make these materials through a conceptual approach.

The fire performance of these fire barriers is subject to an assessment in accordance with experimental test methods based for example on the Euroclass system in the case of building regulations. The fire barriers are required to pass these standardization tests before they can reach market. The standardization tests are also used during material design to ensure that the developed materials meet the requirements. To evaluate the fire performance of the fire barriers, large-scale and intermediate fire tests such as the Room Corner Test (ISO 9705) and Single Burning Item (EN 13823) respectively mimicking a real fire scenario are often used but these tests are expensive as well as time consuming especially during material development. Small-scale tests such as the cone calorimeter (ISO 5660) are then used. In addition, pyrolysis modeling is often used to predict the fire behavior of a material. Pyrolysis models have increased in complexity over the years ranging from thermal models to comprehensive models. Comprehensive models have gained more attention with the development of computer power. Moreover, they consider the actual thermal degradation processes and transport phenomena taking place within the solid material. These include coupled physical and chemical phenomena such heat transfer, morphological changes, expansion, shrinkage, char formation, chemical reactions etc. [7]. Different comprehensive pyrolysis codes have been developed and validated e.g. Gypro/Gypro3D [8-10], ThermaKin [11], NIST Fire Dynamics Simulator (FDS) [12] etc. Other research works have also been successfully implemented in COMSOL Multiphysics [13-15]. However, even though pyrolysis modeling has advanced during the past years, a few studies [16-20] have focused on identifying the important engineering parameters [21] that control the fire behavior of different materials. The knowledge of these parameters helps in understanding which of them should be optimized for the best performance. This work bridges the gap by clearly identifying these parameters based on numerical model systems including fundamental heat transfer mechanisms involved in the fire behavior of different fire retardant (FR) materials. Moreover, a comprehensive review on pyrolysis modeling, sensitivity analysis, and optimization techniques for combustible techniques is presented.

In the fire safety design of buildings, prescriptive and performance-based approaches have often been used. However, the prescriptive approach has shown major drawbacks e.g. the standard fire tests results are not applicable to other fire scenarios therefore designers are not able to evaluate the behavior of the materials under different conditions other than those in the test. The performance-based design approach has proved to have advantages over the traditional prescriptive approach [22, 23]. This approach is based on considering the design process as a multi-objective optimization problem. Computational tools are then used to evaluate several design options in order to determine the favorable solution. Amongst these computational tools are pyrolysis models, sensitivity and optimization techniques. Hidalgo et al. [24] proposed a methodology based on the performance-based approach for the design of thermal barriers for combustible insulation materials by defining the onset of pyrolysis as a failure criterion. However, the authors used an approach based on a simple direct solution and dimensionless parameters resulting in design charts. Moreover, in their approach they did not include the endothermic thermal decomposition of the material and this will be included in this work.

In this context, the objective of this PhD work is to **provide with the fundamentals on how to design efficient fire barriers through understanding the fire behavior of reference fire-retardant (FR) materials when subjected to an external radiant heat flux from the ISO 5660 cone calorimeter.**

Precisely, this work is focused on;

- investigating the fire behavior of reference FR materials through an experimental and numerical approach,
- identifying the governing parameters that control the fire behavior of the reference FR materials,
- developing a design methodology that allows to make an efficient fire barrier that is in accordance with specific requirements for a given fire scenario.

The reference FR materials used in the scope of this study consist of a calcium silicate insulation block (calsil), a closed-cell mullite foam (CF), phenolic foam (PF) and a silicone-based intumescent coating (SBIC) containing expandable graphite (EG). The choice of these materials is based on understanding the fundamental heat transfer mechanisms from an inert, static calsil block (simple model systems) to a reactive and dynamically evolving SBIC (complex model systems). This work is part of the Fire-Bar Concept project (2014–2020 ERC Advanced Grant Agreement no. 670747). One of the goals of the project is to design and assemble materials exhibiting low flammability, protecting substrates and limiting fire spread.

This dissertation is divided into four chapters. Chapter 1 presents a comprehensive review on pyrolysis modelling as well as different sensitivity and optimization techniques. Then, a literature review on the approaches used in the design of fire-safe materials is presented. At the end of the chapter, a general background on fire barriers commonly used is highlighted, leading to the selection of the reference FR materials. Finally, based on previous research works, the reference FR materials are described in terms of their fire behaviors, thermal properties and issues concerning their numerical modeling.

Chapter 2 presents the materials and methods used in this study. The materials and the experimental set-up are described in detail as well as the different methods used to characterize some of the thermophysical properties of the reference FR materials. Then, at the end of the chapter, the numerical tools implemented in this study are presented.

Chapter 3 presents the numerical models implemented to predict the fire behavior of the reference FR materials used in this study. The numerical models are explicitly described as well as the input material properties used. They are then validated, and their applicability and limitations are explained. Sensitivity studies are also presented in this chapter and the governing parameters that control the fire behavior of the reference FR materials are clearly identified.

After having gained a fundamental understanding of how these fire barriers behave in the case of a fire from the previous chapter, Chapter 4 focuses on the conceptualization of a fire barrier that is subjected to a different fire scenario compliant with ISO2685:1998(E) and FAR25.856(b):2003. This chapter will provide with the knowledge on how to design novel fire safe materials based on the performance-based design methodology and optimization techniques.

Finally, at the end of this PhD work, a general conclusion and outlook is presented.

CHAPTER 1. STATE OF THE ART

A set of computational tools is often implemented during the conceptualization process. This chapter reviews the fundamental numerical modeling techniques that are applied in the fire science community for combustible materials. The modeling techniques include pyrolysis modeling, sensitivity analysis and optimization. Moreover, the different approaches that are used in the design of fire safe materials are presented. At the end of the chapter, the various types of fire barriers are presented in a general manner. Finally, the reference fire retardant (FR) materials used in this study are described.

1.1. Fundamental numerical modeling techniques for combustible materials

This first section of this chapter is based on part of a review paper that was published in the Journal of Fire Sciences and is referenced below:

- **Nyazika, T., Jimenez, M., Samyn, F., and Bourbigot, S.,** ***Pyrolysis modeling, sensitivity analysis and optimization techniques for combustible materials: A review,*** **Journal of Fire Sciences, 2019. 37(4-6): p. 377–433**

The section presents the fundamental numerical modeling techniques applied to combustible materials. These techniques include pyrolysis modeling, sensitivity analysis and optimization techniques. The section begins with a general introduction on pyrolysis followed by a classification of pyrolysis models. Given that these pyrolysis models require input parameters, the section also discusses the techniques allowing the estimation of these parameters. These techniques involve direct measurement by thermal analysis as well as solving inverse heat transfer problems using optimization techniques. Finally, the use of sensitivity studies in the fire science community to study how the estimated parameters influence the model response is highlighted.

1.1.1. Introduction

The term pyrolysis often refers to the thermal degradation of the solid-phase caused by external heating under inert atmospheric conditions or in the absence of oxygen [25]. It is a major process contributing to the solid ignition, flame spread and fire growth involving complicated phenomena such as heat transfer through the material, thermal decomposition resulting in the mass transfer that produces combustible or non-combustible gases [26].

The fire behavior of a material can be experimentally investigated at different scales [27, 28]. Thermogravimetric analysis (TGA) [29] and microscale combustion calorimetry (MCC) [30] are often used to study the behavior of the material at microscale while tests such as the fire propagation apparatus (FPA - ASTM E2058) [31-33], cone calorimeter (CC - ASTM E1354) [34] and radiant panel apparatus [35] are used at bench scale. Moreover, at product scale, medium single burning item and room corner test are commonly used. Fire tests at real-scale can also be conducted for example in an apartment with a single bedroom [36].

To numerically predict the fire behavior of a material, pyrolysis should be modeled. Pyrolysis models allow for example, to understand the fire behavior of a material without having to conduct expensive experimental tests. Once the pyrolysis model is validated against experimental data, a sensitivity study can be performed to identify the material properties governing the phenomenon, thereby helping in the optimization of the material behavior during development. Pyrolysis modeling has become a useful predictive tool in understanding the complex physical and chemical processes. Although the modeling of these processes remains a great challenge, significant advancements have been made in the fire community. Due to the increasing interest in the fire safety of combustible materials used in various applications, significant research work has been reported on pyrolysis models [8, 11, 37-43].

These models vary from thermal to comprehensive models depending on their complexity [44-47]. The modeled materials can be divided into non-charring and charring solids depending on their ability to form char after fire exposure. Some charring materials can expand or intumesce to form a porous carbonaceous char when subjected to external heat flux.

A number of reviews on pyrolysis models for different materials exist in literature. A comprehensive review on pyrolysis models was presented by Di Blasi [39] in 1993. The models took into account both the solid and gas phase combustion processes and they were used to describe the physical and chemical phenomena occurring in charring materials such as wood as well as a non-charring material such as poly(methyl methacrylate). The author also outlined how pyrolysis modeling had generally helped in understanding the combustion of solid materials. However, the author concluded that the lack of accurate thermophysical properties and kinetic parameters hindered the accuracy of the model predictions even when a comprehensive model was used. In 1994, Kashiwagi [48] presented a discussion on polymer combustion. At this time, Kashiwagi stated that basic understanding of polymer combustion had progressed for the gas phase thanks to the previous conducted significant research work. However, more research work was required to understand the combustion phenomena in the solid phase. Later in 2000, Di Blasi [41] presented a review on the pyrolysis modeling of charring materials including intumescent materials. The author concluded that comprehensive modeling including complex reaction kinetics for wood had progressively advanced but more work was still needed for charring polymers and intumescent materials.

The same year, Sinha et al. [25] outlined the advances in wood pyrolysis models and focused on issues such as wood composition and morphology. The authors then identified the need for input parameters when dealing with even such complex issues. They recommended that there should be closer interaction between the modeling and experimental efforts. In 2001, Moghtaderi [44] also reviewed the pyrolysis models involving charring materials from over three decades. The improvement of the models in terms of the included physical and chemical processes was presented. They also demonstrated how the input parameters influenced the model outputs and pointed out the difficulty of improving the predicted results without accurate material properties. The same author [45] reviewed in 2006, the numerical models for the thermal decomposition of lignocellulosic materials. The author came up with the similar conclusions as from the previous review in terms of input parameters, except that the complexity of the models was dependent on the modeler making the pyrolysis models non-uniform. In 2005, Lyon and Janssens [49] presented an overview based on the combustion of polymers. Several experimental techniques used in the understanding of the fire behavior of polymers were also presented. From these experimental techniques, several hypotheses were made and mathematical formulations were derived from the properties of the gas and solid phase thereby, providing the experimentalists with information for the design of new materials. Three years later, Laughtenberger and Fernandez-Pello [46] presented pyrolysis models based on non-charring, charring and intumescent materials. Since the conservation equations on which the pyrolysis models were based could be applied universally, they suggested the possibility to formulate a generalized pyrolysis model. The generalized pyrolysis model (Gpyro) was later developed and is presented in [8, 9]. They also provided a database of input parameters of different combustible solids collected from literature. At the same time, Stoliarov and Lyon [11] also developed a generalized pyrolysis model named ThermaKin which was also capable of taking into account a wide range of materials [50].

In 2013, Shi and Chew [51] also presented a review on pyrolysis models based on the same class of materials as those mentioned previously. In their study, the ways in which the physical and chemical phenomena involved in pyrolysis were numerically described were explicitly detailed. They also gathered several input parameters for different materials. They observed that most pyrolysis models focused on wood whereas relatively few models focused on other combustibles as shown in Figure 1. From Figure 1, it can also be noticed which pyrolysis processes have been included in models based on literature. However, no information is given by the authors over how many years the statistics were conducted.

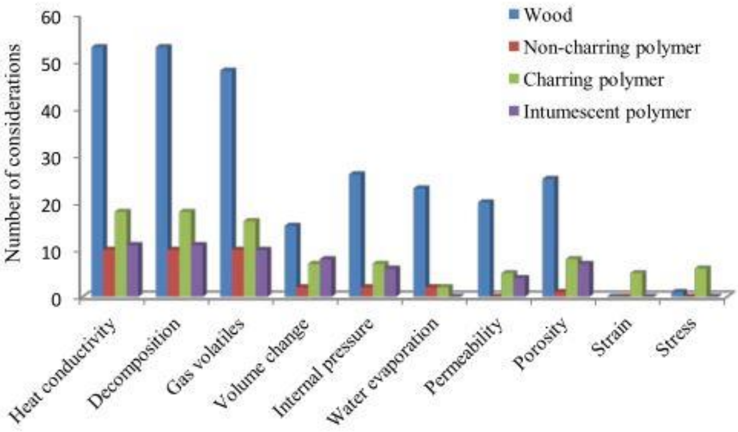

Figure 1. Statistics on 1D models based on different combustible materials [51].

Recently in 2016, Lundström et al. [47] presented a survey of different types of pyrolysis models and focused on their similarities and differences. They also discussed in which cases the models could be applied. They supported the other previous reviews by noting that, when increasing the complexity of the model, more parameters are required. Some of these parameters are difficult to measure and if used as model inputs they may induce uncertainties in the model.

Other noteworthy review papers on smoldering combustion and composites were presented by Ohlemiller [52] and Mouritz et al. [53] respectively. Ohlemiller [52] extensively reviewed numerical models involving coupled physical and chemical phenomena that take place in self-sustained smoldering combustion. During smoldering, the polymer pyrolysis is involved and was considered to be endothermic and competing with the exothermic oxidative polymer degradation amongst other processes such as char oxidation, thereby making smoldering combustion process complex. As a result, the author concluded that the models that existed at that time were greatly simplified and that more work was needed to approach reality. The reader is referred to more recent review paper on smoldering combustion by Rein [54, 55]. Mouritz et al. [53] reviewed the progress in modeling the fire behavior of polymer composites. At that time, the authors concluded that significant progress had been made, although a number of issues such as experimental validation of models that take into account fire-induced damage (e.g. delamination) still needed to be given attention.

Considering the complexity of these comprehensive models and that most of the model input parameters can carry some degree of uncertainty, a sensitivity analysis is required to understand the role and the influence of the input parameters on the modeling outputs of interest. This step, aiming at simplifying the problem, allows checking whether a small change to an input parameter value has an effect on the modeling results. In general, a sensitivity analysis is useful in identifying the parameters that play a major role in the overall pyrolysis process [16]. Understanding the role of the parameter also helps in reducing the number of parameters that need to be estimated or measured, consequently reducing the calculation time during optimization and the complexity of the problem. Several sensitivity analysis techniques have been used in pyrolysis modeling, from local to global sensitivity analyses [19]. The first comprehensive sensitivity analysis using a generalized pyrolysis model was conducted by Stoliarov et al. [18] in the ThermaKin framework.

Comprehensive pyrolysis models have proven to be flexible in describing the pyrolysis of a combustible solid as compared to thermal models by considering the actual thermal degradation processes and transport phenomena taking place. However, these models require a significant number of input parameters [25, 39, 47]. These parameters can be extracted from direct measurement by thermal analysis (e.g. the thermal conductivity from Hot Disk thermal constant analyzer experiments, based on a Transient Plane Source method [15, 37, 56]), searching through the literature or through optimization techniques [57]. Determining parameters this way can be difficult in certain conditions especially at high temperatures, when the material begins to thermally degrade and the same applies to materials that shrink, expand or melt [37]. For example, very few papers deal with the measurement of thermal conductivity of intumescent materials at high temperature [56, 58]. Errors from each of the measured parameters may result in considerable uncertainty [17]. Moreover, in many cases the measured properties are effective and not intrinsic [57]. Obtaining input parameters by searching through the literature can be inexpensive, however, although certain materials may have the same nomenclature, the material properties may vary depending on the manufacturer and a wide range of values can be observed [18]. The other approach for determining input parameters is to use optimization techniques. In this case, the pyrolysis model is coupled with an optimization technique to solve an inverse problem. Gradient-based and direct search methods such as evolutionary algorithms have been implemented to numerically obtain material pyrolysis properties. For example, Meunders et al. [59] used a gradient-based method to estimate the kinetic and thermophysical parameters of polyurethane foam based on small-scale experiments (TGA and cone calorimeter). Some anomalies were observed, for example some values were equal to the values used as bounds which probably indicated problems in finding the global optimal values. Gradient-based methods have some limitations and recently, direct search methods such as evolutionary algorithms have started to gain attention because of they have been found to perform better in certain cases [60].

This part of the chapter presented a brief survey of reviews on pyrolysis models. Up-to-date, a significant effort has been made for the modeling of non-charring, charring and intumescent materials, However, significant work still remains to be accomplished in the field. The next part of the chapter will present a set of computational tools from pyrolysis modeling to optimization techniques. In the context of this study, these computational tools will assist in the objectives of this work. The first section presents the classification of pyrolysis models. The second section presents the experimental and numerical techniques used to estimate material properties used as input data to run the pyrolysis models.

1.1.2. Pyrolysis models

A pyrolysis model is a set of governing equations that describes the physical and chemical processes occurring in a combustible solid when subjected to an external heat flux. It can be used as a stand-alone or coupled to a Computational Fluid Dynamics (CFD) model like Fire Dynamics Simulator (FDS) or FireFoam that takes into account the gas-phase phenomena.

Generally, the steps involved in pyrolysis modeling include (i) experimentally testing the material on a small scale test (e.g. cone calorimeter, thermogravimetric analysis (TGA),…) and (ii) describing the experiments using mathematical models. Input model parameters are then determined by direct measurement, searching through the literature or by optimization techniques. The system of equations together with the accompanying boundary conditions is then resolved numerically and the model is validated against experimental data.

There are numerous ways to classify pyrolysis models [26, 46] and this review broadly classifies the models into two main categories i.e. thermal and comprehensive models. The distinction between thermal models and comprehensive models is that "thermal models predict the conversion of the virgin material into products based on a critical pyrolysis temperature criterion and an energy balance, while the comprehensive models describe the degradation of the material by a chemical kinetic scheme coupled with the conservation equations for the transport of heat and/or mass [44, 45]." This classification has been adopted from the works of Moghtadheri [44, 45]. The critical pyrolysis temperature criterion is the temperature that determines the onset of pyrolysis [61]. The aim of this section is not to extensively present pyrolysis models since they have already been well documented in previous reviews [39, 44, 45] but to give the reader a general overview of the progress in their development over the past years.

1.1.2.a. Thermal models

The easiest approach to pyrolysis modeling is to implement thermal models which do not take into account the reaction kinetics and mass transport. They use few input parameters and due to this, their parameterization requires smaller number of calibration experiments. Moreover, they are also faster computationally [45]. Thermal models can further be divided into algebraic and analytical as well as integral models according to their solution techniques [44]. These different models are described hereafter.

1.1.2.a.i. Algebraic and analytical models

For algebraic and analytical models, an assumption that the gasification rate is proportional to the net absorbed heat flux is made [44, 45, 62]. Equation 1 shows an example of an analytical solution of the energy conservation as a function of the mass loss rate for a thermally thin sample (when Biot number is less or equal to 1) of combustible material when exposed to an external heat flux, assuming that there is no shrinking or expansion during pyrolysis. Moreover, the morphology i.e. the structure of the pores as well as the changes in the thermophysical parameters, are also neglected.

$$\dot{m} = -\frac{q_{ext}A_s}{Q} \qquad \text{Equation 1}$$

where $\dot{m}$ mass loss rate, $\dot{q}''_{ext}$ is the external heat flux , A_s is the surface are and Q is the heat of decomposition.

A more fundamental approach consists of using the integral models [63].

1.1.2.a.ii. Integral models

An integral model is applicable to both charring and non-charring materials depending on the formulation of the equation [61]. In short, for integral models, the original set of partial differential equations describing the problem is reduced to a set of ordinary differential equations, which are easier to solve by considering that the temperature distribution within the solid depends on the space variables. Different temperature profiles have been used in literature such as exponential [64] and in this case a quadratic temperature profile was applied.

The model describes the pyrolysis of a combustible solid when subjected to an external flux. It is basically divided in three stages according to the physical processes occurring in the solid. The first stage is before ignition and heat is transferred into the material by pure conduction (Figure **2**(a)). The temperature increases up to the temperature at which pyrolysis is assumed to start. The second stage occurs during pyrolysis and the solid acts in a semi-infinite manner. The difference in behavior between a charring and non-charring material is shown (Figure **2**(b)) and (Figure **2**(c)). The final stage is when the virgin material has been totally converted.

The 1D model was formulated by describing the materials during the first stage and second stage;

The model for the first stage using virgin material properties;

$$\frac{\partial T_v}{\partial t} = \alpha_v \frac{\partial^2 T_v}{\partial x^2} \qquad \text{Equation 2}$$

The net heat flux on the surface ($\dot{q}''_{net}$)

$$\mathrm{q_{net}} = q_{ext} - h_h(T - T_{amb}) - \sigma\varepsilon(T^4 - T^4_{amb}) \qquad \text{Equation 3}$$

And the boundary condition at $x = L$,

$$\frac{\partial T_v}{\partial x}(x = L) = 0\ (insulated) \qquad \text{Equation 4}$$

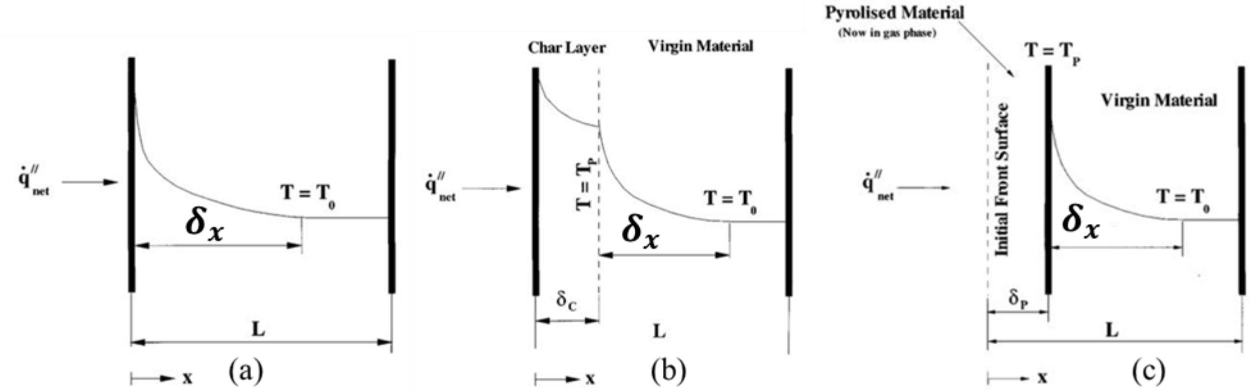

Figure 2 (a) First stage , (b) second stage for a charring solid, (c) second stage for a non-charring solid [61].

Considering the scenario of a solid which undergoes charring, heat is transferred by pure conduction in the char layer as well and the governing equation is given by:

$$\frac{\partial T_c}{\partial t} = \alpha_c \frac{\partial^2 T_c}{\partial x^2} \qquad \text{Equation 5}$$

and it is subject to the initial condition $T_c\left(0, t_p\right) = T_P$, with the applied boundary conditions as:

$$-k_c \frac{\partial T_c}{\partial x}(x = 0) = q_{net} \qquad \text{Equation 6}$$
$$= q_{ext} + q_f - h_h(T_s - T_\infty) - \sigma\varepsilon(T^4 - T_{amb}^4)$$

$$T_c(x = \delta_c) = T_p \qquad \text{Equation 7}$$

with T_c the temperature distribution corresponding to the char layer, T_p the pyrolysis temperature, $\dot{q}_f^{"}$ the heat flux due to the flame. α_c and k_c the thermal diffusivity and thermal conductivity of the char, respectively.

The coupling of the heat transfer between the char and virgin layer is described by the Stefan condition at the pyrolysis front:

$$k_v \frac{\partial T_v}{\partial x}(x = \delta_c) - k_c \frac{\partial T_c}{\partial x}(x = \delta_c) = \dot{m}^{"} Q \qquad \text{Equation 8}$$

Where Q is the heat of pyrolysis and $\dot{m}^{"}$is expressed in terms of the pyrolysis front as:

$$\dot{m}^{"} = (\rho_v - \rho_c)\frac{d\delta_c}{dt} \qquad \text{Equation 9}$$

ρ_v and ρ_c being the densities of the virgin and char materials respectively.

The results from the model presented above were confronted with experimental data and they provided a reasonable level of accuracy and captured the peak of mass flux. To understand the influence of the heat of pyrolysis (Q) on the mass flux, a sensitivity study was conducted as shown in Figure **3**. As observed, the value of the peak of mass flux increases as Q decreases. This is because, as reported by reported by Weng and Fan [65], when Q exhibits a low value, the amount of energy required to decompose the material into volatiles and char is low; as a result the pyrolysis temperature (T_p) is reached very quickly.

In Figure **3**, the curve of the mass flux against time increases up to a maximum followed by a gradual decrease. The heat of pyrolysis has an influence on the maximum value and the gradual decrease is mainly caused by the char formation which acts as a thermal barrier.

An interesting study using a thermal model from Rhodes and Quintiere [66] was conducted by Hopkins and Quintiere [67]. They extracted the thermophysical properties of the material using the experimental results from a cone calorimeter. Thermal models are also computationally cheap enough to couple with CFD models. Moghtaderi et al. [68] successfully incorporated an integral model into a CFD fire code.

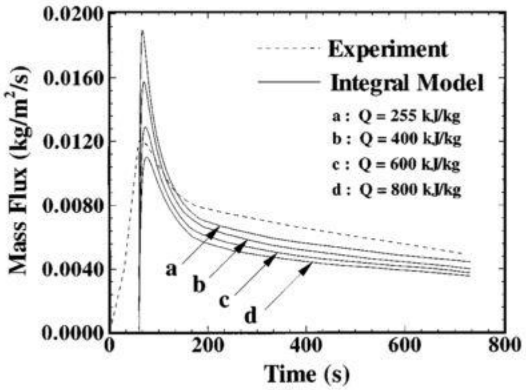

Figure 3. Integral model results confronted with experimental data for white pine under an inert environment [61].

The reader is recommended to consult the following papers [61, 62, 64, 68-72] for more detailed mathematical formulations. A summary of some thermal models is shown in Table 1.

Table 1. Examples of thermal models

Author	**Type of model**	**Material**	**Comments on sensitivity/ parameters**
Moghtaderi et al. [61]	Integral	PMMA	-The effect of the heat of the pyrolysis on the mass flux was studied. The mass flux as well as the peak on the mass flux curve were influenced by the heat of pyrolysis.
Quintiere and Iqbal [71]	Integral	PMMA	-Input parameters were taken from literature.
Steckler et al. [73]	Analytical	PMMA	-Heat of reaction was measured and the other temperature-dependent thermal properties were approximated.
Hopkins and Quintiere [67]	Integral	PMMA, Nylon, PE, PP	-Utilized experimental results from the cone calorimeter to obtain the input thermophysical parameters for the prediction of the time of ignition and the burning rates.
Spearpoint and Quintere [72]	Integral	Wood	- The ignition temperature, the thermal conductivity, and specific heat capacity were mathematically obtained from ignition data whilst the heat of gasification and flame heat flux were obtained by optimization.
Weng and Fan [65]	Integral	White pine	- The influence of input parameters such as the emissivity of the char surface on the mass loss rate were studied.

(PMMA - poly(methylmethacrylate), PE- Polyethylene, PP- Polypropylene)

The main disadvantage of thermal models is that they are too simplified by the hypothesis of the pyrolysis temperature and they do not properly describe the major processes occurring during pyrolysis. For a complete understanding of the phenomena, comprehensive pyrolysis models, which are more representative, have gained more attention from researchers due the development of better computational resources.

1.1.2.b. Comprehensive models

Comprehensive models consider the actual thermal degradation processes and transport phenomena taking place within the solid material. These include coupled physical and chemical phenomena such as heat transfer, morphological changes, expansion, shrinkage, char formation, chemical reactions, in-depth radiation etc. [7]. These phenomena are normally represented as sub-models. Comprehensive pyrolysis modeling has improved progressively. The earliest possible model was presented by Bamford et al. [74] in 1946. It was based on 1D pyrolysis model applied to wood that was exposed to an external heat flux. The model consisted of a heat and mass conservation equation and assumed a first order single step reaction (the boundary conditions are not presented here):

$$\frac{\partial}{\partial t}(\rho C_p T) = \frac{\partial}{\partial x}\left(k\frac{\partial T}{\partial x}\right) - Q\frac{\partial m}{\partial t} \qquad \text{Equation 10}$$

$$\frac{\partial m}{\partial t} = -A.exp\left(-\frac{E}{RT}\right).m \qquad \text{Equation 11}$$

The left hand side (LHS) of the Equation 10 represents the rate of change of energy. The right hand side (RHS) represent the heat transferred by conduction and the heat released by thermal decomposition. Equation 11 is the Arrhenius equation representing the rate of decomposition, where m is the mass of the solid. Even if the model was relatively simple, the predicted temperature at the center of the considered wood slab fitted with the experimental data although there were deviations when applying the model to a thicker slab. The authors further investigated the release of gases when the wood degrades. Many of the pyrolysis models available for combustible solids in the literature are either extensions or modifications of the model developed by Bamford et al. [74]. The same model was implemented in various other works afterwards, such as the work of Roberts and Clough [75]. Other authors went on to improve it by including more physical phenomena.

Tinney [76] improved the model by using a kinetic scheme comprising two consecutive reactions. Matsumoto et al. [77] applied the model to plastics and incorporated a temperature-dependent thermal conductivity obtained from the linearization of experimental data from Wilson [78] using the least squares method and included the char removal phenomena. Kung [79] then later developed a wood pyrolysis model including physical processes such as internal gas convection and the author particularly implemented variable thermophysical input parameters mainly obtained from linear approximation between the virgin and char material. The main disadvantage of the model was that it was not confronted with bench-scale data, however, the author was able to investigate, on a theoretical basis, the influence of parameters such as thermal conductivity of char and thickness of the material on the rate of pyrolysis.

In 1977, a more complete model was developed by Kansa et al. [80]. The model was applied to wood, which was considered as a porous media. Figure **4** shows the various heat transfer phenomena taken into account in the model, namely, 1) incident heat flux ($\dot{Q}_i$), 2) the heat transferred by convection on the surface and in the material ($\dot{Q}_{conv}$), 3) heat lost by radiation ($\dot{Q}_e$), 4) heat transferred by conduction in the material ($\dot{Q}_{cond}$) and 5) wood pyrolysis ($\dot{Q}_x$).

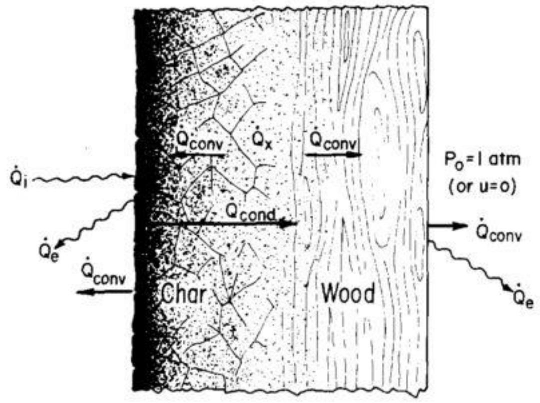

Figure 4. Various heat transfer phenomena taken into account in the model [80].

The complete mathematical description of the model is given below considering that the gas and solid matrices were in non-local thermal equilibrium.

Mass conservation equation of gas in the porous material:

$$\frac{\partial(\delta\rho_g)}{\partial t} + \nabla.\left(\rho_g u\right) = \dot{R}_g;\ \dot{R}_g = -\dot{R}_s \qquad \text{Equation 12}$$

Momentum conservation equation of gas flow in a porous matrix (Darcy's law):

$$\left(\frac{\mu}{\Gamma}\right)u + \beta\rho|u|u + \nabla p = 0 \qquad \text{Equation 13}$$

Energy conservation equation of gas:

$$\frac{\partial(\delta\rho_g h_g)}{\partial t} + \nabla.\left(\rho_g u h_g\right) + \left(\frac{h_T}{\delta}\right)\left(T_s - T_g\right) - \frac{\partial(\delta p)}{\partial t} - \nabla.\left(k_g \nabla T_g\right) + q_g' = 0 \qquad \text{Equation 14}$$

Energy conservation of the solid phase:

$$\frac{\partial[(1-\delta)\rho_s h_s]}{\partial t} - \nabla.[(1-\delta)k_s \nabla T_s] + \frac{h_T\left(T_s - T_g\right)}{1-\delta} + q_s' = 0 \qquad \text{Equation 15}$$

Rate of decomposition of the solid ($\dot{R}_s$) expressed in Arrhenius form:

$$\dot{R}_s = \frac{\partial(1-\delta)\rho_s}{\partial t} = -A\exp\left(-\frac{E}{RT_s}\right) * [\rho_s - \rho_c]^n = 0 \qquad \text{Equation 16}$$

Equation of state of an ideal gas:

$$p = (\frac{R}{M_n})\rho_g T_g \qquad \text{Equation 17}$$

Where u is considered as the superficial gas velocity, p is the pressure, R is the gas constant and n=1.

To complete the model, the initial and boundary conditions for the above system of equations are shown in [80]. Most of the material properties such as the specific heat capacity were linearly approximated from $f(\gamma) = \gamma f_{virgin} + (1-\gamma)f_{char}$, where $f(\gamma)$ stood for the considered material property whereas γ represented the overall extent-of-reaction or degree of decomposition related to the densities/masses in the fully virgin and fully charred conditions, with $\gamma = 1$ representing the fully virgin condition and $\gamma = 0$ representing the fully charred condition. Initially, they used input parameters from literature, then they were optimized using temperature profiles from experimental results. Generally, the numerical and experimental results corresponded with each other at low heat fluxes as compared to high heat fluxes. This was attributed to the non-inclusion of phenomena such as shrinkage, radiation exchange inside the pores as well as an improved kinetic mechanism to fully take into account the physical processes at high fluxes. The comprehensive pyrolysis model formulation presented here shows how these models require more input parameters as compared to semi-empirical formulations.

During this period, considerable work was conducted on modeling the pyrolysis of composites. In 1985, Henderson et al. [81] developed a pyrolysis model for composites which was different from the previous models in the way that decomposition was taken into account using nth order Arrhenius equations and the diffusion of the gases released from the decomposition reactions through the char. Moreover, the work used input properties that were both temperature and mass dependent. The following year, Henderson and Wiecek [82], on the basis of the previous model [81], included thermochemical expansion as well as the storage of decomposition gases. The inclusion of these phenomena improved the capability of the model to predict the fire behavior of composites, and in particular the prediction of pressure profiles in the composite.

In 1987, Vovelle et al. [83] developed a model for the prediction of the mass loss rate of PMMA exposed to a radiant heat flux. The model was also similar to Bamford's model in that it was a combination of the heat transfer equation and the Arrhenius equation assuming a first order reaction. Moreover, they introduced the Landau transformation to take into account surface regression.

Since it is difficult to fully integrate all the complex phenomena in the model, certain assumptions are considered. Basically in the comprehensive pyrolysis approach, the heat transfer, the thermal decomposition represented by a chemical kinetic scheme and mass transport are solved using conservation equations.

In the 2000s, several comprehensive models have since been developed as numerical codes including Gypro/Gypro3D [8-10], ThermaKin/ThermaKin2D [11, 38], Pyropolis [42, 84] and FiresCone [85]. Furthermore, Computer Fluid Dynamics software such as NIST Fire Dynamics Simulator (FDS) [12] and FM Global's FireFOAM [86, 87] also include a pyrolysis model. An example of the Pyropolis overall model structure is shown in Figure **5**.

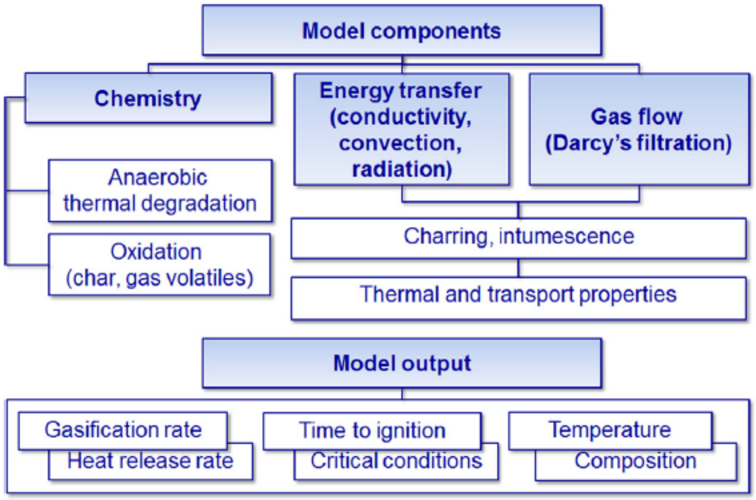

Figure 5. Structure and output of the Pyropolis model [42]

Most of these numerical codes are formulated in a generalized way to take into account all the types of materials. Laughtenberger and Fernando-Pello [8] validated Gypro using a variety of combustible materials which behave differently when subjected to an external flux. The combustible materials used were a non-charring solid (poly(methylmethacrylate)), a charring solid (white pine), an intumescent coating and polyurethane foam (for the study of smoldering combustion). Given the complicated fire behavior of the studied materials, Gypro performed reasonably well.

COMSOL Multiphysics® has also successfully been used to model pyrolysis [13-15, 88]. For example, Girardin et al. [15] predicted the gasification experiments of ethylene-vinyl acetate containing aluminum tri-hydroxide using COMSOL Multiphysics®. Agreement between experimental and numerical results of temperature and mass loss was good. Moreover, the model also allowed conducting a sensitivity study on different scenarios of diffusion by tuning the coefficient of mass transfer.

These codes are developed using the same theoretical basis of coupling momentum, mass and energy conservation equations, although they have different mathematical and numerical formulations. Gpyro uses the Finite Difference Method, COMSOL Multiphysics® and ThermaKin uses the Finite Element Method and FiresCone uses Finite Volume Method. The Finite Difference Method relies on the differential form of the governing equations while the Finite Volume and

Finite Element methods are based on the weak formulation or integral form. Furthermore, radiative heat transfer are not treated in the same manner in FDS and ThermaKin [89]. The effect of this difference was observed in the work of Linteris [90] applied to poly(methylmethacrylate) where the results of mass loss rate (MLR) for both programs corresponded well, apart from the case where there was high in-depth radiation absorption. Linteris et al. [17] also implemented FDS and Thermakin to thermoplastics such as polyamide 6,6, polyoxymethylene and the same conclusions were reported. Kempel et al. [89] used ThermaKin and FDS for predicting the MLR of poly (butylene terephthalate) (PBT) and PBT reinforced with glass fibres (PBT-GF). They reported that given precise input properties, the choice between the two numerical tools was not significant and the characteristic model output (e.g. the peak of mass loss rate (PMLR)) obtained using the two models was within ±4%.

A study to compare ThermaKin, COMSOL Multiphysics® and FDS was conducted by Witkowski et al. [91] using a 1D pyrolysis models applied to cable sheathing materials. They concluded that the choice of model between the three computer programs, using the same input parameters, is not important given the similar nature of the applied governing equations to describe the physical phenomena.

Comprehensive pyrolysis models have the capability to predict the pyrolysis of different combustible materials. However, to implement them, they require input material properties as well as boundary conditions for the experiment being modeled. The next section discusses how model input parameters can be determined.

1.1.3. Parameter estimation

As previously mentioned, to implement the pyrolysis models and predict the fire behavior of combustible materials, the input material properties are required. This section thus discusses how model input parameters can be determined. The first part of this section discusses the determination of model input parameters using experimental techniques and the uncertainties in the measurements. The second part discusses the estimation of parameters considering inverse analysis combined with optimization methods and the chapter concludes with a discussion on the sensitivity analysis techniques.

1.1.3.a. Direct measurement by thermal analysis

Material properties such as thermal conductivity and specific heat capacity can be 'directly measured by thermal analysis', using for example, the Hot Disk thermal constant analyzer which is based on a Transient Plane Source (TPS) method and Differential Scanning Calorimetry (ASTM E1269-11) respectively [14, 15, 92]. In addition, the emissivity can be determined from the hemispherical directional reflectometer and the thermal diffusivity from the Laser Flash Apparatus (ASTM E1461) [93]. Most of these tests are standardized ASTM test methods and a comprehensive presentation of these tests were discussed by Kim and Dembsey [26]. Some of the tests are presented briefly below.

The TPS method was developed by Gustafsson in 1991 [94]. The method is based on a sensor that acts as a heat source and generates the heating power using Joule heating. The sensor is inserted in between an infinite medium and the heat diffuses into the material. The mean sensor temperature rises with time and the temperature function i.e. the shape of the rise is dependent on the type of sensor (e.g. its radius). In an ideal scenario, from the temperature function measurement, the thermal conductivity and diffusivity of the material can be determined from one single experiment from a parameter estimation process. However, in reality they are different factors (such as the material not being infinite) that influence the measurement and different improvements have been proposed by different research groups [94-96]. A typical example is that of Bohac et al. [95] who introduced an improvement in the method by calculating an optimal time window for measurement using the difference analysis together with the analysis of the sensitivity coefficients.

The Laser Flash Analysis (LFA) is also a measurement technique principally used to estimate the thermal diffusivity of a material, in addition, the specific heat capacity and the thermal conductivity can also be deduced. It should be noted that the LFA is based on the flash method developed by Parker et al. [97] in 1961. In general, it is a non-contact method based on heating a sample on one side using a xenon lamp as a heat source. The temperature rise is then captured on the other side of the sample using an infrared detector. The temperature profile that is obtained is then analyzed using an appropriate mathematical model and optimization methods. Finally, the thermal diffusivity is obtained. The mathematical model is generally chosen to find the best fit from the temperature profile. Different such as models exist in literature such as the Adiabatic model [97], Cowan model [98], Cape-Lehman model [99], Radiation model [100] etc.

The thermal decomposition of a material can be studied using TGA, DSC as well as the Simultaneous Thermal Analysis (STA) [101]. The heats of reactions can be extracted from DSC or STA measurements. More precisely, for example, TGA measures mass loss and the mass loss rate of a sample under well-defined heating conditions i.e. heating rate, atmosphere etc. The Arrhenius parameters are then extracted from numerical optimization using TG curves as discussed later in this section [101, 102].

It is noteworthy that even though this technique is often referred to as ‘direct measurement by thermal analysis’, generally, an inverse analysis (using some mathematical model coupled with an optimization method that can either be manual or automated iterative) of the experimental results from the measuring tool is required to extract the relevant thermophysical parameters from the data set as explained above. The definition of the mathematical models, the equations to be resolved and the parameters to be optimized (i.e. what acceptance criteria) are equally important.

Stoliarov et al. [103] investigated the pyrolysis of poly(methyl methacrylate) (PMMA), high-density polyethylene (HDPE) and high-impact polystyrene (HIPS) using the cone calorimeter and gasification experiments. The densities of the materials at room temperature were derived from measuring the mass and the dimensions of the samples. The temperature dependent densities were extracted from literature. The heat capacities as a function of temperature as well as the decomposition thermodynamics i.e. the heats of melting and decomposition were determined using differential scanning calorimetry (DSC) and the method is described in [92]. The thermal conductivity was determined based on the transient line source method. For the measurement of melting polymers, the method is described in [104]. The optical properties, the reflectivity and absorption coefficient were obtained from literature [105, 106]. The Arrhenius parameters were obtained by fitting the reaction rate constants to the first order Arrhenius equation. The uncertainties associated with the property measurements were given as, ±15% for the thermal conductivity, heat capacities and decomposition thermodynamics, ±5% for densities, ±3% for heats of combustion and energies of activation, ±50% for Arrhenius pre-exponential factors and respectively ±20% and ±50% for reflectivity and absorption coefficient.

Linteris et al. [17] measured input parameters for their models in FDS and Thermakin. Uncertainties were taken into account, some are presented here and their effects were explored by conducting a sensitivity analysis. Figure **6** shows the results for the thermal conductivities using different methods (transient plane and line source methods). The relative uncertainties in the thermal conductivity were estimated to be 6%-8% for polypropylene (PP), polyamide 6,6 (PA66), and polyethylene terephthalate (PET) and the uncertainty for polyoxymethylene (POM) was 20%. For properties such as heat capacities and heats of reaction, the error was 16% according to Stoliarov et al. [92] and 3% for reflectance.

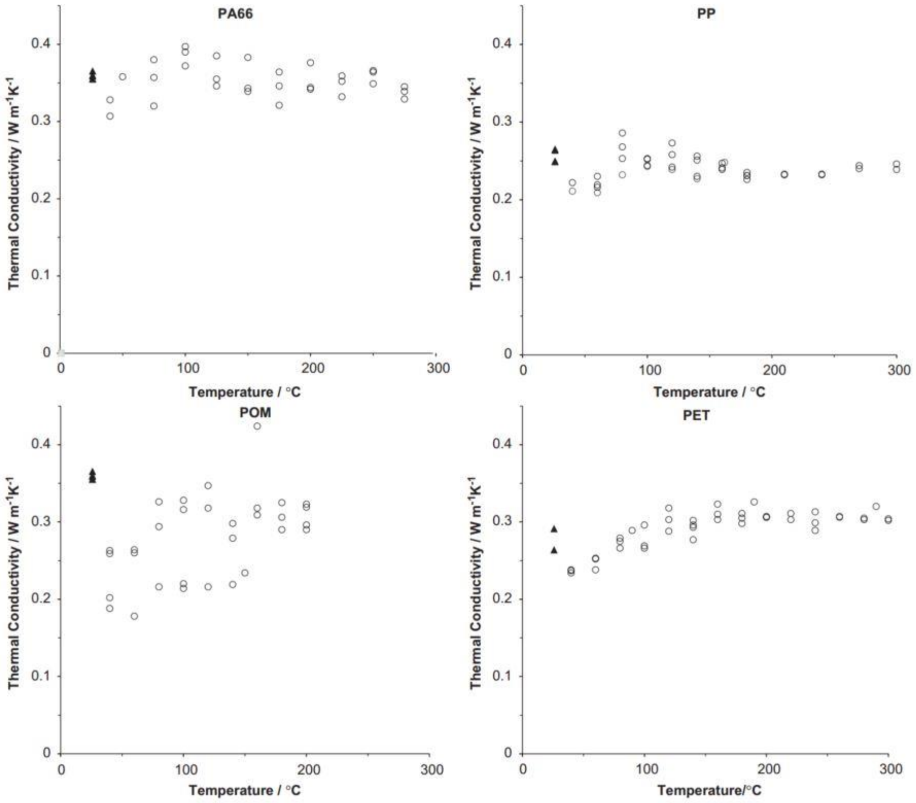

Figure 6. Thermal conductivity measurements of different polymers (PP, PA66, POM, and PET) using the methods : transient plane (Δ) and line (○) [17].

Girardin et al. [14, 15] directly characterized the thermophysical properties of ethylene-vinyl acetate copolymer/ aluminum tri-hydroxide/nanoclays (EVA/ATH/NC). They also used DSC and transient plane source methods. Moreover, for the optical properties, transmittance and reflectance spectra were measured using spectrophotometers equipped with an integrating sphere. The uncertainty in the measurements was ±3% and the method for the determination of absorption coefficients and emissivity is described in [91]. The heat capacity of decomposition gases was also determined by identifying the gaseous products using a controlled-atmosphere mass loss calorimeter connected to a Fourier Transform Infra-Red (FTIR) spectrometer. The procedure is described in [15].

For charring materials, numerical models often require the properties of the formed char. The char is often fragile and non-uniform, making direct measurements difficult [37]. However, Gardelle et al. [56] measured the thermal conductivity of a silicone-based intumescent coating from ambient temperature to 500°C using a hot disk apparatus. They observed that the thermal conductivity decreased from 0.5 ± 0.02 $Wm^{-1}K^{-1}$ to 0.21 ±0.02 $Wm^{-1}K^{-1}$at 400°C owing to the formed carbonaceous char structure and then rises to 500°C due to radiation in the porous structure. Muller [107] also used the same technique to measure the thermal conductivity of intumescent polyurethanes.

Stoliarov et al. [37] used the same experimental techniques as above for determining heat of decomposition and heat capacities of charring polymers and extracted other parameters from literature as well as approximations when no other solution could be found.

Tranchard et al. [108] characterized the thermophysical properties of a carbon epoxy composite exposed to fire. The experimental techniques included TGA, STA, Laser Flash Analysis (LFA) as well as Fourier Transform Infrared (FTIR). These techniques were used to determine the specific heats, anisotropic thermal conductivity, decomposition kinetics and thermodynamics. The application of inverse analysis to parameter estimation of input material parameters for pyrolysis models is presented in the next section.

1.1.3.b. Inverse analysis

A parameter estimation problem can be formulated as an inverse heat transfer problem involving optimization with an objective function which minimizes the error between experimental and model data. This approach involves obtaining input model parameters from e.g. bench scale tests used for temperature measurements or mass loss rates determination. It has been widely used in the fire community [33, 60, 109]. The most noticeable early work on the parameterization of comprehensive pyrolysis models from experiments include that of Stoliarov and Lyon [37, 103]. Lautenberger et al. [60] also worked on parametrization but used an evolutionary algorithm which was later improved by Chaos et al. [33]. These research works are further discussed later in this section.

When conducting optimization, the idea is to compare numerical results from the pyrolysis model and the results from the experiment and a stopping criterion like the relative tolerance on the objective function is normally defined. Calabrese et al. [110] defined the relative tolerance to be lower than 10^{-4} in their study. Comprehensive pyrolysis models are then coupled with numerical optimization methods. A detailed study and guide on parameter estimation applied to comprehensive pyrolysis models was conducted by Kim [26, 57, 111]. As shown on the work flow of their methodology presented on Figure **7**, they categorized the process of parameter estimation in three blocks containing 1) the main parts of the pyrolysis model i.e. initial input values of the material properties, numerical optimization method etc., 2) the block containing the numerical results which are confronted with the experimental results, errors etc. i.e. the validation phase and 3) the block which allows to comment or discuss information on the results of the optimization study etc.

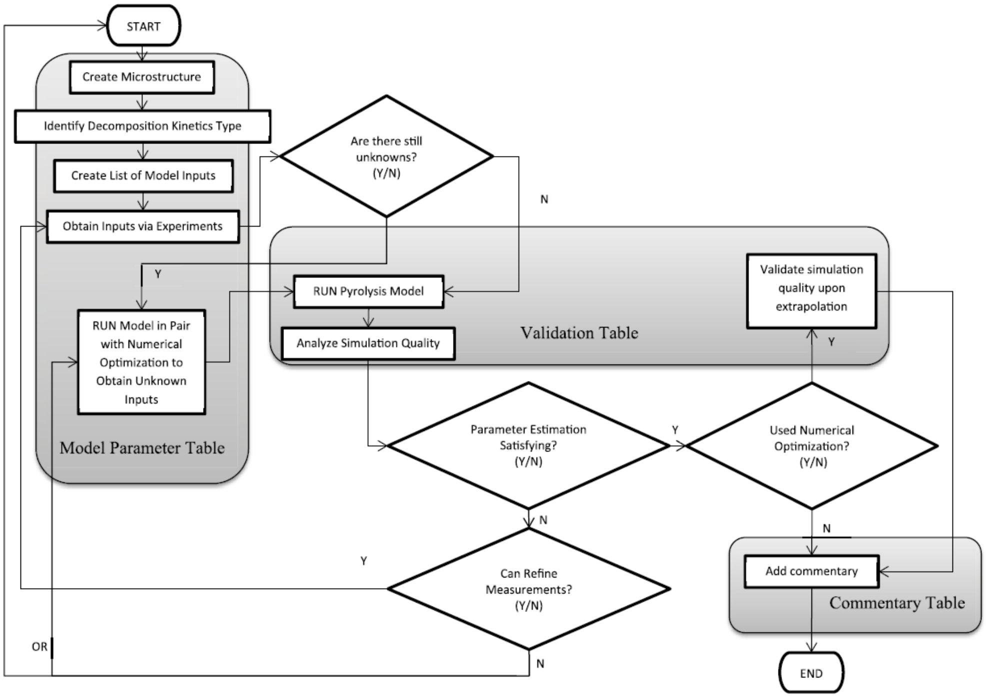

Figure 7. Workflow on how to conduct a parameter estimation study [26, 57].

A number of curve-fitting algorithms have been developed and used over the past years and they have been successfully applied to pyrolysis models. Optimization plays an essential role in the estimation of material properties to be used as inputs for pyrolysis models and it is crucial to identify which optimization technique is best suited for a particular problem in terms of how it converges and overall performance. Besides the selected optimization technique, experiments for which they are applied and the final model validation are highly important. The conducted experiments should be relatively accurate otherwise an incorrect data set can be obtained. For the validation step, the predictions should be compared to the experimental results and an agreement should be observed preferably over a wide range of conditions e.g. different external heat fluxes. If the agreement is not achieved, it means that there was a phenomenon not included in the model or that an incorrect parameter or boundary condition was used. In this case the pyrolysis model should be improved [112].

To solve the inverse heat transfer problem, different types of optimization methods are used. Several optimization methods exist in literature such as manual optimization and automated search techniques [110]. These methods are generally classified by the optimization community as gradient-based versus direct search methods. Using this classification, evolutionary algorithms fall under direct search methods.

In this review, we present gradient-based and direct search methods which are often applied to pyrolysis of combustible materials. Additional class of approaches for finding model parameters from data are Bayesian methods such as Markov Chain Monte Carlo (MCMC). These methods are interesting as they characterize the model parameters from a probability distribution rather than as a single value. Bruns [113] used MCMC to find kinetic parameters from TGA data for HIPS, PC and PVC.

1.1.3.b.i. Gradient-based methods

Several gradient-based methods such as Simplex method, Gradient method, Newton, Levenberg-Marquardt, Sequential quadratic programming (SQP) etc. exist in literature. The gradient-based method often implemented for non-linear problems is the Levenberg-Marquardt method [114-120].

Gradient-based methods have often been applied to estimate material thermophysical properties of materials as well as kinetic parameters. Calabrese et al. [110, 121] proposed a methodology to estimate the effective thermal conductivity applied to a material that intumesces. COMSOL Multiphysics® coupled with the Nelder-Mead algorithm coded in Matlab was used to solve the problem. The Nelder-Mead algorithm is however presented under this section for clarity even though it is a gradient-free method. Experimental data for the optimization target were gathered from temperature measurements from thermocouples that were placed at two different heights inside the intumescent layer. The results demonstrated how the thermal conductivity varies with temperature and the possibility to estimate the thermal conductivity using inverse heat transfer. Bozozoli [122] also applied the same methodology. Since in their case they were only estimating one material property, there was no information on the performance of the algorithm. Theuns et al. [62] determined the material properties of charring combustible solids by implementing an automatic optimization technique called downhill Simplex in multidimensions (which is also known as the Nelder-Mead simplex method) using experimental mass release curves. They set their relative tolerance as 10^{-4}. In their optimization procedure, they also chose bounds to allow for realistic values. Some of the optimized parameters resembled those found in literature while others did not, probably because of differences in the source of the materials. Scott and Beck [123] estimated the thermophysical properties of a composite using a Gauss minimization procedure and temperature measurements at different locations. The obtained parameters corresponded very well with the synthetic values that were used to produce temperature values.

Meunders et al. [59] investigated an optimization method for estimating kinetic and thermophysical parameters of polyurethane (PUR) foam. Experimental information was collected from bench-scale tests such as Thermo-Gravimetric Analysis (TGA) and cone calorimeter. TGA and heat release rate (HRR) results were used as optimization targets for the kinetic parameters and thermophysical properties respectively. In this study, the heats of reaction were taken from literature [124] and the Arrhenius equation was manually adjusted to obtain a good fit against the experimental data from the TGA to estimate the Arrhenius parameters. The obtained set of Arrhenius parameters was then used to determine the thermophysical properties and FDS 6.0.1 was coupled to an optimization algorithm which was based on the gradient method. The comparison between the predicted and experimental HRR was considered consistent for the overall burning time and average HRR. However, the model could not capture the two-stage fire behavior probably because the kinetic scheme was not capable of taking this behavior into account. The bounds prescribed on the material properties for the optimization technique were very large and consequently the estimated parameters would be based on the used pyrolysis model and boundary conditions. Even though the bounds prescribed on the parameters were large, two of the estimated parameters were equal to the upper boundary indicating that there were issues with the modeling approach (Table **2**). It makes sense as the pyrolysis model chosen could not predict the two-step burning of PUR at high fluxes.

Table 2. Bounds prescribed and estimated values [59].

	Units	Lower bound	Upper bound	Estimated Values
Mass fraction (C1)	−	−		0.22
Mass fraction (C2)	−	−		0.67
Activation Energy, *E* (C1)	kJ/kmol	−		1.50×10^{5}
Activation energy, *E* (C2)	kJ/kmol	−		1.85×10^{5}
Pre-exponential factor, A (C1)	1/s	−		1.07×10^{12}
Pre-exponential factor, A (C2)	1/s	−		5.90×10^{12}
Emissivity, ε (C 1)	−	0.70	1.00	0.70
Emissivity, ε (C 2)	−	0.70	1.00	0.78
Specific heat, c_p (C 1)	kJ/(kg·K)	1.50	4.00	3.17
Specific heat, c_p (C 2)	kJ/(kg·K)	1.50	3.00	3.00
Thermal conductivity, k (C 1)	W/(m·K)	0.01	0.15	0.01
Thermal conductivity, k (C 2)	W/(m·K)	0.15	0.23	0.23

Optimization techniques have also been widely used for determining the kinetic parameters using kinetic models. Different kinetic models have been implemented to model the thermal degradation of combustible solids. These kinetics models can be simple one-step or multi-step complex reaction schemes [39]. To understand how the level of complexity of the kinetic model plays a role on pyrolysis modeling, a typical study was conducted by Marquis et al. [125] on polyisocyanurate foam (PIR). They evidenced that simple kinetic models were acceptable to represent thermal decomposition of PIR. Ritchter et al. [126] studied the influence of kinetics of several wood species on their charring behavior. They then concluded that the kinetic model for one wood species can be applied to other wood species and that modelers should pay more attention to their thermophysical properties. For non-charring materials, issues concerning model complexity have been discussed by Bal and Rein [127-129], and Ghorbani et al. [7]. Bal and Rein [128] conducted a brief comparison of three models (implemented in different codes) used for predicting the same experimental results, which revealed that some degree of complexity in mechanisms was unnecessary. They then proved that using complicated kinetic schemes was not necessary once heat transfer processes were simplified. However, for scenarios such as smoldering combustion in polyurethane foam the heterogeneous chemistry has been fully described. Rein et al. [130] implemented a 5-step mechanism to take into account the smoldering combustion of polyurethane foam which was an improvement to the most used 3-step mechanism proposed by Ohlemiller [131]. The model was capable of reproducing the smoldering characteristics such as the thermal and species structure of the reaction-front propagation rate etc. and described both opposed and forward propagation despite inaccuracies.

Many solid-state decomposition kinetic models have been developed over the past years and up-to-date the Arrhenius law is still being used to model the solid decomposition. Equation 18 describes the reaction rate of a solid-phase reaction and gives the relationship between reaction rate and temperature,

$$\frac{d\alpha 1}{dt} = k1(T)f(\alpha 1) \qquad \text{Equation 18}$$

The rate constant $k1(T)$ is expressed in terms of the Arrhenius equation (Equation 19);

$$k1(T) = Aexp^{-(E/RT)} \qquad \text{Equation 19}$$

where, A is the pre-exponential factor (1/s), E is the activation energy (kJ/mol), T is the absolute temperature, R is the gas constant, $f(\alpha)$ is the reaction model related to the solid reaction mechanism (some kinetic models are listed in Table. 5) and $\alpha 1$ is the conversion degree defined by Equation 20:

$$\alpha 1 = \frac{m_0 - m_t}{m_0 - m_f} \qquad \text{Equation 20}$$

Where , m_0 is the intial weight, m_t is the instantaneous weight, and m_f is the final weight.

There are several ways to determine the Arrhenius parameters. They can be extracted from isothermal kinetic data by applying Equation 18. Equation 18 is then adapted into a non-isothermal rate expression (Equation 21) leaving the reaction rate as a function of temperature at a constant heating rate,

$$\frac{d\alpha 1}{dT} = \frac{A}{\beta 1} e^{-\left(\frac{E_a}{RT}\right)} f(\alpha 1) \qquad \text{Equation 21}$$

where $\beta 1$ is the heating rate.

This transformation is based on the assumption that changing the experimental conditions from isothermal to non-isothermal has no effect on the reaction kinetics, which is quite reasonable when dealing with simple single-step process but may have serious implications for multi-step reactions kinetics as discussed by Vyazovkin and Wight [132]. Reaction kinetics is commonly studied by using thermogravimetric analysis (TGA) and derivative thermogravimetric (DTG) curves but can also be studied using Differential scanning calorimetry (DSC) curves [133, 134].

Isothermal or non-isothermal kinetic analysis can be performed by using model-based or model-free methods (Figure **8**). Model free methods such as Friedmann, Kissinger, Flynn-Wall-Ozawa, Kissinger-Akahira-Sunose method [135, 136] have the ability to calculate the activation energy without the assumption of reaction models but they however have some disadvantages, hence, a model to describe the reactions is often applied for the solid thermal degradation.

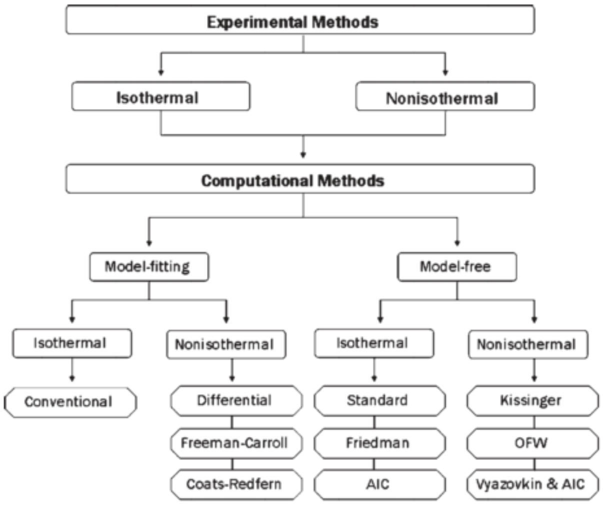

Figure 8. Typical kinetic analysis methods [137].

For a comprehensive understanding on these methods the reader is referred to papers [135, 137-143]. A model-based method is one that fits different reaction models $f(\alpha 1)$ or $g(\alpha 1)$ (Table 3) into the general kinetic equation (Equation 18) and the activation energy and pre-exponential factor are often calculated by non-linear regression analysis (least square optimization) [142]. A number of optimization methods exist for the extraction of the kinetic parameters e.g. gradient-based [117], simulated annealing [144], genetic algorithm (GA) [145, 146], particle swarm algorithm (PSO) [147-149] etc. These algorithms are explained later in this section.

Table 3. Examples of reaction models [150].

Model	Differential form $f(\alpha 1) = \frac{1}{k1}\frac{d\alpha 1}{dt}$	Integral form $g(\alpha 1) = k1t$
	Nucleation models	
Power law (P2)	$2\alpha 1^{1/2}$	$\alpha 1^{1/2}$
Power law (P3)	$3\alpha 1^{2/3}$	$\alpha 1^{1/3}$
Power law (P4)	$4\alpha 1^{3/4}$	$\alpha 1^{1/4}$
Avrami-Erofeyev (A2)	$2(1-\alpha 1)[-ln(1-\alpha 1)]^{1/2}$	$[-ln(1-\alpha 1)]^{1/2}$
Avrami-Erofeyev (A3)	$3(1-\alpha 1)[-ln(1-\alpha 1)]^{2/3}$	$[-ln(1-\alpha 1)]^{1/3}$
Avrami-Erofeyev (A4)	$4(1-\alpha 1)[-ln(1-\alpha 1)]^{3/4}$	$[-ln(1-\alpha 1)]^{1/4}$
Prour-Tompkins (B1)	$\alpha 1(1-\alpha 1)$	$ln[\alpha 1/(1-\alpha 1)] + c^{a}$
	Geometrical contraction models	
Contracting area (R2)	$2(1-\alpha 1)^{1/2}$	$1-(1-\alpha 1)^{1/2}$
Contracting volume (R3)	$3(1-\alpha 1)^{2/3}$	$1-(1-\alpha 1)^{1/3}$
	Diffusion models	
1-D diffusion (D1)	$1/(2\alpha 1)$	$\alpha 1^{2}$
2-D diffusion (D2)	$-[1/ln(1-\alpha 1)]$	$\big((1-\alpha 1)\ln(1-\alpha 1)\big) + \alpha$
3-D diffusion-Jander (D3)	$\left[3(1-\alpha 1)^{2/3}\right]/\left[2(1-(1-\alpha 1)^{1/3}\right]$	$(1-(1-\alpha)1^{1/3})^{2}$
Ginstling-Brounshtein (D4)	$3/\left[2((1-\alpha 1)^{-1/3}-1\right]$	$1-(2/3)\alpha-(1-\alpha 1)^{2/3}$
	Reaction-order models	
Zero-order (F0/R1)	1	$\alpha 1$
First-order (F1)	$(1-\alpha 1)$	$-ln(1-\alpha 1)$
Second order (F2)	$(1-\alpha 1)^{2}$	$[1/(1-\alpha 1)]-1$
Third-order (F3)	$(1-\alpha 1)^{3}$	$1/2[(1-\alpha 1)^{-2}-1]$

[a] Constant of integration.

Since a large number of kinetic models exist, Burnham and Braun [151] reviewed some of these models, they outlined how they work and gave recommendations on the selection of an appropriate model.

Significant effort has been made in the development of numerical methods for the determination of the kinetics of decomposition, however, most studies reported in literature do not explain the physical significance of the obtained parameters and reaction schemes. Development of experimental techniques is required to physically understand the extracted kinetic parameters. An interesting study was conducted by Tranchard et al. [152] relating the obtained kinetic parameters of a composite material to a physical sense. Based on the determination of the degradation pathway of the material, they proposed a multi-step reactions model composed of two main competitive reactions, an auto-catalytic reaction and a n^{th} order reaction. In a similar way, Bourbigot et al. [153] determined the kinetic degradation scheme of a polystyrene-montmorillonite nanocomposite. Results from the kinetic analysis were justified by using the heat release curve from the cone calorimeter. A concise paper on the challenges of modeling the thermal decomposition of solid fuels is presented by Rogaume [154].

Currently, different numerical codes exist to calculate the kinetic triplet such as TA-KIN, NETZSCH thermokinetics software, KINETICS…[138]. For example, NETZSCH thermokinetics software determines the parameters of the model-free and model based approach following the methodology by Opfermann [155]. Anderson et al.[156] investigated three different computer programs (RATE, KINETICS MK and TA-KIN) to determine activation parameters using non-linear evaluation methods. TA-KIN implements the the Levenberg-Marquardt algorithm, RATE implements Simplex algorithm while the KINETICS MK uses the modified Gauss-Newton algorithm. TA-KIN performed very well because it was flexible.

Bruns et al. [157] extracted Arrhenius parameters of thermoplastic materials by using the algorithm based on sequential quadratic programming. TGA curves obtained from several heating rates were used in the study and their pyrolysis model was based on a population balance approach. Generally, the population-based model performed well for the prediction of TG curves and the same was reported by Staggs [30]. However, there were typical issues with the parameter estimation study and there was no conclusion on the extracted parameters because the global minimum could not be reached due to the kinetic compensation effect.

The kinetic compensation effect is a major issue when it comes to finding optimum kinetic parameters [157, 158]. Generally, it is possible to generate the same TG curve by simultaneously varying the values of the activation energy (E) and the pre-exponential factor (A). Ceamanos et al. [158] reported that for polyethylene, the activation energy can vary between 175 and 325 kJ/mol while the pre-exponential factor varied between 10^{10} and 10^{22} s^{-1}. Koga [159] presented a comprehensive review on this topic. A visualization of kinetic compensation is shown in Figure 9 where the objective function (sum of squared errors (SSE)) is plotted for the activation energy against the pre-exponential factor [157] for a "critical molecule size of a monomer unit" using the random scission model. There are two major observations: the first one is the valley for which the experimental data is predicted by the model which highlights the kinetic compensation effect. At A=5.495 10^9 s^{-1} and E=130 kJ/mol a unique shallow minimum was found even though the SSE was relatively flat along the kinetic compensation line. The second observation is the noticeable flat region for large values of A and small values of E which is a consequence of the considered limited range of temperatures for the data points of the experiments.

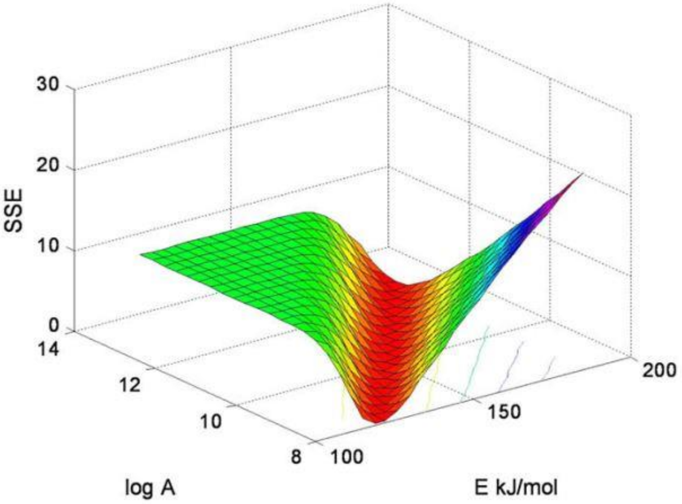

Figure 9. 3D Visual representation of the kinetic compensation for PMMA with random scission model for a "critical molecule size of a monomer unit"[157].

Loulou et al. [120] aimed at applying optimization techniques to obtain the Arrhenius parameters from a proposed kinetic model for the pyrolysis of a cardboard material. Mass loss information from thermogravimetric measurements was used. The Levenberg-Marquardt algorithm was implemented and it was robust in fitting with the experimental data. Constraints were also imposed on the estimated values e.g. to keep the parameters always positive. The comparison between the experimental and simulated data was acceptable given that there were small differences on the curvature of the total mass loss. However, the methodology was affected by the values used initially and this was attributed to the kinetic models being non-linear and consequently they proposed the use of genetic algorithms for better initial guesses. Mamleev and Bourbigot [117] used a method involving modulated thermogravimetry to estimate the Arrhenius parameters. The methodology was the same as the Levenberg-Marquardt method and it sped up the numerical processing time.

For intumescent modeling, Griffin [118] applied the Levenberg-Marquardt method for the estimation of the kinetic parameters of an intumescent coating. Independent first order parallel reactions were assumed. They obtained a correlation coefficient that was higher than 99.5%, however they observed poor fits at inflexion points and at the end of the weight loss curves. An example of the fit between predicted and measured results is shown in Figure **10**.

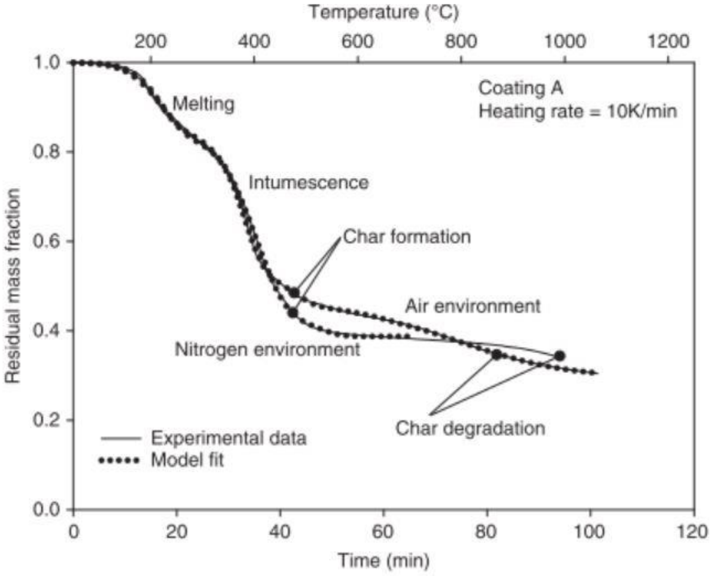

Figure 10. Weight loss and predicted curves [118].

Di Blasi and Branca [160] proposed that an intumescent coating made of three ingredients degrades following independent finite-rate reactions. Thermogravimetric data (TGA) were used for estimating Arrhenius parameters using a direct method. The estimated parameters corresponded to those which were found in a previous study. Reverte et al. [119] also used TGA data and contributed to the research on parameter estimation. A gradient-based method, which was a version of Levenberg–Marquardt method, was implemented. Other numerical methods for the estimation of kinetic parameters were presented.

Rozyki [161] compared the Arrhenius parameters that were estimated from different methods such as the linear method etc. Generally, he concluded that the values of the calculated parameters depended on the estimation method. The use of the non-linear least squares methods was recommended because it allowed calculating statistical weights and it did not bring into play transformations involving algorithms.

A different approach was presented by Lyon [162] to determine the kinetic parameters from TGA data. These data were obtained from different heating rates i.e. 1, 5 and 20 K/min. The methodology was based on using nonisothermal, single step thermal degradation kinetics to express the heat release kinetics combining material properties as well as thermal stability parameters. Using a simplified kinetic model to describe the thermal decomposition for polymers, they managed to predict a good fit between the model and experimental data except for temperatures higher that 700 °C because secondary reactions were not taken into account in the model. For determining the kinetic parameters from TGA data, the Stoliarov's group [163] has used this method as a basis in ThermaKin as well as other studies in FDS [59].

Li and Stoliarov [101, 102] developed a systematic approach for the determination of kinetics and thermodynamics of the thermal decomposition of non-charring and charring polymers based on the simultaneous thermal analysis (STA) using ThermaKin. The ThermaKin model was fitted to the experimental TGA curves to obtain the kinetics of decomposition and then used for the analysis of the heat flow curves from the DSC to determine the parameters related to the thermodynamics of decomposition (sensible, melting and decomposition reaction heats). The parameters obtained from this methodology were capable of reproducing both the experimental TGA and DSC curves. Li et al. [50, 164] used the same procedure as above to determine the Arrhenius parameters, heats of decomposition and the heat capacities. Moreover, other parameters such as the emissivities and the absorption coefficients were determined from independent experiments. Finally, the thermal conductivities were the only unknowns and their values were computed by fitting the gasification sample back surface temperature evolution. In their model development, the optimization problem is well poised and the gasification experiment MLR were not used as fitting targets but were instead utilized in the model validation. This is a critical feature of the Li et al.'s approach [50]

[164] that differentiates it from the majority of other pyrolysis parameterization studies [37, 88, 89, 103, 165]. In most similar studies, MLR was used as an optimization target and thus the model's ability to capture MLR was not viewed as an independent indicator of the model's validity. The same technique was used by McKinnon et al. [166] applied to corrugated cardboard. The authors also used TGA and DSC to determine the reaction mechanism, the enthalpy of decomposition reactions as well as the apparent heat capacities related to the species. Moreover, the heat of combustion of evolved gases for the respective reactions were determined from the pyrolysis-combustion flow calorimetry. This approach has an advantage because it results in a pyrolysis model that is physically representable [167]. A detailed study on this approach is presented by Stoliarov [112].

Another approach consists in fitting all or almost all material properties into a set of cone calorimeter or FPA experiments. By doing so, the problem is both highly complex (multi-dimensional parameter space) and ill-posed (multiple solutions exist representing local minima in the multi-dimensional parameter space). Finding solutions to these problems require sophisticated optimization methods. In this case, direct search methods such as evolutionary algorithm are useful and they are presented in the next section.

1.1.3.b.ii. Direct search methods

The objective of this section is not to describe the evolutionary algorithms but to give an overview of their application in pyrolysis models. Detailed descriptions of these algorithms can be found elsewhere [93, 168-170]. These optimization methods are inspired by the theory of evolution and are often referred to as Evolutionary Algorithms. Gradient-based optimization techniques optimize a single individual whilst evolutionary algorithms are focused on optimizing a population. These algorithms do not identify the global minimum but they do combine traditional mathematical optimization with random exploration of the parameter space, which makes them effective in identifying multiple local minima, the best of which is subsequently selected. In pyrolysis modeling, up-to date, evolutionary algorithms have been successfully implemented.

Genetic algorithms have been applied in other fields such as turbulent reacting flows for the optimization of reaction rate coefficients and they were found to be numerically robust and efficient as well as being flexible and easy to use [83]. In 2001, Şahin et al. [171] used genetic algorithms (GA) to determine the kinetic parameters from thermogravimetric analysis of ammonium pentaborate. They compared the results between the GA method and Coats-Redfern methods and the former presented better results. In 2006, Rein et al. [60, 145], started implementing GA for the estimation of thermophysical and kinetic parameters from cone calorimeter and TGA experiments. Rein et al. [145] obtained the Arrhenius parameters of the pyrolysis and oxidation of flexible polyurethane (PUR) foam by applying a GA together with TGA data. Before applying the GA to PUR they applied the methodology to a case which has been extensively studied, that is the pyrolysis of cellulose [172]. In this preliminary work, the GA methodology was used to estimate the Arrhenius parameters of cellulose (activation energy - E, pre-exponential factor - A) as well as the stoichiometric coefficient ($\vartheta_{c,p}$). Figure **11**(a) shows the performance of the GA at simulating the TGA experiments; the simulated results perfectly correspond with the experimental data for the duration of the experiment. Figure **11**(b) illustrates how the GA performs during search of optimized parameters. It shows how initial individuals perform poorly and how the GA progresses up to convergence. Figure **11**(c) shows the fitness vs generations. The figure shows how the fitness evolves from the start i.e. in a quick manner, then slowing down toward the end of the search.

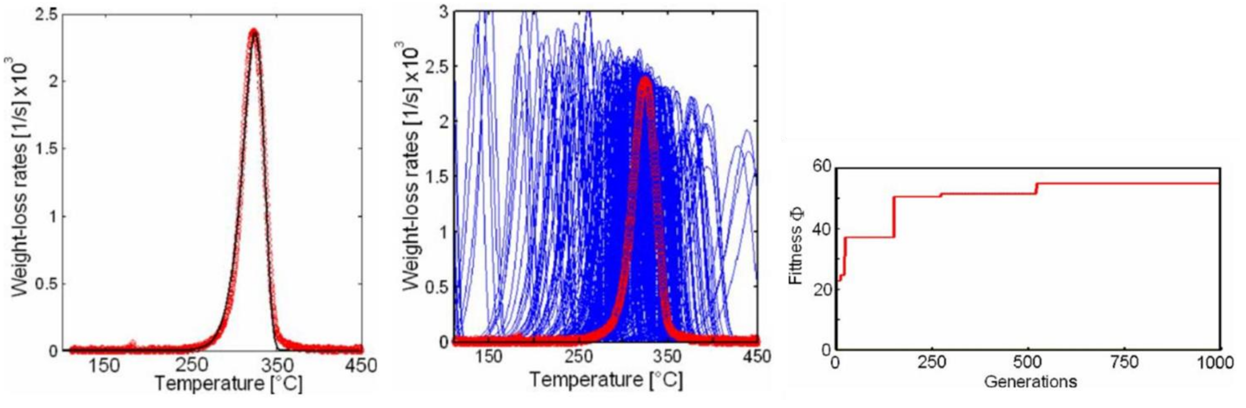

(a) (b) (c)

Figure 11. (a) Comparison of experimental (red) and numerical (black) results of cellulose mass-loss rate curves in nitrogen at 5 °C/min [172], (b) GA (blue) performance during the search of optimized parameters (in red is the experimental curve), (c) Fitness evolution during GA optimization [145].

The optimized kinetic parameters from the GA are shown in Table 4. The parameters agree very well with the parameters obtained from a gradient-based method. Significant scatter (TG scatter) was reported among measured TGA data from several laboratories because of errors in the data which consequently caused differences in the estimated parameters (Table 4).

Table 4. Comparison of estimated parameters [145].

Parameter	GA	TG benchmark	TG scatter	GA-TG difference	Units
E	236	241	12%	2%	kJ/mol
Log $_{10}$ (A)	18,4	18.8	17%	2%	Log $_{10}$ (1/s)
$\vartheta_{c,p}$	0.050	0.052	90%	4%	-

The study suggested that the differences between results from the GA and benchmark were lower than that from the benchmark and experimental data because of the errors observed. For the PUR foam, Arrhenius laws were implemented using a 5 step reactional scheme. The GA performed very well and the estimated parameters well predicted the experimental TGA data at different conditions as well as some physical characteristics associated with smoldering combustion.

Other works involving the use of GA for determining the Arrhenius parameters are included here; Matala et al. [173] applied the methodology which was developed by Lautenberger et al. [60] and Rein et al. [145] involving the use of GA for the estimation of the Arrhenius parameters of several combustible materials from TGA measurements in FDS. The methodology worked very well and further confirmed the use of evolutionary algorithms in estimating input parameters in the field of fire safety. More work was also done on applying the GA, for example the work of Rogaume et al. [174]. They used the GA to calculate the kinetic parameters of five-step kinetic scheme describing the thermal decomposition of polyether polyurethane foam. The experimental and predicted mass loss rate data were consistent.

Lautenberger et al. [60] demonstrated applicability of the previous methodology using cone calorimeter data instead of TGA data applied to redwood and red oak as well as polypropylene. Their optimization targets were the surface temperature and the MLR. In their study, the comparison between calculated and experimental results was acceptable given that the estimated parameters were model dependent (boundary conditions, assumptions), a sensitivity study would be necessary. The GA was also able to estimate the material properties within ~10 % of those found in the literature. However, the advantage of the approach was the possibility to apply it to any pyrolysis model using experimental data from small-scale tests.

In a similar way, Chaos et al. [33] used evolutionary optimization methodologies. Their objective was to study the ability of the SCE and GA "to converge to a global optimum using the least amount of data". In this study, the MLR from the Fire Propagation Apparatus (FPA) was used to generate synthetic data by adjusting the input parameters to get the best fit. This synthetic data was then used to investigate the performance of the SCE and GA algorithms. This exercise showed the ability of SCE to return almost the exact same data as the initial synthetic data. Moreover, it was accurate, efficient and robust. The MLR was used as a target at different heat fluxes i.e. 25kWm^{-2}, 62.5 kWm^{-2} and 100 kWm^{-2} and the SCE further provided excellent agreement as well as residual that was as low as 10 $^{-7}$ as shown in Figure 12. The authors chose the MLR as an optimization target because it was assumed to be measured accurately as compared to the temperature data. This was because the measured temperature data had uncertainties. However, they reiterated that the modeler should use several target data and not limit it when available and accurate. Moreover, additional target data provides confidence in the data set obtained from optimization.

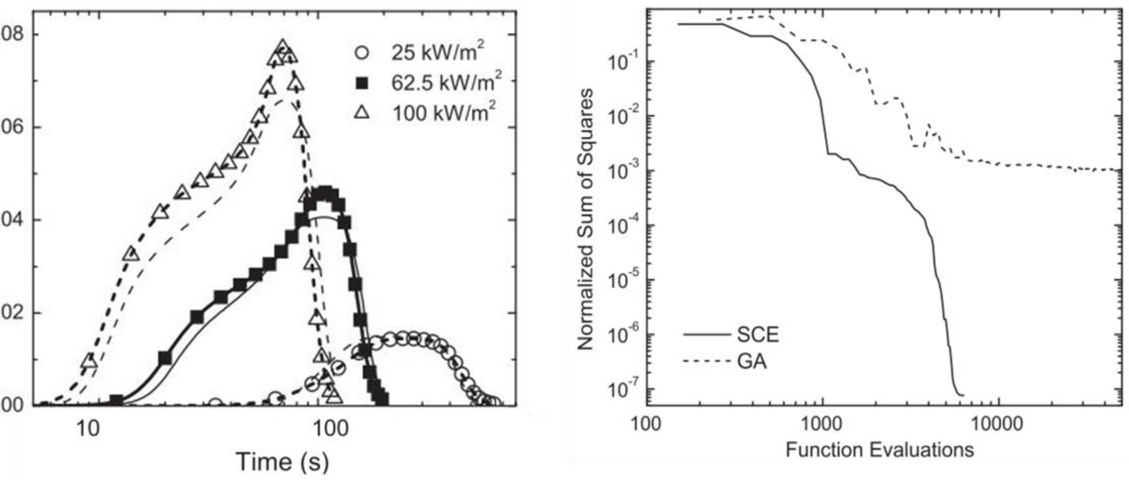

(a) (b)

Figure 12. (a) MLR from optimized parameters (SCE – bold lines, GA – thin lines) vs synthetic data (symbols) for a non-charring material (b) Residuals of the SCE and GA during optimization [33].

The SCE was further recommended by Lautenberger and Fernandez-Pello [175] for general use in the estimation of material properties because of its balance between efficiency and accuracy. They presented a comprehensive review on the application of four different optimization techniques with Gpyro (namely vanilla GA, hybrid GA/simulated annealing, SHC and SCE). They also evaluated the different experimental techniques that can be used when conducting a parameter estimation study.

The same methodology used by Chaos et al. [33] (described above) was successfully used by the same author [176] with application to hardwood pyrolysis. In their study they however decoupled the boundary conditions from the optimization problem by measuring the spectral properties of the material surface. Ding et al. [177] used the FireFoam pyrolysis model to study the pyrolysis of wet wood using the optimized parameters obtained by Chaos [176]. Chaos et al.[178]. also investigated the flame spread and fire response of corrugated cardboard using the CFD program FireFoam. This study was conducted on vertically orientated panels and exposed to an external propane sand burner. For this particular test, the heat release rate and the smoke generation were evaluated. In addition, surface temperatures and heat flux were determined so as to add to the validation data set. Using the pyrolysis model in FireFoam, input material properties were obtained using optimization against experimental data from the FPA. These properties were then used for the CFD simulations and the model results overpredicted the peak of HRR. Moreover, a sharp decay was observed towards the end of the combustion process and this was probably due to the char oxidation which was not taken into account in the model. In addition, the same methodology [33] was also applied by Zeinali et al. [87] for the determination of input model parameters to examine the pyrolysis and flame spread on medium density fiberboard (MDF) using FireFoam.

Interesting work was presented by Ghorbani et al. [7, 179] who also studied the two algorithms GA and SHC using six different models to describe the pyrolysis of polyvinyl chloride. The authors further presented the limitations of the optimization technique that was implemented. The models differed in their thereby affecting the number of unknown properties as well as the algorithm used. The optimization targets were experimental data obtained from the cone calorimeter i.e. MLR and temperature at the back surface. Some of the properties, such as the char density estimated by the GA, were too low and without any physical sense. This was attributed to the typical parameter estimation problem of the non-existence of a unique solution. Both the algorithms were capable of globally capturing the MLR curves. Precisely, they successfully predicted the time to ignition and the predictions for the time of the first peak, magnitude of the first peak, total burn out time, time for the second peak, magnitude of the second peak, total burn out time and total mass loss were within 20%, 10%, 30%, 15%, 10% and 5% respectively. For the temperature curves, the predictions were capable of capturing the early moments up to around 100 °C and experimental values beyond this temperature were not taken into account because they were considered unreliable. The authors reported that these models were only valid for the set of conditions used during model calibration after applying them to a scenario involving flame spread. To overcome this problem, in addition to the cone calorimeter or FPA, DSC, DSC and/or STA could be used for calibrating the models as well as improving the bench-scale tests and measurements. Capote et al. [180] presented a methodology combining the cone calorimeter and STA to estimate thermophysical properties and the kinetic parameters respectively. The methodology was similar to that of Stoliarov and Li [112] in that it separated the individual pyrolysis processes during optimization i.e. the STA results were used to obtain the kinetic parameters and then the cone calorimeter data (MLR) as the optimization target for the thermophysical properties. The cone calorimeter tests were conducted at external hea fluxes of 25kW/m^2, 40kW/m^2, 50kW/m^2 and 75kW/m^2. The methodology was applied on polyethylene and optimization was conducted by implementing evolutionary algorithms in Gpyro. The initial values were obtained both from measurements and from literature. The methodology was able to provide with a reasonable set of properties. However, the following relative errors were observed; 0% at 75kW/m^2 and 27% at 50kW/m^2 for the ignition times, 135% at 25kW/m^2, 45% at 40kW/m^2, 4% at 50kW/m^2 and 32% at 75kW/m^2 for the peak MLR and 21% at 25kW/m^2, 35% at 40kW/m^2, 3% at 50kW/m^2, and 4% at 75kW/m^2 for the time to peak. In general, the optimization performed well at 50kW/m^2 and the ignition times for the other heat fluxes were acceptable. Moreover, errors for the peak MLR were higher than those of the ignition times.

Generally, the major drawback associated with parameter estimation problems, especially with gradient based algorithms, is the non-existence of a unique solution because the complicated pyrolysis phenomenon is numerically described using simplified models. In this case, methods based on evolutionary algorithms are necessary [181, 182]. Marquis et al. [181] worked on proving that a unique solution existed which satisfied the initial conditions for a given model. Kinetic parameters were obtained using the GA and mass loss rates under air and nitrogen atmospheres were used as optimization targets. They implemented the Picard–Lindelöf based on a model for the pyrolysis of polyether–polyurethane foam. They managed to prove that a unique solution actually existed which satisfied the initial conditions for a given model in certain conditions.

Several papers in literature have been reported to evaluate the performance of the different types of evolutionary algorithms. Webster and co-workers [7, 168, 179] examined the use of an algorithm called stochastic hill-climber for the estimation of material properties from mass loss rates from bench scale data. The results were compared to results obtained using genetic algorithms. The stochastic hill-climber (SHC) algorithm performed much better for pyrolysis parameter optimization. Lauer et al. [183] compared the performance of different optimization algorithms i.e. the Fitness Scaled Chaotic Artificial Bee Colony algorithm (FSCABC), Artificial Bee Colony algorithm (ABC) and SCE. In terms of accuracy as well as efficiency, both the FSCABC and the SCE performed very well. Ira, Hasalova et Jahoda [184] also dealt with both the GA and SCE for estimating wood thermophysical properties from TGA experiments. In their study, in overall, SCE performed slightly better than the GA.

More advanced optimization techniques are also found in literature. Saha et al. [185] studied the pyrolysis of several thermoplastics and focused on searching for the optimized kinetic model as well as the kinetic parameters. Instead of using the model-fitting methods because of their drawbacks, they applied a hybrid GA (HGA) on 15 different kinetic schemes using TGA data. The HGA reduced the calculation time because it was based on the general GA but used a different method for the search of parameters thereby increasing convergence. The kinetic models that performed very well were the nucleation and growth models together with the n*th* order. Other research work was done by Li et al. [146] to reach the same objective as mentioned previously. In their work, they implemented the GA coupled with the Kissinger's Method (K-K method). As compared to the regular GA, the K-K method was highly efficient because the Kissinger's Method is first used to search for the possible initial parameters and then these parameters are fed into the GA. Park et Yoon [149] used the repulsive particle swarm optimization (RPSO) algorithm to numerically determine the material pyrolysis parameters. The RPSO algorithm was an improved particle swarm algorithm. Ritcher et al. [126] implemented the Multialgorithm Genetically Adaptive method which used several optimization algorithms to estimate the kinetic parameters of wood. The several combined optimization algorithms used were GA, PSO, Adaptive Metropolis Search as well as the Differential Evolution. This algorithm was both accurate and less time consuming compared to others.

In a similar way, a very interesting study was conducted by Raudensky [160]. The authors focused on the notion of artificial intelligence in parameter estimation for materials. They compared a genetic algorithm as well as an algorithm based on neural networks. Neural network algorithms emanate from how the brain of a human works. Both algorithms performed well although they all had advantages and limitations. Genetic algorithms were stated to take time during simulation whereas neural networks required acceptable initial values. They proposed that a combination of both algorithms would improve the results. Najafi and Woodbury [186] used neural networks to estimate the heat flux at the surface of a material using temperature information, then they also discussed their limitations and benefits.

In summary, within the framework of pyrolysis modeling, optimization can broadly be used to solve two main categories of problems. The first category is where most of the model input parameters are determined from independent experiments [50, 164]. Then the few remaining parameters are optimized using, for example, the gasification sample back surface temperature evolution. In this case, optimizations are not time consuming and can be carried out by manually method adjusting parameter values or by the gradient-based methods until satisfactory agreement is achieved. The second category of optimization problems involves fitting all or almost all material properties into a set of Cone or FPA experiments. These problems have been discussed and include the use of evolutionary algorithms [33, 175, 179, 187]. These algorithms are not guaranteed to find the global minimum (no algorithm is capable of that) but they generally combine traditional mathematical optimization with random exploration of the parameter space, which makes them effective in identifying multiple local minima, the best of which is subsequently selected based on physical consideration. However, Ghorbani [7] stated that the estimated values from this approach, when using one set of target data, sometimes do not provide reliable predictions outside the range of conditions in which the calibration was realized. Several research works have focused on trying to overcome this problem. These works involve a systematic approach of combining cone calorimeter or FPA data with TGA, DSC and/or STA data. In this way, it is possible to separate the individual phenomena involve in pyrolysis [112, 164]. Moreover, improved measuring techniques and controlled bench-scale tests have been implemented [50].

In all the cases described above, it is essential to have the knowledge on how the estimated parameters influence the model outputs of interest. The next part highlights the use of sensitivity studies in the fire community.

1.1.3.c. Sensitivity analysis

In general, a sensitivity analysis permits the quantification of the role of parameters in the model predictions. The application of sensitivity analysis to chemical problems dates back to as early as 1981. Rabitz [188, 189] presented an overview of sensitivity theory for the application to chemical problems. In 1994, a comprehensive review presenting more than a dozen sensitivity analysis methods intended for those not familiar with the techniques was presented by Hamby [190]. Some of the techniques applied in the fire-related field are presented here.

Generally, when the most influential parameters are determined, it allows the elimination of the less important parameters and the modeler concentrates on the experimental or numerical determination of the most sensitive parameters in order to increase model accuracy. Sensitivity analysis (SA) methods can generally be classified into three classes i.e. 1) screening, 2) local, 3) global [191, 192].

Screening is a qualitative method that only involves the ranking of input parameters according to their sensitivity. They are advantageous for complex problems as compared to other SA methods because they are computationally economic. Gillet [193] conducted a sensitivity analysis using the screening method on a one dimensional intumescent coating model.

On the other hand, the local sensitivity methods are quantitative and are carried out by changing each input parameter at a time and maintaining the other parameters constant. This method provides the gradient of the model output with respect to a nominal set of input parameters. Chaos [16] performed a sensitivity analysis on a given pyrolysis model that was a simplification of Gpyro [8] applied on both a charring and non-charring combustible solid. In their study, instead of varying the parameters by an arbitrary uncertainty value such as in [19], they used a complex-step differentiation approach to compute the normalized first-order local sensitivity coefficients. The outputs of the model were the temperature of the surface and the MLR. Figure **13** shows some of the results of the sensitivity of the surface temperature at different heat fluxes with respect to the input parameters in the case of a non-charring combustible solid. Note that the kinetic parameters were grouped because of the compensation effect. From the first row in Figure **13**, an increase in the heat flux (from 25 kWm^{-2} to 100 kWm^{-2}) caused the sample surface to reach a higher temperature in the steady state. Near the end, the temperature decreases slightly in both cases. This was explained to be the effect from the mass loss of the material which reduced the thickness consequently reducing the absorbed in-depth radiation and heating rate. The parameters were divided into material properties i.e. thermal conductivity (k_v), heat capacity ($C_{p,v}$), density (ρ) then optical parameters (emissivity (ε_v), absorptivity (α_v), absorption coefficient (κ) and parameters related to reaction kinetics (Ea/lnZ, reaction order (n) , heat of pyrolysis (ΔHp)).

Regarding the surface temperature sensitivity coefficients, they generally exhibit an initial unsteady stage during the first moments and then remain relatively steady except for the parameters related to reaction kinetics. This observation shows the effect of varying the input parameters. The materials properties lower the heating rate because of the dynamic thermophysical properties. The heat flux reaching the surface is dependent on the optical properties and absorptivity is the most sensitive to the increase in temperature. The parameters related to the reaction kinetics hardly have an influence at this stage because conduction controls the heat transfer phenomena. When the material starts to decompose, Ea/LnZ becomes the most influential parameter. ΔHp lowers the temperature of the surface and the effect is demonstrated by its sensitivity coefficient curve. Moreover, from Figure 13, it can be observed that some of the sensitivity coefficients change from a negative value to a positive value with time. This demonstrates how values obtained by optimization could be affected due to compensation effects between the parameters i.e. a variation in some parameters during optimization gives rise to a change in other parameters. Bal [127] extensively studied these effects.

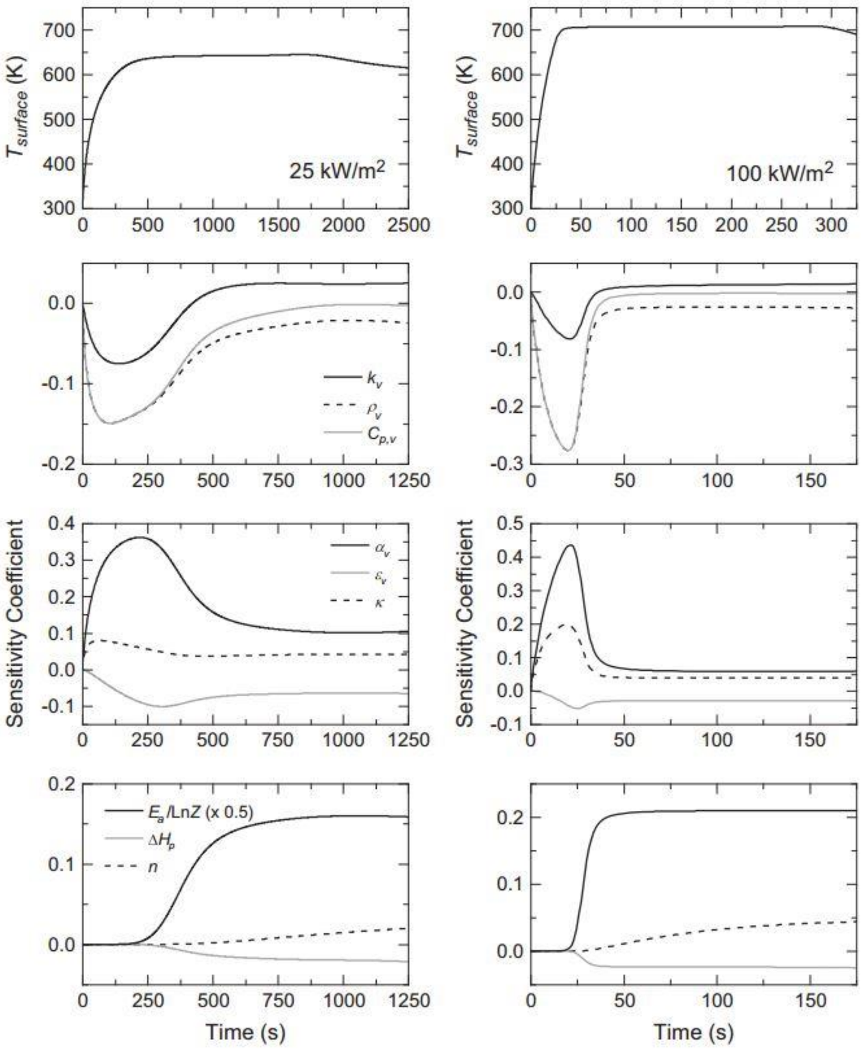

Figure 13. Sensitivity of the temperatures of the surface at different heat fluxes 25 kWm^{-2} (left column) and 100 kWm^{-2} (right column). with respect to the input parameters in the case of a non-charring combustible solid [16].

Their targets were the MLR and surface temperature and most of the parameters qualitatively exhibited relatively the same sensitivity curves. The most sensitive parameters were α_v and Ea/LnZ. Chaos [16] also conducted a sensitivity study on the time to ignition, average MLR, and peak MLR. For charring material, the thermophysical properties for both the virgin and char state except for the heat capacity of the char had an influence on the time to ignition, average MLR, and peak MLR, in particular at low heat fluxes. Moreover, Ea/LnZ significantly influenced the average and peak of MLR. Figure 14 shows the results for the non-charring material. The ignition was not influenced by ΔHp but it was significantly influenced by Ea/LnZ as well as by α_v, k_v , $C_{p,v}$ and ρ also affected the ignition time given that these properties play a role during the initial heating phase of the material (Figure 13). As for the average and the peak MLR, Ea/LnZ, ΔHp, α_v and ε_v were the most influential parameters.

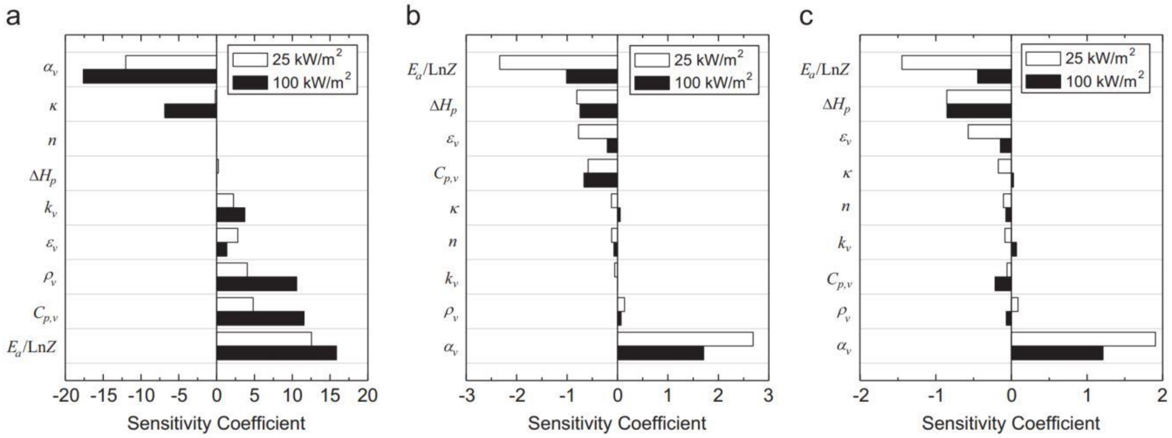

Figure 14. Global sensitivity analysis for non-charring material (a) time to ignition, (b) average MLR, (c) peak MLR [16].

The results observed by Chaos [16] were consistent with those from Stoliarov [18] and Linteris [90] in that the thermophysical properties as well as κ had an impact on the time to ignition. Moreover, the average MLR was also noticed to be sensitive to ΔHp and $C_{p,v}$. However, when considering the impact on the peak of MLR, the results were only consistent with those of Stoliarov [18].

Global sensitivity methods are also quantitative and they focus on how all the parameters influence the outputs of the numerical model. They vary all the inputs at the same time as well as providing information concerning statistical distributions which is necessary for a deeper understanding of the role of the parameters. These methods are useful when a significant number of parameters is involved [19].

Ramroth et al. [19] used a finite-element pyrolysis model to simulate the fire behavior of a composite and then conducted both a local and global sensitivity study. All the parameters were varied by an uncertainty of 1%. As a preliminary step, the sensitivity of the temperature on the cold surface to material properties were calculated in terms of the local sensitivity coefficients. Statistical information related to uncertainty was then obtained by using the Monte Carlo method. Figure **15**. shows results concerning the local sensitivity coefficients. Figure **15**(a) shows the change in the value of every property with time. The change in colors from left to right represents the change of the parameter with time. The values above zero demonstrate that if the material property is increased, the temperature value which is the output is also increased and vice-versa for the values below zero. Figure **15**(b) ranks the material properties with the evolution of time. The higher the position at any given instant shows that the parameter is the most influential and vice-versa. However, varying the parameters by 1% did not significantly affect the results.

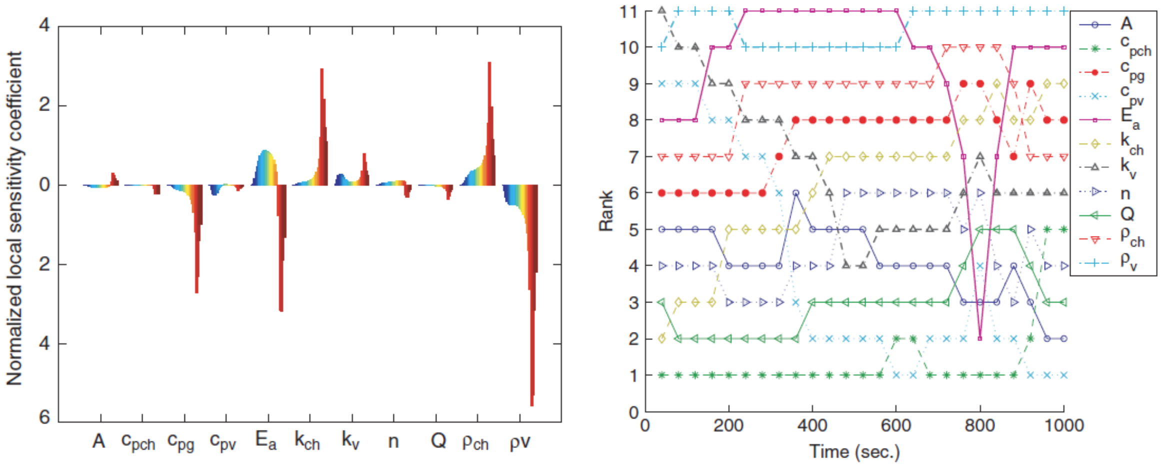

(a) (b)

pre-exponential factor - A [s^{-1}]; specific heat of the char - c_{pch} [Jkg^{-1}K^{-1}]; specific heat of the product gases - c_{pg}, [Jkg^{-1}K^{-1}]; specific heat of the virgin composite - c_{pv}[Jkg^{-1}K^{-1}]; activation energy -E_a [Jkmol^{-1}]; conductivity of char - k_{ch}[Wm^{-1}K^{-1}]; conductivity of the virgin composite - k_v [Wm^{-1}K^{-1}]; Reaction order – n; heat of decomposition – Q[Jkg^{-1}]; density of char - ρ_{ch}[kgm^{-3}]; density of the virgin composite - ρ_v [kgm^{-3}].

Figure 15. (a) Normalized local sensitivity coefficients (b) Ranking of the material properties as a function of time [19].

Moreover, they conducted a comparison of the results from the local and global sensitivity study results. The results agreed in many ways, however, there was contrast in a few instances. At early times of the calculation, the most sensitive parameters in both methods were obviously c_{pv}, k_v and ρ_v because heat transfer is controlled by pure conduction until degradation starts and the importance of E_a comes into play. During the simulation, which is the degradation phase, both methods showed c_{pg}, E_a, k_{ch} and ρ_v to be of significance. However, the local sensitivity method, showed ρ_{ch} as significant, whilst the global sensitivity method indicated A as important. Finally, near the end of the calculation, $c_{pg}, \rho_{ch}, k_{ch}$ and ρ_v were more influential as per both methods.

However, according to the local sensitivity method, E_a and k_v were more significant at this time, while they were not for the global sensitivity method. Both methods demonstrated that c_{pch}, n and Q were not of significance. The discrepancies between these two analyses were solely attributed to the nature of the methods.

Stoliarov et al. [18] conducted a study on the pyrolysis of polymeric materials as well as a sensitivity study using ThermaKin. The sensitivity analysis was carried out based on the predicted MLR curves. The motivation of their study was to investigate which properties could be guessed with reasonable accuracy based on existing property data and which properties must be measured for each material to provide reasonable predictions. In this analysis, each property was varied within the range representing the majority of synthetic polymers. This range was different for each property. Figure **16** shows the mean and maximum variations. Regarding the maximum variations, the signs shows how the peak or average mass loss rate responds to an increase of the input parameter. Their conclusion was that the parameters related to kinetics (E/A) and decomposition (h_{dec},char yield) were of great influence to the peak and average mass loss rates as shown in Figure **16**. Moreover, the average mass loss rate was sensitive to α (Figure **16**(b)).

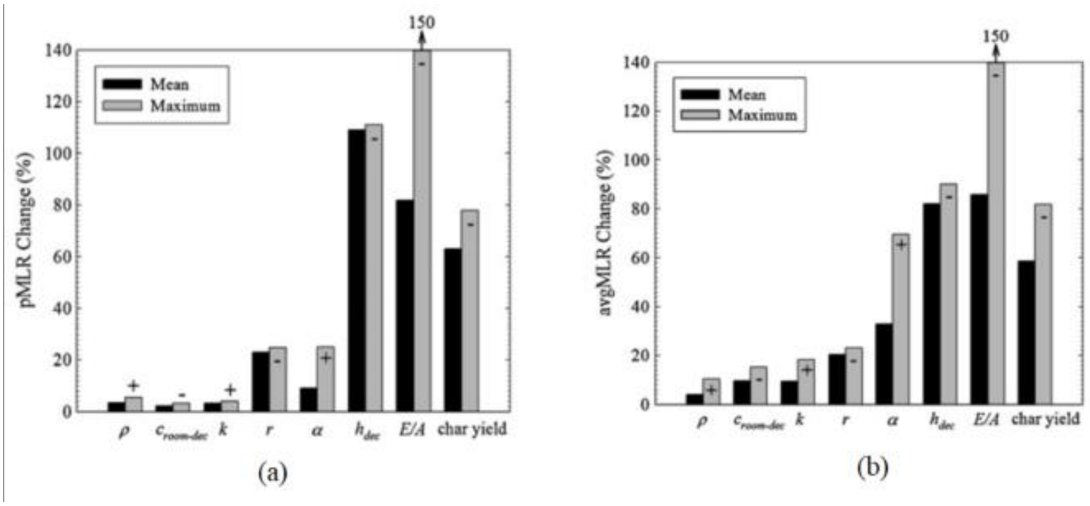

density – ρ; heat capacity describing temperature range, $c_{room-dec}$; thermal conductivity – k; reflectivity – r; absorption coefficient – α; heat of decomposition - h_{dec}; activation energy – E; pre-exponential factor – A.

Figure 16 (a) Peak mass loss rate sensitivity to material properties (b) Average mass loss rate sensitivity to material properties [18].

Linteris [90] further conducted numerical simulations on PMMA exposed to radiant fluxes to understand the effect of property variations using FDS and ThermaKin. Both programs were used to calculate the mass loss rate and to evaluate its sensitivity to material properties. The nominal property values that were used were taken from [66]. The values were varied by a factor of 2-2.5 around the nominal values. As reported, these variations were greater than those applied by Stoliarov et al. [18] for typical polymers. This was done so as to take into account new materials with a wide range of properties. In their study, they reported that the heat of reaction was the most sensitive and the activation energy the least sensitive parameter. The result suggested that for the prediction of the mass loss rate, the heat of reaction needed to be measured with accuracy. It is a key property defining the fire response of a non-charring combustible solid as it contributes to the energy needed to transform a unit mass of solid to materials to volatiles [92]. According to Linteris [90], for the conditions assumed, activation energy was the least important parameter which was in contrast with results from Stoliarov [18]. This was attributed to the different ranges in which E and A were varied in the two works revealing how the sensitivity of the parameters are model dependent.

As discussed earlier, material properties that are directly measured by thermal analysis have a certain degree of uncertainty that can induce errors in the numerical predictions. In this case, a sensitivity analysis helps in in understanding how much percentage uncertainty can be accepted so as to obtain minimum error in the predictions. Stoliarov et al. [194] noted that one of the potential sources of discrepancy between their numerical model and experimental results was the uncertainties in the material properties. In this case, a sensitivity analysis brings additional insights on the uncertainty quantification. Girardin et al. [14] modeled the pyrolysis of EVA/ATH/NC. The particularity of their work was the measurement of temperature-dependent thermophysical parameters. The numerical and experimental results were in reasonable agreement, however, to fit the final mass loss curves with accuracy, the mass transfer need to be adjusted. In their work, a sensitivity study was conducted on the kinetic parameters and the mass transfer coefficient. They concluded that the later was the only parameter to help fit the model and they reported that the diffusion of the gases did not have a significant effect on the temperature but rather on the mass loss curves. However, they did not conduct a sensitivity analysis to quantify the uncertainty from each of the property measurements which could have further explained differences between the numerical and experimental results.

Linteris et al. [17] measured inputs parameters for their models in FDS and Thermakin as described in the direct measurement by thermal analysis section. Figure 17 shows sensitivity of the mass loss rates to changes in the materials properties. Different percentage variations were used in the sensitivity study for the properties. The basis of the variations for the thermal conductivity was on the standard deviation in the mean of the measured properties (Figure 6) for each material. The variations were given as ±7% for the thermal conductivity for all polymers except for POM which was ±20%. ±16% was taken for the heat of reaction and specific heat based on the uncertainty in the measurements that was reported in [92]. The Arrhenius parameters, activation energy and pre-exponential factor, were varied by ±50% and ±3% based on uncertainties give in literature [103]. The uncertainty values for the absorption coefficient were chosen based on its dependency on thickness of the material [195]. The variations are extensively explained in Linteris et al. [17] to try and understand the source of differences between the calculated and experiment mass loss rates at some points mainly for PA66. The left column in Figure 17 shows the influences of H (heat of reaction), A (pre-exponential factor) and E (activation energy) while the right column shows the influences of a (absorption coefficient), C (heat capacity) and all (All) properties at once. The signs + and – indicate the value bounds corresponding to each property. E_{cr} denoted that E was simultaneously varied with A in a way to alter the temperature on the surface. In general, the thermal conductivity did not have an influence on mass loss rate but affected the ignition time. The parameter that exhibited the largest effect on the mass loss rate results, depending on the conditions of simulation, was the heat of gasification and the least was the coefficient of absorption. It appeared that the uncertainties that were observed in the properties that were experimentally determined were not the reason for the differences between the calculated and experiment mass loss rates for PA66. They therefore attributed the discrepancies to other physical burning features which needed to be understood and included in the model.

Kempel et al. [89] used FDS and ThermaKin to calculate the mass loss rate of two polymers namely poly (butylene terephthalate) (PBT) and PBT reinforced with glass fibres (PBT-GF). The former burns to leave no residue while the later does.

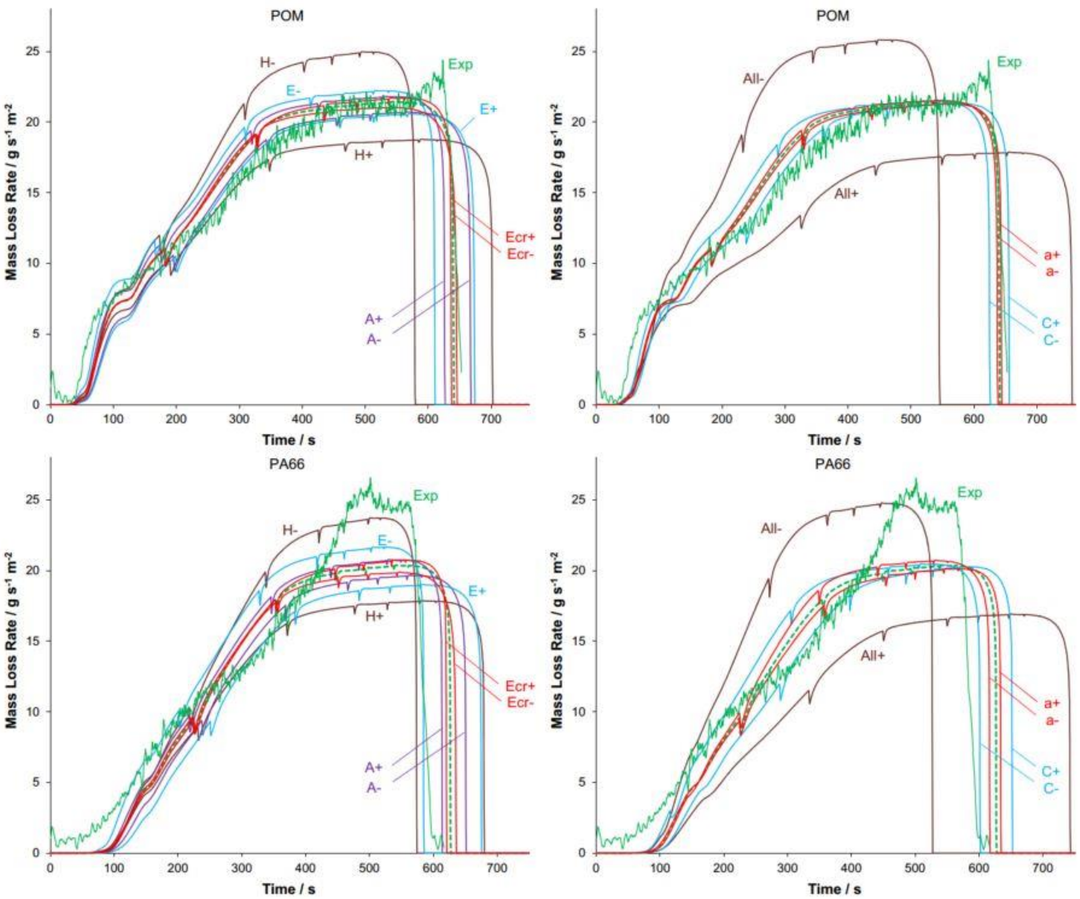

activation energy – E; pre-exponential factor; A - pre-exponential factor; heat of reaction – H; absorption coefficient – a; heat capacity – C; all the parameters combined – All.

Figure 17. The sensitivity of calculated mass loss rates to E, A, and H (left column) and a, C, and all parameters (All) (right column) for POM and PA66 [17].

Three different sets of material properties were used i.e. data from the material supplier, properties determined at room temperature and temperature dependent properties. Temperature dependent properties gave better correspondence between model and experiment demonstrating the importance of the precision of the input properties on the performance of the model. Of interest in this section was the sensitivity analysis. The material properties were varied by ±20% and for both materials, the time to mass loss (tML) was sensitive to changes in Cp and k. The rest of the materials properties hardly had an influence on the tML. The peak of mass loss rate (pMLR) corresponding to PBT was influenced by variations in Hdec while the pMLR corresponding to PBT-GF was influenced by the variations in k, Hdec and Cp.

Bal and Rein [128] presented a different methodology as compared to the other sensitivity methods focused on input parameters. Their methodology focused on the effect of adding the heat, mass and chemical processes during the development of model on the model output. They concluded that generally once the heat transfer processes were simplified in the model, the model was not sensitive to complicated kinetic schemes and simple ones would be acceptable.

When applied to decomposition kinetics, a sensitivity study helps to understand how the change in the Arrhenius parameters affects the results of the kinetic model both in a qualitative and quantitative way [192]. Batiot et al. [191] applied a method using the local and global SA to study a kinetic model using a one-step mechanism. The Sobol's technique was applied as global sensitivity method. The work demonstrated how the mass loss rate is influenced by the Arrhenius parameters and also highlighted issues concerning the compensation effect of these parameters. A local sensitivity method was implemented by Dong et al. [196] on kinetic models applied to the pyrolysis of cellulose i.e. the 1st and nth order. The models were much more influenced by the activation energy and the logarithmic pre-exponential factor. They concluded that for optimization purposes, it was advisable to use the logarithmic pre-exponential factor rather than the pre-exponential factor because it was hardly sensitive.

In summary, it should be mentioned that the outcome of sensitivity studies strongly depends on the specific question being answered as seen above. Often, researchers seek to understand the sensitivity of key model predictions (mean HRR, time to ignition, surface temperature, etc.) to the uncertainties in the measured properties by varying the properties within a certain percentage of uncertainty. This percentage is not always the same for all the researchers and is not applied uniformly to all properties e.g. Kempel et al. [89] varied all the properties by ±20% while Linteris [17] varied the properties with different percentages. On the other hand, Stoliarov et al. [18] and Linteris [90] varied the properties within a certain range of values representing the studied polymers. It should be noted that the chosen range was different between the two authors. Moreover, the outcome of the sensitivity studies also depends on their targets. However, collectively, these studies show that the thermophysical properties of the material together with the absorption coefficient have a significant influence on the ignition time and that the heat of pyrolysis affects the average MLR. Moreover, both Stoliarov et al. [18] and Chaos [16] found that the heat of pyrolysis and the reaction rate were the most influential on the peak MLR. Kempel [89] also found that the heat of pyrolysis was influential on the peak MLR. The difference between the results from Stoliarov et al. [18] and Linteris [90] is mainly on how the Arrhenius parameters influence the ignition time and the average MLR; Linteris observed that Ea/LnZ was the less influencing parameter which was contrary to Stoliarov et al. [18] and Chaos [16]. This difference can be attributed to the considered range of variations in the parameters by Linteris [90] which were not consistent and different from Stoliarov [18].

As noted in the introduction, this section of the chapter is based on a review paper that will be published soon. For the interest of the reader, the review paper continues with a section on the application of the presented computational tools to non-charring, charring and intumescent materials.

1.1.4. Conclusion on numerical modeling techniques

This section presented fundamental modeling techniques that are used in fire safety in a general manner. The pyrolysis modeling techniques which can be modified or extended for the prediction of the fire behavior of combustible solids were extensively reviewed in terms of the mathematical expressions and physical significance. The sensitivity and optimization techniques were also discussed. The computational tools presented above are commonly implemented in the fire safety design of materials. The next section will briefly review the application of these tools in the design methodologies for fire barriers.

1.2. Design methodologies for fire barriers

In general, Ashby [197] states that "for the development of a material to meet given requirements, it generally requires that a compromise be struck between several, usually conflicting, objectives". The author reviewed different multi-objective optimization methods so as to address this problem. The problem is basically presented as having one or more functions (e.g. to support a load, to transmit heat etc.). In the design, the designer has an objective (e.g. to make it cheap, light, or safe or a combination) and is subject to constraints (e.g. it is supposed to function within a certain range of temperature etc.) as illustrated in Table 5.

Table 5. Definitions for the design problem [197].

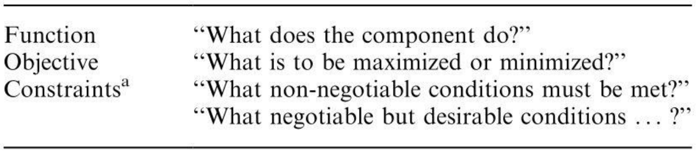

Function	"What does the component do?"
Objective	"What is to be maximized or minimized?"
Constraints[a]	"What non-negotiable conditions must be met?" "What negotiable but desirable conditions … ?"

Daryabeigi [198] investigated the coupled conductive and radiative heat transfer in a multi-layer thermal insulation system used for re-entry space vehicles. The multi-layer system was comprised of thin ceramic/composite foils which had high reflectance gold coatings and were separated using fibrous insulation. The insulation system was modeled and validated against experimental data. As a final step, the model was implemented for the design of optimal multi-layer arrangements. The main objective for thermal insulation for re-entry space vehicles is to have low mass and at the same time protect the vehicle from high temperatures. As a control experiment, pure fibrous material (thickness =76.2mm) was used. The objective was to limit the temperature of an aluminum plate from exceeding a design limit of 177°C and the model predicted that a density of 60.48 kgm^{-3} (equivalent 4.61 kgm^{-2}) was required. A parametric study was then conducted on the design variables i.e. the number of reflective foils, spaces between foils and location of foils in the multi-layer system. Trial number 1 was optimal giving a mass gain of 3.8 % as compared to the pure fibrous material.

Table 6. The results of different design trials (a negative value signified a gain in mass) [198].

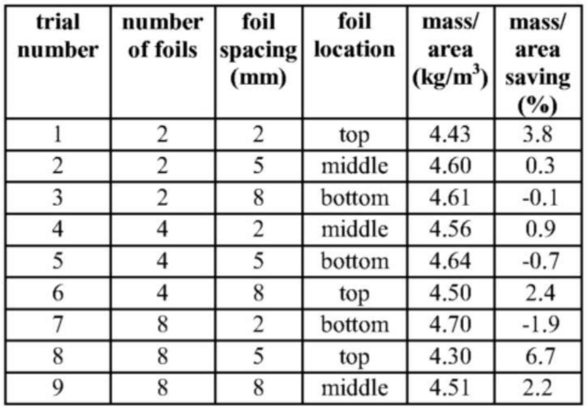

trial number	number of foils	foil spacing (mm)	foil location	mass/ area (kg/m^3)	mass/ area saving (%)
1	2	2	top	4.43	3.8
2	2	5	middle	4.60	0.3
3	2	8	bottom	4.61	-0.1
4	4	2	middle	4.56	0.9
5	4	5	bottom	4.64	-0.7
6	4	8	top	4.50	2.4
7	8	2	bottom	4.70	-1.9
8	8	5	top	4.30	6.7
9	8	8	middle	4.51	2.2

A similar technique was used by Kumar et Mahulikar [199] but they focused more on the thermal properties and optimized dimensions of different multi-layer thermal protection materials.

In fire safety design of buildings, there are two main approaches that are used i.e. prescriptive and performance-based [200]. A prescriptive approach basically uses codes that are based on strict specifications that are required to achieve safety requirements [201, 202]. The materials or products are tested using standard codes and their performance is determined as a material classification and as pass-fail criteria. The drawbacks of using this approach have thoroughly been noted by Hidalgo et al. [23]. A comprehensive study on the EU regulatory framework as well as that of the National Fire Protection Association (NFPA) was done and the drawbacks concerning traditional fire safety methods used for the design of insulation materials were noted. The major drawbacks were that the standard fire test results were not representative of real fires, the results from a specific test would probably not be applicable to a different scenario therefore designers would not be able to evaluate the behavior of the materials under different conditions other than those in the test etc. In the same study, the authors used a different methodology for the failure criteria which was based on the fundamental understanding of the material behavior. The failure criterion was based on the onset of pyrolysis. The critical temperature was obtained from TGA and tests on flammability conducted on the cone calorimeter from prior experimental studies [203]. Their methodology was based on the performance-based approach which is explained next.

Hurley et Rosenbaum [204] quoted the definition of performance-based design from the SFPE Engineering Guide to Performance-Based Fire Protection as “an engineering approach to fire protection design based on (1) agreed fire safety goals and objectives, (2) deterministic and/or probabilistic analysis of fire scenarios, and (3) quantitative assessment of design alternatives against the fire safety goals and objectives using accepted engineering tools, methodologies, and performance criteria.” This approach can be considered as a multi-objective optimization problem where several criteria can be used to obtain the best design [23]. Computational tools are then implemented when using this approach. Meacham et Custer [200] presented an overview of the performance-based fire safety engineering. This approach is flexible, promotes innovation and allows cost savings [205].

Hidalgo et al. [23, 24] presented a design methodology for combustible thermal barriers used as insulation systems for buildings. The methodology was to help in the performance-based design of buildings based on a failure criterion defined for thermal insulation materials (polyurethane, polyisocyanurate, phenolic foam etc.). They defined the failure criterion as the onset of pyrolysis

(pyrolysis temperature – critical temperature) on the surface of the insulation material (Figure 18). The design methodology was aimed at the definition of an optimized thickness as well as thermal properties of a thermal barrier for several fire scenarios. The non-combustible thermal barrier would delay the thermal front reaching the surface of the insulation material.

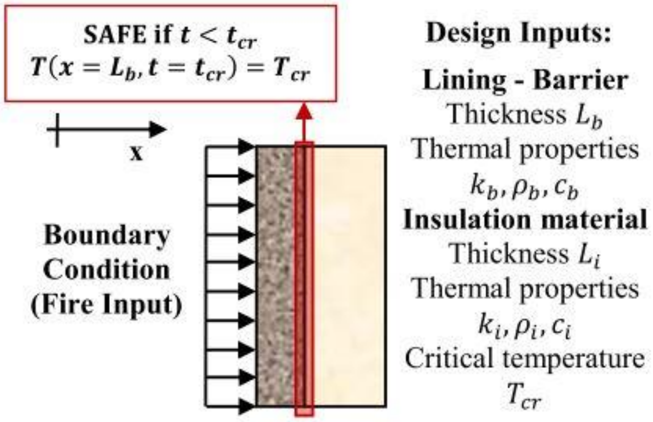

Figure 18. Definition of the design problem [24].

The solving of the system of equations (Equation 22 - Equation 26) would allow the prediction of the critical time where $T(x = L_b, t = t_{cr}) = T_{cr}$.

$$\dot{q}''_{net} = -k_b.\frac{\delta T}{\delta x}\Big|_{x=0^+} \quad for\ x = 0$$

Equation 22

$$\frac{\partial(k_b.\frac{\delta T}{\delta x})}{\partial x} = \rho_b.c_b.\frac{dT}{dt} \quad for\ 0 < x < L_b$$

Equation 23

$$-k_b.\frac{\delta T}{\delta x}\Big|_{x=L_b^-} = -k_i.\frac{\delta T}{\delta x}\Big|_{x=L_b^+} \ for\ x = \ L_b$$

Equation 24

$$\frac{\partial(k_i.\frac{\delta T}{\delta x})}{\partial x} = \rho_i.c_i.\frac{dT}{dt} \quad L_b < x < L_b + \ L_i$$

Equation 25

$$-k_b.\frac{\delta T}{\delta x}\Big|_{x=L_b^-} = \dot{q}''_{loss} \ \approx 0\ for\ \ x = L_b + \ L_i$$

Equation 26

In which $\dot{q}''_{net}$– net heat flux (Wm^{-2}), k_b, ρ_b, c_b, and L_b and k_i, ρ_i, c_i are the thermal conductivity ($Wm^{-1}K^{-1}$) , density (kgm^{-3}), specific heat capacity ($Jkg^{-1}K^{-1}$) and thickness of the barrier (m) and the insulation respectively and finally $\dot{q}''_{loss}$ – heat loss (Wm^{-2}) at the back surface of the insulation.

Their methodology generally helped in the quantitative design of thermal barriers for combustible materials based on preventing the onset of pyrolysis.

1.2.1. Conclusion on design methodologies

Design methodologies used in fire safety were presented. The design problem for fire barriers can generally be considered as an optimization problem where the objective is to protect the substrate by imposing a constraint such as the onset of pyrolysis for polymeric foams, thereby obtaining the optimum barrier properties for different fire scenarios. This is based on the performance-based approach and it has shown to be flexible [206]. The next section puts into context the different fire barriers that are used for fire protection and thermal insulation. The section will lead to the selection of model fire barriers that were used in this study.

1.3. Fire barriers

A fire barrier is generally a material that prevents the spread of fire as well as smoke in some cases. Fire barriers based on thermal insulation systems are often used to prevent the transfer of heat from the fire to the substrate materials. Figure 19 shows the most common types of thermal insulation materials used for buildings. The percentage contribution by volume of the materials to the European thermal market is glass wool (36%), stone wool (22%), expanded polystyrene (EPS) (27.1%), extruded polystyrene (XPS) (6.4%), PUR/PIR (8.1%), flexible insulation (0.4%) and finally phenolics (0.1%). Mineral wool (glass and stone wool) contribute more because of their good insulation properties and flexibility in different applications. Even though EPS has low fire retardant properties, it is generally used for external wall thermal insulation particularly in eastern Europe given its low price [207, 208]. The use of these insulation materials depends on durability, cost, compressive strength, fire resistance, ease of application, thermal conductivity etc. [209].

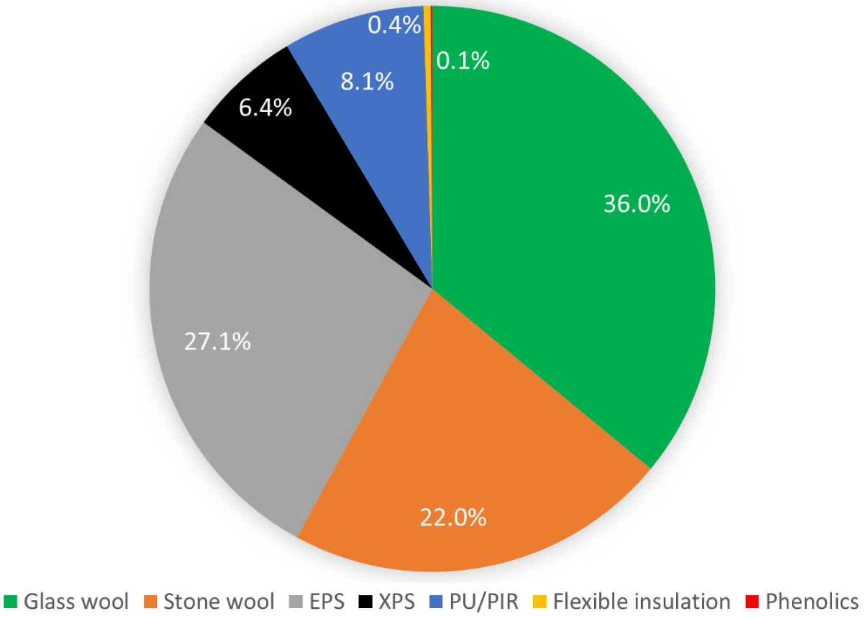

Figure 19. The European Thermal Insulation Market by volume [207].

Other thermal insulation materials exist on the market such as calcium silicate, microporous insulants, gypsum etc. [210] and some of their service temperatures are shown in Figure 20. Non-combustible materials typically have a higher maximum service temperature as compared to combustible materials.

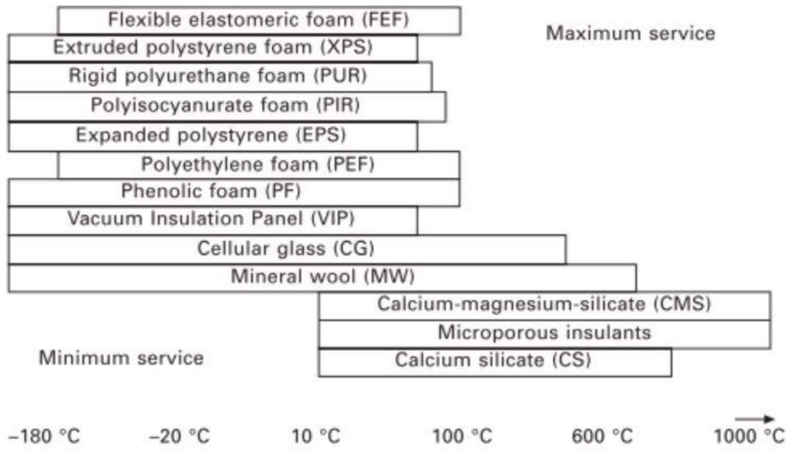

Figure 20. Service temperatures of different insulation materials [211].

Generally, the thermal insulation materials, based on their composition, can be categorized into inorganic (e.g. glass wool) and organic materials (e.g. PUR/PIR) [209] with other materials falling into combined (e.g. calcium silicate) and new technology materials (e.g. transparent or dynamic materials) [212]. Dynamic materials such as intumescent coatings are also widely used for thermal insulation as well as for fire protection. Their application is one of the oldest and one of the most efficient ways to protect materials from fire [5].

Al-Homoud [209] and Aditya et al. [213] presented a review on the most common building thermal insulation materials in terms of their performance characteristics and applications. Generally, inorganic thermal insulation materials have higher fire resistance and, thermal insulation properties and lower costs for the same thermal performance as compared to organic thermal insulation materials. Stec and Hull [214] assessed the fire toxicity of several building insulation materials. The fire toxicity in increasing order was stone wool, glass wool, polystyrene, phenolic, polyurethane to polyisocyanurate foam.

Zhang et al. [215] studied the effect of varying the heat flux from the cone calorimeter on the combustion behavior of several thermal insulation barriers (dimensions 100x100x35 mm^3) used for exterior walls. The heat release rates of the materials at 50kWm^{-2} are shown in Figure 21. It was clearly observed that rock wool, adhesive polystyrene granules and phenolics exhibited low heat release rates which is an evidence of good fire restistance. The other materials were ignited and exhibited higher release rates.

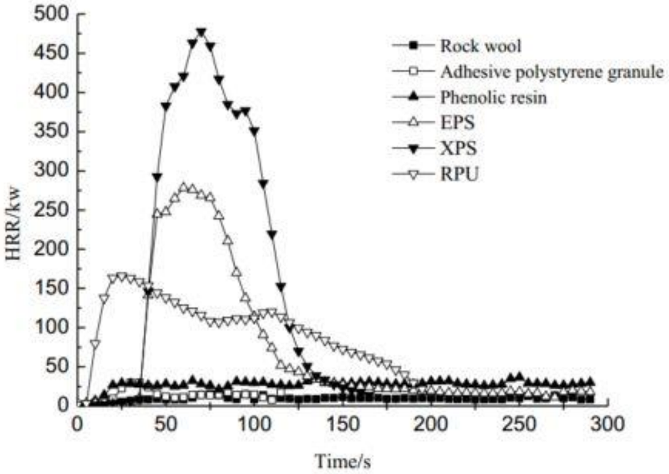

Figure 21. Heat release rates of different thermal insulation materials at 50kWm^{-2} [215].

Rock wool did not ignite but several phenomena were observed such as thermal expansion, color change volatile release. Adhesive polystyrene granule exhibited an ignition time of 17s with a peak HRR of 29.56 kWm^{-2}. Phenolic and rigid polyurethane foam (rigid PU) exhibited a typical thermosetting (non-melting/ charring) behavior while expanded polystyrene (EPS) and extruded polystyrene (XPS) exhibited a typical thermoplastic behavior (melting). Smoldering combustion was observed on the surface of the phenolic foam while the rigid PU ignited and violently burnt. The fire risk of the materials in terms of descending order was XPS>rigid PU>EPS> adhesive polystyrene granule> phenolic resin> rock wool based on the fire danger indexes.

Given the fire behaviors of the fire barriers presented above, a selection of model materials for this work was done. As a reminder, the scope of this work involves the identification of the governing parameters that make an efficient fire barrier. To simplify the identification process, the choice of the reference materials was based on increasing the complexity in the development of the mathematical models. The starting point was a non-combustible, non-porous calcium silicate insulation block and a porous closed-cell mullite foam block. For combustible materials, phenolic foam which is known as the “king of insulation” [216] and a silicone based intumescent coating were selected. It is noteworthy that phenolic foam exhibits similar fire behavior as rigid PU/PIR. The silicone-based intumescent coating was chosen since it was developed in our laboratory and extensive work on its chemical behavior was established, this work completes the understanding of its physical behavior.

In this context, the next sections will present a literature review on the selected model fire barriers in terms of their fire behaviors and thermal properties. As seen in the first section of this chapter, before considering any numerical modeling, the fire behavior of a materials should be understood. Moreover, the thermal properties are required as inputs for the models and they will be presented when available. Since the models presented in the first section of this chapter form the basis of pyrolysis modeling, the different modifications that are required for the different materials are also presented.

1.3.1. Calcium Silicate

1.3.1.a. Generalities

Calcium silicate (Ca_2SiO_4) is categorized as an inorganic fiber-reinforced thermal insulation material that is composed mainly of hydrous calcium silicate and cellulose reinforcing fibers. Their production basically involves a process of autoclaving a slurry mixture of lime and powdered silica as well as adding mineral fibers then a final step of forming the mixture into the preferred shape depending on the end use [217]. Different types of calcium silicate with different thermophysical properties such as density, porosity and thermal conductivity are found in literature. They can be either non-porous or porous. Koronthalyova et Matiasovsky studied four different types of Calsil with the bulk density variyng from 200 kgm^{-3} to 280 kgm^{-3} [217]. The microstructure of a typical porous calsium silicate is shown in Figure 22.

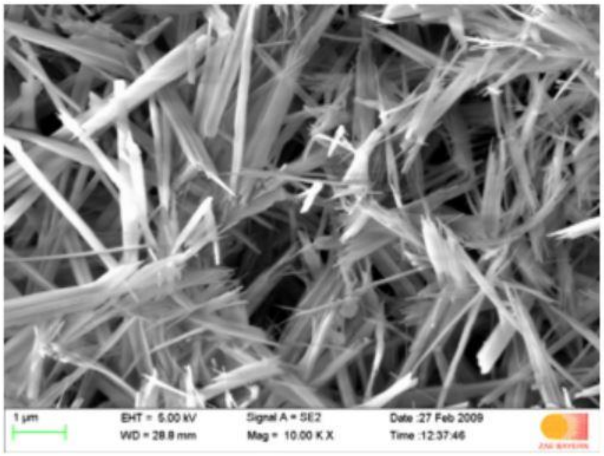

Figure 22. Scanning Electron Microscope picture of a typical calcium silicate specimen [218].

Calsil insulation products have mainly been used for different thermal insulation applications in buildings, transportation etc. It can also be used as a wall-façade and it is actually preferred as compared to asbestos and gypsum insulation. This is because asbestos insulation has health risks while gypsum insulation can dissolve in water making it not suitable for exterior use [219].

Calsil is a non-combustible thermal insulation material and it has excellent fire resistance properties since it does not thermally degrade and exhibits no flame spread [220]. Moreover, it has a high maximum service temperature that can reach up to 1050–1100 °C [210] and has good thermal properties making it an efficient fire barrier. Some of the thermal properties are discussed in the next section.

1.3.1.b. Thermal properties

The thermophysical properties of CalSil depend on how it was fabricated as well as compositions. For example, Ebert et Hemberger [218] found that the thermal conductivity of their Calsil varied from 0.0846 $\text{Wm}^{-1}\,\text{K}^{-1}$ at 300 K to 0.173 $\text{Wm}^{-1}\text{K}^{-1}$ at 1100 K compared to the values found by Wulf et al. [221] shown in Figure 23. Wulf et al. [221] measured the effective thermal conductivity of an isotropic calcium silicate material using several methods. The results are shown in Figure 23 and there were no major differences of the thermal conductivity values between the methods used.

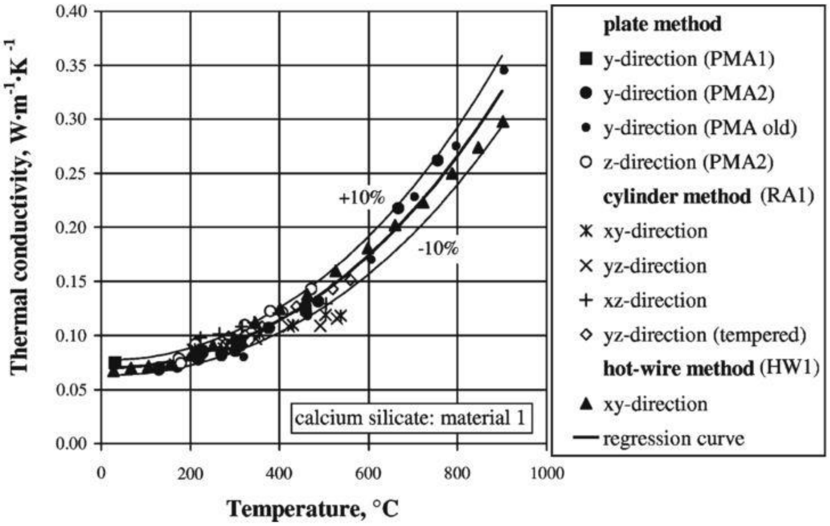

Figure 23. The thermal conductivity of isotropic calcium silicate determined from several methods.

Gellert [210] noted that the specific heat capacity of a calcium silicate material with density between 115-390 kgm^{-3} is 1000 Jkg^{-1}K^{-1}. The same value was used in a numerical model by Van Belleghem [222].

1.3.1.c. Numerical Modeling

Numerical modeling concerning calcium silicate has mainly focused on the hygroscopic behavior of calcium silicate i.e. the modeling the drying behavior of the material. Van Belleghem et al. [222] coupled a computational fluid dynamics (CFD) model with a heat, air and moisture (HAM) model to study the drying behavior of a calcium silicate insulation block. Gellert [210] noted that the thermal conductivity of an inorganic insulation material is not dependent on its internal structure if the materials consists of small pores and when they are equally distributed. In this case, heat is transferred by pure conduction in the material. When the material is porous different heat transfer mechanisms should be taken into consideration and these are discussed in the following section.

1.3.2. Closed-cell mullite foam

1.3.2.a. Generalities

Ceramic foams are a type of porous thermal insulation materials that are non-combustible and exhibit high porosity, low density and low thermal conductivity [223]. They make great fire barriers given their good thermal properties [224]. They have a high porosity that can be greater than 60 vol% consisting of either closed and/or opens cells [2] that are made from a variety of oxide or non-oxide ceramic materials depending on the application. The materials can be silicon carbide, alumina, zirconia or silica. Huo et al. [225] prepared zirconia ceramic foams which performed better at high temperatures as compared to alumina ceramics.

Ceramic foams can be produced from different methods for example the replica, sacrificial template and direct foaming technique. Closed cell foams can be fabricated by blowing air into the molten material or by using a foaming agent which is introduced into the slurry mixture and then calcinated at the right temperature [19]. They are generally used in different engineering applications such as refractory walls, thermal and acoustic insulations, lightweight applications etc. In particular, closed cell ceramic foams are generally used for thermal insulation and as fireproof materials whilst open cell foams are used for filtration applications such as diesel engine exhaust filters. [220, 226, 227].

Figure 24. shows the cross-sectional view of two different foams produced by at the same sintering temperature and different solid loading. Their morphologies show spherical pores since they were produced using the direct foaming method.

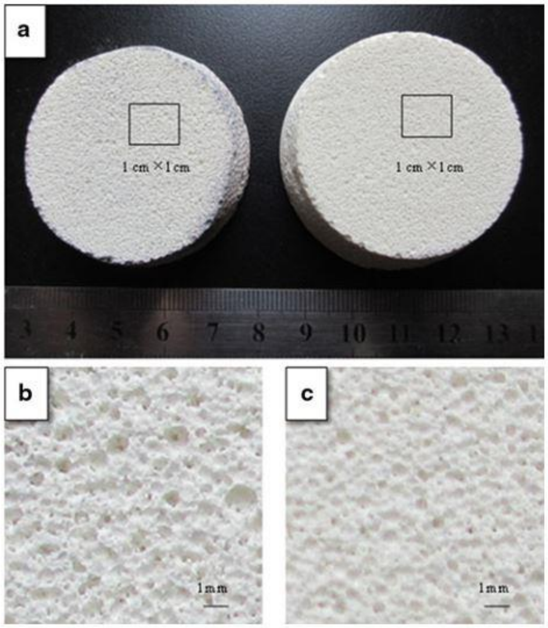

Figure 25. (a) Cross-sectional views of two different foams (b) magnified square for the sample on the left (porosity = 82.85 vol%) (b) magnified square for the sample on the right (porosity = 80.25 vol%) [228]

Heat transfer in closed cell foams can take place through conduction, radiation and convection. Convection is generally neglected for cell sizes of less than 3mm [229]. Conduction takes place through the solid cell walls and struts as well as through the gas-filled pores whilst radiation is throughout the foam. Given a closed cell foam of low density, filled with a gas of low thermal conductivity, at low temperatures, the gas heat transfer accounts for 40%-50% the total heat transfer while radiation and solid conduction contribute equally approximately [230]. At high temperatures, heat transfer through radiation can significantly rise owing to the solid material emitting energy that is proportional to T^4 [224]. The contribution of the heat transfer mechanisms to the thermal conductivity is discussed in the next section.

1.3.2.b. Thermal properties

Hildmann et Schneider [231] determined the heat capacity of mullite using several types of differential scanning calorimeters and found that it varied from 0.4150 $Jg^{-1}K^{-1}$ to 1.3427 $Jg^{-1}K^{-1}$ between the temperatures -125°C and 1400°C. Barea et al. [232] determined the thermal diffusivity of mullite foam by using the laser flash method and then deduced the thermal conductivity (Figure

26) using the relation between thermal conductivity, thermal diffusivity and the specific heat capacity. The thermal conductivity steadily decreased from 4.63 $Wm^{-1}K^{-1}$ to around 3.15 $Wm^{-1}K^{-1}$ for the dense material (0% porosity) because of its crystalline nature. As for the porous materials, the thermal conductivity decreased moderately and that of material with 57vol% porosity was more or less constant.

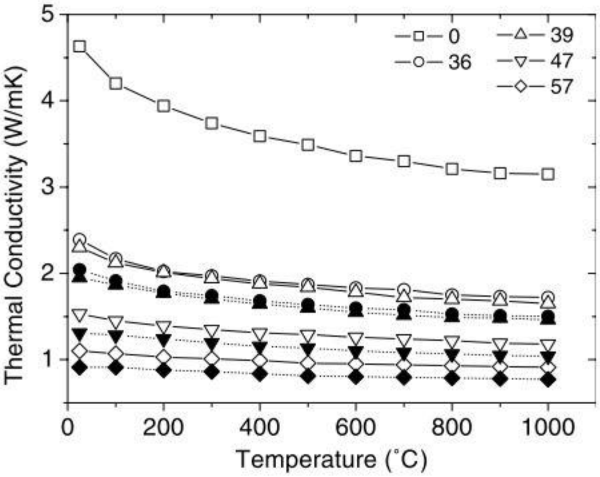

Figure 26. Temperature dependent thermal conductivity of mullite specimens with different porosity percentages (legend). The full symbols represent values after thickness correction [232].

Generally, the thermal conductivity of the porous materials was lower than that of the dense material.

1.3.2.c. Numerical Modeling

In the modeling of the heat transfer in closed cell ceramic foams, the thermal conductivity is the parameter of concern and several analytical models have been used and are presented below.

The overall effective thermal conductivity of an optically thick porous material is generally modelled by the superposition of each mechanism (Equation 27) i.e. contribution of conduction in the solid material (k_s), conduction in gas phase (k_g) and radiation in the material (k_{rad}) [230, 233]:

$$k_{eff} = k_s + k_g + k_{rad} \quad \text{Equation 27}$$

The convection contribution within the cells is assumed negligible because in most cases the pore size is small. To lower the thermal conductivity, porous materials should have large pore volume fraction [234]. Since porous materials such as closed cell mullite foam can be seen as a system composed of two phase i.e. the solid matrix and air, the overall effective thermal conductivity is normally used for the description of heat transfer of this material. The thermal conductivity does not only depend on the porosity but also on the microstructure. Modeling the effective thermal conductivity of porous materials is of interest. Actually, different analytical models exist for the effective thermal conductivity of porous materials. The fundamental structural models that take into account the conduction contribution include Series, Parallel, two forms of Maxwell-Eucken and the Effective Medium Thoery (EMT) (Table 7). Since these structural models are based on certain material structures, sometimes they are not applicable. For example, Gong et al. [234] observed that a highly porous mullite foam consisted of many interconnected pores and a few isolated pores. Moreover, the solid matrix and air were not randomly distributed, as a result, both the Maxwell-Eucken models and the EMT were not applicable.

Table 7. Five fundamental effective conductivity analytical models for porous materials [235].

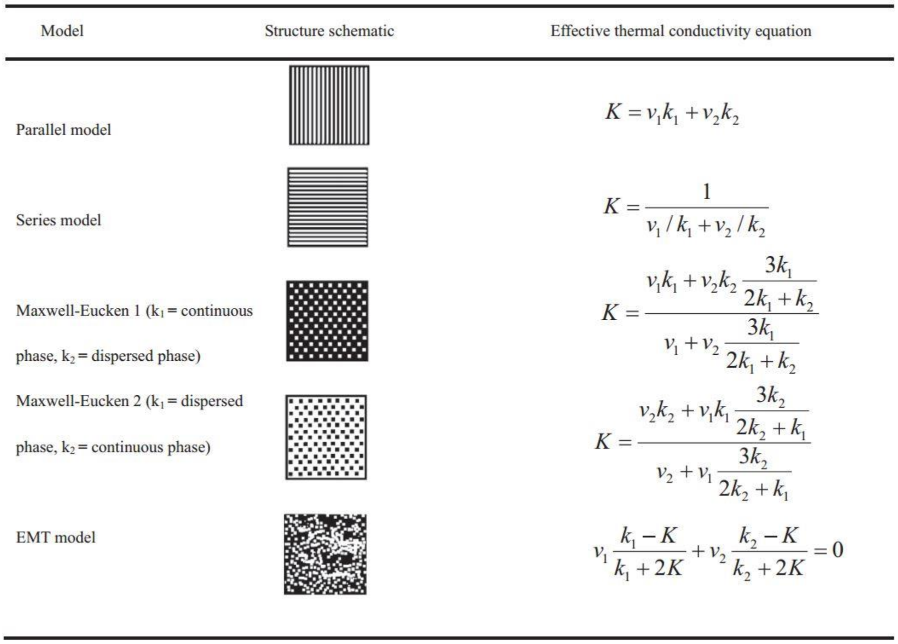

Model	Structure schematic	Effective thermal conductivity equation
Parallel model		$K = v_1 k_1 + v_2 k_2$
Series model		$K = \dfrac{1}{v_1 / k_1 + v_2 / k_2}$
Maxwell-Eucken 1 (k_1 = continuous phase, k_2 = dispersed phase)		$K = \dfrac{v_1 k_1 + v_2 k_2 \dfrac{3k_1}{2k_1 + k_2}}{v_1 + v_2 \dfrac{3k_1}{2k_1 + k_2}}$
Maxwell-Eucken 2 (k_1 = dispersed phase, k_2 = continuous phase)		$K = \dfrac{v_2 k_2 + v_1 k_1 \dfrac{3k_2}{2k_2 + k_1}}{v_2 + v_1 \dfrac{3k_2}{2k_2 + k_1}}$
EMT model		$v_1 \dfrac{k_1 - K}{k_1 + 2K} + v_2 \dfrac{k_2 - K}{k_2 + 2K} = 0$

υ and k are the volume fraction and the thermal conductivity respectively. Component 1 and 2 are the solid matrix and air respectively.

Due to this complex structure of mullite foam containing several of the basic structures, a universal model has been proposed. The universal model is based on a combination of the fundamental models and can be found in the work of Wang et al. [236]. From Equation 28, the fundamental models are obtained by the choice of d_i and k'. When $d_i = 0$, or $k' \rightarrow 0$ we obtain the Series model, when $d_i = \infty$, or $k' = k_i$ we obtain the Parallel model, when $d_i = 3$, or $k' = k_2$ we obtain the Maxwell-Eucken equation and finally when $d_i = 3$, or $k' = K$ we obtain the EMT equation.

$$k_{s+g} = \frac{\sum_{i=1}^{m} k_i \nu_i((d_i k')/\,(d_i - 1)k' + k_i)}{\sum_{i=1}^{m} \nu_i((d_i k')/\,(d_i - 1)k' + k_i)} \qquad \text{Equation 28}$$

d_i is a parameter that can have a physical sense as related to for example, the sphericity of the dispersed phase. Generally it is taken as $d_i = 3$. The parameter k' had no obvious meaning but when Equation 28 was applied to porous ceramics, however, it was understood to have a connection with pore size and distribution. Han et al. [237] took these parameters as $d_i = 3$ and $k' = 0.18$ for an anorthite ceramic material while Guo et al. [238] used $d_i = 3$ and $k' = 0.4$ for a mullite ceramic material. These aforementioned analytical models take into account heat transfer by conduction in the solid and gas. Radiation heat transfer models are used to take into to account radiation in the material and are discussed next.

Loeb [239] derived an equation for radiation contribution to the thermal conductivity through a pore. It was given by Equation 29:

$$k_{rad} = 4\omega d\varepsilon\sigma T^3 \qquad \text{Equation 29}$$

In which d is considered as the diameter of the pore, σ the Stefan-Boltzmann constant, ε emissivity of the radiant surface, ω is the geometrical factor which depends on the structure of the pores and for spherical pores for example, $\omega = \frac{2}{3}$. Similar expressions have been used in literature [232, 235, 240], for example, Barea et al. [232] used a similar one for the contribution of radiation to the thermal conductivity in a highly porous mullite foam.

Other radiation models have been implemented for porous cellular foams. Generally, a Rosseland approximation is used when the material is assumed to be optically thick and when the foam absorbs and scatters isotropically. Detailed explanations are found in Siegel et Howell [241]. In that case the radiation contribution is expressed as in Equation 30:

$$k_{rad} = \frac{16n1^2\sigma T^3}{3\sigma_{e,R}} \qquad \text{Equation 30}$$

where $\sigma_{e,R}$ – Rosseland mean extincition coefficient, n1 – refractive index, σ – Stefan-Boltzmann constant. This radiation model has been used by different authors for different materials such as fibrous materials [242] and for polymeric cellular foams as will be explained later in the chapter. Indeed, compared to the expression derived by Loeb, this approximation requires the determination of the Rosseland mean extinction coefficient which involves more parameters.

Other works have used the radiative heat transfer equation (RTE) by relating the spectral intensity fields of the material [243]. A comprehensive review on the conductive and radiative heat transfer study in ceramic and metal foams at high temperatures was conducted by Coquard et al. [224].

1.3.3. Phenolic foam

1.3.3.a. Generalities

The main difference between closed cell ceramic foams and closed cell polymeric foams is that the latter is combustible and undergoes thermal decomposition at high temperatures when exposed to an external flux. Rigid closed cell polymeric phenolic foams (e.g. PF, PIR, PUR etc.) are organic and are basically produced from liquid phenol formaldehyde resin, foaming agent and hardener. When the mixture is stirred rapidly, foaming occurs due to an exothermic reaction of the resin and the foaming agent. This process is followed by setting of the foam [244]. The phenol formaldehyde resin is also used in the production of composite materials. Phenolic foams are considered as effective fire barriers and they are generally used for thermal insulation for different applications such as buildings and their resins can be found in the construction of re-entry space vehicles where they can transform into an ablative char [245].

The burning characteristics of phenolic foam is different in comparison with dense foams because there is generally an accumulation of heat at the surface due to its low thermal inertia, therefore, the heat contributes to pyrolysis and combustion. Phenolic foams are thermoset materials that form a char layer and limits the spread of fire to the underlying foam. Moreover, they tend to glow when exposed to an external heat flux [246].

Anderson et al. [247] conducted an experimental study so as to understand the onset self-sustained downward smoldering of PUR foam. The foam was exposed to an external heat flux from the cone calorimeter for different times and temperature and mass loss rates were recorded. Three stages were observed i.e. the warm-up and the smoldering stage that is controlled by external heat flux and the self-sustained stage controlled by heat generated from heterogeneous smoldering reactions when the heat flux is removed.

In a general way, for a polymeric foam (e.g polyisocyanurate [248]) heated by an external radiative heat flux, remaining water in the foam evaporates first and when the surface reaches sufficient temperature, the pyrolysis phenomena starts. Char is formed and volatiles are released as the thermal wave progresses into the virgin material. The char layer plays the role of an insulator because of its low conductivity by reducing heat transfer by conduction thereby reducing the rate of pyrolysis. In the presence of oxygen, the surface of the char layer is oxidized and surface recession is observed. On the surface of the foam, different phenomena can occur such as smoldering [247], transition from smoldering to flaming as well as ablation for phenol formaldehyde resin based materials [249].

1.3.3.b. Thermal properties

Tseng et Kuo [244] measured the effective thermal conductivity of different samples of phenolic foam with different densities (Figure 27). The effective thermal conductivity was measured on an apparatus based on the heat flow meter method. Sample A and sample C had densities of 46.3 kgm^{-3} and 66.6kgm^{-3} respectively.

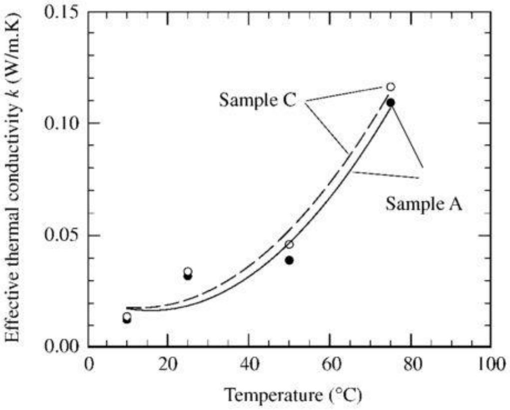

Figure 27. Effective thermal conductivity of different phenolic foams samples of different densities [244].

In the given temperature range (Figure 27), the effective thermal conductivity increased in a quadratic manner with temperature. Schiavoni et al. [250] noted low thermal conductivities of phenolic foam ranging between 0.018 – 0.028 $Wm^{-1}K^{-1}$ and a specific heat capacity of 1.3 – 1.4 $kJkg^{-1}K^{-1}$ at ambient temperature.

The thermal stability of phenolic and lignophenolic closed cell foam was studied by Carvalho et Frollini [251] under air and nitrogen using thermogravimetric analysis (TGA) and differential scanning calorimetry (DSC). The thermal decomposition of the foam depended on the atmosphere used. The TGA curves are shown in Figure 28. Under air four steps of degradation were observed. The first step is between ambient temperature and 100°C. The loss of weight for phenolic (P) foam was attributed mainly to water evaporation. As for lignophenolic (LP), the loss of weight was more prominent and this was due to the presence of an aqueous solution of phenolsulphonic acid. The second step was between 100°C and 300°C. It was attributed to the volatilization of residual monomers. The third step was between 300°C and 400°C. It was marked as the start of the thermal decomposition of both foams. The fourth step occurred at temperatures greater than 400°C and it was stated as the main decomposition step characterized by the random breaking of chain linkages and the release of water, CO_2, CO etc. The same behavior was noticed for the thermal decomposition of both foams for the nitrogen atmosphere up to around 400°C. However, the dependence of the process on atmosphere was observed for temperatures higher that 400°C.

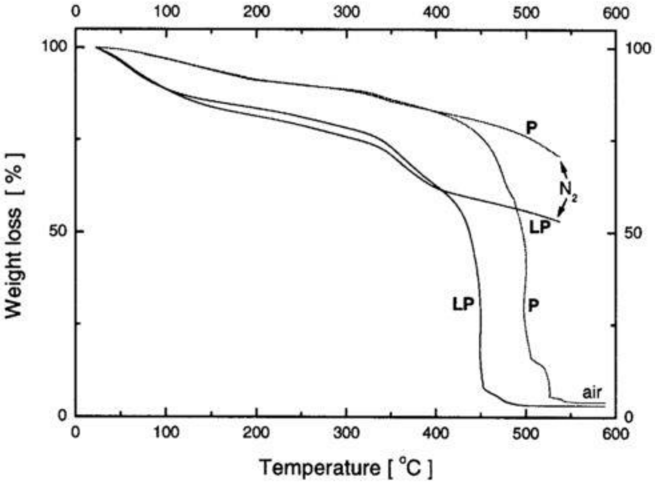

Figure 28. Thermogravimetric analysis curves of lignophenolic (LP) and phenolic (P) foam under air and nitrogen (N_2) at 10°Cmin^{-1} [251].

Since polymeric rigid foams are combustible, their fire behavior is a matter of concern, Hidalgo et al. [252] focused on the behavior of closed cell foams i.e. polyisocyanurate (PIR) and phenolic foam (PF) in the case of a fire using a cone calorimeter. Thermocouples were inserted at every 0.2 cm through the thickness of the materials. In the case of phenolic foam, Figure 29 (a) shows the temperature profiles at an external heat flux of 25 kWm^{-2} and Figure 29 (b), shows the heat release rate (HRR) per unit square meter of 10 cm thick sample. On the temperature profiles, they observed a plateau of temperatures around 100°C and this was attributed the desorption of water. Concerning the HRR, they noticed that PF behaved in a similar manner as PIR. In general, the foam formed a char after flaming followed by smoldering after flame out on the surface.

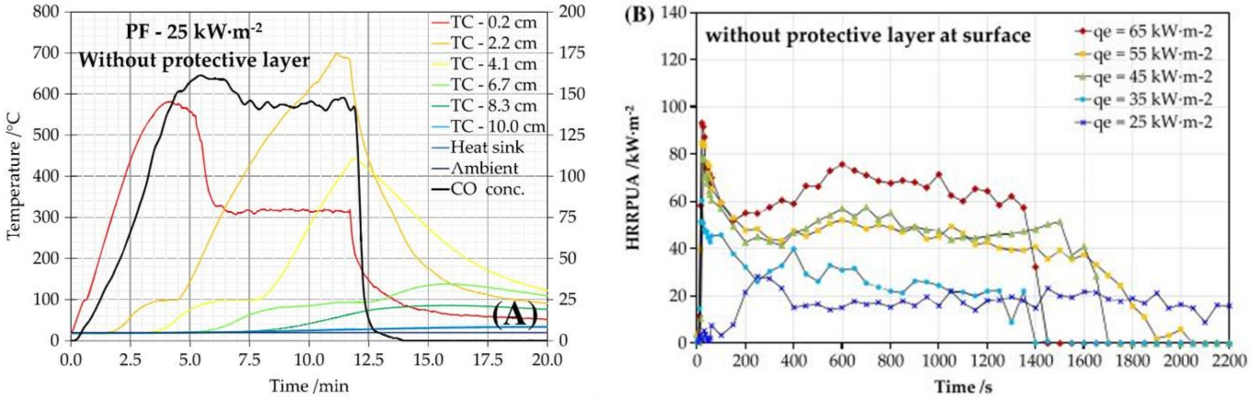

(a) (b)

Figure 29. (a) temperature profiles at 25 kWm^{-2} (b) HRR (kWm^{-2}) of phenolic foam when exposed to various radiative heat fluxes [252].

They also observed that the surface of the sample regressed due to smoldering. Moreover, spalling and cracking phenomena as well as popping sounds were noted. Visually, they observed discoloration of the foam from pink-brown to yellow then finally black during the combustion process.

Branca et al. [253] studied the fire behavior of a typical rigid foam (polyurethane (PUR) foam) under the cone calorimeter. Figure 30 (a) shows the closed cell structure of the virgin PUR foam and Figure 30 (b) shows the loss of the closed cell structure after being exposed to a heat flux of 25 kWm^{-2}. After exposure to the external heat flux the pore size was significantly reduced and consequently the contribution from radiation becomes less as compared to conduction. They also determined the kinetic parameters of the foam using TGA curves in air.

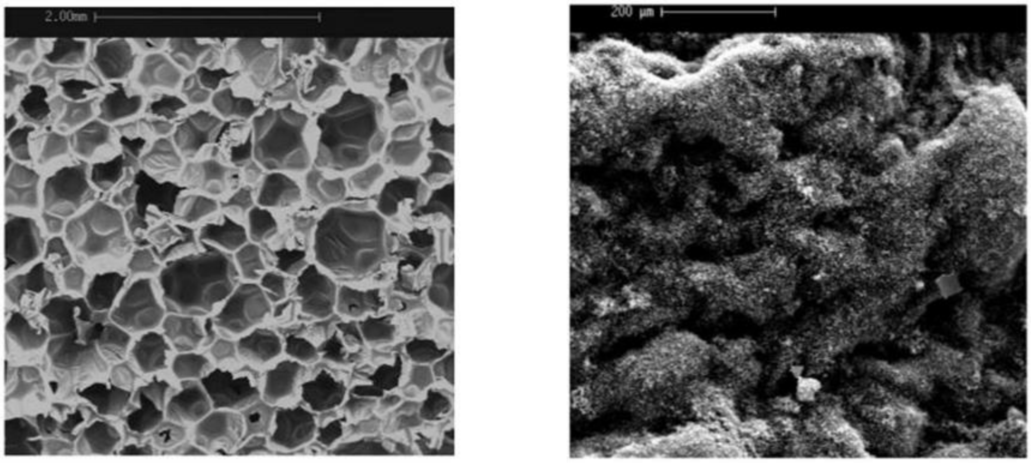

Figure 30. Scanning Electron Microscope images of (a) virgin PUR (20x) (b) surface of PUR after exposure to a heat flux 25 kWm^{-2} under the cone calorimeter (100x) [253].

1.3.3.c. Numerical modeling

Analytical models for the overall effective thermal conductivity of polymeric foams have also been developed based on the contribution of the heat transfer mechanisms. The overall effective thermal conductivity is expressed in the same manner as for closed cell foam shown in Equation 27. However, for the conduction contribution, for polymeric foams, different models such as Equation 31 taking into account the information about the morphology (e.g. pore size) have been used. Conduction heat transfer (in solid (k_s) and gas (k_g)) has often expressed as in Equation 31 [230]:

$$k_{s+g} = \delta k_g + k_s \frac{(1-\delta)}{3}\left[f_s\sqrt{\frac{a}{b}} + 2(1-f_s)\left(\frac{a}{b}\right)^{\frac{1}{4}}\right] \qquad \text{Equation 31}$$

where,

a – longitudinal pore size
b – transverse pore size
f_s – fraction of solid materials in foam
δ – foam porosity

Wang and Foster [254] implemented the same effective thermal conductivity model for the modeling of heat transfer in a polyisocyanurate core used in sandwich panels. They further added the radiation contribution (k_{rad}) which was based on the Rosseland approximation. In their work, Rosseland mean extinction coefficient was determined by using Equation 33. The derivation of these equations is explicitly explained in [230, 255].

$$k_{rad} = \frac{16}{3\sigma_{e,R}}\sigma T^3 \qquad \text{Equation 32}$$

where

$$\sigma_{e,R} = 4.10\frac{\sqrt{\left(\frac{f_s\rho_f}{\rho_s}\right)}}{d} + \left(\frac{(1-f_s)\rho_f}{\rho_s}\right)K_w \qquad \text{Equation 33}$$

in which, σ – Stefan-Boltzmann constant, ρ_s – solid density, ρ_f – foam density, d – dimension of pore in the direction of heat transfer, $\sigma_{e,R}$ – Rosseland mean extinction coefficient, K_w – cell wall extinction coefficient.

Similar radiation models have been used by different authors for smoldering applications [130, 256, 257]. Tseng and Kuo [244] used the same radiation thermal conductivity for phenolic foam but instead they used the transmittance spectra from the a Fourier transform infrared spectrometer (FTIR) to obtain the extinction coefficient spectra using Beer's law and then they calculated the Rosseland mean extinction coefficient.

Gpyro uses a different expression for the contribution of conduction to thermal conductivity that is in a generalized form for combustible materials, however, the contribution of radiation is in the same form as Equation 32. Gpyro has been also been validated for predicting the fire behavior of charring, non-charring, intumescent and smoldering materials [8]. Phenolic foam exhibits the fire behavior of a typical rigid polymeric foam when exposed to an external heat flux. Most studies have focused on modeling the smoldering of polyurethane. One of the earliest work dates back to 1984 were Ohlemiller [131] presented a comprehensive review. Generally, the foam is considered as a porous matrix and these models have been based on solving 1D coupled solid species, solid energy, gas-phase energy, gas-phase continuity as well as the oxygen concentration conservation equations. Different modes of smoldering have been studied i.e. forward [258] and opposed [130]. A three-step kinetic mechanism for PUR has often been used [52, 259]. Rein et al. [130] implemented an improved five-step kinetic mechanism for modeling the two modes of the smoldering of PUR in microgravity conditions. The kinetic parameters were obtained using genetic algorithms (GA). Other research works employing the almost the same methodology are for the smoldering of wood [185], packed fuel beds [260], cigarettes [256]etc.

Other ablation based models have been used for phenolic based resin materials [261-264]. Milos et al. [265] defines ablation as the "combination of processes, including chemical reaction, sublimation and vaporization, that consumes material at the material surface". As compared to the smoldering models presented above, basically, these models do not include the resolution of the conservation equations of the oxygen species at the surface and in the bulk gas. Moreover, the Arrhenius equation is not modified by multiplying it with a term representing the evolution of oxygen. The physical phenomena that cause surface regression are taken into account in the boundary condition at the surface.

1.3.4. Silicone-based intumescent coatings containing expandable graphite

1.3.4.a. Generalities

Intumescent coatings are often used as efficient passive fire protective methods on metallic structures. When exposed to heat, they begin to swell and expand to form an insulative char layer of low conductivity which limits mass and heat transfers between the heat source and the substrate. They normally consist of three ingredients i.e. an acid source (e.g. ammonium polyphosphate), a carbon source (e.g. (di)pentaerythritol) and a blowing agent (e.g. melamine) [266] which results in 'chemical expansion'. However, these coatings are generally organic and have disadvantages such as 1) exothermic reactions which hinder the thermal insulative behavior of the barrier, 2) the final char layer might have low cohesion and 3) the released organic volatiles can be flammable and toxic [56]. In this context, silicone based intumescent coatings (SIBC) containing expandable graphite (EG) have been developed in our laboratory. SBIC/EG exhibits good physical barrier properties in the case of both cellulosic and hydrocarbon fire scenarios thanks to the fast formation of an expanded structure having low thermal conductivity [56, 267, 268]. With EG, the expanded structure is obtained through the decomposition of the intercalation compounds inserted between the carbon layers of graphite which cause graphite exfoliation and is considered 'physical expansion'. Gardelle et al. [267] studied the fire behavior of silicone-based coatings using an experiment similar to the 'torch test' and a heat radiator test. They showed that the fire barrier properties were improved when a modifier was incorporated. However, they observed that the coatings behaved differently under pure radiative and radiative/convective fire scenarios. Under pure radiative conditions, the coatings cracked and this was attributed to the high vibration energy of Si-O bond in the infrared region. These cracks eventually caused low fire performance of the silicone-based coatings. In another study, Gardelle et al. [56] studied silicone-based coatings by using expandable graphite a blowing agent. The fire behavior of the coating was conducted in a hydrocarbon fire scenario (standard UL1709). They concluded that the fire performance increased with the percentage of expandable graphite (Figure 31). This was explained by the fast formation (18%/s) of the formed char layer (3400% expansion) which exhibited a low conductivity (Figure 33).

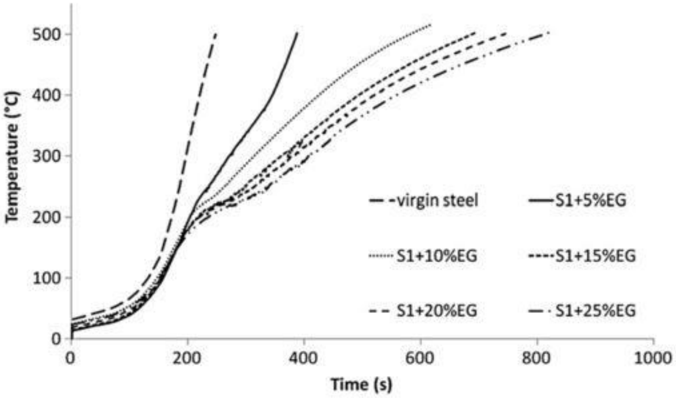

Figure 31. Backside steel temperature profiles as a function of time for different compositions [56].

Different silicone-based coatings containing expandable graphite have also tested by adding for example an organoclay [269] or a catalyst [270].

1.3.4.b. Thermal properties

The temperature-dependent thermal conductivity (Figure 32) of silicone based intumescent coatings (silicone and silicone/modifier) were measured from ambient temperature up to 600°C using a transient plane source method (Hot Disk TPS250 S). The thermal conductivity varied from 0.1 $Wm^{-1}K^{-1}$ to 0.35 $Wm^{-1}K^{-1}$ [267].

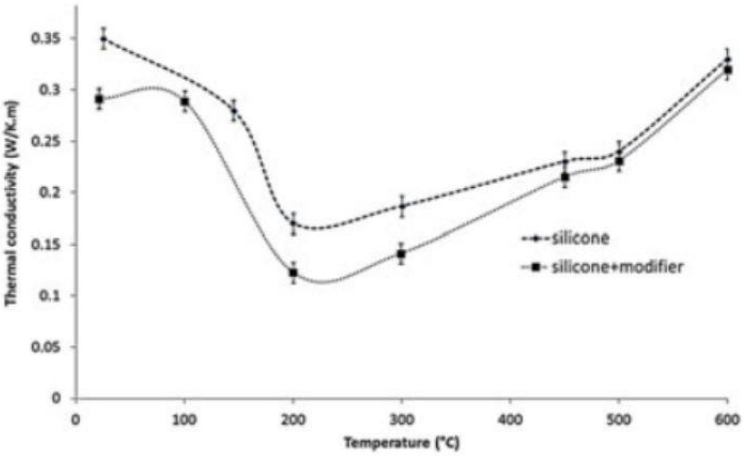

Figure 32. Measured temperature-dependent thermal conductivity of virgin silicone and silicone/modifier [267].

Gardelle et al. [56] measured the thermal conductivity of a silicone-based coating containing 25% of expandable graphite (EG) from ambient temperature to 500°C. (Figure 33). The thermal conductivity decreased from 0.5 ± 0.02 $Wm^{-1}K^{-1}$ to 0.21 ± 0.02 $Wm^{-1}K^{-1}$ at 400°C owing to the char formation. From 400°C – 500°C, the thermal conductivity increased up to 0.35 $Wm^{-1}K^{-1}$ probably due to heat transfer by radiation in the char layer. The cohesion of the char layer was improved as compared to another commercial coating (Figure 33).

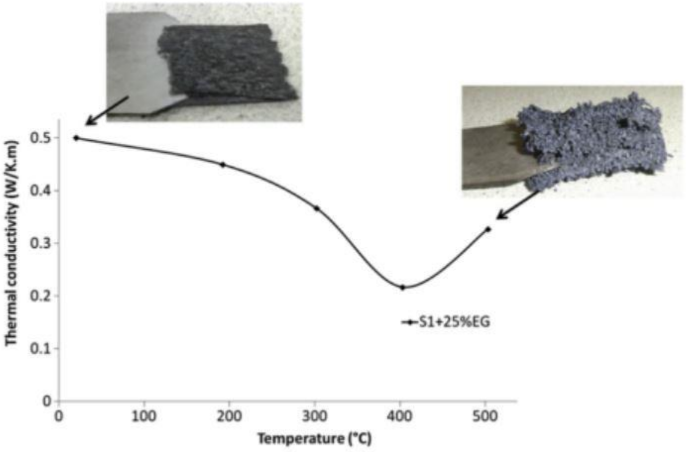

Figure 33. Measured temperature-dependent thermal conductivity of silicone/25% EG [56].

Figure 34 shows the expansion rate of a silicone-based coating/EG that was applied on a carbon fiber reinforced polymer substrate when exposed to a jet fire test. It was determined by monitoring the expansion of the char using an infrared camera (FLIR System A40) during the experiment. The coating expanded rapidly up to 2400% at the initial moments of the experiments. A steady state was reached at 120s and the average expansion rate was 23%/s [271].

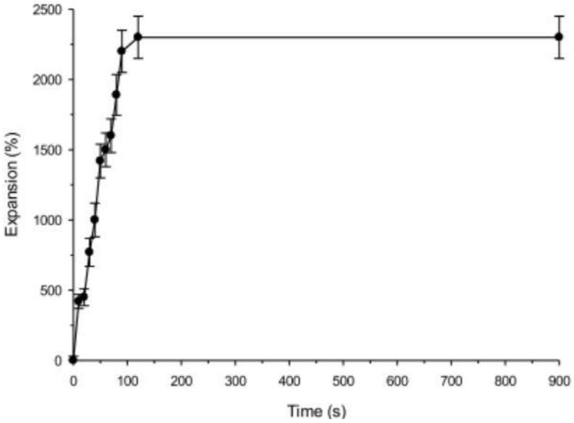

Figure 34. Expansion rate of a typical silicone-based coating/EG applied on a carbon fiber reinforced polymer substrate [271].

1.3.4.c. Numerical Modeling

Intumescent materials expand or swell to form a carbonaceous char of low conductivity when exposed to fire. Their expansion is therefore an important parameter that should be considered when modeling their fire behavior [272]. One of the earliest models to numerically represent the physical and chemical phenomena of an intumescent coating when exposed to an external flux was presented by Anderson et al. [273] in 1984. In this model, expansion was explicitly taken in to account by assuming it to be a dependent on the mass loss. In 1985, Anderson et al. [97], conducted complementary work but this time they implemented a frontal model. Over the past decades, several pyrolysis models of intumescent materials have been developed in literature varying from simple models [273, 274] to complex models involving multi-step reaction mechanisms [118, 160, 275, 276]. Griffin [118] reviewed and discussed the limitations of the intumescent models including those of Anderson. The main limitations included 1) the one dimensionality of the models given that the intumescent materials do not expand symmetrically during bench scale tests, 2) the unavailability of a complete set temperature-dependent thermophysical properties, 3) the use of expansion factors to represent swelling because of the not so well understood processes etc. These limitations often result in discrepancies between model predictions and experimental results.

Staggs [275] developed a model that used a different kinetic scheme as compared to that used by other researchers such as Di Blasi et Branca [160], Di Blasi [276], and Griffin [118]. In this work a competitive one was used instead of parallel and only the kinetics involved in expansion was taken into account to describe the intumescent phenomena. Observations from the study emphasized the need to understand the phenomena that drives expansion and more work is required in the general modeling of this process. Other researchers have assumed that the fire behavior of an intumescent system can be assumed to be equivalent to a material going through phase change [277, 278]. Cirpici et al. [279, 280] used an analytical model and a numerical simulation method to simulate the expansion of a water based intumescent coating. The analytical method was based on bubble growth model by Amon and Denson and the numerical method was based on the Smoothed Particle Hydrodynamics (SPH). From the brief review on intumescent coating modeling, most intumescent coating models address coatings that are based on epoxy or water [281, 282] which involve the traditional intumescent ingredients resulting in 'chemical expansion'. Moreover, it can be clearly noticed that there is no convention on the expansion mechanism that is considered in the models.

Bourbigot and Duquesne [283] used a quantitative approach to model the heat transfer in an intumescent coating using COMSOL Multiphysics®. To take into account the expansion of the coating, a moving mesh using the Arbitrary Lagrangian Eulerian (ALE) method was used. Statler et Gupta [13] also used the moving mesh technique implemented in COMSOL Multiphysics® to simulate the expansion of a char forming polycarbonate exposed to an external heat flux. The numerical heat release rate results were in good agreement with the experimental data.

As for models concerning SBIC/EG which involve 'physical expansion', only growth models on the expansion mechanisms of EG are available in literature. Of course, these growth models require more parameters which are difficult to determine. Ye et al. [284] developed a growth model for the expansion mechanism of EG based on the Griffiths cracks. The model was in agreement with experimental data (expansion of EG grain measured using a high speed graphite grain [285]). Mysyk et al. [286] focused on a theoretical and experimental study graphite intercalation compounds. This study was based on the fact that the compounds increased in volume with temperature to the sixth power when heated due to several processes. The change in volume and mass was monitored during the experiments. Finally, the numerical model was coherent with the experimental results.

1.3.5. Conclusion on fire barriers

The different fire barriers that are commonly used were presented in this section as well as the selected model fire barriers for this study. Experimental bench-scale tests such as the cone calorimeter or furnace test have been used to determine the fire behavior of material. As seen in this section of this chapter, the fire behavior of calcium silicate, closed cell mullite foam, phenolic foam and intumescent coating are different. The complexity of the numerical modeling increases from calcium silicate to the intumescent coating depending on their fire behavior and the involved heat transfer mechanisms when the materials are exposed to an external heat flux. Specific issues concerning numerical modeling the behavior of each material were also discussed.

1.4. Conclusion

This chapter reviewed the fundamental pyrolysis modeling techniques that are used to predict the fire behavior of combustible solids in the fire science community. The design methodologies for fire barriers which make use of the aforementioned numerical techniques were also presented. Finally, the fire barriers that are commonly used were discussed. Finally, a selection of the reference fire barriers was done based on the objectives of this work.

Both thermal and comprehensive models have been developed. Thermal models have shown to be computationally faster than comprehensive ones because they use a small number of parameters, therefore their parameterization requires a smaller number of calibration experiments. However, generalized comprehensive pyrolysis models are more representative of the pyrolysis phenomena which have been validated with reasonable accuracy for non-charring, charring, and intumescent materials and sometimes taking into account phenomena of smoldering. For intumescent materials, expansion has been considered differently in the pyrolysis models depending on the modeler. The main problem is the not-so-well understood phenomena that drive expansion and some modelers have resorted to including fitting parameters which do not necessarily have a physical meaning. Indeed, a comprehensive understanding of the fire behavior of materials at experimental level is required first so as to improve the current models. Even though 1D model formulations have a low run cost, 2D or 3D models are more reliable and accurate.

Numerical techniques such as SA and optimization have become necessary. Several sensitivity methods have successfully been used, and they have become a powerful tool in understanding the model responses to the input parameters. SA has proved to be useful in pyrolysis modeling by allowing the study of the response of a model based on its input parameters. It can guide the development and optimization of better pyrolysis models. Nevertheless, it is noteworthy that the SA results are model specific and depends on the experimental conditions: it should be analyzed depending on the modeled case. In addition, there is a lack of generality in the methodologies when conducting sensitivity studies which can make it difficult to determine the ‘‘true’’ important parameters.

Optimization techniques have been successfully used to obtain model input parameters. Gradient-based algorithms are much more efficient for small problems involving a few number of parameters. When there are many parameters, experimental measurements can be used to reduce the number of parameters to be estimated. They have successfully been implemented but the major drawback like any other optimization techniques is in attaining the global optimum. Problems in attaining this optimum have been often attributed to errors that arise from the selected initial values. To counter these drawbacks, modern evolutionary algorithms have often been implemented. However, these evolutionary algorithms are based on heuristic approach and they are not optimized for problems involving a few number of parameters because they are time-consuming. Among the most used evolutionary algorithms (GA, SCE, and SHC), the SCE method has proved to perform very well probably because it combines the strength of Nelder–Mead method (downhill simplex), controlled random search, GA, and complex shuffling. More advanced optimization techniques are starting to gain attention to overcome some obstacles, for example, coupling Kissinger’s method with GA where Kissinger’s method is first used to search for the possible initial parameters and then these parameters are fed into the GA accelerating the process. Combining these optimization techniques helps in reducing their drawbacks thereby increasing their efficiency. Moreover, to improve the optimization results the modeler can also fit a combined set of bench-scale data, for example, TGA data and CC data. Systematic approaches involving several experimental data and decoupling the individual processes in pyrolysis have also been developed. It is noteworthy that the selected optimization technique and final model validation are highly important.

As the comprehensive understanding of the fire behavior of materials at experimental level continues to improve together with the modeling techniques, further understanding of the complex pyrolysis phenomena should be achieved. In the context of this study, this explicit review provided with a complete state of the art in order to accomplish the objectives of this work.

Design methodologies that make use of the presented numerical pyrolysis modeling techniques that are based on the performance-based approach have shown to be flexible for designers and they promote innovation.

The fire barriers such as organic polymeric materials have commonly been used and their use is expected to increase over the years in the context of energy efficiency [208]. The problem with these materials is that they are combustible and they can contribute to a fire. Indeed, flame retardants can be incorporated in the materials to reduce their flammability but there is need to design new materials which have the ability to resist and limit the spreading of a fire. The goal of this study is therefore to conceptualize a fire barrier that undergoes a thermal stress from the fundamental understanding of the fire behavior of reference FR materials (i.e. calcium silicate, closed cell mullite foam, phenolic foam and a silicone based intumescent coating containing expandable graphite) using an experimental and numerical approach. The reference materials were chosen because they are typical fire barriers that are used in different applications especially in the building and construction industry. The study will provide with basics on how to make an efficient fire barrier when a material undergoes a thermal stress.

The fire behaviors of the reference FR materials are different and their complexity in modeling increases from calcium silicate which might involve pure conduction to intumescent coatings which involve a complex set of physical and chemical phenomena during the formation of an expanded char. This choice will help in fully understanding how the different fire barriers behave from simple to complex model systems. The strategy of this work will be to experimentally determine the fire behavior of the model materials. Characterization of some of the material properties will be conducted and numerical models will be developed to predict the fire behavior of the reference FR materials and then validated against experimental data. Sensitivity studies will be conducted in order to understand the influence of input material properties on the model response which will lead to the understanding of the material fire behavior. Finally, the models will be used to conceptualize efficient fire barriers for given fire scenario with given constraints by implementing the design methodologies and optimization techniques presented here. A flow chart of the strategy is shown in Figure 35.

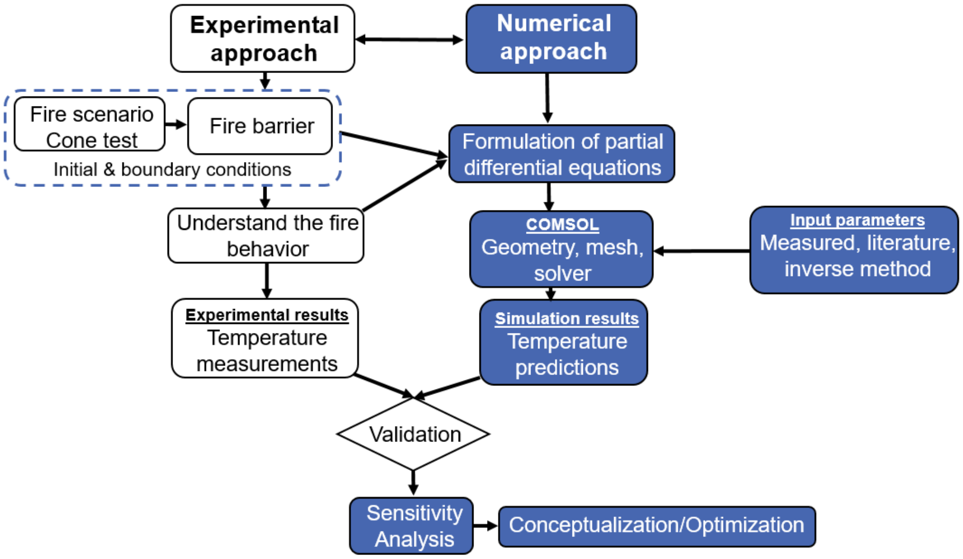

Figure 35.Flow chart of the strategy used in this work.

The next chapter will present the reference FR materials, the experimental and numerical tools that were used in this study.

CHAPTER 2. MATERIALS AND METHODS

This chapter presents the materials and methods used in this work. The first section is dedicated to the presentation of the reference FR materials used. The second section describes the experimental methods used to study their fire behaviors. In addition, characterization methods for the estimation of the material properties required as input data for numerical models are described. Finally, in the third section, the numerical tools implemented in this study are briefly presented.

2.1. Materials

This first part of this chapter presents the materials as well as properties provided by the suppliers. Only the silicone based coating was provided in different components and the preparation method is described.

2.1.1. Steel

Stainless steel 310S plates of dimension 100 x 100 x 3 mm^3 were used as substrates. The plates were provided by Oxycoupage Sciage Service, France. It was chosen as a substrate because it is widely used for structural and architectural applications [287-289]. Figure 36. shows the behavior of steel at high temperatures. It can be observed that for temperatures under 400 °C, steel does not lose its yielding strength, however, at 600°C the yielding strength reaches 40 %. On the other hand, at 600 °C the Young's modulus is at 30%. Intumescent coatings are often used to delay the steel from reaching its failure temperature [290]. In this work, the silicone-based intumescent coating (SBIC) was applied on the steel plates and the procedure will be explained later in the chapter. The steel plates are also glued to the unexposed surface of the phenolic foam (PF) keep good thermal contact with the water-cooled sample holder.

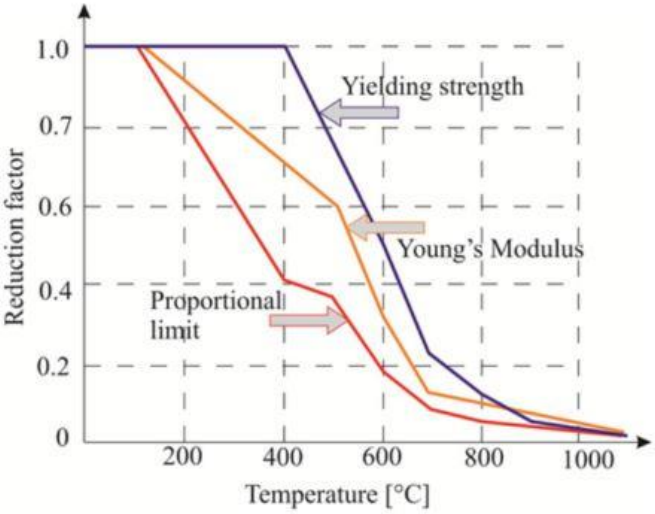

Figure 36. Behavior of steel when exposed to a fire [290].

2.1.2. Calcium Silicate

The calcium silicate insulation blocks (CALSIL N) used in this study were of dimensions 100 x 100 x 50 mm^3 and they were supplied by Distrisol, France. The calcium silicate blocks were used to represent inert, non-combustible and non-porous fire retardant materials. The calcium silicate (calsil) blocks were in accordance with ASTM C 533 type II. Some of the properties of the calsil that were provided by the supplier are shown in Table 8. The complete technical sheet of the calcium silicate blocks is presented in Appendix 1. It can be observed that calsil exhibits relatively low thermal conductivity varying from 0.075 $Wm^{-1}K^{-1}$ at 200 °C to 0.110 $Wm^{-1}K^{-1}$ at 600°C. Moreover, it has a maximum service temperature of 1000 °C in a neutral atmosphere.

Table 8. Properties of Calsil N.

Characteristics			**Calsil N**	**Units**
Maximum service temperature	In neutral atmosphere		1000	°C
Density			240	kgm^{-3}
Thermal conductivity	at	200°C	0.075	$Wm^{-1}K^{-1}$
		400°C	0.090	
		600°C	0.110	
Chemical composition		Al_2O_3	0.490 %	
		SiO_2	44.10 %	
		CaO	42.73 %	
		Fe_2O_3	0.09 %	
		AlKs	0.42 %	
		SO_3	0.11 %	

2.1.3. Closed cell mullite foam

The closed cell mullite foam (CF) blocks (QN-23) used in this study were of dimensions 100 x 100 x 50 mm^3 and they were supplied by Bylim Special Products, Netherlands. It is generally used for high temperature insulation applications. In this work, CF blocks were used to represent inert, non-combustible and porous fire retardant materials. Some properties of the ceramic foam that were provided by the supplier are shown in Table 9. The complete technical sheet is presented in Appendix 1. Similar to calsil, CF exhibits a relatively low thermal conductivity ranging from 0.15 $Wm^{-1}K^{-1}$ at 400°C to 0.35 $Wm^{-1}K^{-1}$ at 1000°C. Moreover, it has a porosity of 0.85 with an average pore size of 100 µm.

Table 9. Properties of QN-23.

Characteristics		QN - 23	Units
Safety application temperature		1260	°C
Bulk density		500	kgm^{-3}
Thermal conductivity at	400°C	0.15	$Wm^{-1}K^{-1}$
	600°C	0.17	
	800°C	0.19	
	1000°C	0.35	
Chemical composition	Al_2O_3	≥ 37%	
	Fe_2O_3	≤ 1.0%	
	SiO_2	≤ 55%	
Porosity		85%	
Average pore size		100	µm

2.1.4. Phenolic foam

The phenolic foam (PF) insulation blocks (Kooltherm ® K5) were supplied by Kingspan, Belgium. The phenolic foam core was sandwiched between two protective thin layers (thickness $\approx$1mm each) made from glass tissue and altogether made a thickness of 50 mm. These layers are generally used to avoid contact between the foam and air and the composites are destined for use in External Thermal Insulation Composite Systems (ETICS). The core is a rigid thermoset modified resin insulant manufactured with a blowing agent that has zero Ozone Depletion Potential (ODP) and low Global Warming Potential (GWP). In this work, the protective layers were removed since the study was focused on the phenolic foam core. The PF was used to represent a combustible, charring and porous fire retardant material. Some of the properties from the supplier are shown in Table 10. The complete technical sheet is presented in Appendix 1. The PF also exhibits a relatively low thermal conductivity at 0.02 $Wm^{-1}K^{-1}$ for the thicknesses ranging from 45 mm to 120 mm.

Table 10. Properties of Kooltherm ® K5

Characteristics	Kooltherm ® K5	Units
Density	~35	kgm^{-3}
Thermal conductivity (EN 13166: 2008)	0.020 (45 mm < thickness ≤ 120mm)	$Wm^{-1}K^{-1}$
Thermal Resistance (R-value)	2.50 (thickness 50mm)	m^2K/W
Closed cells	≥ 90%	
Foam core	< 5%	
BS 5111–1: 1974 (Smoke Obscuration)	(Negligible smoke obscuration)	
Foam Core (EN 13501-1) (Reaction to fire classification)	C-s2,d0	

During the experiments, the foam tended to deform thereby loosing contact with the water-cooled sample holder. To maintain the PF in contact with the water-cooled sample holder, it was glued to a steel plate using a very thin layer of epoxy hardener.

2.1.5. Silicone based intumescent coating

The silicone-based intumescent (SBIC) coating formulation consisted of silicone resin (Silastic ® LC 40-3000 BASE); composed of trimethylated silica, dimehtylvinylated silica (Dow Corning (DC)), the catalyst (Silastic ® LC 40-3000 YELLOW-CUR); comprised of SiH functional siloxane (DC), ceramic fibers, Ceepree CGB 3BAM (Chance & Hunt Ltd) and expandable graphite (80-98% carbon; ASBURY carbons) which were all supplied by Advanced Insulation Systems (AIS), England. The components are thoroughly mixed using a high-speed mixing device. The composition of the formulation is given in Table 11:

The SBIC was used to represent a ‘self-expanding’ passive fire protection system due to the expandable graphite. The SBIC was then applied on 100 x 100 x 3 mm^3 steel plates after proper preparation of the surface, including degreasing and sand blasting steps.

Table 11. Composition of the SBIC/EG coating

Material	**Percentage (%)**
Silicone resin	58.82
Ceramic Fibers	2.94
Ceepree (Glass frit/FR additive)	14.71
Low expansion graphite	15.29
High expansion graphite	8.24
Mass (%)	100
Part B-Catalyst (weight %)	6

Teflon molds were used to obtain a repeatable coating thickness of 4mm. The coated plates were left overnight at room temperature and then cured at 40°C for 6h as a customized procedure.

To understand the fire behavior of the materials presented in this section, fire tests as well as characterization of the materials were conducted. In summary, the experimental methods and protocols used in this work are described in the next section.

2.2. Experimental methods

2.2.1. Fire testing

The fire behavior of the materials was studied by exposing the surface of the materials to an external radiant heat flux from a cone heating element based on the ISO 5660 [291].The cone heating element can provide with a heat flux ranging from 0-100 kWm^{-2}. In this work, the cone heating element was used to provide different recommended levels of irradiation i.e. $25kWm^{-2}$, $35kWm^{-2}$ and $50kWm^{-2}$. The external radiant heat flux is calibrated using a water cooled heat flux meter. The experiments were conducted without any piloted ignition source and under normal air conditions. In addition, the samples were placed in a horizontal configuration. The infrared (IR) camera was used to track the surface movement of PF and SBIC, the procedure will be explained later in the chapter. The complete experimental set-up is shown in Figure 37.

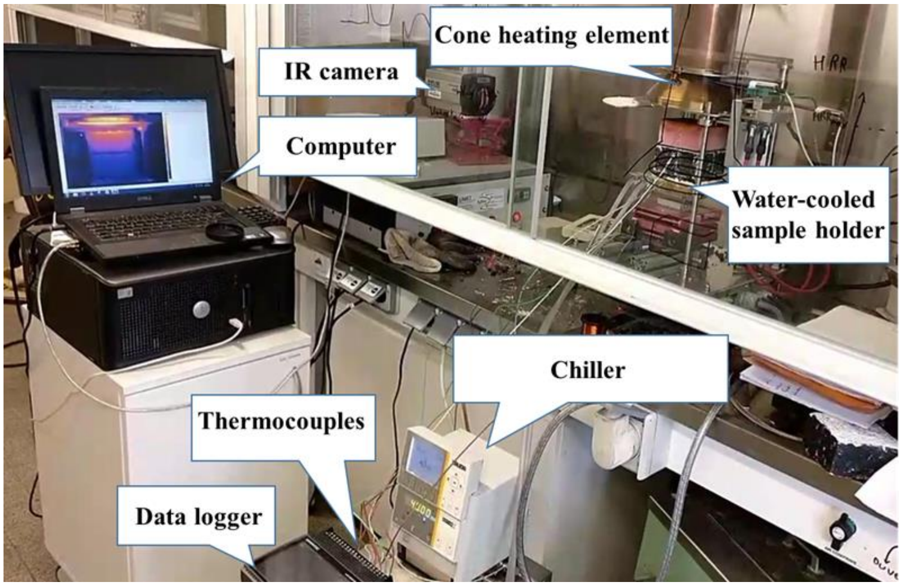

Figure 37. The complete experimental set-up used for fire testing.

This bench-scale test was chosen because the experiments are conducted under controlled fire test conditions making it possible to determine the boundary conditions for numerical modeling. Moreover, a water-cooled sample holder with a well-defined temperature condition was used to the assumption of the adiabatic condition at the backside of the sample [88]. A well-known Dirichlet boundary condition was then applied at the backside of the copper plate. The water-cooled sample holder was connected to a chiller with the temperature maintained at 40°C. Several studies [109, 217, 292, 293] have modified the sample holder for different objectives. For example, De Ris and Khan [109] used a sample holder comprising of 4 layers of ceramic paper wrapped in an aluminium tape at the sides and back in order to minimize heat losses from the sample. Sabarilal and Kumar [217] used an aluminium block as a sample holder in order to quantify the heat transfer at the unexposed surface of the sample. Lucherini et al. [292] used a water-cooled sample holder to study its effect on thin intumescent coatings applied on steel.

Figure 38 shows a close-up shot of the experiment applied to steel-calsil-copper. The temperature measurements were recorded using K-type thermocouples of diameter 0.5 mm and 3mm at different in-depth locations at the center of the material. The 3 mm thermocouples were only used for PF because they were more stable during the experiments. The temperature measurements were repeated three times and the average temperature profiles will be presented in Chapter 3. Where the temperature at the backside of the steel plate was required, a thermocouple was welded at the backside as shown in Figure 38. The thermocouples were then connected to a Graphtek GL220 midi logger. During the experiments, another thermocouple was attached between the copper plate and sample holder in order to track the temperature evolution. The thermal contact between the copper plate and water-cooled holder was enhanced using a very thin layer of thermal paste from Servisol, United Kingdom. Different configurations were used for the materials and they will explicitly be illustrated in the next chapter together with their accompanying boundary conditions. A typical configuration for steel-calsil-copper is shown in Figure 38.

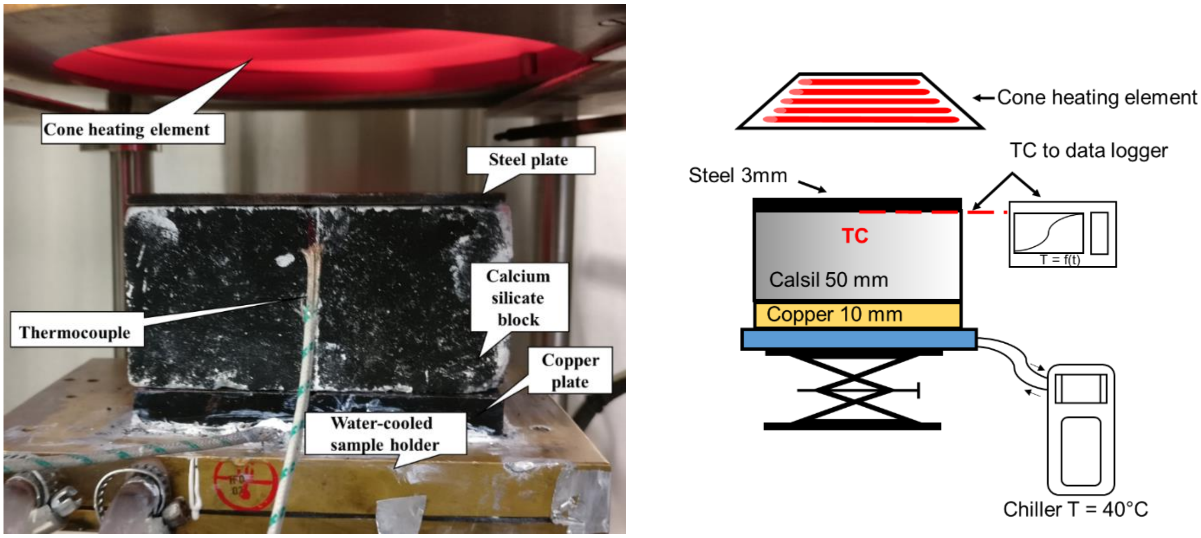

(a) (b)

Figure 38. (a) Close-up shot and (b) schematic of the experiment showing steel-calsil-copper.

Before the tests, the calsil, ceramic block, copper plate and steel plate were painted with a black heat-resistant paint (Jelt noir mat 700 °C, ITWPC Spraytec, France) so as to ensure a well-defined surface emissivity and then left to dry at ambient temperature.

For all the materials except for the intumescent coating, the thermocouples were placed parallel to the surface that was exposed to the external flux in order to reduce errors from the disturbances in temperature readings as recommended by Beck [294] especially for low thermal conductivity materials. This disposition was favorable because it did not hinder the thermal contact between the copper plate and sample. For the intumescent coating, thermocouples were inserted from the backside of the steel plate perpendicular to the exposed surface so that the thermocouples could not move or hinder the expansion of the coating.

The main source of errors was observed from the thermocouple positioning. As discussed by Reszka [295] the error, δ [mm] can be quantified as a function of the misalignment angle, β for both dispositions of the thermocouples. Equation 34 and Equation 35 express the errors when the thermocouples are placed from the back or side respectively. l_{back} and l_{side} represent the lengths of the thermocouple embedded in the material from the back and from the back respectively.

$$\delta_{back} = l_{back}(1 - cos\beta) \quad \text{Equation 34}$$

$$\delta_{side} = l_{side}\, sin\beta \quad \text{Equation 35}$$

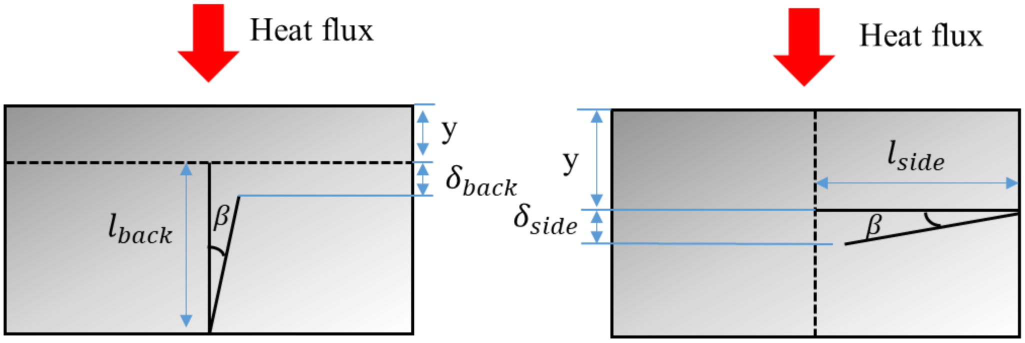

Figure 39. Thermocouples depth errors from position misalignments when thermocouple is inserted from the back (l_{back}) and from the side (l_{side}).

For a calsil block of dimensions 100 x 100 x 50 mm^3, for example, for a thermocouple expected to be at an in-depth position of 25 mm (y) at the center of the material i.e. l_{side} $= 50$ mm and for a thermocouple inserted from the back (SBIC) at a height of 15 mm ($l_{back} =$ 15 mm), the errors as a result of misalignments are shown in Table 12. It can clearly be observed that position misalignments contribute to errors in the thermocouple positioning resulting in uncertainties in the temperature measurements. The sensitivity of the temperature profiles to the thermocouple positioning will be demonstrated in the next chapter.

Table 12. Errors as a result of thermocouple misalignments.

Misalignment angle	**2°**	**4°**
$\boldsymbol{\delta_{back}}$ **(mm)**	0.0091	0.037
$\boldsymbol{\delta_{side}}$ **(mm)**	1.74	3.49

Having described the fire test, the next section presents the characterization of the materials using thermal analysis. The measured material properties will be complemented by those extracted from literature and then used to run the developed numerical models.

2.2.2. Thermal analysis and determination of the thermophysical properties

2.2.2.a. Thermogravimetric analysis

Thermogravimetric analysis (TGA) is generally used to determine the thermal decomposition of a material and it is based on the change in mass of a material with the increase in temperature. In this work, the analysis was carried out at different heating rates and under different atmospheres (air or nitrogen) using a SDT Q600 from TA Instruments, US (Figure 40).

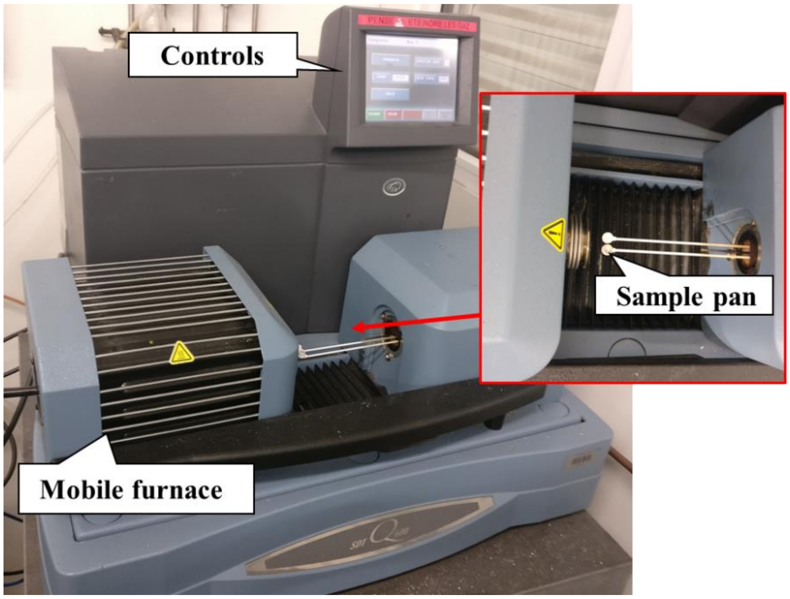

Figure 40. SDT Q600 from TA Instruments, US.

Powdered samples of 5.0 ± 0.5 mg were used and placed in an open alumina pan. Experiments were performed under air and nitrogen at 100 mL.min^{-1}. An isotherm of 30 minutes under air and 120 minutes under nitrogen was first performed to ensure a stable atmosphere. Then the samples were heated from 30°C to 800°C at different heating rates ranging from 1°C.min^{-1} to 20 °C.min^{-1}. The experiments were performed at least three times so as to ensure repeatability. The TGA results were used to study the thermal stability of the materials as well as determine the kinetics of decomposition. The kinetics of decomposition were determined using a Thermokinetics 3 software package from Netzsch, Germany. The principle is well described by Opfermann [155]. The theory related with the determination of kinetics of decomposition was extensively explained in Chapter 1.1.3.

2.2.2.b. Thermal diffusivity

The thermal diffusivity of the materials was measured using a Laser Flash Aparatus (LFA) – LFA 467 Hyperflash from Netzsch, Germany shown in Figure 41.

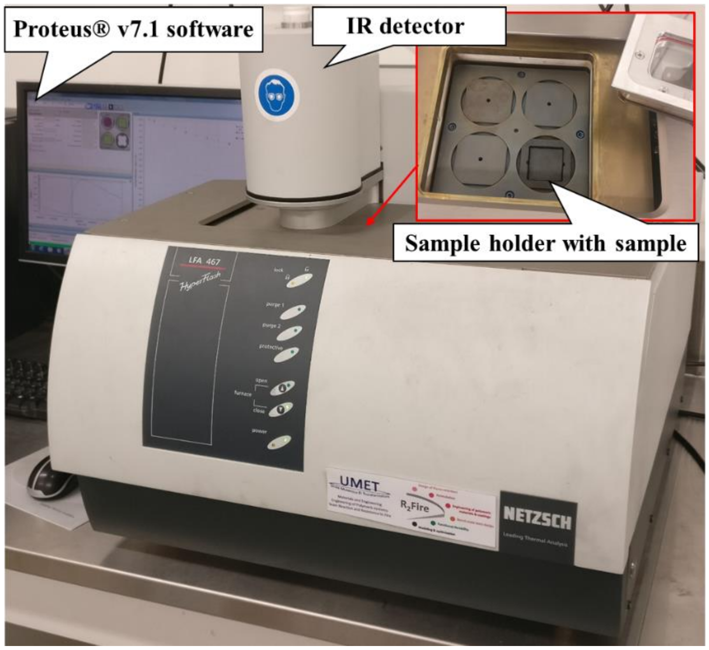

Figure 41. LFA 467 Hyperflash from Netzsch.

The apparatus uses a non-contact method by heating one side (front) of the sample by a xenon lamp as a flash source and heat flows through the thickness. On the other side (rear), an infrared (IR) detector records the temperature profile [97]. The thermal diffusivity is deduced from Equation 38;

$$\alpha = 0.1388\frac{L^2}{t_{1/2}}$$ Equation 36

where L is the sample thickness and $t_{1/2}$ is the half-time measurement i.e. the time required for the temperature of rear surface of the sample to reach half its maximum value. The obtained temperature profile is analyzed using a mathematical model included in the Netzsch Proteus ® v7.1 LFA analysis software and the thermal diffusivity is determined using an optimization technique. Moreover, Netzsch Proteus ® v7.1 LFA analysis software offers a new Penetration model that improves measurements for porous materials and materials having a rough surface [296].

The flash technique is a standardized method according to ASTM E 1461. The LFA apparatus worked in the range 30°C to 500°C. To avoid overheating of the IR detector, liquid nitrogen is used. The flash method is advantageous because it is less time consuming [297] and small sample dimensions are needed. In addition, other properties such as the specific heat capacity and the thermal conductivity can be estimated. The estimation of these parameters from LFA results is as discussed in the following sections.

All the samples were coated using a conductive graphite coating (GRAPHIT 33, CRC Industries Europe, Belgium) to avoid any reflections from the material surface and 3 ± 0.5 mm thick samples were used. The experiments were conducted at least three times and were repeatable within 5% margin of error. The thermal diffusivity of the non-combustible materials i.e. calsil and CF were measured from ambient temperature up to 500 °C and the thermal diffusivity of the combustible materials i.e. PF and SBIC were measured from ambient temperature up to 80 °C and 150 °C respectively. These temperatures were chosen in order to avoid thermal degradation of these materials in the LFA furnace.

2.2.2.c. Specific heat capacity

The specific heat capacity can be determined by estimation using the comparative method or by the conventional measurement using the Differential Scanning Calorimetry (DSC). In this work, the comparative method was used in order to show the possibility of obtaining realistic thermophysical properties using this method. The method has proven to be efficient especially at low temperatures below 200 °C [298] and it is directly incorporated in the Netzsch Proteus ® v7.1 LFA analysis software. Kövér et al. [298] obtained good agreement between values obtained by the comparative method, literature and DSC measurements. Moreover, the obtained results should be adequate for conducting a sensitivity analysis.

This method is based on the understanding that the maximum temperature (T_{max}^{sample}) from the temperature profile recorded by the IR detector is "primarily related to the thermal mass (density (ρ), radius (R) and thickness (L)" of the *sample* as well as the *Gain* applied during the measurements. By comparing T_{max}^{sample} to the maximum temperature obtained for a reference material (T_{max}^{pyro}) of known specific heat capacity (c_p^{pyro}), c_p^{sample} i.e. the specific heat capacity of the sample can be calculated using Equation 37 [299]. In this work, pyroceram (*pyro*) which is recommended for low diffusivity materials [300] was used as a reference material.

$$c_p^{sample} = \frac{T_{max}^{pyro}}{T_{max}^{sample}} * \frac{P^{sample}}{P^{pyro}} * \frac{Gain^{sample}}{Gain^{pyro}} * \frac{\rho^{pyro}}{\rho^{sample}} * \frac{L^{pyro}}{L^{sample}} * \frac{(\rho^{sample})^2}{(\rho^{pyro})^2} * c_p^{pyro} \qquad \text{Equation 37}$$

where P is the pulse energy.

2.2.2.d. Thermal conductivity

The thermal conductivity of a material can be deduced by applying Equation 38 and using parameters estimated from the LFA (α_{sample} and c_p^{sample}).

$$k_{sample} = \alpha_{sample} \cdot c_p^{sample} \cdot \rho^{sample} \qquad \text{Equation 38}$$

2.2.2.e. Emissivity

The total hemispheric emissivity of the materials was determined at room temperature by using a Vertex 70v vacuum FTIR spectrometer from Bruker equipped with an integrating sphere A562G having a high reflectance diffuse gold coated interior surface (Figure 42). The emissivity was determined based on reflectance measurements. The measurements were conducted at room temperature and within the infrared region (8 µm – 14 µm).

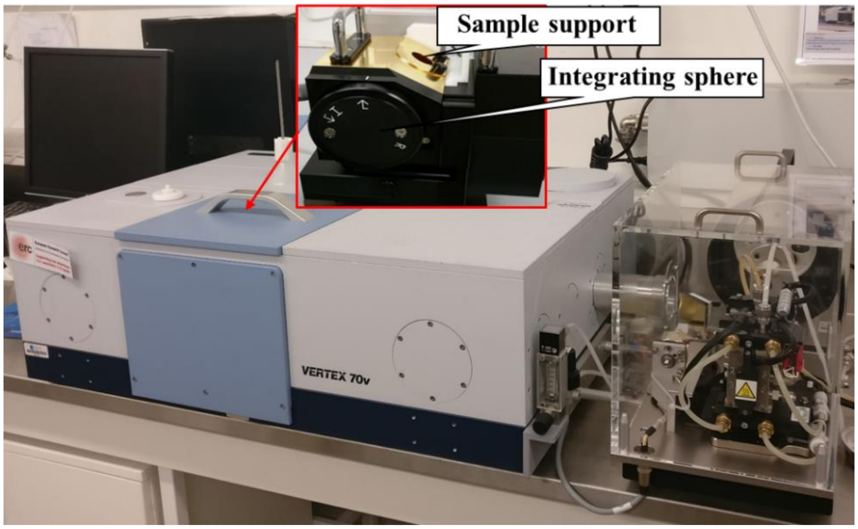

Figure 42. Vertex 70v vacuum FTIR spectrometer

Small samples were also painted black similar to the samples used for the fire test.

The principle of the integrating sphere is based on collecting the laser light that is reflected by the sample and uniformly distributed in the sphere by the interior surface [301].

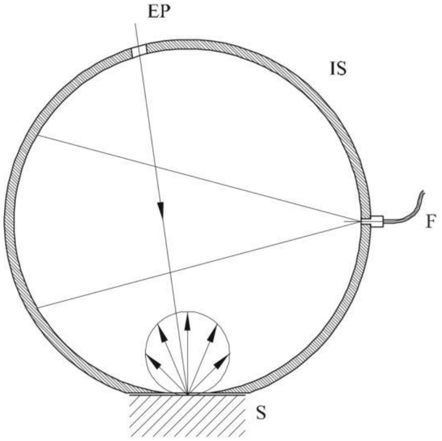

Figure 43. Diagram describing the principle of a simple integrating sphere reflectometer with EP – Entrance Port, S – sample, IS – integrating sphere, F, fiber to detector [302].

The signal from the sample is referenced to that from a reflectance standard with known reflectance (in this work a gold reference was used) and in an ideal case the ratio of the radiances is equal to the reflectances of both materials (Equation 39);

$$\frac{S_{sample}}{S_{ref}} = \frac{R_{sample}}{R_{ref}} \qquad \text{Equation 39}$$

Where S_{sample}, S_{ref} are the signals from the sample and reference materials respectively. R_{sample} and R_{ref} are the reflectances from the sample and reference materials respectively.

By using Kirchoff's law, considering opaque materials, the normal spectral emissivity (ε) can be obtained from the measured spectral hemispherical reflectance (R_s) for normal incidence and can be expressed as Equation 36;

$$\varepsilon = 1 - R_{sample} \qquad \text{Equation 40}$$

Then this spectral emissivity is used to obtain the total hemispherical emissivity by integration over direction and spectral range as weighted that of a black body (R_{BB}).[303, 304] and is given by Equation 41;

$$\varepsilon_T^{\Omega} = \frac{\int_{\lambda_1}^{\lambda_2} (1 - R_{sample}) * R_{BB} d\lambda}{\int_{\lambda_1}^{\lambda_2} R_{BB}\, d\lambda} \qquad \text{Equation 41}$$

where λ is the wavelength.

2.2.2.f. Surface movement

To monitor the surface movement i.e. expansion rate of SBIC and surface recession rate of PF, an infrared camera (IR) ThermoVisionTM A40 from FLIR systems, US was used to record the experiments as previously shown in the complete experimental set-up in Figure 37. The captured images were analyzed using Image J software developed at the National Health Institution and the Laboratory for Optical and Computational Instrumentation (University of Winsconsin). Using this approach, the surface movement was assumed to be homogenous and occurring in one dimension.

In the next section, the COMSOL Multiphysics ® commercial software package implemented in this work will be briefly presented. The software package is used to model the fire behavior of the materials in order to predict the experimental temperature profiles. The material properties characterized in this section and those extracted from literature are used to run the models. Moreover, the integrated Deformed Mesh Interface is used to take into account the moving boundaries for PF and SBIC while the Optimization and Sensitivity Interface allows to determine the keys parameters as well as assist in the conceptualization process.

2.3. Numerical tools

2.3.1. COMSOL Multiphysics®

COMSOL Multiphysics® is a finite-element method (FEM) based computational tool comprising of a powerful partial differential equation (PDE) solving engine [305]. It has a user-friendly graphical user interface (GUI) and it is well adapted for solving 1D, 2D and 3D multiphysics modeling problems with several add-on modules for different applications ranging from Heat Transfer, Structural Mechanics, Acoustics, Chemical Species Transport, Fluid Flow etc. It can also be implemented through Java® or MATLAB® script programming, however this requires an additional license.

Figure 44 illustrates a typical workflow diagram of the main modeling steps that are implemented in COMSOL Multiphysics®. A brief description of how the computational tool functions is presented here. After launching the software, it prompts you to choose between the different dimensions i.e. 1D, 2D or 3D. This work is based on a 2D study which is adequate in keeping a physical representation of the modeled phenomena. The next step is the creation of the required geometry followed by selection of materials. COMSOL Multiphysics® contains a database of materials and there is a possibility to implement user defined material properties.

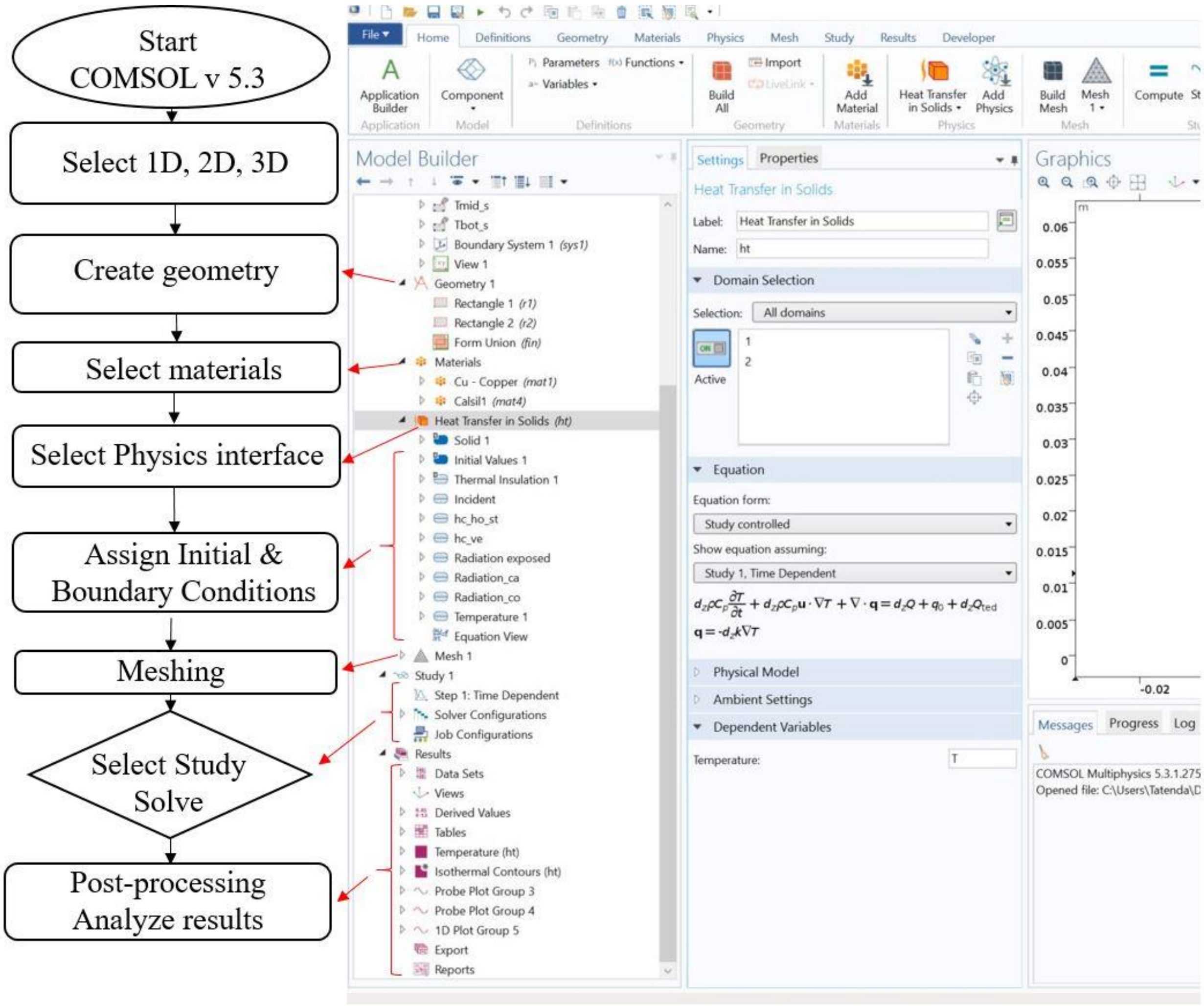

Heat Transfer in Solids

Label: Heat Transfer in Solids

Name: ht

Domain Selection

Selection: All domains

1

2

Active

Equation

Equation form:

Study controlled

Show equation assuming:

Study 1, Time Dependent

$$d_z\rho C_p\frac{\partial T}{\partial t}+d_z\rho C_p\mathbf{u}\cdot\nabla T+\nabla\cdot\mathbf{q}=d_zQ+q_0+d_zQ_{ted}$$

$$\mathbf{q}=-d_zk\nabla T$$

Physical Model

Ambient Settings

Dependent Variables

Temperature: T

COMSOL Multiphysics 5.3.1.275

Opened file: C:\Users\Tatenda\D

Figure 44. Workflow of the main modeling steps implemented in COMSOL Multiphysics ®.

The material properties determined in the previous section are then directly implemented either by using the interpolation function for temperature/time dependent parameters or as constant parameters. The next step includes choosing the relevant Physics interfaces depending on the modeled phenomena. Physics interfaces used in this study include, the Heat Transfer in Solids, Heat Transfer in Porous Media, Darcy's Law, ODE and DAE, Deformed Mesh and, Optimization and Sensitivity. The initial and boundary conditions are then assigned then meshing is done. The details for the initial and boundary conditions, the mesh and the used physics interfaces will be explicitly detailed in Chapter 3. The study step allows you to choose between, for example a time or stationary study and also add functions such as parametric sweep, sensitivity or optimization. Once a study step is added, COMSOL Multiphysics® automatically sets up the solver configurations by default depending on the selected Physics interfaces. In the case that non-convergence is observed or the results are not satisfactory, these solver configurations can be changed by the user. Finally, the results are obtained and analyzed. A complete description on how COMSOL Multiphysics® works is provided in the COMSOL Multiphysics® Reference Manual [306].

The numerical simulations were run on a computer with a processor Intel ® Core ™ i5-5300 with 2.3 GHz CPU speed and 16 GB installed memory on 64-bit Windows 10 operating system.

2.4. Conclusion

In this chapter, the first section presented the fire barriers as well as their preparation before the experiments. In the second section, the experimental methods and protocols used in this work including the fire test and the characterization techniques of thermophysical properties were described. The last section briefly presented the commercial software package, COMSOL Multiphysics ® v 5.3. The next chapter will present the fire behaviors of the reference FR materials and the thermophysical properties that were obtained using the experimental methods described in this chapter. Moreover, from the results of the fire tests, numerical modeling of the fire behavior of the materials will be conducted

.

CHAPTER 3. MODELING THE FIRE BEHAVIOR OF FIRE BARRIERS

This chapter is focused on the modeling of the behavior of different fire barriers when exposed to an external radiative heat flux. The strategy implemented to build-up the predictive numerical models is the following. First, an experimental study is performed in order to characterize and understand the fire behavior of the fire barriers. Based on these experiments, the physical and/or chemical phenomena describing the fire behavior are deduced and included in the models. For the materials exhibiting complex fire behavior (such as phenolic foam (PF) and the silicone-based intumescent coating (SBIC)), an effort was made to include the necessary physical and/or chemical phenomena while limiting the number of the required input material properties. Consequently, deliberate simplifications and fairly crude assumptions were made. The applicability and the limitations of the models are also discussed. Once the numerical model was proposed, the relevant input properties which were obtained from direct measurements and/or literature are then discussed. The model is then validated by comparing the experimental and numerical temperature profiles. Finally, sensitivity studies were conducted to identify the most identify the most influential parameters on the model response. The accompanying initial, boundaries conditions as well as the mesh details will also be explicitly described.

With the above in mind, the chapter begins with a preliminary study on the determination of optimized boundary conditions of the experimental set-up using the temperature profile at the center backside of a steel plate when exposed to an external radiative heat flux. Then, the separate sections that fully describe the fire behavior of the fire barriers with increasing complexity i.e. from the calcium silicate (calsil) block, the ceramic foam (CF), the phenolic foam (PF) to the silicone-based intumescent coating (SBIC) are presented. Finally, the chapter ends with some concluding remarks.

3.1. Identification and quantification of boundary conditions

3.1.1. Preliminary study: description of the steel plate scenario

To accurately identify and quantify the boundary conditions of the system, a preliminary study using the temperature profile on center backside of a steel plate when exposed to an external radiative heat flux was conducted (Figure 45). To improve the thermal contact between the steel plate and calsil block, a small groove was made on the surface of the calsil block in order to take into account the diameter of the thermocouple. Using the temperature profile from the steel plate, all the conditions are well-known including the exact thermocouple position and the study eliminates the uncertainty in the thermocouple positioning in the in-depth of the materials that was discussed in Chapter 2.2.1. The painted steel plate (thermally thin with Biot number <0.1) of dimensions 100 x 100 x 3 mm^3 was equipped with a thermocouple which was welded on the center backside of the plate and was placed on top of a 100 x 100 x 50 mm^3 calcium silicate (calsil) block which was then placed on a 100 x 100 x 10 mm^3 copper plate. This multi-layer system (steel plate-calsil-copper plate) was mounted on a water-cooled sample holder as shown in Figure 45.

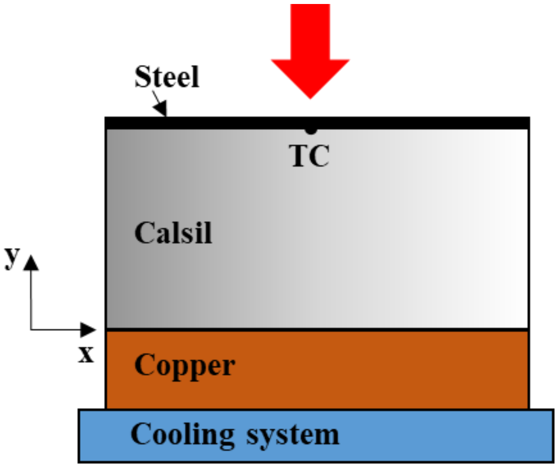

Figure 45. Experimental set-up for the identification and quantification of the boundary conditions.

To predict the temperature profile at the center backside of the steel plate, a numerical model was developed. Using the Heat Transfer in Solids module in COMSOL Multiphysics® and assuming pure conduction in all the materials as well as a perfect thermal contact between the layers, the following heat transfer equation, also known as Fourier-Kirchhoff equation (Equation 42), was solved together with the accompanying initial and boundary conditions specified hereafter. In

Equation 42, the term on the left hand side (LHS) represents the rate of change of internal energy in the material and the term on the right hand side (RHS) represents the heat transfer by conduction.

$$\rho_i {C_p}_i \frac{\partial T}{\partial t} = \nabla.(k_i \nabla T) \qquad \text{Equation 42}$$

where *i* represents steel (st), calsil (cs) or copper (co).

3.1.1.a. Initial and boundary conditions

The boundary condition imposed on the exposed surface of the steel plate is expressed in Equation 43 given Kirchoff's identity that absorptivity and the emissivity (ε) are equal [307]. The expression takes into account heat transfer by radiation (first term on the RHS) as well as convection (second term on the RHS).

$$q_{net} = \varepsilon(q_{inc} - \sigma T^4) + h_h(T_{amb} - T) \qquad \text{Equation 43}$$

where q_{net} is the net heat transfer to the sample, q_{inc} is the incident radiant heat flux from the cone heater, h_h is the convective heat transfer coefficient on the horizontal exposed surface, T_{amb} is the ambient temperature, ε is the emissivity of the surface and σ is the Stefan-Boltzmann constant.

The incident radiant heat flux can be approximated as the sum of the contributions from all the radiating sources [308] giving Equation 44;

$$q_{inc} = \sum_i \varepsilon_i F_i \sigma T_i^4 \qquad \text{Equation 44}$$

where ε_i is the emissivity of the i^{th} surface, σ is the Stefan-Boltzmann constant, $\mathrm{F_i}$ is the view factor and T_i is the temperature.

Taking into consideration the radiation contribution from the cone heating element and ambient environment and assuming that both their emissivities are equal to unity, Equation 44 can be written as Equation 45;

$$q_{inc} = \sigma(FT_r^4 + (1 - F)T_{amb}^4) \qquad \text{Equation 45}$$

where T_r is the temperature of the cone heating element that is set as 685 °C so as to deliver a heat flux of 35 kWm^{-2} on the surface of the sample at a distance on 25 mm from the lower base of the frustum (Figure 46). It is noteworthy that experiments at 25 kWm^{-2} and 50 kWm^{-2} were also conducted and the evolution of the experimental temperature profiles (TC) were similar signifying that the same heat transfer mechanisms were taking place. (only the results of the 35 kWm^{-2} test are presented here). In a similar way, the results for calsil and CF are presented for the 25 kWm^{-2} and 35 kWm^{-2} tests respectively. Other results for different heat fluxes are shown in Appendix 2.

F represents the view factor and is expressed using Wilson's formula [309] who studied the uniformity of the radiant heat fluxes in the cone calorimeter and is shown in Equation 46. This formula made it possible to take into account the changes in the surface-to-surface radiation between the cone heater and the surface of the sample which is associated with expansion or ablation of the material e.g. for the intumescent coating and phenolic foam.

This formulation results in a radiant heat flux that is uniform at the central 50mm area on the exposed surface of the sample [310].

$$F = \frac{1}{2}\left[\left(1 - \frac{1 + H_2^2 - R_2^2}{\sqrt{Z_2^2 - 4R_2^2}}\right) - \left(1 - \frac{1 + H_4^2 - R_4^2}{\sqrt{Z_4^2 - 4R_4^2}}\right)\right] \qquad \text{Equation 46}$$

where $H_2 = \frac{z}{a}, R_2 = \frac{r_2}{a}$ and $Z_2 = 1 + H_2^2 + R_2^2$, $H_2 = \frac{h+z}{a}, R_4 = \frac{r_4}{a}, Z_4 = 1 + H_4^2 + R_4^2$.

Figure 46 shows the configuration of the cone as well as the representation of the letters used in the view factor expression.

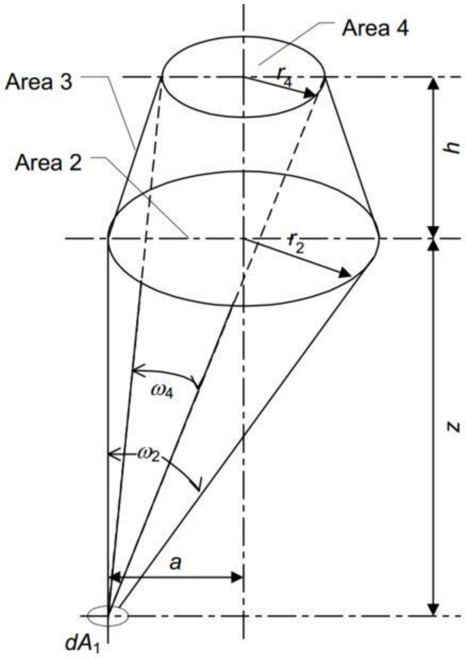

Figure 46. Schematic diagram of a radiant cone and an exposed elemental surface dA_1 [309].

The dimensions of the cone for the calculation of the view factor were taken from the ISO 5660-1:2015 [310].

Finally, during heating, the net heat flux on the exposed surface of the sample is given by Equation 47 by substituting Equation 45 into Equation 43;

$$q_{net} = \varepsilon_{st}\sigma(FT_r^4 + (1-F)T_{amb}^4) - \varepsilon_{st}\sigma T^4 + h_h(T_{amb} - T) \qquad \text{Equation 47}$$

The boundary condition on the sides is given by Equation 48. In Equation 48 , the first term on the RHS represents the heat transfer by radiation while the second term represents the heat transfer by convection. The same boundary condition is applied on the exposed surface when the shutter of the cone calorimeter is closed.

$$-n\,(-k\nabla T) = \varepsilon_i\sigma(T_{amb}^4 - T^4) + h_v(T_{amb} - T) \qquad \text{Equation 48}$$

where h_v is the convection heat transfer coefficient on the sides and *i* represents steel (st), calsil (cs) or copper (c).

A Dirichlet boundary condition was set as T=40°C at the backside of the copper plate. The initial temperature condition is set as $T_{ini} = 100.8$ °C.

The quality of the mesh was verified to assure that the results were independent of the grid and the mesh was finer at the exposed surface to take into account the large temperature gradient due to the radiant heat flux. This procedure was applied to all the models in this work. The complete computational mesh used was comprised of 2000 quadrilateral elements with a maximum element size of 0.002m, a minimum element size of 7.5 x 10^{-6} m and an average element quality of 0.9997. The system of equations was resolved using the direct solver PARDISO. The same solver was used for calsil and CF.

3.1.2. Thermophysical properties

3.1.2.a. Thermal properties

Knowing the relationship between the thermal conductivity, density and the specific heat capacity as shown in Equation 49, and taking $\rho_i c_{p_i} = 1$, the only parameter which requires to be determined is the thermal diffusivity of the materials (α_i). Moreover, this manipulation allows to directly implement the thermal diffusivity using the Heat Transfer in Solids module. (From Equation 49 $k_i = \alpha_i$).

$$\alpha_i = \frac{k_i}{\rho_i C_{p_i}} \qquad \text{Equation 49}$$

The thermal diffusivity of steel and calsil as a function of temperature are shown in Figure 47. Both thermal diffusivities were in the same order of magnitude as those found in the literature. For steel, Brum et al. [311] reported the thermal diffusivity ranging from 3.25 x 10^{-6} m^2s^{-1} at 0°C to around 4.7 x 10^{-6} m^2s^{-1} at 500°C. For calsil, Wei et al. [312] reported a value of 3.54 x 10^{-7} m^2s^{-1} at room temperature.

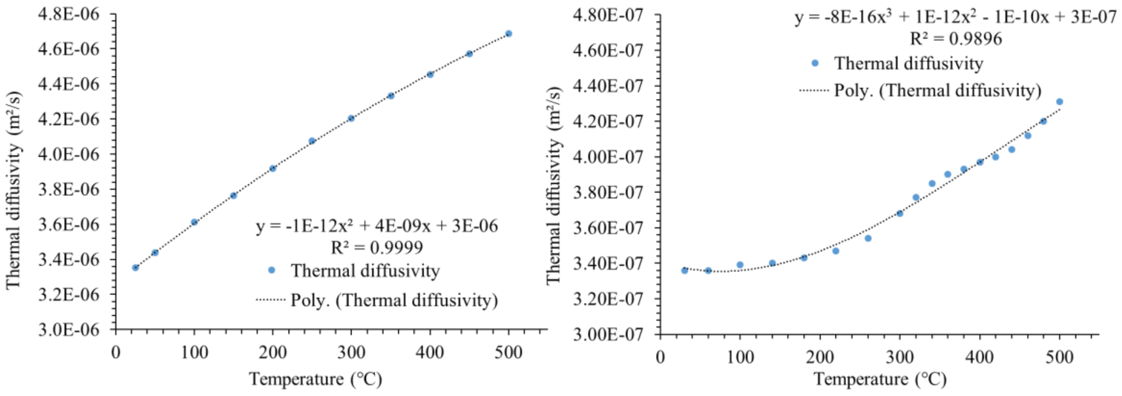

(a) (b)

Figure 47. (a) Thermal diffusivity of steel and (b) calsil as a function of temperature.

The copper plate properties were taken from the COMSOL Multiphysics database and are shown in Table 13.

Table 13. Thermophysical properties of the copper plate at room temperature.

	Density	**Specific Heat Capacity**	**Thermal conductivity**
Copper	8960 kgm^{-3}	384 $Jkg^{-1}K^{-1}$	401 $Wm^{-1}K^{-1}$

3.1.3. Comparison of experimental and predicted results

In this preliminary study, the temperature profile at the center backside of the steel plate was used to validate the model given that the exact position of the thermocouple was well-known. The comparison between the simulated and the experimental temperature profile is shown in Figure 48. When the shutter of the cone calorimeter is opened at t=0s, the temperature increases in around 600s up to a steady state at approximately 530°C. At t=5376s, the shutter is closed leading to a temperature decrease which represents the cooling phase. An excellent fit is observed between the two temperature profiles and this permits to validate the imposed boundary conditions for the model.

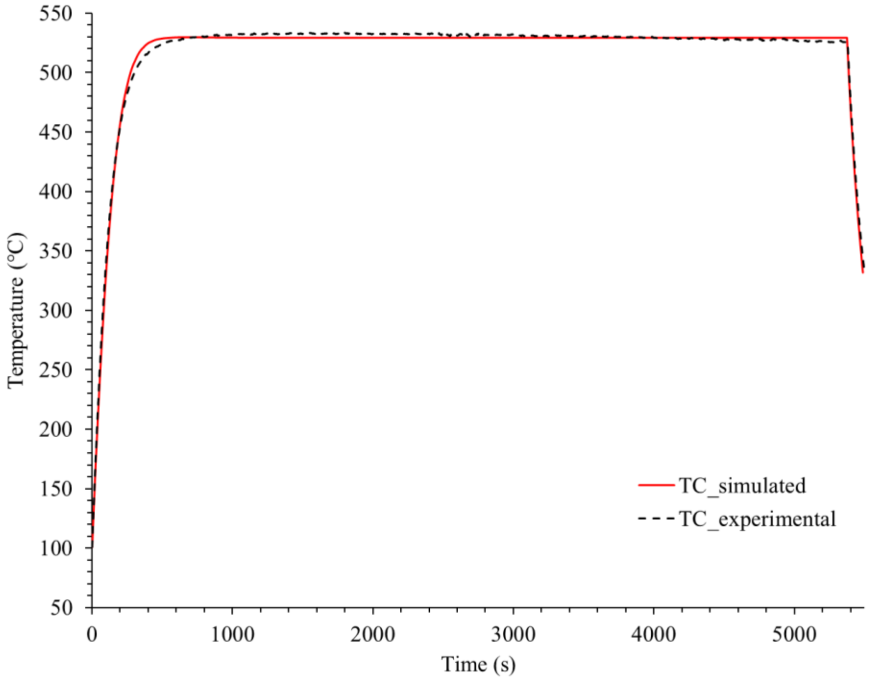

Figure 48. Comparison between numerical and experimental temperatures at the center back side of the steel plate for an external heat flux of $35 kWm^{-2}$.

From the above described model, the values associated with surface boundary conditions i.e. $h_h = 24\ Wm^{-2}K^{-1},\ h_v = 10\ Wm^{-2}K^{-1}$ and $\mathrm{T_{amb}} = 20°C$ as well as the measured emissivity for the painted steel and copper ($\varepsilon_s = \varepsilon_c = 0.987$), emissivity of the painted calsil block ($\varepsilon_s = 0.94$) were validated. The values of both convection heat transfer coefficients are obtained through an inverse heat transfer analysis and they are consistent with the values found in literature [313-316]. Typical high values of the horizontal convection heat transfer coefficient have also been reported and the values generally vary between 7-34 $\mathrm{Wm^{-2}K^{-1}}$[317].

The preliminary study permitted the identification and the quantification of optimized boundary conditions for the experimental set-up using the temperature profile at the center backside of a steel plate. These optimized boundary conditions are transposable assuming that all the experiments were conducted in the same conditions and they will be applied for the other materials given that the same experimental set-up was used. The next section focuses on the fire behavior of the calsil block with thermocouples inserted at different in-depth locations in the material.

3.2. Calcium silicate

In this section, the objective was to study the fire behavior of calcium silicate when exposed to an external radiative heat flux. A similar experimental set-up to the steel plate set-up was used and is described next.

3.2.1. Experimental study

The experimental set-up to study the fire behavior of the calsil insulation block is shown in Figure 49. The results shown here are when the calsil block is exposed to an external radiative heat flux of 25 kWm^{-2}. At this flux the temperature of the cone heating element was set at 623 °C so as to provide a heat flux of 25 kWm^{-2} on the surface of the sample at a distance on 25mm. Thermocouples were inserted at different in-depth positions in the calsil block. From the unexposed surface of the calsil block, TC1, TC2, TC3 are positioned at 40mm, 25mm, 10mm respectively as shown in Figure 49.

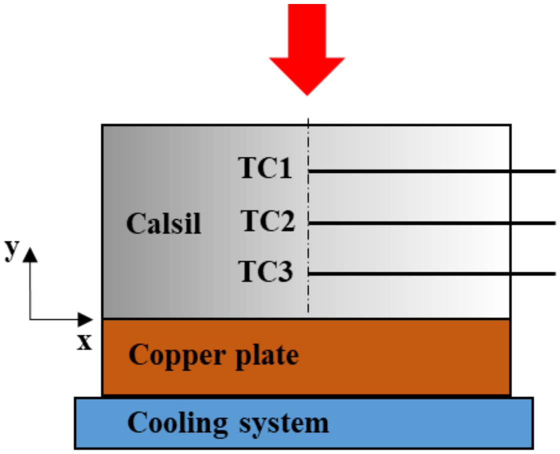

Figure 49. Experimental set-up for the fire behavior of calsil.

The same model and boundary conditions used in the previous section are applied here except that the initial temperature condition was taken as 43.6°C (the average initial temperature between TC1, TC2 and TC3). The complete computational mesh that used for this case was comprised of 1900 quadrilateral elements with a maximum element size of 0.002m, a minimum element size of 7.5 x 10^{-6}m and an average element quality of 0.9868.

Given that all the material properties are known and assuming that experimental conditions were the same as in the previous case with steel, the only unknown is the exact position of the thermocouples. This parameter is unknown because of experimental errors associated with placing the thermocouples in the material [318]. These errors are explained in detail in Chapter 2.2.1. Before validating the model, a sensitivity analysis on the thermocouple positioning with respect to the temperature profiles at the different positions was conducted using the numerical model. The sensitivity of the thermocouple positioning is shown in Figure 50. The thermocouple positions were varied as shown in Figure 50 (TC1 = 40 mm ± 2mm, TC2 = 25mm ± 2mm and TC3 = 10 mm ± 2mm) and it can be observed that the temperature profiles are sensitive to the thermocouple positioning. It can be concluded that when setting up the experiment, an error of 2mm in the thermocouple position can generate an error of approximately 20°C on the temperature measurements.

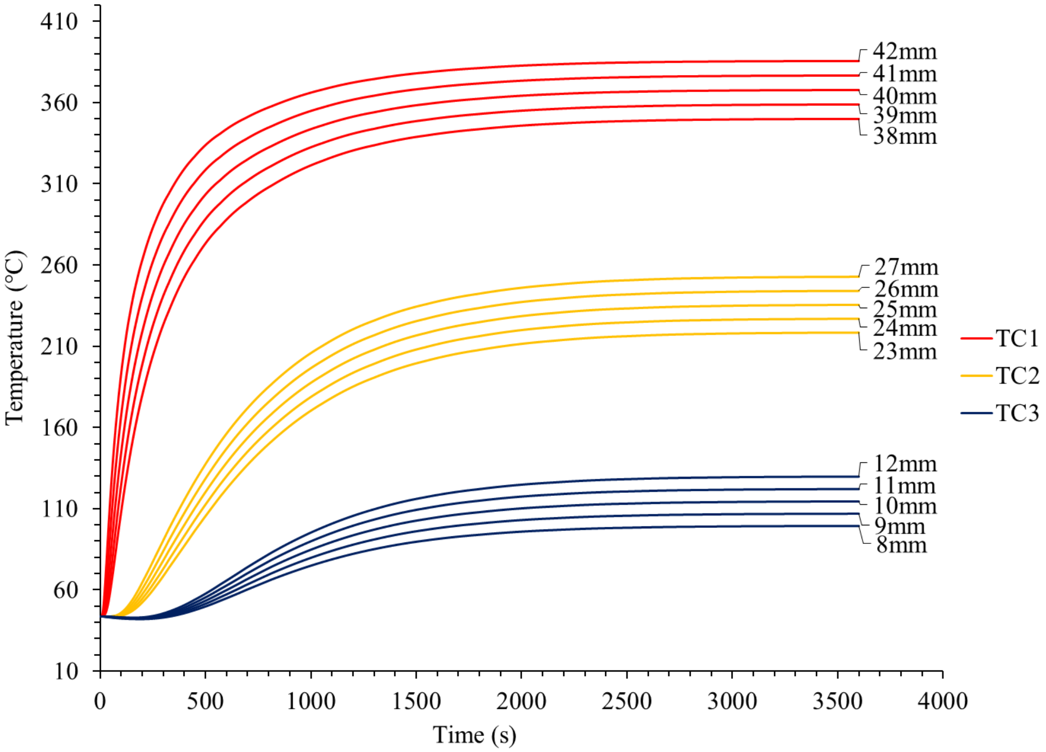

Figure 50. Simulated sensitivity of the temperature profiles with respect to the in-depth thermocouple positioning.

3.2.2. Comparison of experimental and predicted results

Figure 51 shows the comparison of experimental and predicted results for calsil exposed to a radiative heat flux of 25kWm^{-2}. Generally, the experimental temperature profiles TC1, TC2 and TC3 rise up to a steady state and only heat transfer by conduction is assumed to take place. From the results obtained in Figure 50, in order to validate the model and obtain a good fit between the experimental and predicted temperature profiles, the positioning of the thermocouples was adjusted. The positions that gave the best fit for TC1, TC2, TC3 were 39mm, 28.2mm and 11.2mm respectively. Given the uncertainties from the thermocouple positioning, these values are acceptable and the model is validated.

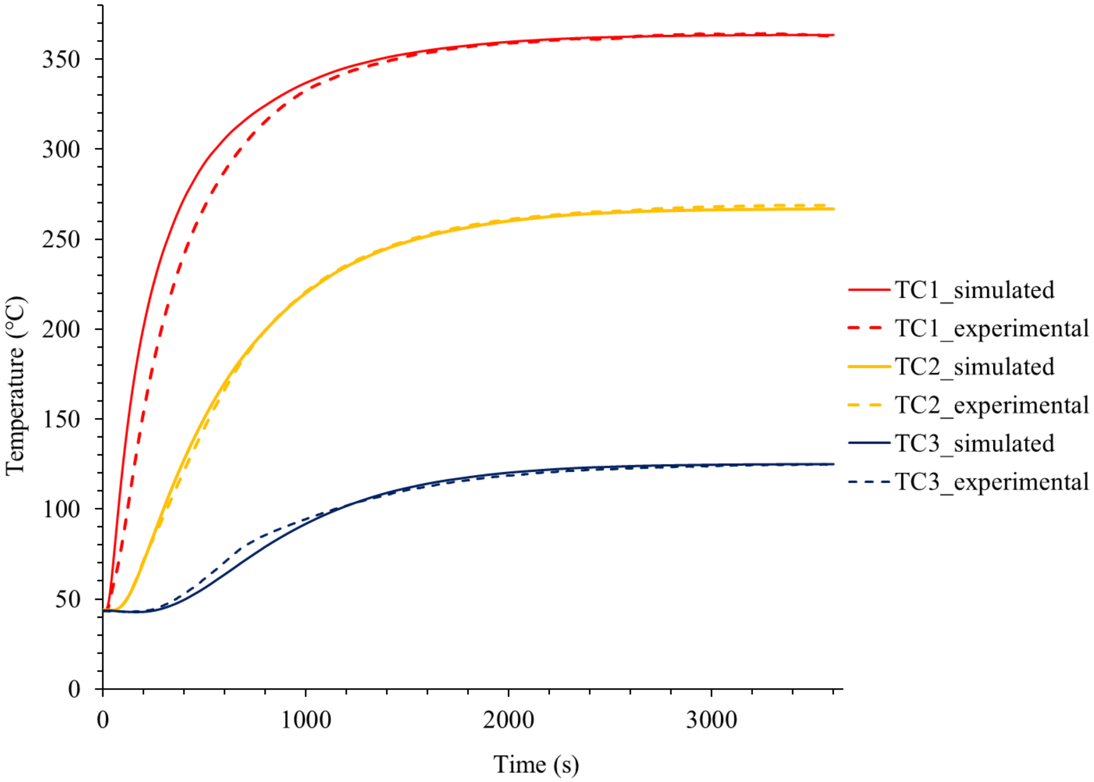

Figure 51. Comparison of experimental and predicted results for calsil exposed to a radiative heat flux of 25kWm^{-2}.

Having validated the model against experimental results, a sensitivity analysis was conducted to understand the influence of the diffusivity of calsil (α_{cs}) as well as parameters related to its boundary conditions on the temperature profiles.

3.2.3. Sensitivity study

The sensitivity study was conducted by using the local sensitivity coefficients. Considering a model response to be given by $\eta(x, y, t, \beta)$ where x, y are spatial variables, t is time and β is a parameter vector, a local sensitivity coefficient X_i is defined as the first derivative of η with respect to β_i (Equation 50) [19, 319].

$$X_i = \frac{\partial \eta}{\partial \beta_i} \qquad \text{Equation 50}$$

The sensitivity coefficient is essential because it indicates the magnitude of change of the response η due to pertubations in the values of the parameters β_i. It allows to calculate the change $\Delta\eta$ that is generated from a variation $\Delta\, \beta_i$ of the parameter β_i such that;

$$\Delta\eta = X_i\, \Delta\beta_i \qquad \text{Equation 51}$$

The sensitivity coefficients were evaluated using the forward difference approximation which is generally given by Equation 52 for the *j*th observation, *i*th parameter and *l*th dependent variable;

$$\frac{\partial \eta_l}{\partial\, \beta_i} = X_{li}(j) \approx \frac{\eta_l(\,\beta_1, \dots\dots, \,\beta_i + \delta\, \beta_i, \dots, \,\beta_p) - \eta_l(\,\beta_1, \dots\dots, \,\beta_i, \dots, \,\beta_p)}{\delta\beta_i} \qquad \text{Equation 52}$$

Where $\delta\beta_i$ is some relatively small quantity and is taken as $\delta\beta_i = 10^{-1}\beta_i$ in this study, which is within a range of realistic experimental values i.e. 10%. In this section, $\Delta\eta$ is the change in temperature at different in-depth positions i.e. TC1, TC2 and TC3 while $\beta_i = [\,\alpha_{cs}, T_r, T_{amb}, \varepsilon_{cs}, h_h, h_v, T_{imp}]$.

Figure 52, Figure 53 and Figure 54 show the sensitivity of TC1, TC2 and TC3 with respect to (w.r.t) the thermal diffusivity and parameters related to the boundary conditions respectively. The sensitivities are given as a function of time and show the transient response of the model to a change in the input parameters. It is observed that some parameters related to the boundary conditions highly influence the temperature profiles. In Figure 52 and Figure 53, T_r is the most influential parameter during the entire simulation time. α_{cs} is also influential after T_r but mostly during the heating (conduction) phase and then starts to diminish up to zero when the steady state is reached. At this point the parameters T_{amb}, ε_{cs}, h_h, T_{imp} become influential. The importance of T_r diminishes towards TC3 and the opposite is observed for T_{imp}.

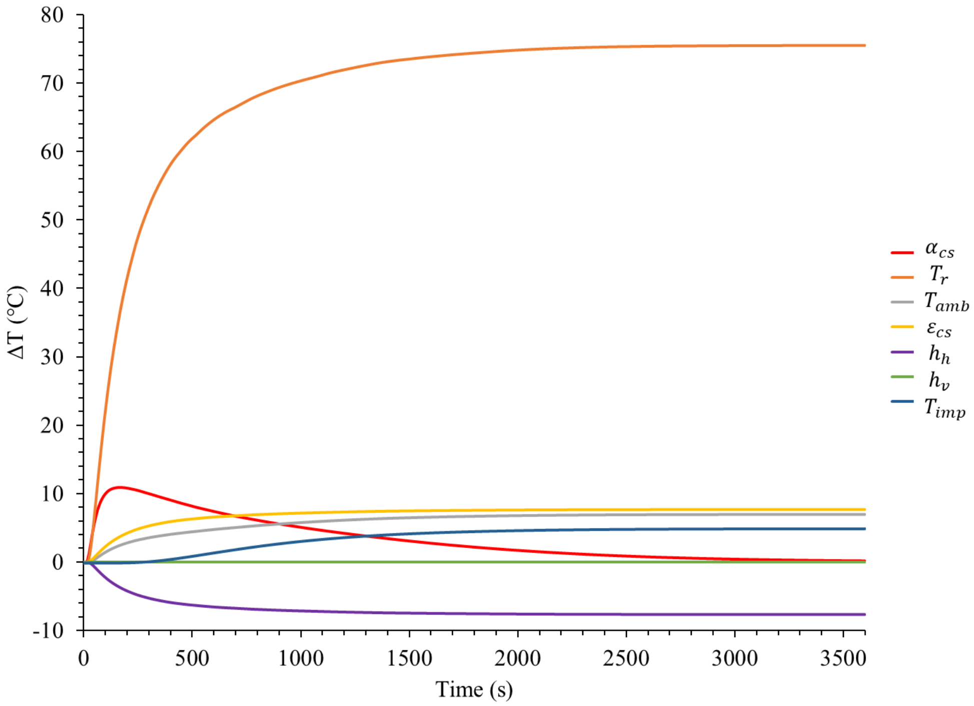

Figure 52. Sensitivity of TC1 with respect to (w.r.t) the thermal diffusivity and parameters related to the boundary conditions for calsil.

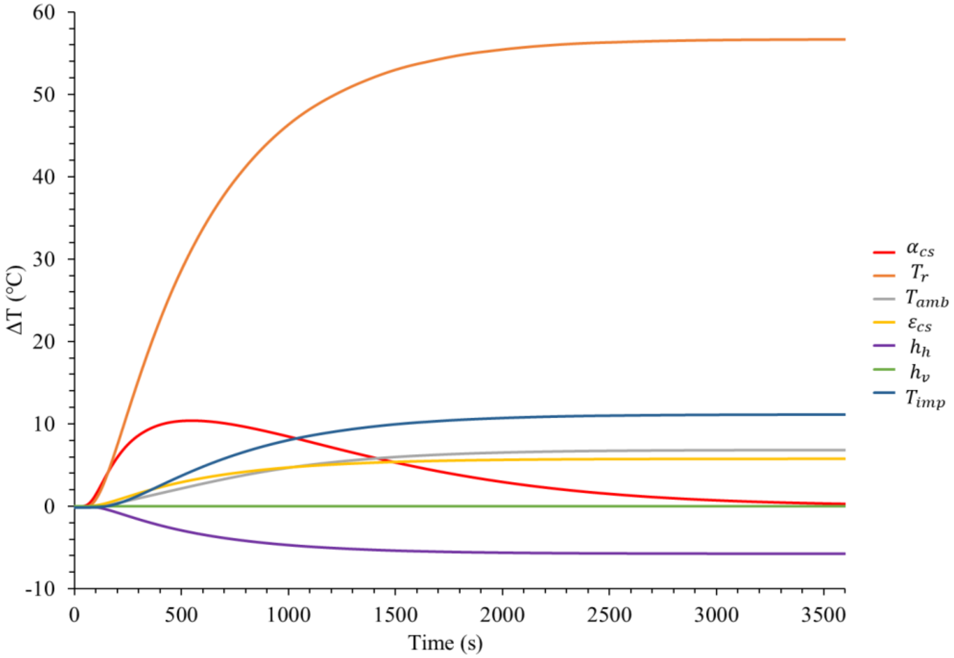

Figure 53. Sensitivity of TC2 with respect to (w.r.t) the thermal diffusivity and parameters related to the boundary conditions for calsil.

The importance of T_{imp} increases towards TC3 which is near the thermocouple near chilled sample holder (Figure 52 to Figure 54).

In Figure 54, it becomes the most influential parameter. The change in temperature (ΔT) for h_h exhibits negative values for all the thermocouples indicating that an increase in h_h reduces the temperature of TC1, TC2 and TC3. h_v has a negligible effect on TC1, TC2 and TC3. To summarize these observations, global model responses are deduced from the results in Figure 52, Figure 53 and Figure 54 by considering the sensitivity of maximum temperature change (ΔT_{max}) as shown in Figure 55.

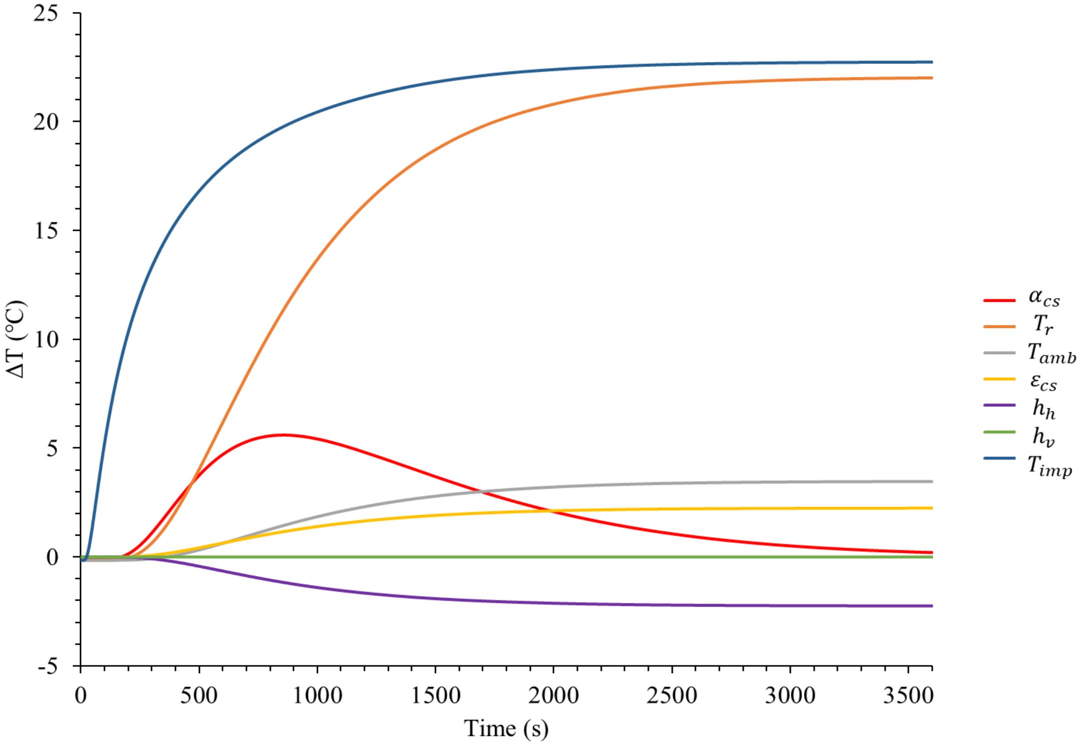

Figure 54. Sensitivity of TC3 with respect to (w.r.t) the thermal diffusivity and parameters related to the boundary conditions for calsil.

From Figure 55, it can be concluded that the sensitivity depends on the location of the thermocouple and that the boundary conditions play a major role in the model predictions. In a general manner, the sensitivity of ΔT_{max} w.r.t. to α_{cs}, $T_r, T_{amb}, \varepsilon_{cs}, h_h$ decreases from TC1 to TC3 while it increases for T_{imp}. This can be explained by the fact that the location of TC3 is far from the exposed surface therefore the effect of $T_r, T_{amb}, \varepsilon_{cs}, h_h$ reduces as compared to T_{imp}

which increases because it is the boundary condition near TC3. Salvador et al. [167] also reported the importance of boundary conditions on the numerical model response (model applied to cardboard/polyethylene), however, the authors did not provide quantifiable data such as that presented here. Livkiss et al [20] also concluded that the boundary conditions were influential to a heat transfer model response applied to stone wool sandwich panels. Besides the boundary conditions, the model was also sensitive to the thermal diffusivity.

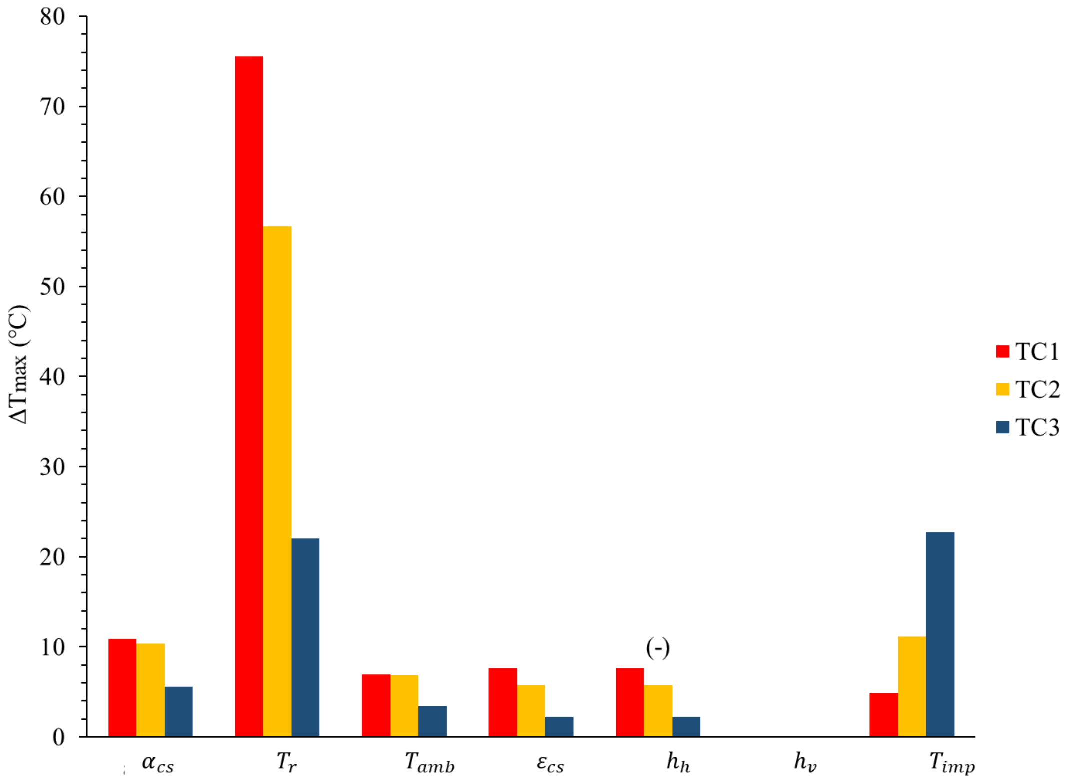

Figure 55. Maximum temperature change sensitivity to the thermal diffusivity and parameters related to the boundary conditions for calsil.

This section focused on the fire behavior of calsil and involved the modeling of heat transfer by pure conduction in the material. In the next section, using the same experimental set-up as before, a more complex scenario involving heat transfer by conduction and radiation through a porous closed-cell mullite foam will be studied.

3.3. Closed-cell mullite foam

3.3.1. Experimental study

In this section, the fire behavior of a closed-cell mullite foam block (CF) was examined. The results shown here are when the CF block was exposed to an external radiative heat flux of 35 kWm^{-2}. The experimental set-up is shown in Figure 56 and thermocouples are placed from the bottom of the CF block. TC1, TC2, TC3 are positioned at 40mm, 25mm, 10mm respectively.

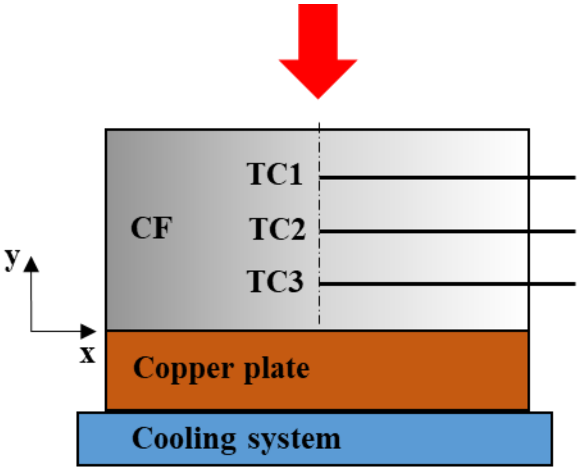

Figure 56. Experimental set-up for CF exposed to a radiative heat flux of 35kWm^{-2}.

The measured thermal diffusivity as a function of temperature of the CF block is shown in Figure 57. It is consistent with the values found in the literature for typical porous ceramic materials, e.g. Garcia et al. [320] reported values between 3 x 10^{-7}m^{2}s^{-1} and 6 x 10^{-7} m^{2}s^{-1} from room temperature to 800°C. The thermal diffusivity of CF is relatively low as compared to the individual components i.e. air and mullite and it will be discussed later in the section.

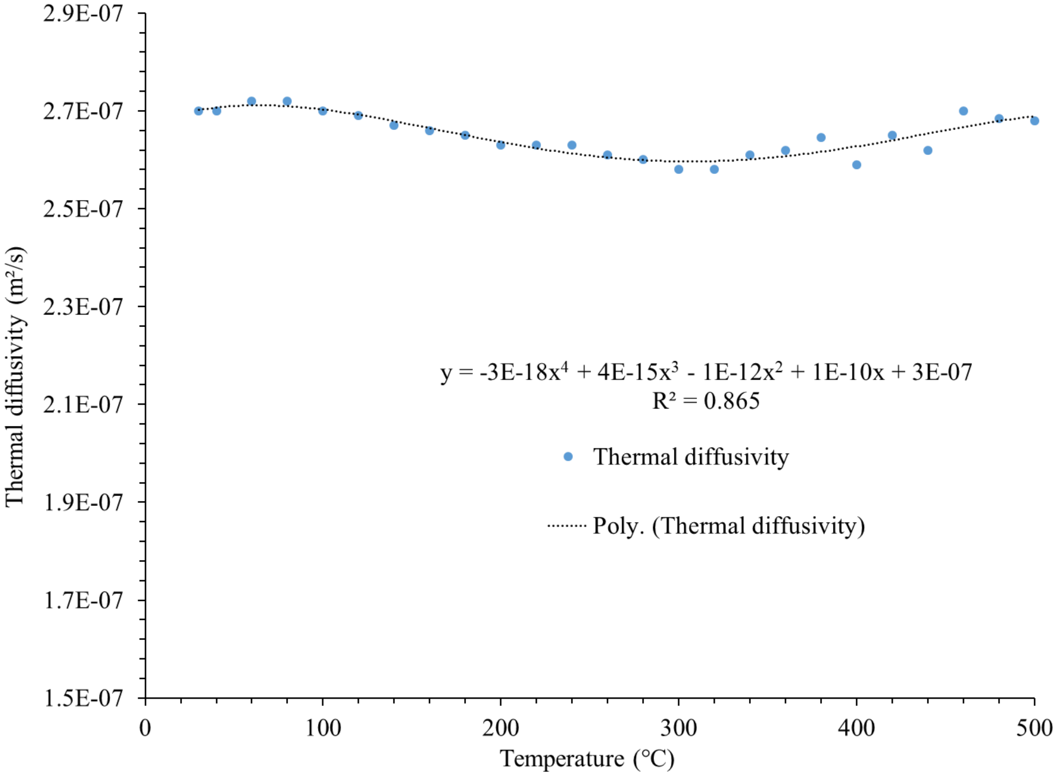

Figure 57. The measured apparent thermal diffusivity of CF as a function of temperature.

It should be noted that using the measured apparent thermal diffusivity of CF together with the numerical model used for Calsil, satisfactory agreement is observed between the simulated and experimental temperature profiles. The results (not shown here) from the numerical model were used to validate the thermocouple positions. However, the model does not take into account the properties of the individual components which is of great interest in the conceptualization of a material especially with the new developments in additive manufacturing for fire resistant materials [321]. Consequently, a numerical model taking into account these properties is proposed and discussed in the next section.

For the modeling case of CF, given that the model required many input parameters, for clarity, their determination is explained at the same time as the development of the model.

3.3.2. Numerical Model

The CF block is a closed-cell porous medium consisting of a two-phase system comprising of a continuous solid mullite phase and a gaseous phase which is dispersed in voids. The voids exist as closed-cells and their distribution is generally in discrete form. Due to this morphology, different heat transfer mechanisms have to be taken into account as explained in Chapter 1.3.2.c. A numerical model is therefore proposed to predict the fire behavior of the CF mullite block when exposed to an external heat flux of 35 kWm^{-2}.

Given the complex morphology of CF a macroscopic heat transfer approach is implemented. A simplified model (one-energy equation) involving the hypothesis of the local thermal equilibrium (LTE) is considered. The LTE assumes that the temperatures of the solid and gas phase are in equilibrium. Moreover, the material is assumed to be isotropic and the viscous dissipation and work done by the pressure changes are not taken into account [322].

Using these assumptions, the following model was implemented in COMSOL Multiphysics® using the Heat Transfer in Porous Media module.

In Equation 53, the term on the LHS represents the rate of change of internal energy in the material and the term on the RHS represents the heat transfer by conduction. Note that the convection term is not taken into account given that the CF block is composed of closed cells therefore restraining gas flow into the material.

$$(\rho C_p)_m \frac{\partial T}{\partial t} = \nabla .(k_m \nabla T) \qquad \text{Equation 53}$$

m represents the apparent properties of the material, where $(\rho C_p)_m$ is the overall heat capacity per unit volume and $\mathrm{k_m}$ is the overall thermal conductivity. The different terms in Equation 53 are further expressed in the following equations to represent the two phases. Moreover, the overall heat production term per unit volume is not added given that the CF block does not degrade during the experiment.

In Equation 54, the first term on the RHS represents the volumetric heat capacity for the solid (s) and the second term represents the volumetric heat capacity of the gas (g) phase and δ is the porosity of the CF block which is taken as 0.85 from the manufacturer’s data.

$$(\rho C_p)_m = (1-\delta)\left(\rho C_p\right)_s + \delta(\rho C_p)_g \qquad \text{Equation 54}$$

For the evaluation of the term $(\rho C_p)_m$, all the properties of the solid and gas phase need to be known and are given below.

The density of the solid phase, ρ_s, was determined from the expression of the density of porous solids [323, 324] (Equation 55);

$$\delta = 1 - \frac{\rho_a}{\rho_t} \qquad \text{Equation 55}$$

where ρ_a is the apparent density which is associated with the external volume of the material including all the pores and ρ_t $(= \rho_s)$ the true density of the material which is associated with the volume of the material without the pores for a given mass of material. The apparent density was determined by using the expression $\rho_a = \frac{m_a}{V_a}$ by measuring the mass (m_a) and by calculating the volume (V_a) from the measurements of the length, the width and the thickness of the CF block. The obtained value was 547.14 kgm^{-3}. Since all the other parameters were known, rearranging Equation 55 gave ρ_s, which was equal to 3647.6 kgm^{-3}. Schneider et al. [325] reported values ranging from 3200 kgm^{-3} to 3600 kgm^{-3} for mullite ceramics and their derivatives.

Given that the properties of mullite have extensively been reported in literature [231, 325], the specific heat capacity of mullite (C_{ps}) was obtained from Hildmann and Schneider [231] who conducted an extensive study on this property using different types of differential scanning calorimeters (DSC) (Figure 58).

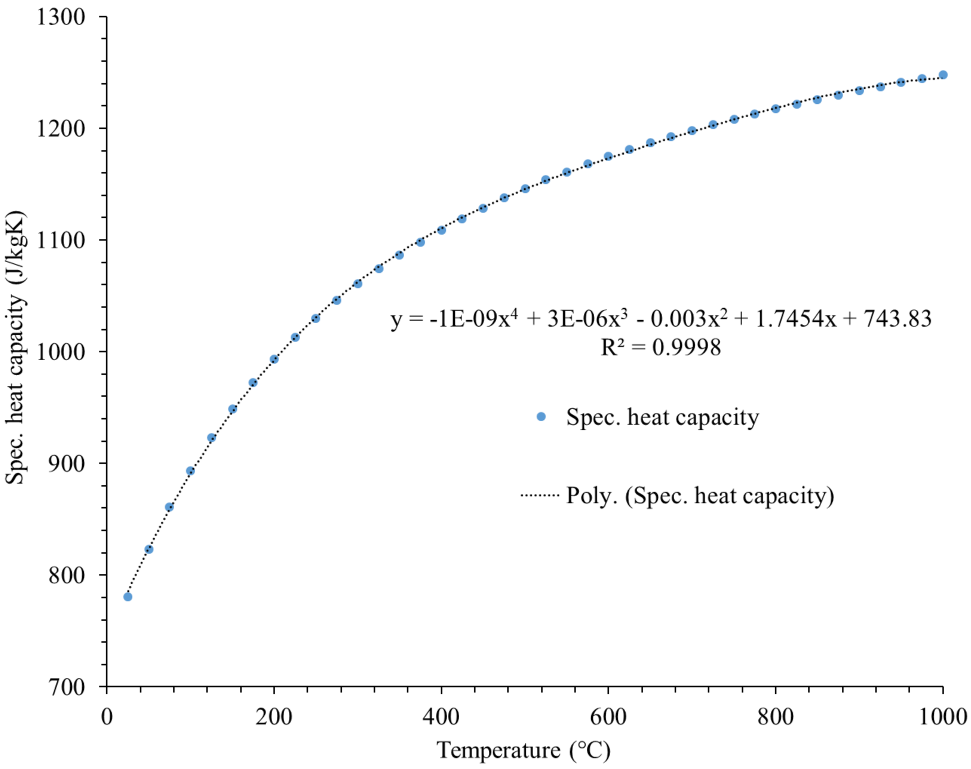

Figure 58. Specific heat capacity of mullite as a function of temperature (from [231]).

The gas phase was assumed to be air and its properties was extracted from the COMSOL Multiphysics® database.

The overall thermal conductivity is expressed in Equation 56 as a sum of different contributions i.e. contribution of conduction in the solid material (k_s), conduction in gas phase (k_g) and radiation in the material (k_{rad}).

$$k_m = k_g + k_s + k_{rad} \qquad \text{Equation 56}$$

As mentioned in Chapter 1.3.2, given the complex structure of the CF block, a universal model is used and it is expressed in Equation 28. The universal model takes into account heat transfer by conduction in the solid (k_s) and gas (k_g).

$$k_{s+g} = \frac{\sum_{i=1}^{m} k_i v_i((d_i k')/\,(d_i - 1)k' + k_i)}{\sum_{i=1}^{m} v_i((d_i k')/\,(d_i - 1)k' + k_i)} \qquad \text{Equation 57}$$

v_i and k_i are the volume fraction and the thermal conductivity of the gas or solid respectively.

The thermal conductivity of air (k_g)was also extracted from the COMSOL Multiphysics® database and the thermal conductivity of mullite (k_s) was estimated as 6.07 $Wm^{-1}K^{-1}$ at 100°C and 3.7656 $Wm^{-1}K^{-1}$ at 1400°C as reported by Shackelford and Alexander [326]. Linear interpolation was made so as to obtain values starting from room temperature. Values of the same order of magnitude were also reported by Hildmann and Shneider [327] who measured the thermal diffusivity of mullite and deduced the thermal conductivity. Moreover, Sneider et al. [325] reported values of 6.978 $Wm^{-1}K^{-1}$ at 20°C and 3.489 $Wm^{-1}K^{-1}$ at 1400°C.

The parameters d_i and k' were taken as 3 and 0.4 respectively, from literature as reported by Guo et al. [235] for a typical mullite ceramic material. Their physical significance is detailed in Chapter 1. For the radiation contribution (k_{rad}), the equation derived by Loeb [239] was implemented (Equation 29);

$$k_{rad} = 4\omega d \varepsilon_{pores} \sigma T^3 \qquad \text{Equation 58}$$

The diameter of the pores (d) was taken as 100µm, which was the average pore size supplied by the manufacturer, the pores were assumed to be spherical and the geometrical factor (ω) was taken as $\frac{2}{3}$, emissivity of the radiant surface of the pores (ε_{pores}) was estimated to be equal to 1.

As seen, the overall thermal conductivity is dependent on the porosity, the structure and the emissivity of the pores [328].

The same boundary conditions implemented for the calsil block as well as the same mesh details were also used for the CF block. In this case the initial temperature was taken 40 °C.

3.3.3. Comparison of experimental and predicted results

As in the case of the calsil block, the sensitivity of the temperature profiles (TC1, TC2, TC3) to the thermocouple positioning need to be considered. Using a similar approach to that of the calsil block, the thermocouple positions were adjusted and the locations that resulted in the best fit for TC1, TC2, TC3 were 42.3mm, 28.2mm and 11mm respectively. These values were acceptable considering that they were similar to those obtained using the numerical model implementing the diffusivity of CF. The comparison between the numerical model for the CF block and the experimental data is shown in Figure 59. The good agreement between both curves permitted the validation of the macroscopic approach of the numerical model.

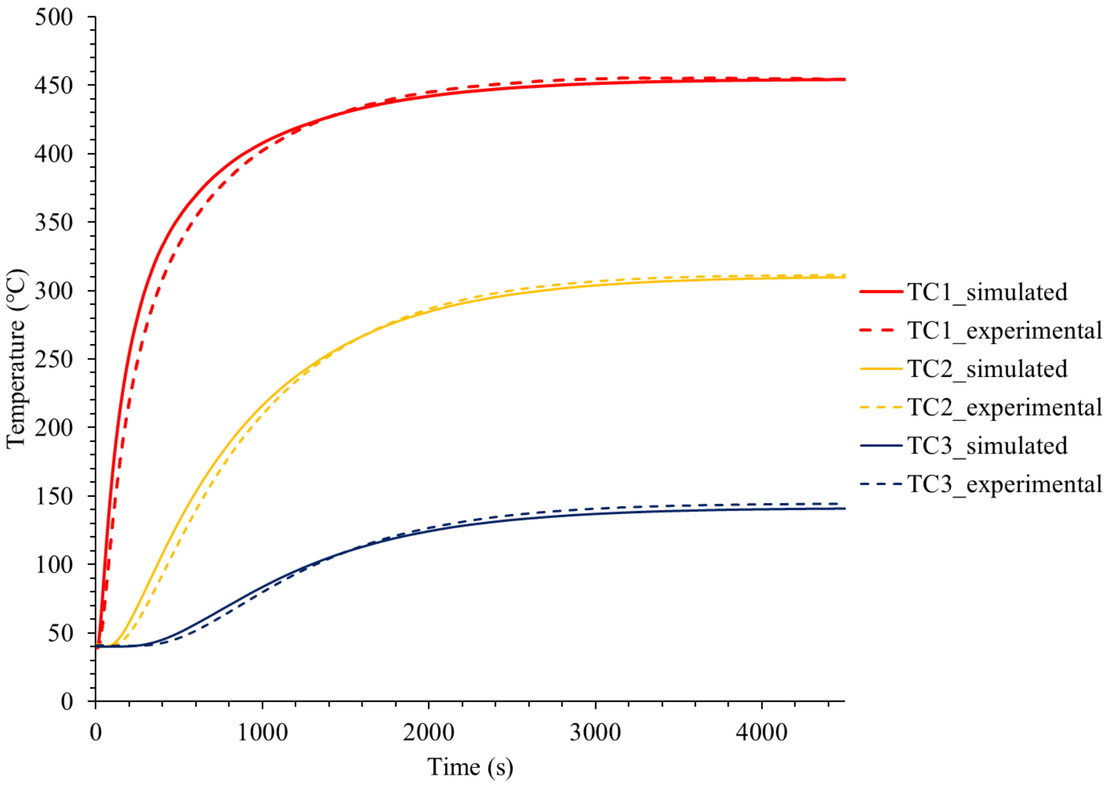

Figure 59. Comparison of experimental and predicted results for CF exposed to a radiative heat flux of 35kWm^{-2}.

3.3.4. Sensitivity study

A sensitivity study was then conducted to understand the influence of the material properties on the temperatures profiles (TC1, TC2 and TC3). A perturbation of +10% is applied on all the parameters. The material properties considered are for both the gas and solid phases. The effect of the boundary conditions will not be studied assuming that they relatively have the same influence as for the case of Calsil. Since the overall thermal conductivity is dependent on the porosity, thermal conductivity of the components, geometrical factor, diameter of pores, emissivity of pores the effect of these individual properties were considered instead. Moreover, the effects of the density, specific heat of the gas and the solid matrix as well as the emissivity of the surface are also considered. In short, $\beta_i = [\delta, \varepsilon_{CF}, C_{ps}, \rho_s, k_g, k_s, d, \gamma, \varepsilon_{pores}, C_{pg}, \rho_g]$.

Figure 60, Figure 61 and Figure 62 present the sensitivity of TC1, TC2 and TC3 w.r.t the selected input material properties respectively as a function of time. It is noteworthy that the sensitivities of C_{ps} and ρ_s superimpose. In Figure 60, the change in temperature, ΔT w.r.t δ rapidly rises to a maximum and then decreases to around 10°C. A similar shape of the curve is observed in the negative values for C_{ps} and ρ_s, however in this case the curve increases to zero. ε_{CF} increases rapidly up to a steady state of ΔT at around 8°C. The curves k_g and k_s also rises then decreases after a maximum value of ΔT and k_g exhibits a slightly higher influence as compared to k_s. This could be explained by the fact that the gas phase occupies most of the material due to the high porosity of the CF. Similar trends are observed in Figure 61 and Figure 62. It can be observed that the most influential parameters are δ, C_{ps}, ρ_s, k_g and k_s. The thermal properties e.g. effective thermal conductivity of the CF are highly dependent on the porosity, δ, which explains it's importance as for TC1 and TC2. However, for TC3, ρ_s and C_{ps} become the most influential. The general behavior of the sensitivity curves could be explained by the fact that the thermal diffusivity of air is higher than the thermal diffusivity of the solid mullite material. The thermal diffusivity of air is estimated as 2.2 x 10^{-5} m^2s^{-1} [329] and that for solid mullite as 2.18 x 10^{-6} m^2s^{-1}. The gas properties C_{pg} and ρ_g have a negligible effect on the temperature profiles.

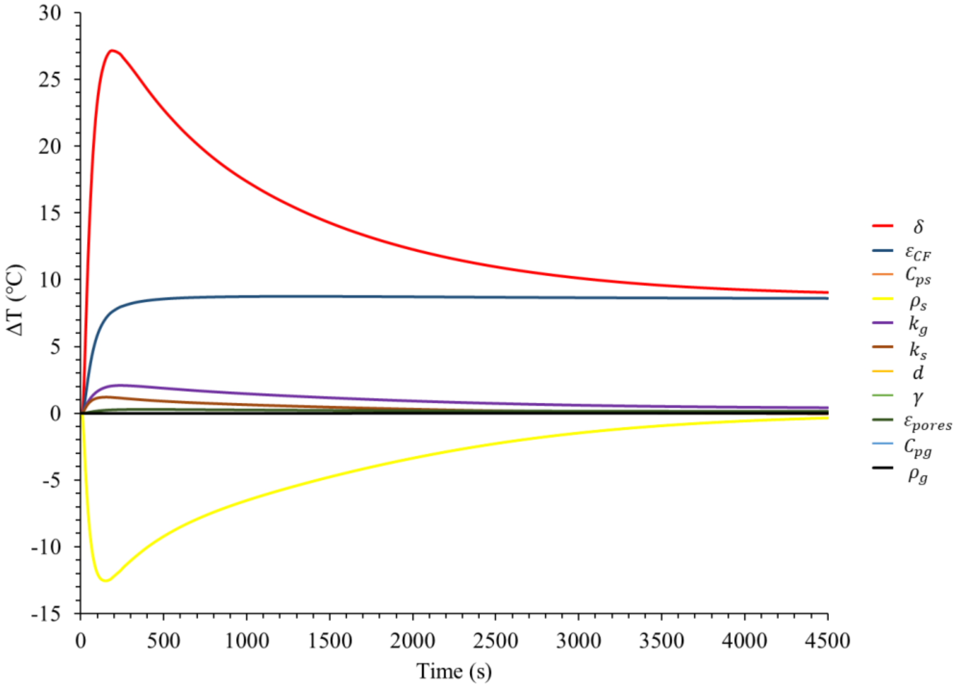

Figure 60. Sensitivity of TC1 with respect to (w.r.t) the input parameters for CF.

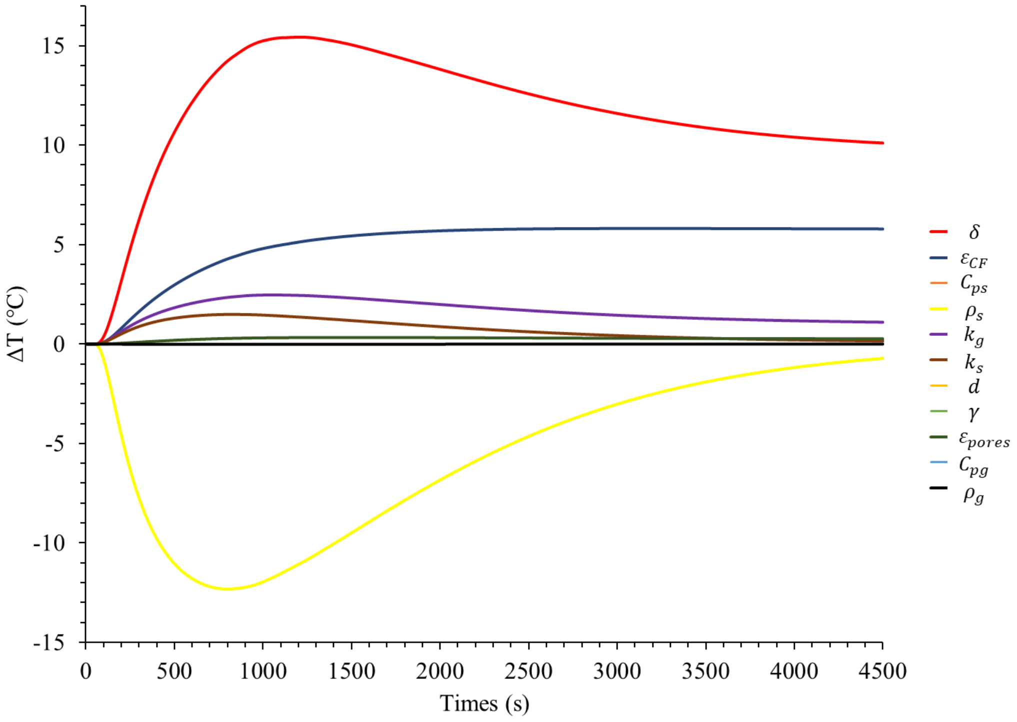

Figure 61. Sensitivity of TC2 with respect to (w.r.t) the input parameters for CF.

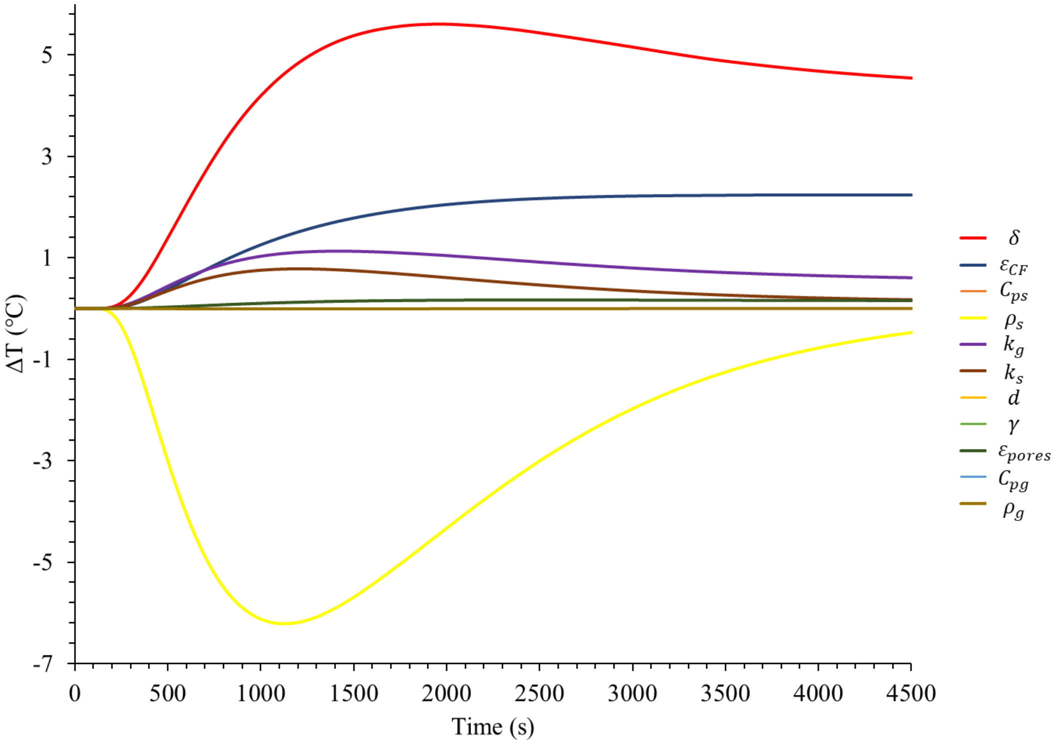

Figure 62. Sensitivity of TC3 with respect to (w.r.t) the input parameters for CF.

To easily understand the global influence of the input parameters on the model response, the maximum temperature change (ΔT_{max}) induced by a disturbance of 10% in the input parameter values at different thermocouple locations (TC1, TC2 and TC3) was used as shown in Figure 63. The negative signs on top of some of the parameters indicate that an increase in the parameter results in a decrease in the temperature values. It is observed that the sensitivity of ΔT_{max} w.r.t. $\delta, \varepsilon_{CF}, C_{ps}, \rho_s, k_g, k_s$ decreases from TC1 to TC3 and $\delta, C_{ps}, \rho_s, \varepsilon_{CF}$ are the most influential parameters. It can be concluded that the accumulation of energy in the gas is negligible as compared to that of the solid. In our knowledge, a similar sensitivity study has never been reported in literature.

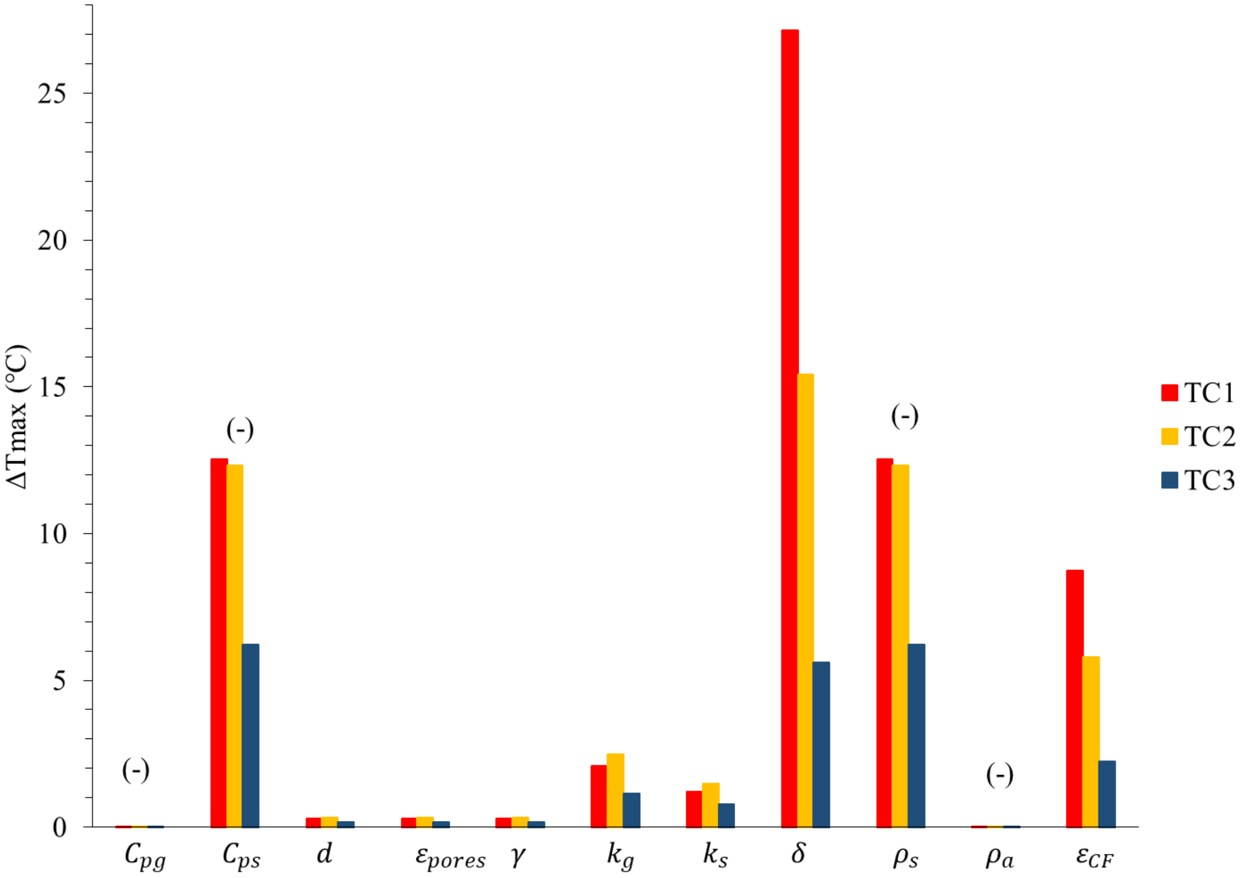

Figure 63. Maximum temperature change sensitivity with respect to the input parameters for CF.

In this section the fire behavior of CF was modeled and a sensitivity study on the material properties was conducted. As observed in the experiments, the CF block was not thermally degradable within the limits of the experiments. Up to now, both studies on calsil and CF have focused on static and non-thermally degradable insulation materials. In the next section, the fire behavior of phenolic foam (PF) which is involves ablation of the surface and thermal degradation will be modeled.

3.4. Phenolic foam

3.4.1. Experimental study

As mentioned in Chapter 1.3.3, closed-cell polymeric foams such as phenolic foam (PF), are combustible and undergo thermal decomposition when exposed to an external heat flux. Modeling their fire behavior is a challenge due to the complex coupled physical and chemical phenomena which occur on the surface and in-depth of the material. Experiments were conducted using the cone heating element to understand the fire behavior of PF when exposed to a radiative heat flux of 25kWm^{-2} and a numerical model was proposed. A heat flux of 25kWm^{-2} was chosen to avoid the complex phenomena of smoldering to flaming combustion as well as the rapid cracking of the foam. A comparison of the cross-section of the PF at 600s at 25kWm^{-2} and 50kWm^{-2} is shown in Appendix 2 in Table 22. However, it should be noted that no smoldering to flaming was observed at 50kWm^{-2} after 600s.

In this case, two experiments with different types and disposition of thermocouples was used. At first, three type-K thermocouples of diameter 0.5mm were used and placed at locations 35mm, 25mm and 10mm from the unexposed surface of the PF block. However, it was observed that these thermocouples moved due to the fire behavior of the material therefore the temperature readings were somehow not correct but gave an order of magnitude as discussed later in the section 3.4.1.b. These readings were used for thermally mapping the temperature ranges of the char layer, pyrolysis zone and virgin layer. To solve the issue with the thermocouples, two type-K thermocouples of diameter 3mm comprising of a probe made from Inconel were then used and placed at the position TC1 and TC2 at 30mm and 15mm respectively. Indeed, it is known that thermocouples of small diameter are more accurate, however, in this case, the 3mm type-K thermocouples did not move too much away from their location. In order to maintain the same boundary conditions as in the previous sections, the experimental set-up shown in Figure 64 was used. Moreover, the PF-steel plate system was used on top of the calsil block in order to avoid thermal contact problems between the steel and copper plate. A similar set-up was adopted for SBIC as will be seen later in Chapter 3.5.1. This set-up can also be considered as a multi-layer system used for thermal insulation on buildings.

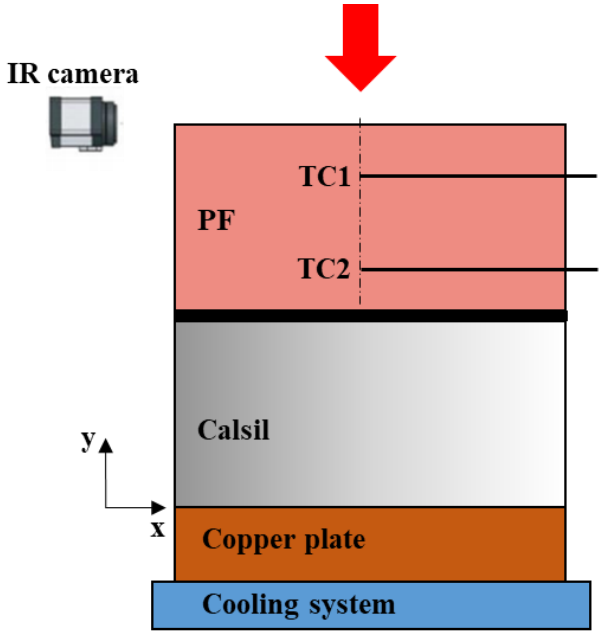

Figure 64. Experimental set-up for PF exposed to a radiative heat flux of 25kWm^{-2}.

3.4.1.a. Post-test visual observations

When the PF is exposed to the radiative heat flux, the surface and in-depth temperatures begin to increase. When the vaporization temperature of water is reached, residual water evaporation from the surface begins. The water content is a by-product of the condensation cure reaction which causes the development of micropores during the manufacture of the PF [330]. It is assumed that the water evaporation in the micropores of the PF induces a pressure build-up near the exposed surface of the material. After all the water has left the material, temperatures continue to increase up to the pyrolysis temperature which causes the onset of pyrolysis reactions and the material is converted to char and volatile gases. Due to the internal pressure build-up caused by the physicochemical processes i.e. the evaporation of water as well as the resistance of the char to the volatile gas flow close to the surface, a slight expansion (Figure 65) of the material is observed and finally cracks are formed on the exposed surface [210, 331]. When the cracks are formed, the closed-cells are opened and the char becomes permeable allowing the easy flow of the pyrolysis gases to the surface. At this point the material is divided into a char layer, pyrolysis zone and virgin layer as shown in Figure 65. During the thermal decomposition process, the virgin foam changes color from pink to yellow and then finally turns black. Moreover, it can be noticed that the thermal degradation of PF is not uniform with higher degradation zones around the center compared to the edges indicating that the heat transfer phenomena is not one-dimensional.

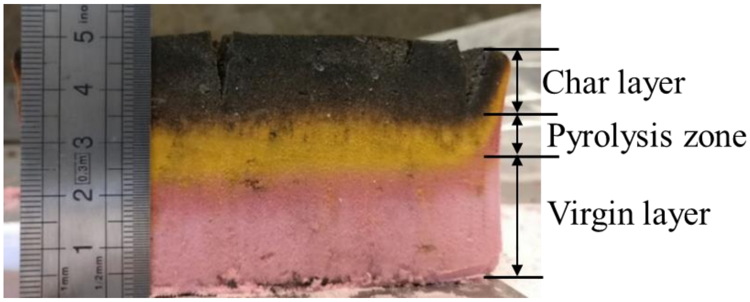

Figure 65. Slight expansion and layers formed during the decomposition process at t=180s.

As the experiment progresses (as shown in Table 14 from t=180s to t=600s), the thickness of the char layer increases and the cracks propagate into the material as the pyrolysis front moves towards the virgin layer [332]. During this process, the oxygen available in the surrounding atmosphere may percolate into the cracks leading to char oxidation, smoldering or glowing combustion (Figure 66) [193, 248, 333]. Moreover, no transition of smoldering to flaming combustion is observed. As a result of these phenomena, ablation is observed and the surface recedes.

At the end of the experiment, when the shutter of the cone calorimeter is closed, surface smoldering stops signifying that it is controlled by the external radiative heat flux and hence it is not self-sustained. This is probably due to the closed-cells which do not allow easy diffusion of oxygen into the foam therefore not supporting smoldering.

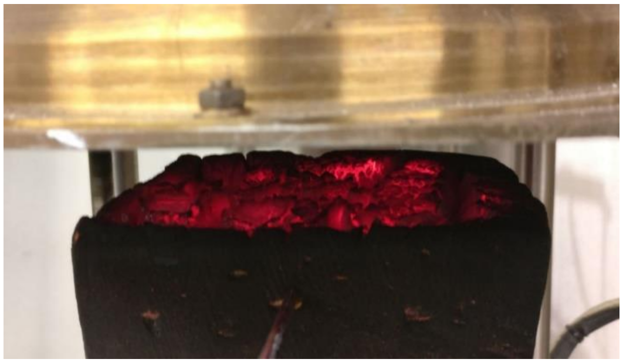

Figure 66. Snapshot showing the smoldering combustion on the surface of the PF during the experiment.

Table 14 shows the visual observations when the PF was exposed to an external radiative heat flux at different heat exposure times.

Table 14 Exposed surfaces and cross-sections of PF at different radiative heat exposure times.

	t=180s	**t=600s**
Exposed surface		
Cross-section		
Infrared images	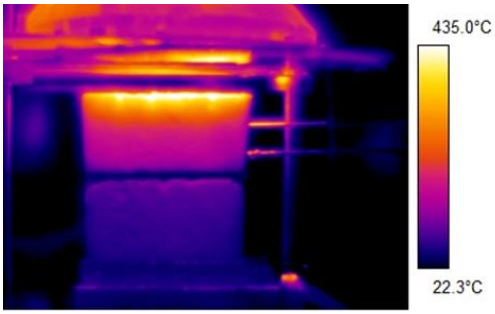	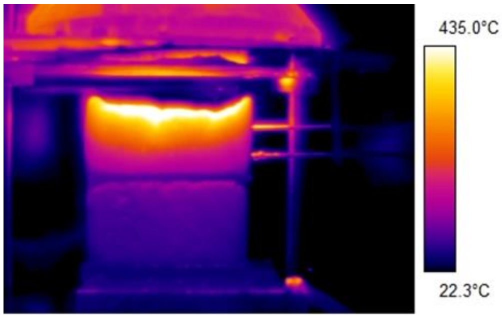

3.4.1.b. Thermal mapping

To estimate the temperature ranges of the different thermal degradation zones, three thermocouples were inserted at different locations in the thickness of the PF. The thermocouples were placed at 10mm, 25mm and 35mm from the unexposed surface. Figure 67 shows the temperature profiles of PF at different times i.e. (a) 180s and (b) 600s with superimposed thermal degradation layers. It can be observed that the temperature of the char layer ranges from 380°C to 560°C and that of the pyrolysis zone ranges from approximately 180°C to 300°C. For the char layer a minimum value of 380°C is chosen according to Figure 67 (b) The dotted red line at 10mm corresponding to a temperature of 300°C is more or less in the pyrolysis zone. In Figure 67 (b) the temperature of the thermocouple at 35mm shows a lower value than the thermocouple at 25mm possibly because it moved and was exposed to air due to the receding surface. The error bars show the standard deviations from 3 experiments for each of the thermocouple position. Some temperature profiles strayed away due to errors in thermocouple positioning induced by the moving foam and were not considered. The reading of the thermocouples in the virgin layer has less errors compared to those towards the exposed surface where irregular cracking and surface recession occur.

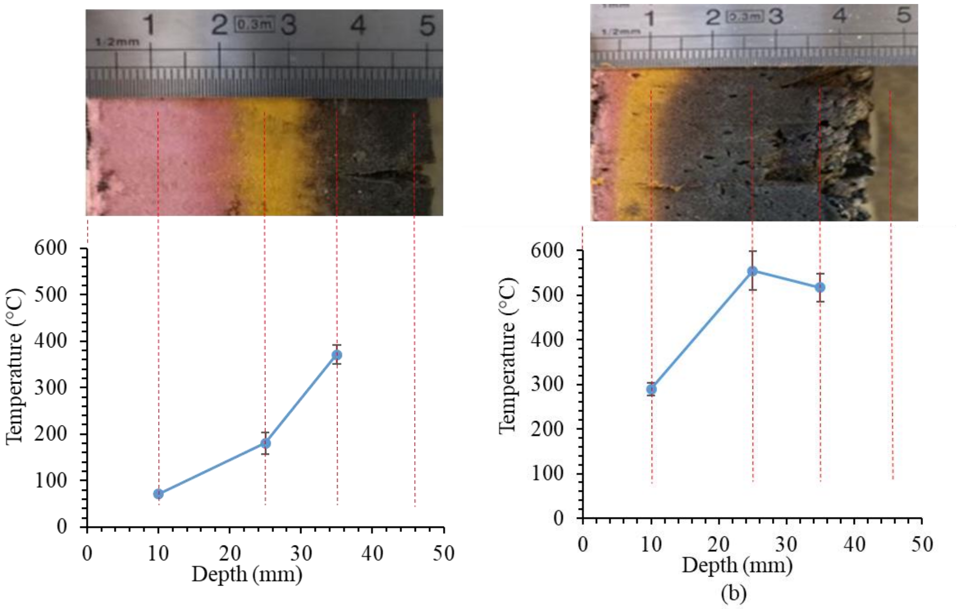

Figure 67. In-depth temperature profiles of PF at (a) 180s and (b) 600s.

3.4.1.c. Thermal stability of PF

To model the fire behavior of a material, it is important to understand how it decomposes therefore the knowledge of their thermal stability is of prime interest. Figure 68 presents the thermogravimetric (TG) and derivative thermogravimetric (DTG) curves of PF at a heating rate of 10°Cmin^{-1} under an air and nitrogen atmosphere i.e. thermo-oxidative and inert conditions respectively. For the TGA experiments under air, four main mass loss steps can be observed from the peaks on the DTG curves: the first is between 150°C-250°C, the second is between 250°C-300°C then a steep mass loss between 350°C-530°C and a final small mass loss between 530°C-570°C with a residual weight of 3.54% at 800°C. The four main mass loss steps are attributed to water evaporation, volatilization of residual monomers, thermal decomposition of the foam and finally the random breaking of chain linkages resulting in the release of water and gases such as CO_2, CO. [251]. The final mass loss step can also be attributed to the secondary char oxidation reactions. For the TGA experiments under nitrogen, three main mass loss steps can be identified: the first and second are similar to those under air and the third mass loss step is between 410°C-550°C. This third mass loss step can be noted as the main step of thermal decomposition. The final step residue shows the dependence of the thermal stability of PF on the atmosphere with a residual weight of 47% at 800°C.

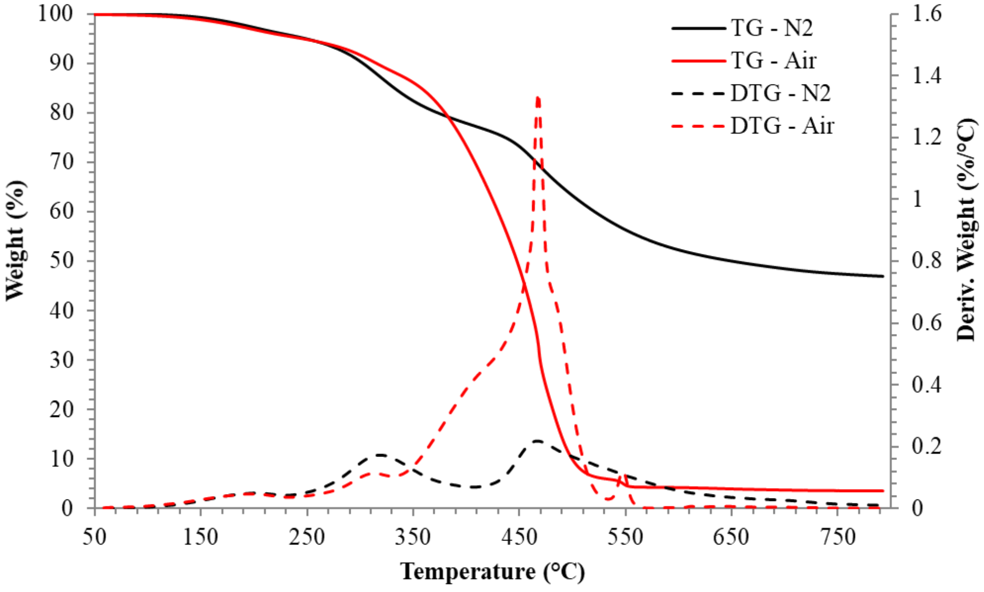

Figure 68. TGA and DTG curves of PF at 10°Cmin^{-1} under an air and nitrogen atmosphere.

With the knowledge from the experimental observations described above, a numerical model is proposed to predict the fire behavior of PF.

3.4.2. Numerical Model

3.4.2.a. Model Assumptions

The main objective of this study is to develop a 2D model gathering the fundamental governing equations for the heat transfer phenomena involved when PF is exposed to fire. Given the complexity of the coupled phenomena observed during the experiments a phenomenological approach was implemented and several assumptions were made in order to minimize the number of input model parameters. Moreover, the numerical model was developed in the view of investigating the sensitivity of the modeling results with respect to the input model parameters.

In the literature, different models have been implemented to study the fire behavior of smoldering or ablative materials. These models were discussed in Chapter 1. The numerical model implemented here is based on the models for ablative materials [264, 334, 335]. It was chosen because it takes into account most of the phenomena involved when PF is subjected to a thermal constraint. Moreover, the phenomena at the surface is represented by adding a term to the boundary conditions on the exposed surface simplifying the problem as compared to other models which require the solving of the conservation of the gas species (e.g. oxygen) [54].

The main assumptions and simplifications are stated as follow. The pyrolysis gases and carbonaceous char are assumed to be in local thermal equilibrium. The pyrolysis gases are ideal, non-reactive and their flow is driven by Darcy’s law. The thermal decomposition is assumed as nth order one step reaction. The moisture transport is not considered. The surface ablation of PF was assumed to be homogenous and occurring in one dimension i.e. the y-axis.

Considering the above reported assumptions, the proposed model takes into account the thermal decomposition of the material, heat transfer, the gas generated and transport through the char layer as well as the pressure field. The governing equations include the mass conservation in the gas phase and energy conservation accompanied by the thermal decomposition expressed in the form of the Arrhenius equation. The full model is implemented in COMSOL Multiphysics® using the modules for Heat Transfer, Darcy’s law, Domain ODEs and DAEs and Deformed Geometry. The system of equations was resolved using the direct solver MUMPS. The same solver was also used later for SBIC.

The full model is described in the next section as well as the complementary assumptions made in the model.

3.4.2.b. Governing equations

As shown in Figure 64, the experimental set-up is made up of four distinct layers i.e. the copper layer, the calsil layer, the steel layer and the PF layer. Perfect thermal contact is assumed between the layers and in the next section, only the governing equations for the PF will be explicitly described since the governing equations for the other layers were described before.

3.4.2.b.i. Internal energy conservation equation

The in-depth energy balance is expressed as shown in Equation 59. The rate of change of internal energy in the gas phase is assumed to be negligible compared to that of the solid as deduced from the sensitivity study for CF and the same assumption has successfully been applied in the literature ([79, 336]). The term on the LHS represents rate of change of internal energy in the solid while the first term on the RHS represents the energy transferred by conduction, the second term represents the thermal decomposition of the material and the last term represents the heat transferred by the diffusion of the pyrolysis gases.

$$\rho_s C_p \frac{\partial T}{\partial t} = \nabla.(k.\nabla T) - Q\frac{\partial \rho_s}{\partial t} - \begin{bmatrix} \dot{m}'_{gx} \\ \dot{m}'_{gy} \end{bmatrix}.\nabla h_g \qquad \text{Equation 59}$$

Where ρ_s is the density of the decomposing solid, T is the temperature, C_p is the specific heat capacity, k is the thermal conductivity and Q the enthalpy of reaction and h_g is the enthalpy of the gases.

The thermal conductivity and the specific heat capacity are also expressed as a linear function of the decomposition degree ($\alpha 1$) and for both the virgin and the char state, Equation 60 and Equation 61 respectively:

$$k = k_v(1 - \alpha 1) + k_c \alpha 1 \qquad \text{Equation 60}$$

$$C_p = C_{pv}(1-\alpha 1) + C_{pc}\alpha 1 \qquad \text{Equation 61}$$

3.4.2.b.ii. Internal decomposition equation

The thermal decomposition of the material was taken into account by assuming a nth order global Arrhenius model. This model is fundamental and simplifies the problem in terms of minimizing the number of parameters to be determined. It has successfully been used for charring ablative materials [210, 263, 335, 337, 338].

The decomposition degree $(\alpha 1)$ is expressed in Equation 62. It describes the pyrolysis process in terms of the bulk density (ρ_s) that is converted from an initial virgin state (ρ_v) to a fully charred state (ρ_c). It quantifies the conversion process from an initial value of 0 to 1 when the material is fully charred [334].

$$\alpha 1 = \frac{\rho_v - \rho_s}{\rho_v - \rho_c} \qquad \text{Equation 62}$$

where, ρ_v the density of the fully-virgin state and ρ_c is the density of the fully-charred state.

The rate of change of the bulk solid density is given in terms of the rate of change of the decomposition degree by Equation 63.

$$\frac{\partial \rho_s}{\partial t} = -(\rho_v - \rho_c)\frac{\partial \alpha 1}{\partial t} \qquad \text{Equation 63}$$

he rate of change of the decomposition degree is expressed in Equation 64.

$$\frac{\partial \alpha 1}{\partial t} = Ae^{-\frac{E}{RT}}(1-\alpha 1)^n \qquad \text{Equation 64}$$

where A is the pre-exponential factor, E is the activation energy, R is the universal gas constant and n is the order of reaction.

3.4.2.b.iii. Mass conservation equation in the gas phase

The pyrolysis gas mass flux $(\dot{m}_g')$ is defined as negative when flowing in the same direction as the positive x- or y-direction. It is represented in *x* and *y* directions. Assuming that the density of the solid is superior to the density of the gas and the pyrolysis gases escape the char region instantaneously due to the formation of cracks, the mass conversation is given by Equation 65 [79, 264, 338, 339]. The term on the LHS represents gases flowing out of the PF while both terms on the RHS represents rate of change of the bulk density in terms of $\alpha 1$.

$$\nabla . \begin{bmatrix} \dot{m}'_{gx} \\ \dot{m}'_{gy} \end{bmatrix} = (\rho_v - \rho_c) \frac{\partial \alpha 1}{\partial t} \qquad \text{Equation 65}$$

Assuming that the pyrolysis gases behave ideally and that gas flow is governed by Darcy's law, we have Equation 66 representing the equation of state of an ideal gas and Equation 67 representing Darcy's law.

$$\rho_g = \frac{PM_n}{RT} \qquad \text{Equation 66}$$

$$\begin{bmatrix} \dot{m}'_{gx} \\ \dot{m}'_{gy} \end{bmatrix} = -\rho_g \frac{\Gamma}{\mu} \nabla P \qquad \text{Equation 67}$$

Where ρ_g is the pyrolysis gas density, P is the pressure, R is the universal gas constant, Γ is the permeability and μ dynamic viscoscity.

Equation 65, Equation 66 and Equation 67 links the mass conservation equation in the gas phase with the internal pressure.

3.4.2.b.iv. Initial and boundary conditions

The boundary condition on the exposed surface is adapted from Equation 47 and additional terms are added given that, in this case, the PF is thermally degrading and there is flow of the pyrolysis gases and thermochemical phenomena at the surface. The two last terms represent the total chemical energy at the surface [261, 340, 341]. The term $-\dot{m}'_{gy} h_g$ represents the energy flux into the surface from the decomposition reactions and the term $\dot{m}'_{gy} h_c$ represents energy flux consumed in the surface chemical reactions providing a positive feedback [334-336].

$$q_{net} = \varepsilon_s \sigma (F T_r^4 + (1 - F) T_{amb}^4) - \varepsilon_s \sigma T^4 + h_h (T_{amb} - T) - \dot{m}'_{gy} h_g + \dot{m}'_{gy} h_c \qquad \text{Equation 68}$$

where h_c is the heat of combustion.

The addition of such terms to the exposed surface boundary condition has been implemented in the fire science community. Tranchard et al. [336] added the same terms for the study of a carbon epoxy composite exposed to fire. Galgano et al. [193, 342] and Boonmee and Quintiere [333] took into account the char oxidation for the glowing combustion of wood by adding a similar term to the surface boundary condition. Similarly, ablation models [261, 263, 334, 335, 341] implement the same terms coupled with chemically reacting boundary flow at the surface of the ablating material.

The boundary conditions on the sides are shown for the right side in Equation 69 and for the left hand side in Equation 70 following the convention that the gas mass flux ($\dot{m}_g'$) is defined as negative when flowing in the same direction as the positive x- or y-direction.

$$-n\,(-k\nabla T) = \varepsilon_s\sigma(T_{amb}^4 - T^4) + h_v(T_{amb} - T) - \dot{m}_{gx}' h_g \qquad \text{Equation 69}$$

$$-n\,(-k\nabla T) = \varepsilon_s\sigma(T_{amb}^4 - T^4) + h_v(T_{amb} - T) + \dot{m}_{gx}' h_g \qquad \text{Equation 70}$$

In addition, the internal pressure and the pressure boundary conditions are set as 1atm and the initial temperature as 25°C.

The complete computational mesh used was composed of 2700 quadrilateral elements with a maximum element size of 0.0022m, a minimum element size of 8.32 x 10^{-6}m and an average element quality of 1. The 3mm type-K thermocouples were not included in the model because a numerical analysis showed that they did not influence the temperature results at the specific locations. This also simplified the mesh and inverted mesh problems were avoided. Figure 69 shows the mesh quality of the (a) initial (t=0s) and (b) final mesh after t=600s. Figure 69 also shows the mobile mesh position at t=0s and t=600s.

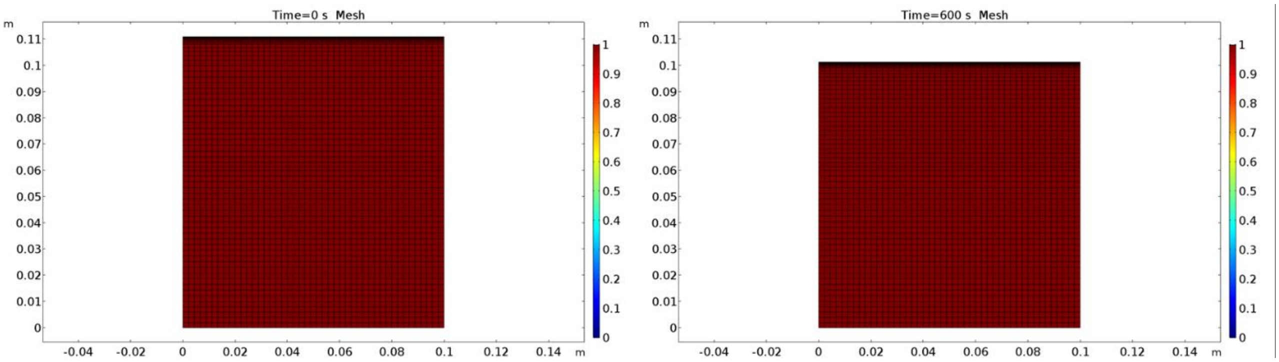

Figure 69 Mesh quality of the (a) initial mesh and (b) final mesh after t=600s.

Having defined a system of equations accompanied by initial and boundary conditions as well as the details of the meshing, the numerical model requires input parameters which will be discussed in the next section.

3.4.3. Thermophysical properties of PF

The knowledge of the material input properties is required to implement the numerical model. These properties are discussed in this section. These properties were estimated in order to implement realistic values. It is noteworthy that in literature, most of the time, when the goal of the model is to understand the influence of the parameters on the model response, crude characterization of properties is often adequate [16, 18, 19]. Moreover, the measured and estimated properties were linearly extrapolated in order to implement them at high temperatures.

3.4.3.a. Thermal properties

The density of the virgin PF was measured as 33.68 kgm^{-3} as compared to 35 kgm^{-3} that was given by the manufacturer. The thermal properties of the virgin and char PF are presented in this section. Figure 70, Figure 71, Figure 72 show the thermal diffusivity, specific heat capacity and thermal conductivity of the virgin PF respectively. These properties increase with temperature for the given range. Tseng and Kuo [244] reported the same behavior for the thermal conductivity and obtained values varying from 0.02 Wm^{-1}K^{-1} at 10°C to 0.11 Wm^{-1}K^{-1} at 80°C. Moreover, the value provided by the manufacturer was 0,020 Wm^{-1}K^{-1}. Hildago et al. [203] reported average ambient temperature values of the thermal conductivity as 0.021 Wm^{-1}K^{-1} – 0.024 Wm^{-1}K^{-1} and the specific heat capacity as 1500 Jkg^{-1}K^{-1} for PF with a density of 38 kgm^{-3}.

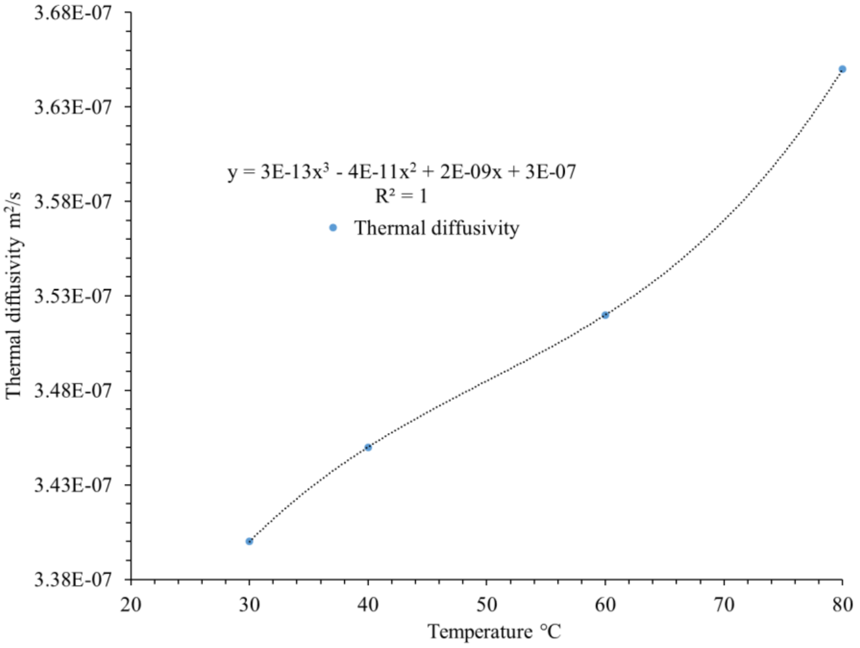

Figure 70. Thermal diffusivity of virgin PF.

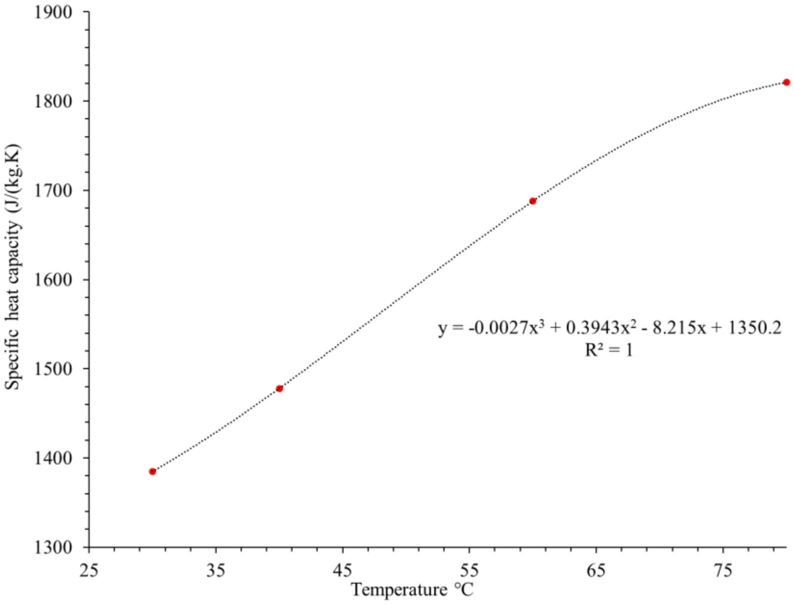

Figure 71. Specific heat capacity of virgin PF.

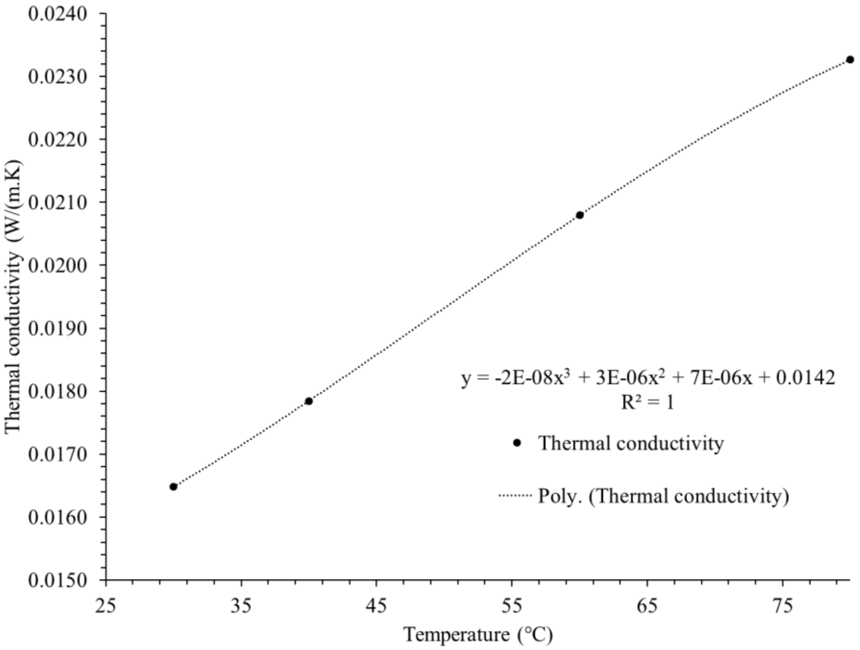

Figure 72. Thermal conductivity of virgin PF.

The char properties were determined in the same way as the virgin properties [343]. Small char samples were cut from the char layer after a fire test at t=600s and the actual char density (ρ_c) was also measured and 31.63 kgm^{-3} was obtained. Figure 73, Figure 74 and Figure 75 show the thermal diffusivity, specific heat capacity and thermal conductivity of the PF char respectively.

The thermal diffusivity of the PF char does not vary a lot with temperature and is almost constant. However, the specific heat capacity and the thermal conductivity of the PF char increased with temperature. In addition, the thermophysical values of the char were higher than those of the neat properties. It can possibly be explained by the fact that the chars that are produced from aromatic polymers can have a “dense and continuous structure that can accelerate the rate of conduction” as reported by Mouritz and Gibson [344]. From literature, phenolic polymers contain a high aromatic ring content that form a large amount of char [345]. No data on the char properties of PF was found in literature. However, to have an idea of the order of magnitude as compared to some charring materials, Valencia [27] reported the following values of rigid polyurethane (PUR) foam at room temperature: virgin specific heat capacity = 1300 Jkg^{-1}K^{-1} and virgin thermal conductivity = 0.04 Wm^{-1}K^{-1} and for char specific heat capacity =2500 Jkg^{-1}K^{-1} and the char thermal conductivity as =0.12 Wm^{-1}K^{-1}. Furthermore, Wilson [346] reported values for a low density phenolic-nylon char. The specific heat capacity ranged from 1600 Jkg^{-1}K^{-1} to 2200 Jkg^{-1}K^{-1} for a temperature range of 537°C to 2757°C and the thermal conductivity from 1.26 Wm^{-1}K^{-1} to 4.17 Wm^{-1}K^{-1} for a temperature range of 634°C to 2388°C. With this in mind, Chen et al. [176] reported that the thermal capacity of the char layer did not influence their pyrolysis model results (mass loss and temperature profiles) in which they studied three different charring materials. Since a sensitivity analysis will be conducted, the impact of these measurements on the model response will be examined.

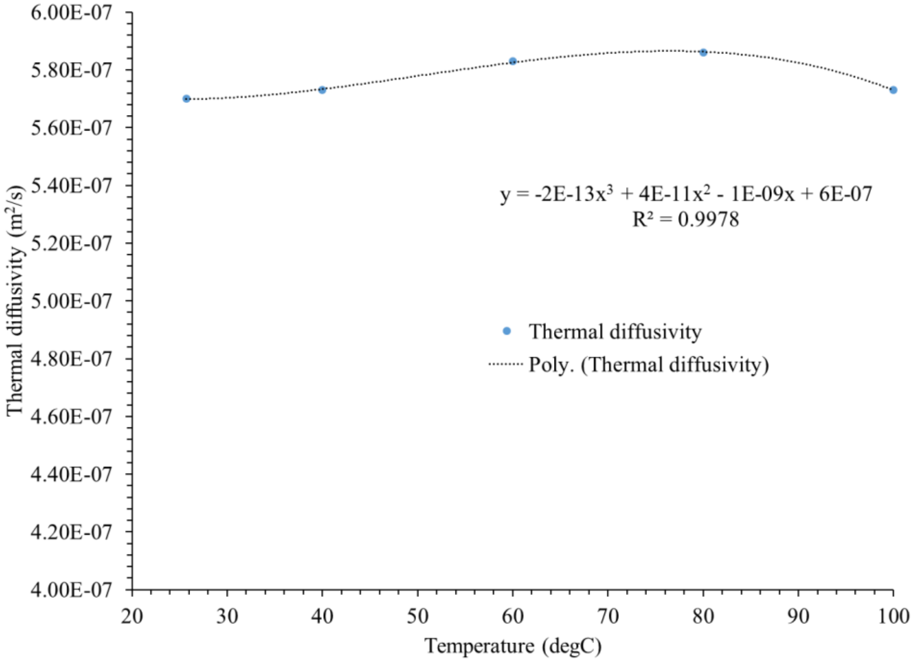

Figure 73. Thermal diffusivity of PF char.

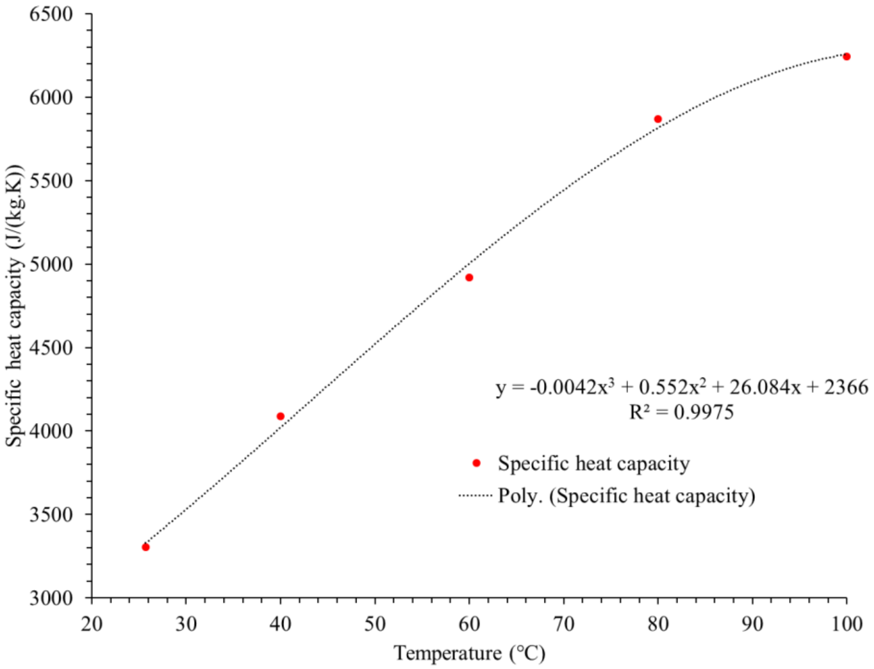

Figure 74. Specific heat capacity of PF char

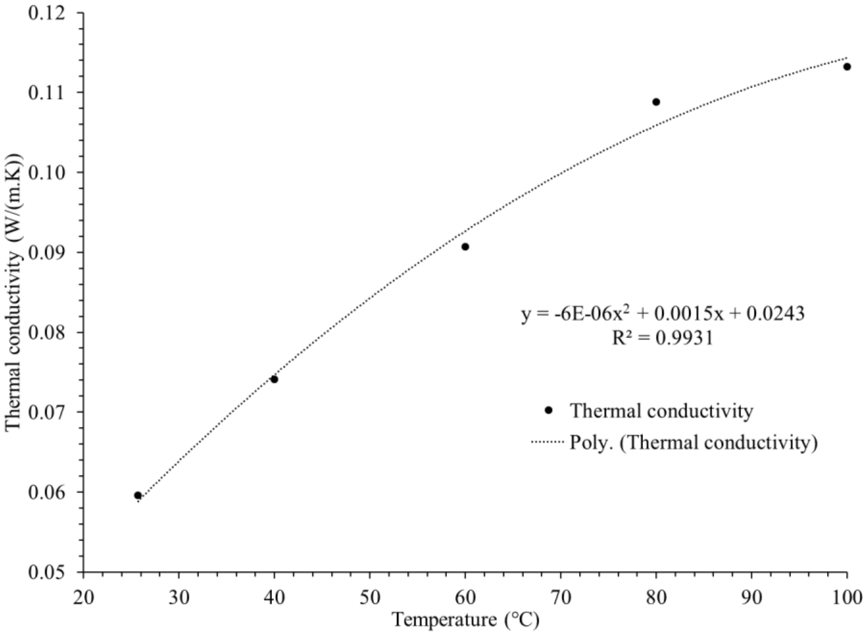

Figure 75. Thermal conductivity of PF char.

The measured emissivity (ε_s) of the painted virgin PF was 0.94 and it was taken as constant.

The heat of combustion (h_c) was extracted as 16 MJkg^{-1} from Hidalgo et al. [252] who determined it based on the cone calorimeter heat release rate and experimental mass loss of a typical phenolic foam.

No data was found in literature for the specific heat of decomposition gases for phenolic foam, therefore, it was estimated from values which have been used for phenolic ablative materials such as silica-phenolic [249] 2390 + T Jkg^{-1}K^{-1} where T is in °C. Similarly, the enthalpy of reaction (Q) was taken as -418,7 Jkg^{-1} from the same reference. Other properties that are complex to determine are the permeability as well as the dynamic viscosity of the gases. The permeability was assumed constant with a value of 1.60E-11m^2 extracted from a database known as the Theoretical Ablative Composite for Open Testing (TACOT v.3) material [347]. It is noteworthy that, since PF is a closed-cell foam, normally at ambient conditions its permeability is zero. However, due to its fire behavior when exposed to an external heat flux, the closed cells break and the permeability changes with temperature. The dynamic viscosity was assumed to be that of air and it was taken from the COMSOL Multiphysics® database.

To simulate the rate of decomposition of the material, the Arrhenius parameters (*E, A* and *n*) are required. These parameters will be determined in the next section.

3.4.3.b. Kinetics of thermal decomposition of PF

The thermal stability of PF under air is of interest in this study given that no flame was present on the surface therefore it is assumed that the oxygen would interact with the surface leading to the oxidation of the char. For the determination of the Arrhenius parameters i.e. the activation energy, the pre-exponential factor (A) and the reaction order (n), a Thermokinetics software package from Netzsch [155] was implemented. The thermal decomposition of PF was studied at different heating rates (2, 5, 10, 20 °Cmin^{-1}) under air. Assuming a one-step nth order reaction, the comparison between the experimental and kinetic model decomposition DTG curves for PF is shown in Figure 76 and the obtained values for the Arrhenius parameters are shown in Table 15. The main peaks are not captured but the kinetic model remains acceptable for engineering purposes.

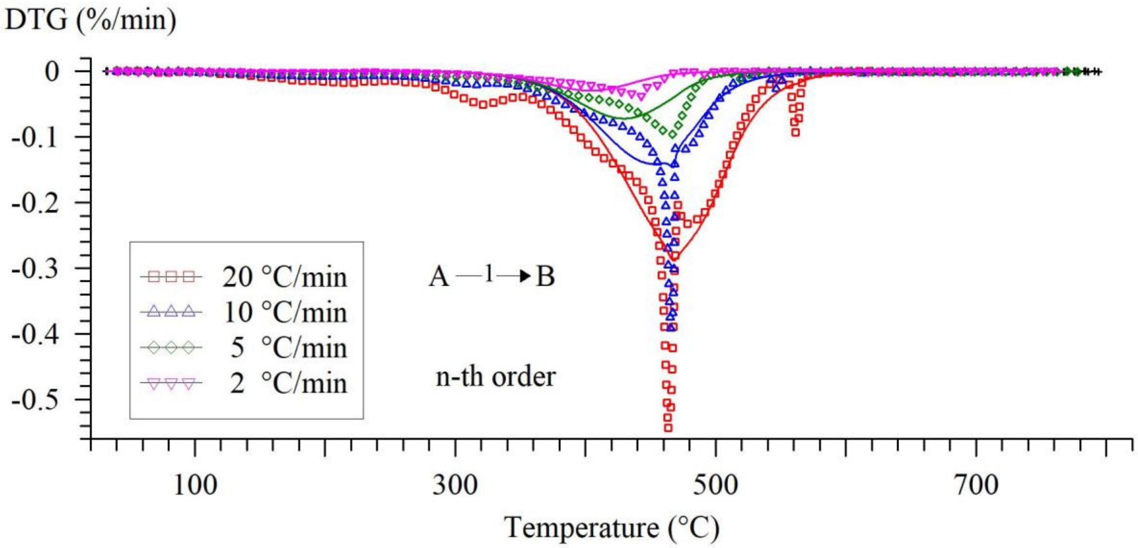

Figure 76. Comparison between the experimental (symbols) and kinetic model decomposition (solid) DTG curves for PF.

Table 15.Kinetics of decomposition of PF assuming a one-step nth order reaction.

Material	**Reaction**	**log A (s^{-1})**	**E($kJmol^{-1}$)**	**Reaction order**
PF	1	7.26	132.30	1.43

Alonso et al. [348] obtained values of activation energy which varied from 100 $kJmol^{-1}$ to 160 $kJmol^{-1}$ as a function of mass loss for phenolic resin using the Flynn-Wall-Ozawa method under an air atmosphere. It is consistent with the present results.

3.4.3.c. Surface recession profile

Figure 77 shows the surface recession profile of the PF obtained during the experiment using the IR camera as detailed in Chapter 2. The ablation of the material occurs generally in four steps with different surface recession rates i.e. between 0s – 240s, 240s – 400s, 400s – 480s and finally 480s – 600s. The surface recession profile is dependent on the physical and chemical phenomena that are occurring on the surface and eventually in the thickness of the material. The surface recession rate is almost constant towards the end of the experiment probably because most of the virgin material would have converted to char and the pyrolysis front is near the steel plate which is in contact with the chilled sample holder. The final thickness after 600s is 38.3mm. The surface recession profile is used to simulate the ablation of PF in the numerical model.

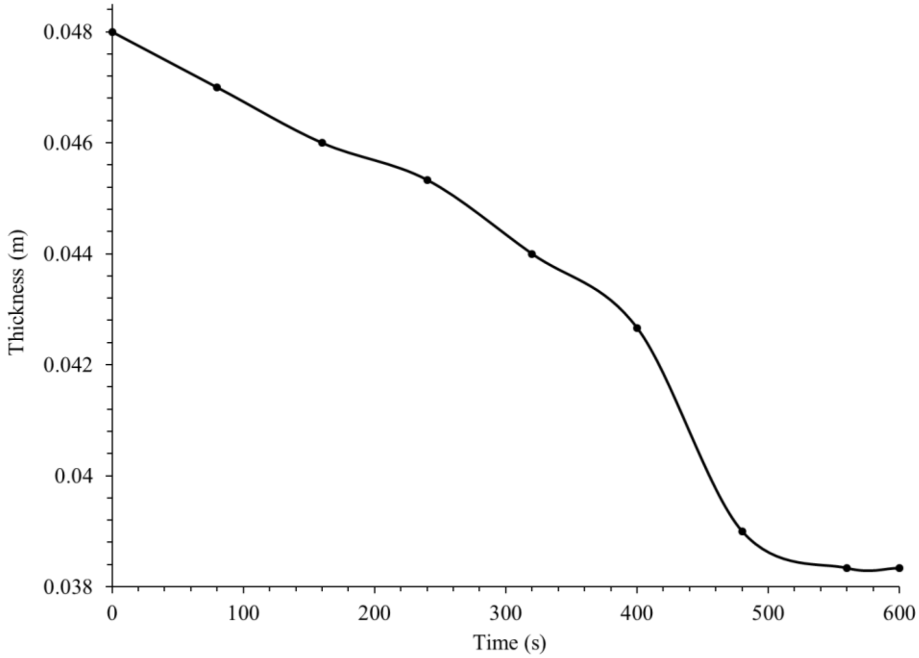

Figure 77. Surface recession as a function of time.

3.4.4. Comparison of experimental and predicted results

Figure 78 shows the comparison of the experimental and predicted temperature profiles of PF at different in-depth locations. The maximum standard deviation between three repeated experiments for TC1 during the first 200s seconds is 6.23°C and that for TC2 during the first 300s is 11.81 °C. Moreover, the uncertainty in the thermocouple positioning is estimated as ±3mm. On the experimental temperature profiles, TC1 increases steadily from 40s up to around 100°C (t=146s) where a plateau is observed. The plateau is attributed to the evaporation of water. Just after this phenomenon at around 158s, a sharp rise in temperature is observed. This temperature rise can be attributed to the coupled physical and chemical processes occurring both at the surface and in the thickness of the material. These processes include smoldering combustion at the surface, surface ablation and the irregular cracking at the surface which propagates into the material. These phenomena increase the flow of heat into the material as well as the decomposition rate of the material. TC2 follows the same trend and a steady temperature rise is observed at 170s, however, the sudden rise in temperature is observed later at 338s. This is because at this point the surface, pyrolysis front as well as the cracks would have progressed into the material towards the underlying material and location of the thermocouple [295, 333, 349].

As shown on Figure 78, the model can only capture the temperature changes at short times. For TC1, it predicts the temperature up to the point where the plateau is observed. Afterwards the plateau is not predicted given that the moisture transport is not included in the model. The surface phenomena related to smoldering was taken into account in the model but the sudden temperature rise could not be captured probably because of the cracking of the surface. For TC2, the model is able to predict the temperature profile up to approximately 170s. After 170s, the temperature rise is not captured by the model and the model underpredicts the temperature. This is also attributed to the cracking that is not taken into account in the model. Moreover, given the estimated uncertainty in the thermocouple positioning, the model can be considered satisfactory since it is consistent with the experimental results within a given range of time. With this in mind, the numerical model can be validated within the time range before the cracking is observed. Although, at times higher than 146s, there is no agreement, it is however adequate to implement the model for sensitivity studies and in the conceptualization of typical fire barriers. It can be concluded that the onset of pyrolysis, which is the main cause of cracking, initiates the failure of the PF.

Indeed, a model including the thermomechanical and hygrothermal behavior of PF would yield better predictions. Several studies have attempted to explain and numerically model the phenomena involving the fire thermo-mechanical response of phenolic-based composites as well as their hygrothermal behavior [53, 350]. However, modeling the structural response of a material is complex and requires the thermo-mechanical properties of PF and it is beyond the scope of this study.

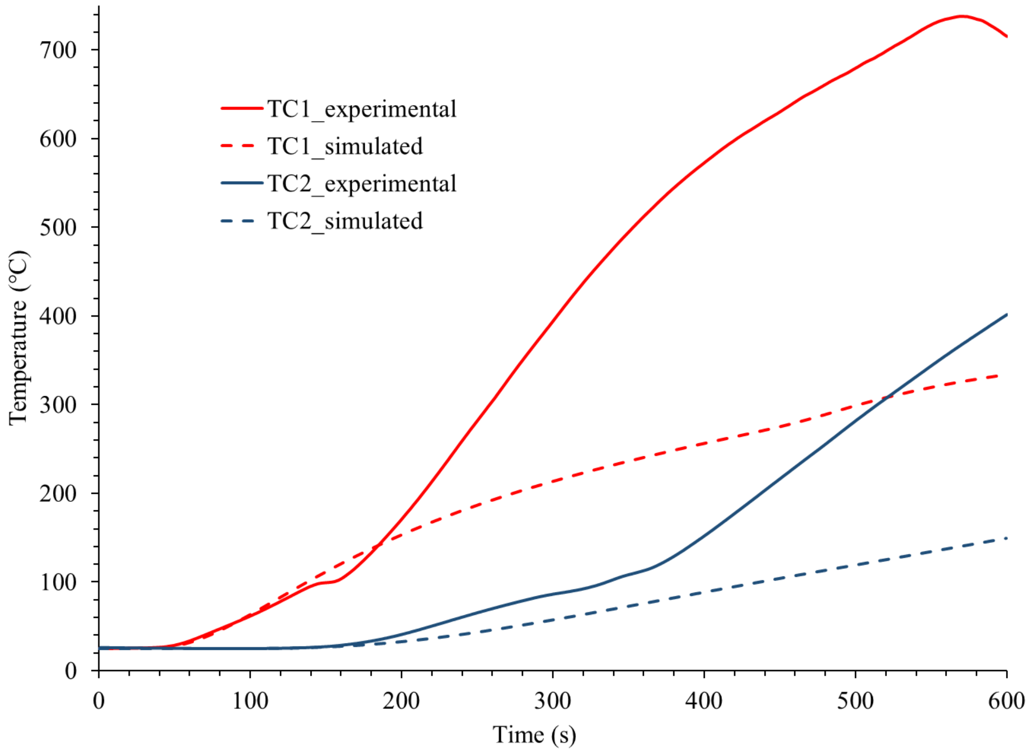

Figure 78. Comparison of experimental and predicted results for PF exposed to a radiative heat flux of 25kWm^{-2}.

In this section, the fire behavior of PF was modeled. The predicted results were confronted with the experimental results and it was concluded that the numerical model is valid within a certain time frame as discussed above. However, for the purposes of conducting a sensitivity analysis that includes all the physical phenomena defined in the numerical model, the model is assumed to be valid for the duration of the simulation.

3.4.5. Sensitivity study

Given the assumption mentioned above, the sensitivity analysis on the PF was based on TC1 and TC2 with respect to the selected input parameters and it is shown in Figure 79 and Figure 80 respectively. A perturbation of +10% is applied on all the parameters. It is shown that virgin properties i.e. ρ_v, C_{pv}, k_v, and ε_s are the most sensitive parameters. Gathering ρ_v, C_{pv} k_v gives the influential role of the virgin thermal diffusivity on the temperature profiles. In both the figures, the change in temperature (ΔT) begins to rise after approximately 20s and 160s for TC1 and TC2 respectively due to the low diffusivity of PF. This corresponds to the temperature profiles for TC1 and TC2 shown in Figure 78. The virgin properties $(\rho_v, C_{pv}\ k_v)$ control the rate of temperature rise in the material as observed by their sensitivity transients. ΔT is also sensitive to ε_s because it plays the role of controlling the amount of external radiative heat flux absorbed by the material. Similar observations using the surface temperature as the sensitivity target were reported by Chaos [16] for a charring material and they were attributed to the pyrolysis/charring process being relatively slow at an external radiative heat flux of 25kWm^{-2}. Moreover, the ablation rate (*abl*) is also an important parameter that influences the model response.

The global response of the model using the maximum temperature change w.r.t to the input parameters is presented in Figure 81. The negative signs on the histogram indicate that a 10% increase in the respective parameter will result in a decrease in the maximum temperature value (ΔT_{max}). The sensitivity of ΔT_{max} w.r.t. ρ_v, C_{pv}, k_v, ε_s, ρ_c, C_{pc}, k_c and *abl* decreases from TC1 to TC2 indicating that the sensitivity study is dependent on the location of the thermocouple.

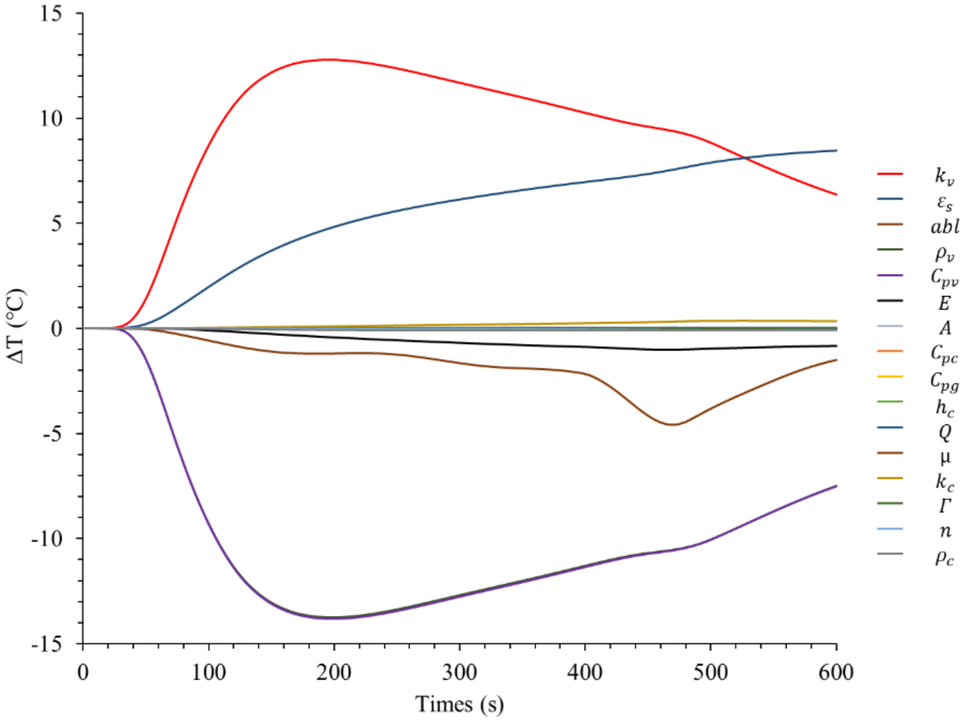

Figure 79. Sensitivity of TC1 with respect to (w.r.t) the input parameters for PF.

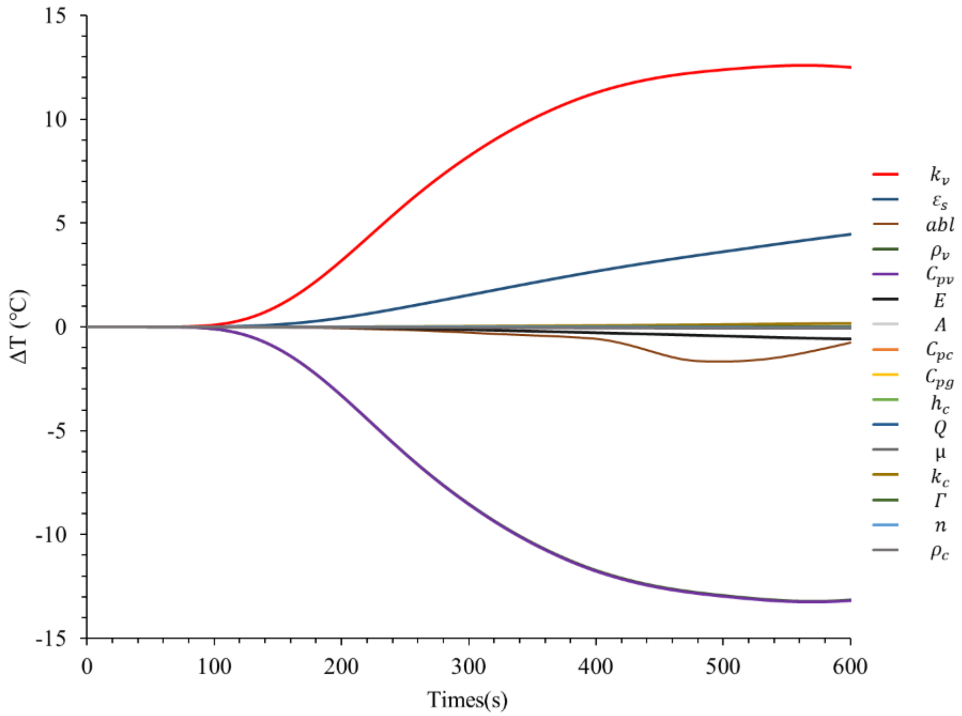

Figure 80. Sensitivity of TC2 with respect to (w.r.t) the input parameters for PF.

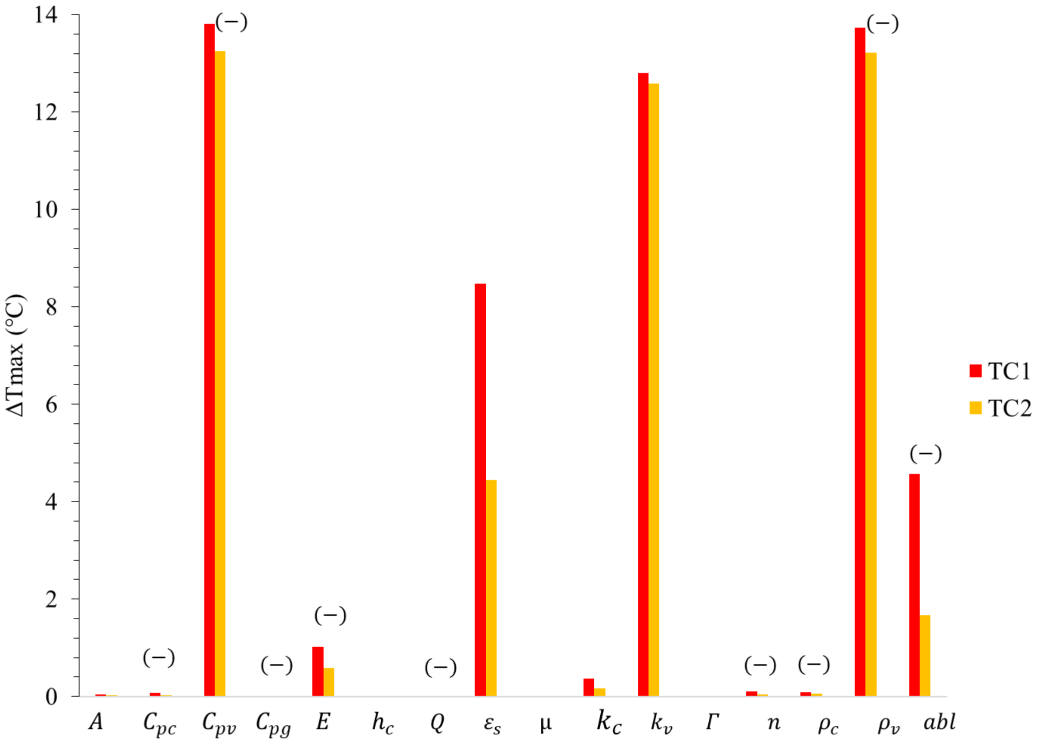

Figure 81. Maximum temperature change sensitivity to the input parameters for PF.

The fire behavior of PF was modeled and a sensitivity analysis to understand the influence of the input material parameters on the model response was conducted. PF chars and ablates resulting in surface recession when exposed to an external radiative heat flux. Given the complexity of its fire behavior, the applicability and the limitations of the numerical model were discussed. In the next section, the fire behavior of a silicone-based intumescent coating (SBIC) is described.

3.5. Silicone-based intumescent coating

3.5.1. Experimental study

SBIC is a passive fire protection coating which expands to form an insulative char layer of low conductivity thereby protecting the substrate when exposed to a thermal stress. As compared to PF, it presents a complexity in numerical modeling due to the intumescent phenomenon (large expansion). To study the fire behavior, the coating was exposed to an external heat flux of 50 kWm^{-2}. The tests for the SIBC were conducted at 50 kWm^{-2} because at this heat flux, it exhibited considerable expansion and good perfomance. The experimental set-up is shown in Figure 82 and the thermocouples used to record the temperature gradients in the SBIC (TC1 and TC2) are inserted into the coating in a vertical position through a drilled hole at the center of the steel plate (see Figure 82). TC1 is initially in air at 15mm from the backside of the steel plate. TC2 is embedded in the SBIC at 5mm from the backside of the steel plate. TC3 is welded at the backside center of the steel plate and TC4 is inserted at 25mm from the backside surface of the calsil block.

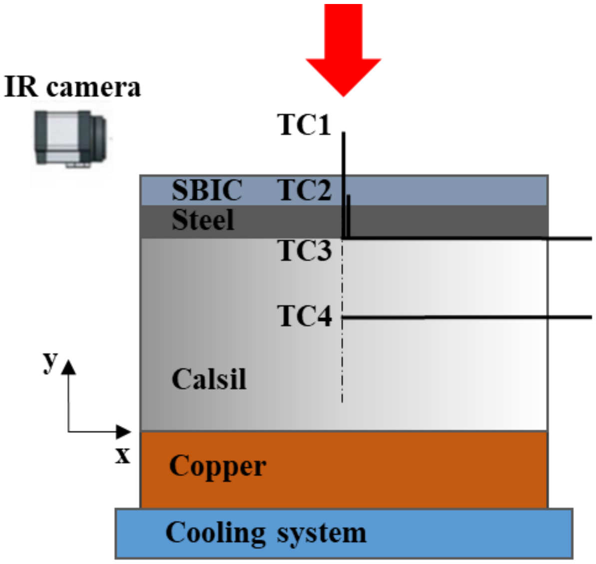

Figure 82. Experimental set-up for SBIC exposed to a radiative heat flux of 50 kWm^{-2}.

3.5.1.a. Post-test visual observations

Table 16 shows pictures of the expansion of SBIC as a function of time. During the first few seconds, SBIC begins to expand with noticeable worm-like structures due to the expandable graphite. Around 82s ± 20s, the coating ignites and a white layer is formed. The white layer is assumed to be silica [270].

Table 16. Expansion of SBIC

t=60s	**t=450s**	**t=900s**
		

The flame observed on the surface slowly fades away up to around 664s ± 14s. As it fades away, the flame can be seen as attached on some cracks (see Table 16 (t=450s)). During the experiment, the SBIC continues to expand up to a maximum thickness and the experiment is stopped at 900s.

Even though no temperature information was deduced from the infrared camera, it allowed to capture the expansion of the SBIC as shown in Figure 83.

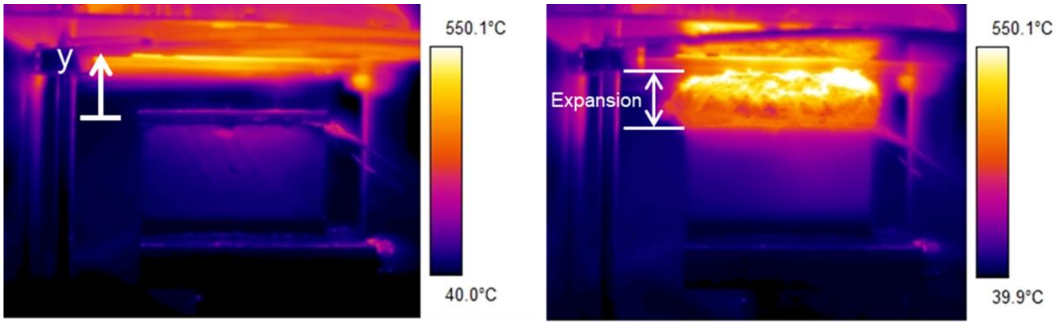

(a) (b)

Figure 83. Infrared images for SBIC at (a) t=0s and (b) t=900s.

The final cross-section of the char is shown in Figure 84(a) and is composed of top white layer and the bulk char. The bulk char is mainly composed of expanded graphite embedded in the complex silicone degraded matrix [56, 270]. Moreover, cracks which limit the fire performance of the SBIC under an external radiative flux are observed on the surface of the char (Figure 84(b)).

These cracks are assumed to be caused by the high vibration energy of Si-O bond that occurs in the infrared field [267, 270].

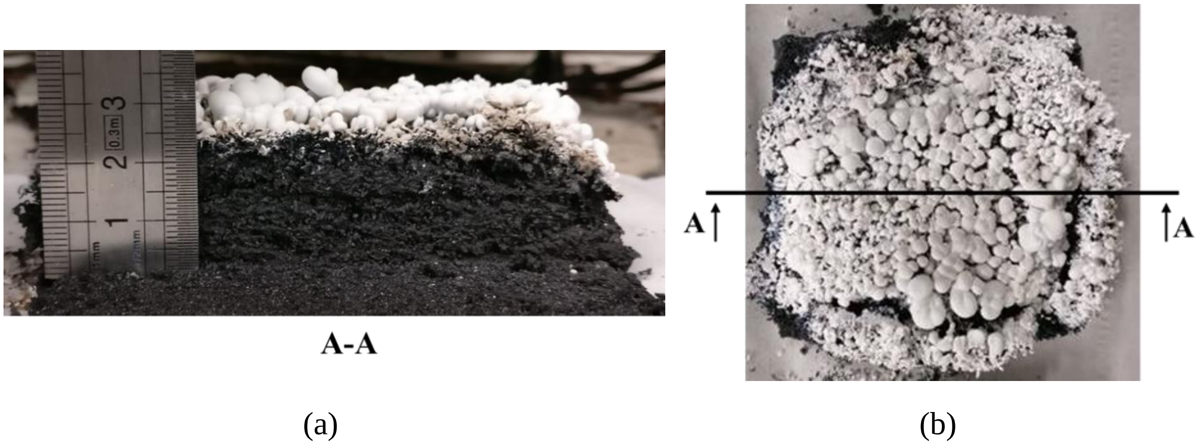

(a) (b)

Figure 84. (a) Cross-section and (b) surface of SBIC after 900s of heat exposure.

3.5.1.b. Fire performance

Figure 85 shows the experimental temperature-time curves at the center backside of the uncoated and coated steel plates. The temperature of the uncoated steel plate rises up to a steady state at approximately 600 °C whereas that of the coated steel rises up to a maximum of around 400°C demonstrating the physical barrier properties of the coating. A sharp linear increase in the temperature around 450s is observed for the coated steel plate even though we would expect it to reach a steady state since the char layer is near full expansion. It should be noted that after 900s the SBIC had reached its maximum thickness (see Figure 92). This behavior is attributed to the cracking of the SBIC which enhances heat transfer into the material.

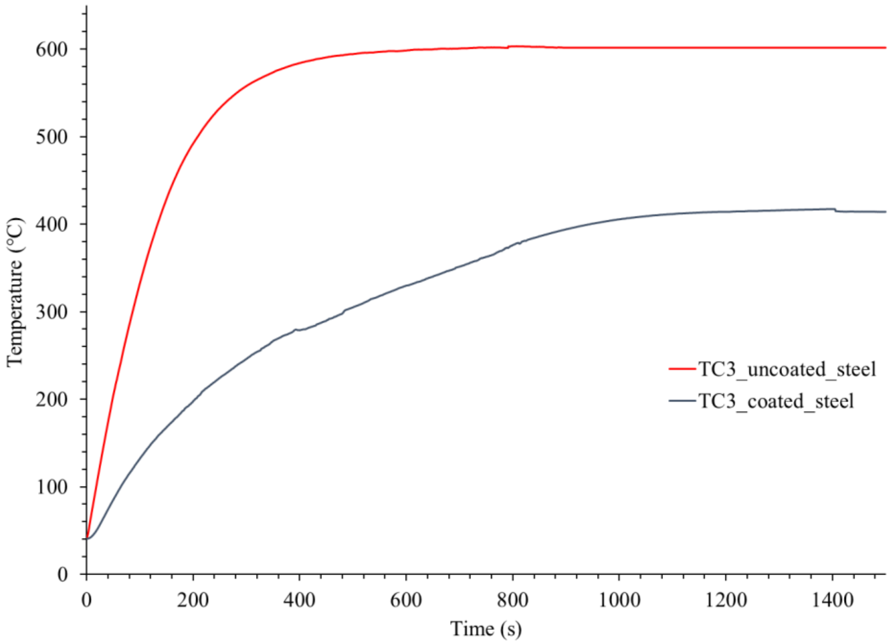

Figure 85. Experimental temperature profiles at the center backside of the uncoated and coated steel plates when exposed to an external heat flux of 50 kWm^{-2}.

3.5.1.c. Thermal stability of SBIC

Figure 86 shows the TG and DTG curves of SBIC at 10°Cmin^{-1} under a nitrogen atmosphere. It is observed that there are two main mass loss steps. The first mass loss step occurs between 170°C and 270°C and the second between 390°C and 670°C. The first step can be attributed to the release of oligomers of silicone and the second step is attributed to the release of aromatic compounds from the silicone resin as reported by Gardelle et al. [267]. The SBIC exhibits a 45.8 % residue at 800°C.

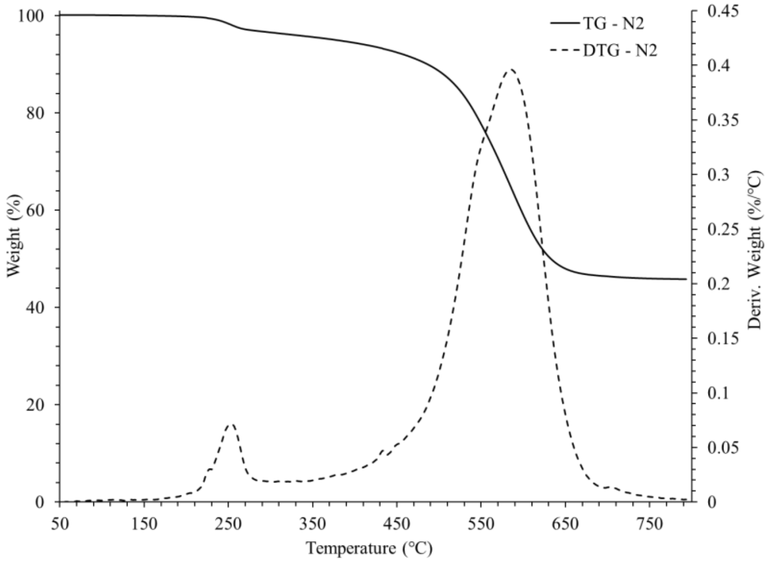

Figure 86. TG and DTG curves of SBIC at 10°Cmin^{-1} under a nitrogen atmosphere.

3.5.2. Numerical model

3.5.2.a. Model assumptions

In a similar way as for the modeling of the fire behavior of PF, the main objective of this study was to develop a 2D model gathering the fundamental governing equations for the heat transfer phenomena involved when SBIC is exposed to fire. Given the complexity of the coupled phenomena observed during the experiments a phenomenological approach was implemented and several assumptions were made in order to minimize the number of input model parameters. From the experimental analysis conducted above, the 'intumescence' phenomenon was considered as a heat transfer problem with a moving boundary in our mathematical formulation. The expansion of the SBIC was assumed to be homogenous and occurring in one dimension i.e. the y-axis. Moreover, the numerical model was developed in the view of investigating the sensitivity of the modeling results with respect to the input model parameters.

Using these assumptions, the full model is implemented in COMSOL Multiphysics® using the modules for Heat Transfer, Domain ODEs and DAEs and Deformed Geometry. Finally, the full model is described in the next section.

3.5.2.b. Governing equations

As shown in Figure 82, the experimental set-up is made up of four distinct layers i.e. the copper layer, the calsil layer, the steel layer and the SBIC layer. Only the governing equations for the SBIC layer are described here since those of the other layers have been explained in the previous sections.

Given that it was difficult to determine the char properties of SBIC because the char would easily break, effective properties were implemented. To avoid redundancy and repeating similar equations, Equation 59, Equation 62, Equation 63 Equation 64 were simplified and adapted to the SBIC scenario and Equation 71 was obtained [351].

Equation 71 shows the energy balance in the SBIC layer. The term on the LHS represents the rate of change of internal energy and the first term on the RHS represents heat transfer by conduction while the second term represents the internal heat energy released due the endothermic decomposition processes involving chemical reactions such as the rapid sublimation of sulfuric acid involved in the expansion of the graphite worms [352]. The decomposition process is modelled using an Arrhenius equation and assuming a nth order reaction. This is indeed a crude assumption; however, it minimizes the number of Arrhenius parameters to be determined. It gathers the fundamental parameters i.e. the activation energy, the pre-exponential factor (A) and the reaction order (n) on a one-step basis and it is adequate for identifying their influence during sensitivity studies. Moreover, other studies have successfully modeled intumescence by assuming a one-step first order reaction [13, 274, 353, 354]. Mequita et al. [353] used a first order reaction to model the intumescent behavior of two coatings exposed to an external radiative heat flux from a cone calorimeter. The model was capable of providing a reasonably good prediction of the temperature at the rear surface of the steel plate. Similarly, Gillet et al. [274] implemented a one-step first order reaction in their mathematical model for the prediction of temperature and mass loss of an intumescent coating exposed to fire and Boiling Liquid Expanding Vapor Explosion (BLEVE) scenarios. The model was able to simulate the back surface temperature profile and mass loss with accuracy. The energy transferred due pyrolysis gas mass diffusion was not considered because it was assumed that the gases escape immediately through the entangled network of graphite worms without any interaction. In addition, this assumption is further reasonable when cracks are formed.

$$\rho_s C_p \frac{\partial T}{\partial t} = \nabla.(k.\nabla T) + \rho_0 Q A e^{-\frac{E}{RT}} (1-\alpha 1)^n \qquad \text{Equation 71}$$

In the case of SBIC, effective properties are implemented given that the char properties were difficult to determine because the residue easily broke and it was fragile.

3.5.2.b.i. Initial and boundary conditions

For the exposed surface, the boundary condition given in Equation 47 is implemented for SBIC as a starting point. It is then numerically adapted to take into account the effect of expansion on the surface-to-surface radiation heat exchanges between the surface of the cone heater and the moving exposed surface. Moreover, a condition to take into account the heat feedback from the combustion flame is implemented by adding the flame heat flux (q_f) to the RHS of Equation 47 resulting in Equation 1.

$$q_{net} = \varepsilon_s \sigma (F T_r^4 + (1-F) T_{amb}^4) - \varepsilon_s \sigma T^4 + h_h (T_{amb} - T) + q_f \qquad \text{Equation 72}$$

The condition is added based on the visual observation of the ignition and flame off time which was discussed earlier. No conventional way was found in the literature concerning the treatment of the convection term in the presence of a flame on the sample surface. It has been implemented either by modifying the radiative and convection terms, adding q_f or using a flame temperature [13, 355-357]. Therefore, it remains the choice of the modeler to include it in the model or not.

Most of the time, in pyrolysis models, q_f, is taken between 10 kWm^{-2} to 20 kWm^{-2} [8, 11, 356, 358]. In this case, considering that the flame was small, a value of 10 kWm^{-2} was chosen. A condition was implemented for q_f to be applied from 80s (ignition time) up to 664s (flame off) based on visual observation.

The boundary condition on the sides that is given in Equation 48 is also used for SBIC and at the back side of the copper plate, a Dirichlet boundary condition is imposed as T=40°C. The initial condition is set as T=40°C i.e. the temperature of all the materials.

The complete computational mesh used was composed of 2900 quadrilateral elements with a maximum element size of 0.002m, a minimum element size of 7.5 x 10^{-6}m and an average element quality of 0.9999. Figure 87. shows the mesh quality of the (a) initial (t=0s) and (b) final mesh after t=900s respectively. Likewise, in Figure 87 , the position of the mobile mesh is shown at (a) t=0s and (b) t=900s.

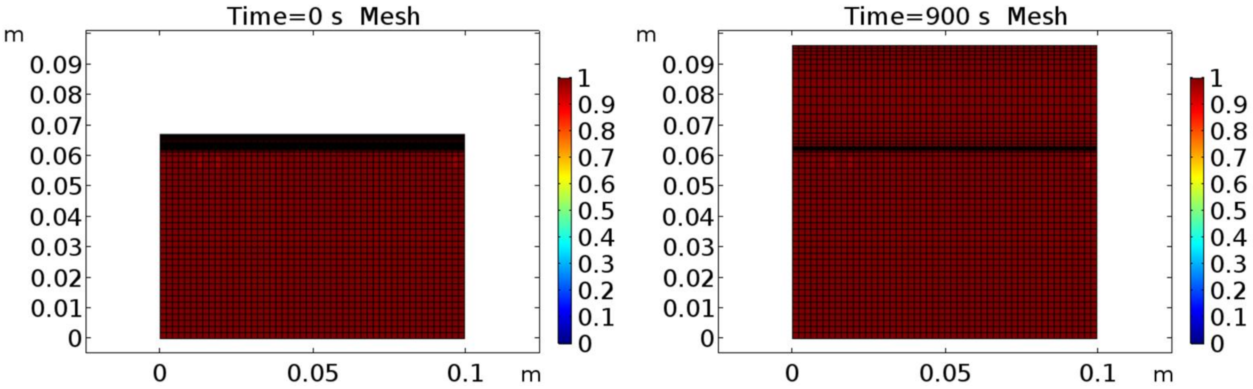

Figure 87. Mesh quality of the (a) initial mesh and (b) final mesh after t=900s.

Having defined the governing equations and the accompanying initial and boundary conditions, the relevant input properties were determined and are presented in the next section.

3.5.3. Thermophysical properties

3.5.3.a. Thermal properties

The measured thermal properties of SBIC are shown in Figure 88, Figure 89, Figure 90. Figure 88 shows the thermal diffusivity of virgin SBIC as a function of temperature up to 150°C. The thermal diffusivity decreases from room temperature up to 150°C. Lucherini and Maluk [359] also reported thermal diffusivity values of an intumescent coating that were decreasing from 2.45×10^{-7} m^2s^{-1} at 30°C to 1.2×10^{-7} m^2s^{-1} at 245°C.

Figure 89 shows the specific heat capacity of virgin as a function of temperature. Values in the same order of magnitude have been obtained for intumescent coatings in the literature [360]. Moreover, Lucherini and Maluk [359] reported specific heat capacity values that increased from 1293 $Jkg^{-1}K^{-1}$ at 30°C to 1686 $Jkg^{-1}K^{-1}$ at 245°C.

Figure 90 shows the thermal conductivity of SBIC that was obtained using the comparative method. The thermal conductivity decreases from around 0.60 $Wm^{-1}K^{-1}$ at ambient temperature to 0.48 $Wm^{-1}K^{-1}$ at 150°C. Similar thermal conductivity values for silicone-based coatings were reported in literature [56, 271].

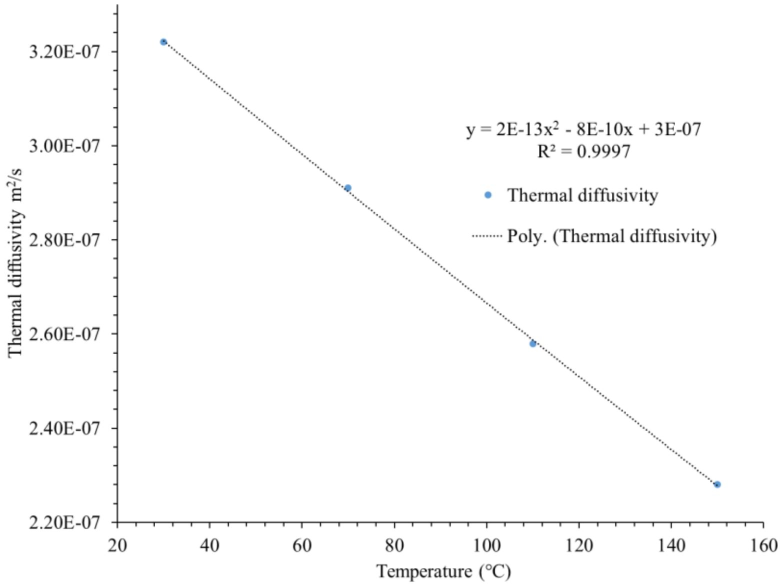

Figure 88. Thermal diffusivity of virgin SIBC.

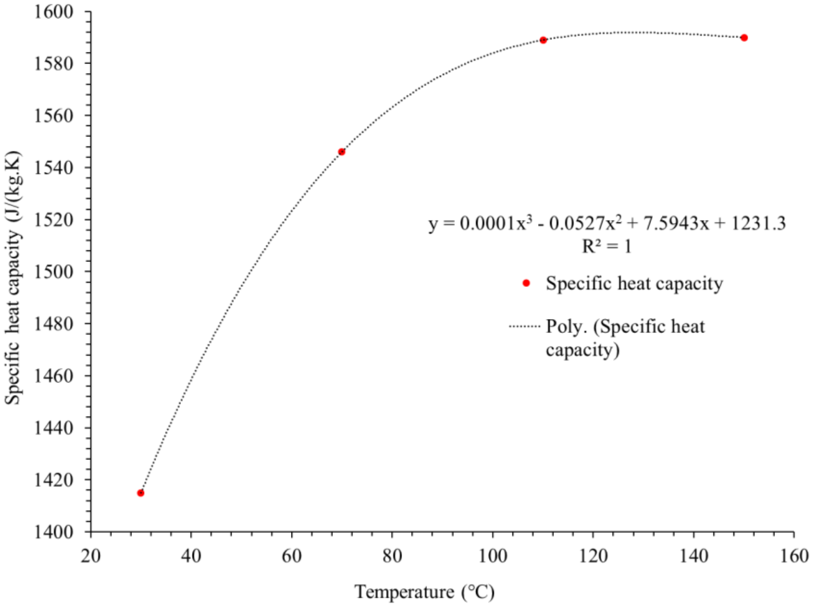

Figure 89. Specific heat capacity of virgin SBIC.

Bourbigot et al. [271] reported that the thermal conductivity of a silicone-based coating decreases from 1Wm^{-1}K^{-1} at ambient temperature to 0.35 Wm^{-1}K^{-1} at 300°C and increases up to 0.45 Wm^{-1}K^{-1} at 700°C, consequently, in this study, for temperatures higher that 150°C, the thermal conductivity is assumed constant at 0.47 Wm^{-1}K^{-1}. This is physically acceptable given it is in the same order of magnitude as the values previously reported in literature. A similar assumption is also applied the specific heat capacity above 150 °C.

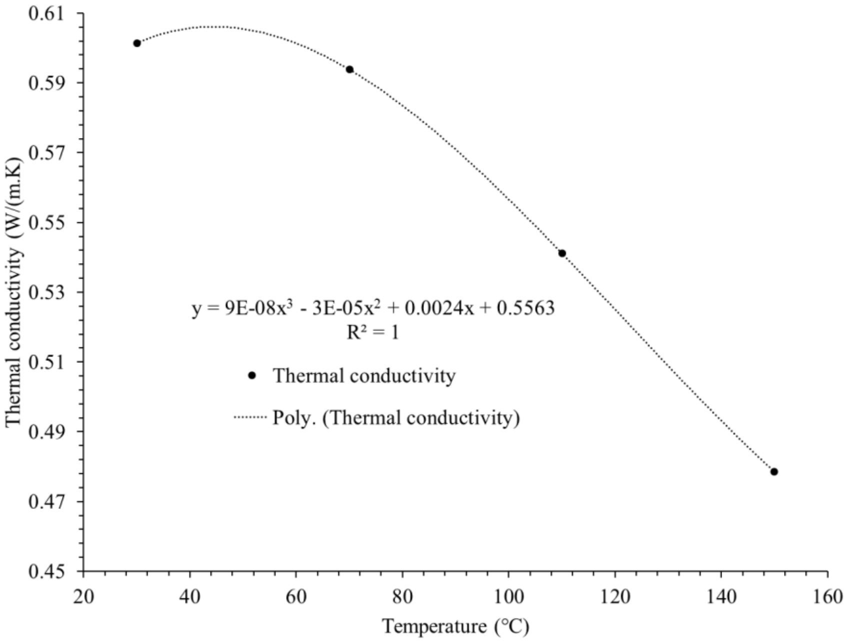

Figure 90. Thermal conductivity of virgin SBIC.

The measured emissivity of virgin SBIC was obtained as 0.914 from the method described in Chapter 2.2.2.e. As observed after the experiment, the surface of SBIC had white powder which signified the change in the emissivity, it was however not taken into account and a constant value was used. The density of the virgin SBIC was estimated as 1320 kgm^{-3}.

To simulate the rate of decomposition of the material, the Arrhenius parameters (*E, A* and *n*) are required. These parameters will be determined in the next section.

3.5.3.b. Kinetics of decomposition of SBIC

The thermal decomposition of SBIC was studied at different heating rates (1, 5, 10 and 20°Cmin^{-1}) under a nitrogen atmosphere. As mentioned earlier, a one-step nth order reaction was assumed and the Arrhenius parameters i.e. the activation energy (E), the pre-exponential factor (A) and the reaction order (n) were determined using a thermokinetics software package from Netzsch [155]. The comparison between the experimental and kinetic model decomposition DTG curves for SBIC is shown in Figure 91 and the obtained values for the Arrhenius parameters are shown in Table 17. The kinetic model can successfully capture the main mass loss step and this validates the assumption of the one-step nth order reaction.

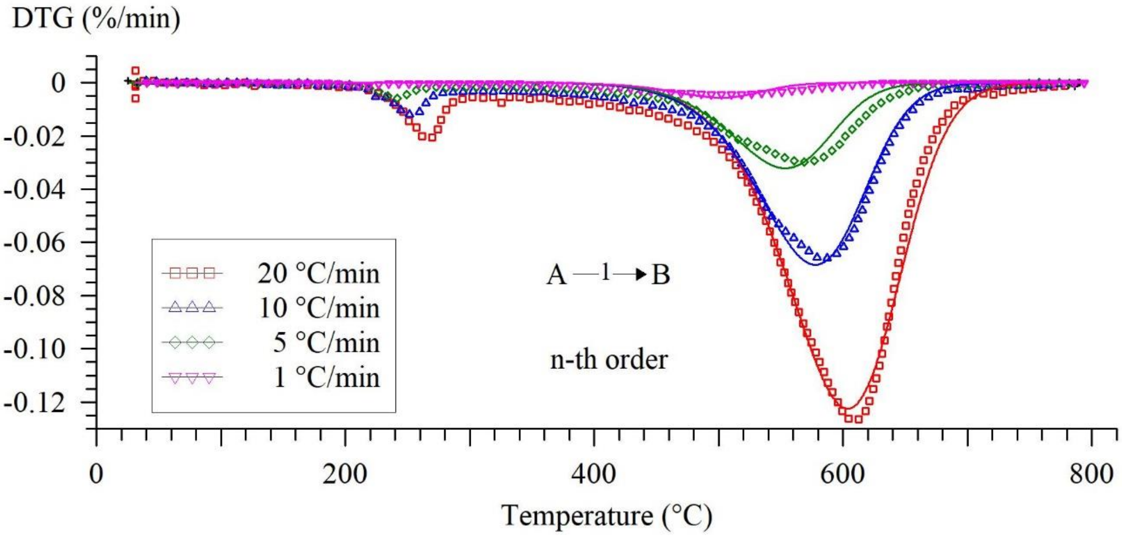

Figure 91. Comparison between the experimental (symbols) and kinetic model decomposition (solid) DTG curves for SBIC.

Table 17.Kinetics of decomposition of SBIC assuming a one-step nth order reaction.

Material	**Reaction**	**log A (s^{-1})**	**E($kJmol^{-1}$)**	**Reaction order**
SBIC	1	7.012	153.17	1.23

The enthalpy of reaction (Q) was extracted from literature as -6.31x10^{-5}Jkg^{-1} [360].

3.5.3.c. Expansion profile

The expansion profile of SBIC is shown in Figure 92. The expansion occurs in three steps; the first between 0 and 300s were the expansion increases quite steadily with a high expansion rate, then slows down up to 450s around 580%. The expansion then increases again after 560s to reach its maximum of around 729%. The high expansion rate during the first step is attributed to the fast expansion of the graphite ‘worms’. The expansion rate slows down because the char layer would have been formed and the underlying virgin SBIC is protected from the external radiative heat flux probably slowing down the rate of decomposition even though there are cracks on the surfaces. This process continues with a lower rate until the maximum expansion is reached and all the virgin SBIC is converted to char.

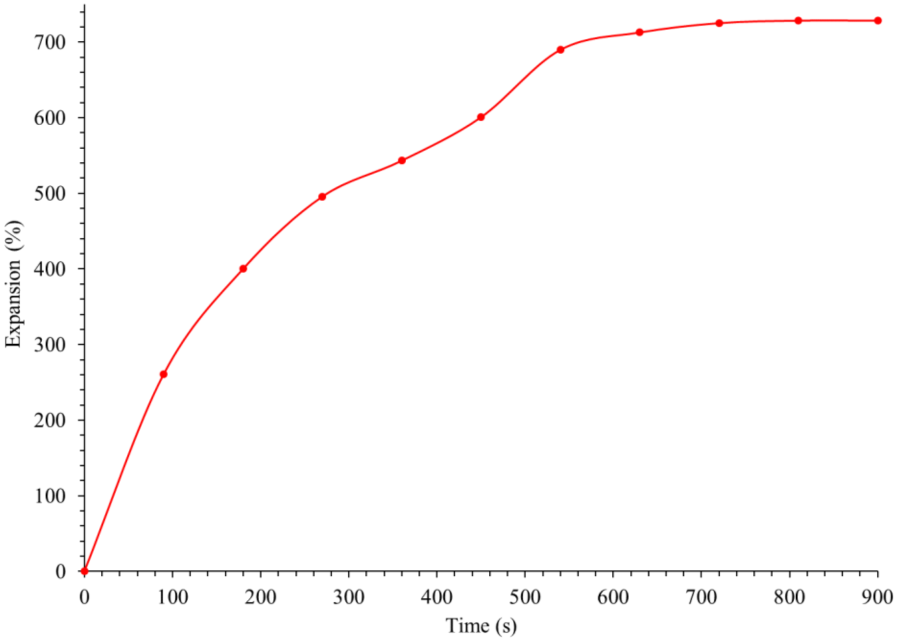

Figure 92. Expansion of SBIC as a function of time.

3.5.4. Comparison of experimental and numerical results

Figure 93. compares the experimental and predicted temperature profiles at different thermocouple locations in the SBIC. At the beginning of the test, TC1 is in air and the reading starts at 110s; this is the moment when the expanding SBIC reaches the position of the thermocouple TC1. At this point, TC1 begins to get covered by the expanding coating and the temperature starts to decrease up to approximately 450°C. The temperature decrease is attributed to the barrier of the expanding insulative char. For the temperature profiles TC2 and TC3, from 0s to 140s (<220°C), the heat transfer is assumed to be pure conduction and it is hence governed by the radiative heat source, thermal diffusivity and expansion of the coating. Moreover, the onset of thermal decomposition is observed from around 220°C (Figure 86) corresponding to approximately 140s on Figure 93. Generally, from 450s and onwards, the temperature profiles of TC1, TC2 and TC3 tend to increase rapidly which is surprising since we would expect that they should be reaching a steady state given that the char layer is near full expansion. The rapid increase in temperature is attributed to the cracking of the SBIC which was previously explained.

As for the comparison, for TC1, the numerical model generally underpredicts the temperature profile. However, the shape of the curve is coherent with the experimental results up-to approximately 450s. The underprediction can be attributed to the cracking of the SBIC (which is not taken into account in the model) and the uncertainty in the thermocouple position. To confirm this statement, it should be noted that a sensitivity analysis was conducted on the effect of the thermocouple position and it was found that a perfect fit up to 450s is achieved at 18mm. For TC2 and TC3, an excellent agreement is observed for t<450s. In general, the model fails to capture the sudden temperature increase from 450s because of the cracking phenomenon explained previously which is not included in the model.

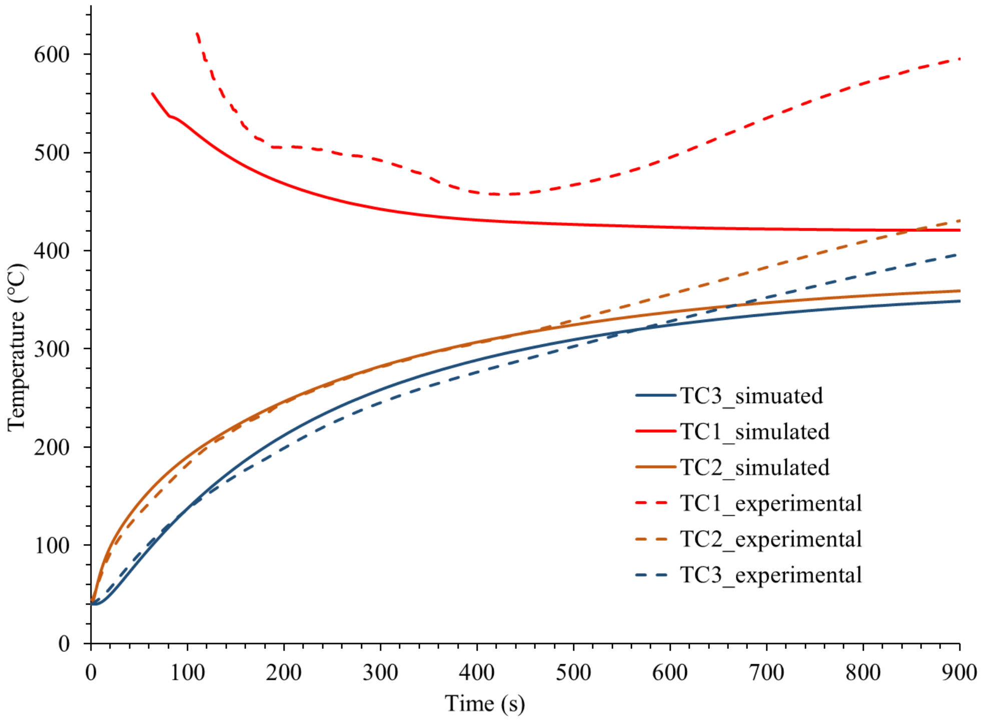

Figure 93. Comparison of experimental and predicted results for SBIC exposed to a radiative heat flux of 50kWm^{-2}.

In conclusion, the presented model showed that it is capable of coherently predicting the temperature profiles when t<450s. For t>450s, the SBIC exhibits cracking and this phenomenon was not taken into account because it is beyond the scope of this work. However, there is a possibility of assuming that from the onset of cracking, the thermal conductivity of the SBIC is altered and therefore a coefficient could be added. Nevertheless, with the given results, the numerical model is adequate for conducting a sensitivity study since it takes into account the main physical processes involved in intumescence.

In this section, the fire behavior of SBIC was modeled. The predicted results were compared with the experimental results and it was concluded that the numerical model is valid up to a certain time frame as discussed above. However, for the purposes of conducting a sensitivity analysis that includes all the physical phenomena included in the numerical model, the model is assumed to be valid for the duration of the simulation.

3.5.5. Sensitivity study

As observed in the previous sections, the sensitivity studies are dependent on the position of the thermocouples. However, for the case of SBIC, its main purpose is to protect the steel plate from reaching failure temperatures [361]. Therefore, only the bottom steel TC3 is considered and the sensitivity of TC3 w.r.t the input parameters is shown in Figure 94. Given that the numerical model is assumed to be valid for the duration of the simulation, the sensitivity analysis is conducted up to t=900s. A perturbation of +10% is applied on all the parameters. The transient sensitivity responses show that $E, \varepsilon_s, k, \rho_0, C_p$ and the expansion rate ($swell$) are the most influential parameters. At early times up to 100s, E does not influence the model response, nevertheless its effect is observed just after 100s and this moment is considered as the onset of the thermal decomposition process. The sensitivity w.r.t E steadily increases from the onset of the thermal decomposition process and becomes important than the other parameters at times higher than approximately 300s. The decomposition process is an endothermic reaction which reduces the amount of energy reaching the back surface of the steel plate therefore any phenomenon that reduces the rate of decomposition causes a rise in the temperature at the back surface of the steel plate. This explains the reason why if E is increased by 10%, there is an increase in the temperature values at the back side of the steel because it slows down the rate of the decomposition process. To confirm this result, it can be observed that the sensitivity w.r.t to the endothermic enthalpy of reaction (Q) is negative for the duration of the simulation. Similarly, for the sensitivity w.r.t $swell$, the change in temperature (ΔT) is negative for the duration of the simulation. This signifies that an increase in $swell$ results in an efficient SBIC which slows down the rise of temperature at the back surface of the steel plate. The sensitivities w.r.t ρ_0, C_p and A exhibit the same behavior and they are also negative for the duration of the simulation. As for the sensitivity w.r.t k, ΔT is positive for the duration of the simulation. ΔT rapidly rises during the first few seconds up to approximately 100s. This can be explained by the fact that between t=0s and t=100s, heat is transferred by conduction in the SBIC. During this phase, the energy accumulated in the material is not sufficient to start the thermal decomposition process. It can also be observed that ΔT reaches a maximum at the onset of the decomposition process and the curve starts to decrease. Moreover, the correlation between the curves of ΔT for k, ρ_0, C_p give an indication of the role of the thermal diffusivity of SBIC. The reaction order, n, has a negligible effect on ΔT.

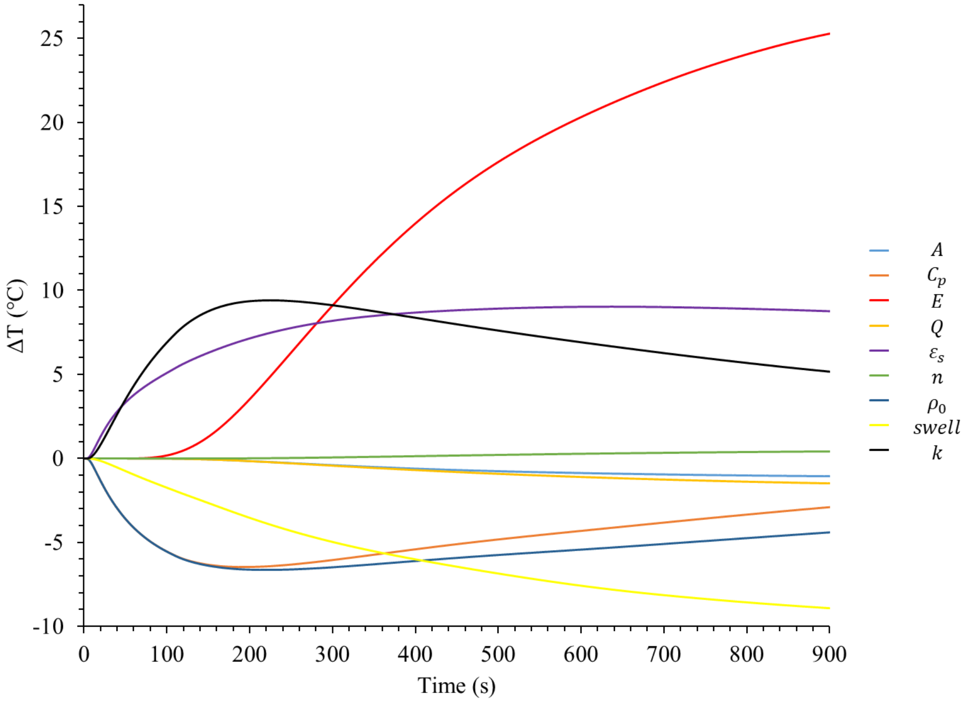

Figure 94. Sensitivity of TC3 with respect to (w.r.t) the input parameters for SBIC.

Global model responses use the maximum temperature change and it is shown in Figure 95. The negative sign signifies that an increase in the parameter results in a temperature decrease. In general, E is the most influential parameter followed by $k, \varepsilon_s, swell, \rho_0, C_p, Q, A$ and n is the least influential parameter.

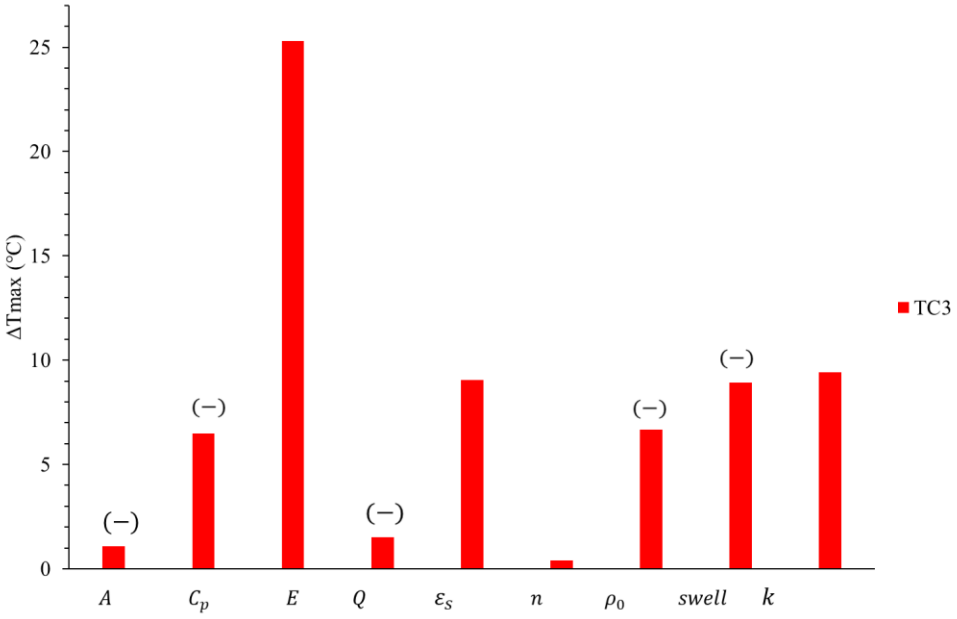

Figure 95. Maximum temperature change sensitivity to the input parameters for SBIC

.

3.6. Conclusion

This chapter focused on modeling the fire behavior of the fire barriers used in this work i.e. calcium silicate (calsil), closed-cell mullite foam (CF), phenolic foam (PF) and a silicone-based intumescent coating (SBIC). The main objective was to develop computational tools that would help in clearly identifying the governing parameters involved in the fire behavior of each fire barrier through sensitivity studies. The chapter was divided into five main parts. The first part was a preliminary study based on the steel plate scenario which was used to determine the optimized boundary conditions of the experimental set-up followed by four detailed studies including the experimental and numerical studies on the fire behavior of the respective fire barriers. The input material properties were obtained from direct measurement and/or literature.

In the first part, i.e. the preliminary study allowed the identification and quantification of the optimized boundary conditions given that all the experimental conditions for this case were well-known. The optimized boundary conditions were then successfully transposed to the other materials assuming the same experimental conditions were kept and given that the experimental set-up was the same throughout. In the second part, the fire behavior of calsil was studied. The same experimental set-up as for the first part was used except that the steel plate was removed and thermocouples were placed in the thickness locations of the material. The main input parameter i.e. the thermal diffusivity of calsil was experimentally determined. The model was capable of predicting the temperature profiles and it was validated through adjusting the thermocouple locations which was justified by the uncertainty as a result of experimental errors in placing the thermocouples during the setting up of the experiment. Finally, a sensitivity analysis was conducted at the three thermocouple positions (TC1, TC2, TC3) w.r.t the thermal diffusivity of calsil and the parameters related to the boundary conditions $(T_r, T_{amb}, \varepsilon_{cs}, h_h, h_v, T_{imp})$ by introducing a perturbation of +10% on the parameters. The sensitivity results were presented using the change in temperature (ΔT) as a function of time and in a global manner using the maximum temperature change (ΔT_{max}). Positive and negative values of ΔT and ΔT_{max} were obtained. The positive values signified that a 10% increase in the respective parameters resulted in an increase the temperature and the opposite for the negative values of ΔT and ΔT_{max}. T_r was the most influential parameter for the upper thermocouples (TC1, TC2) while T_{imp} was the most influential parameters for TC3. This result highlighted the importance of well-defined boundary conditions and their influence on the model response. The thermal diffusivity and emissivity of the painted calsil block were also influential parameters on all the thermocouples. From this simple case of modeling heat transfer by pure conduction in the calsil block, a more complex model taking into account heat transfer by conduction and radiation in a porous CF was developed.

In the third part of the chapter, the fire behavior of CF was studied. The CF was successfully modeled using a macroscopic heat transfer approach. Similar to the case of calsil the model was validated by adjusting the thermocouple locations. In this case, a numerical model implementing the measured thermal diffusivity of CF was used to successfully verify the thermocouple locations. Finally, a sensitivity analysis was conducted on the thermocouples (TC1, TC2, TC3) w.r.t to the material properties i.e. the porosity, thermal conductivity of the components (gas and solid matrix), geometrical factor, diameter of pores, emissivity of pores etc. It was concluded $\delta, C_{ps}, \rho_s, \varepsilon_{CF}$ were the most influential parameters.

In the fourth part, the fire behavior of PF was studied. In this case, the thermal degradation and ablation of PF were taken into account as compared to the case with CF. The material exhibited cracks at the surface of the material and they propagated into the in-depth of the material. This behavior posed a problem in modeling the fire behavior of the material. However, a numerical model which included most of the physical phenomena taking place in the material was developed.

Reasonable assumptions were imposed and the numerical model was capable of predicting the temperature within a time interval before the cracking phenomena was observed on the experimental temperature profiles. It would be interesting to include a thermomechanical model that takes into account the thermal stresses in the material as well as a complex decomposition kinetic model. For the purposes of conducting a sensitivity analysis including the physical phenomena considered in the model, the model was assumed to be valid for the duration of the simulation. It was then concluded that ρ_v, C_{pv}, k_v, and ε_s were the most influential parameters

Finally, in the fifth part, the fire behavior of SBIC was studied. The fire behavior of SBIC was also complex because it was a charring and intumescent material. Moreover, it exhibited cracks on the surface due to the external radiative heat flux from the cone heating element and it was difficult to determine its thermophysical properties at high temperature. However, acceptable crude assumptions were made on both the thermophysical properties and the developed model. A simplified one-step nth order kinetic model was capable of capturing the main mass loss step of SBIC thereby limiting the number of required input parameters. The numerical model was validated within a timeframe that was t<450s for TC3 and TC2 the temperature at the center backsurface of the steel plate and 5mm from the backsurface of the steel plate respectively. An under prediction was observed for TC1 the thermocouple at 15mm from the backsurface of the steel plate which attributed to thermocouple position uncertainty and cracking of the SBIC surface. Lastly, a sensitivity analysis was conducted w.r.t TC3 and the most influential parameters were E, k, ρ_0, C_p and the expansion rate ($swell$).

In conclusion, in this chapter, computational tools were developed to simulate the fire behavior of the fire barriers used in this work. After imposing reasonable assumptions, especially for PF and SBIC, the computational tools were capable of clearly identifying the governing parameters involved in the fire behavior of the materials through sensitivity studies. The applicability and limitations of the numerical models were also discussed. The developed engineering tools will provide with the means of conceptualizing different optimized fire barriers for a given fire scenario and constraints as will be presented in Chapter 4.

CHAPTER 4. CONCEPTUALIZATION OF FIRE BARRIERS

This chapter is dedicated to the development of a methodology for the conceptualization/design of fire safe innovative insulation materials. The methodology is developed based on the performance-based design approach using the numerical models developed in Chapter 3. The methodology will also allow, through virtual testing, the optimization of fire barrier concepts without the need to conduct expensive and time-consuming fire tests.

A general description of the methodology is detailed in the first section. Based on this methodology, the fundamentals on how to make efficient fire barriers will be presented in the second section. In this section, the different fire barrier concepts based on the reference materials used in this study i.e. calcium silicate (calsil), ceramic foam (CF), phenolic foam (PF) and a silicone-based intumescent coating (SBIC) are presented. Finally, some concluding remarks will be given. At the end of the chapter, certain fundamental rules on how to design efficient fire barriers based on imposed requirements and a given fire scenario are clearly stated.

4.1. Design Methodology

The design methodology developed in this work is based on the performance-based design (PBD) process. Figure 96 reminds the reader of the flowchart for the PBD process [362, 363]. The process is comprised of different steps and it is flexible because it does not specify which methods or models are supposed to be used to carry out the specific tasks for a particular design. In a general manner, the steps can be grouped into the following; 1.) Define Scope, Goals and Objectives 2.) Define performance criteria, 3.) Define Design fire scenario 4.) Run trial designs 5.) Check perfomance criteria 6.) Choice of design. These steps are well defined and explicitly explained in [362, 363].

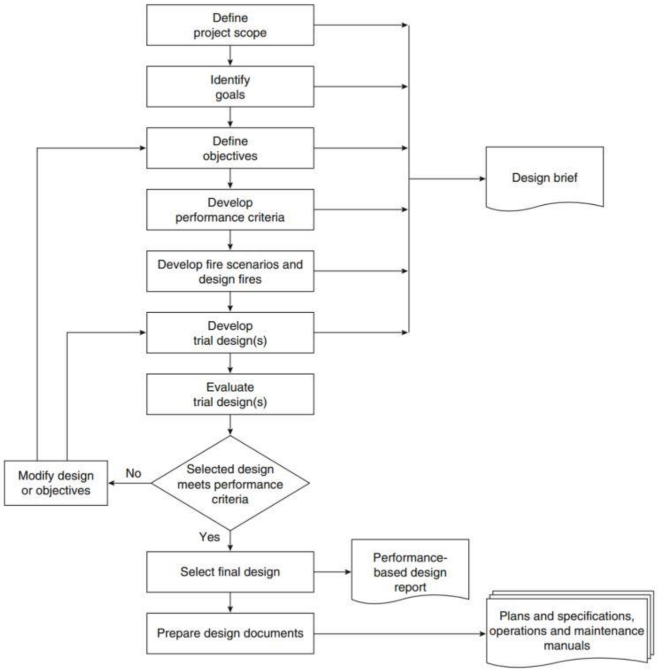

Figure 96. Flowchart for the PBD process [362, 363].

Briefly and in the context of this PhD work, examples of the relevant steps are explained as follows:

1) The project scope in this context identifies the boundaries of the PBD process. These can include which part of the building is being considered for the PBD process. For example, a whole building, components of the building such as wall claddings or small samples of the building materials [205]. The goal can be defined as the “desired overall fire safety outcome expressed in qualitative terms”.

This gives a general understanding on the final performance of a component in the case of a fire. For example, Hidalgo et al. [24] used a thermal barrier on the surface of a combustible insulation material with the goal of delaying or preventing the surface from pyrolysis so that it does not contribute to fire. These goals can be obtained from different sources e.g codes defined by regulatory boards or they can be defined by the designer. For example, ISO2685:1998(E) stipulates that a material has to be 'capable of withstanding the application of heat by a standard flame for 5 min'. In a similar manner, the National Fire Protection Association (NFPA) 5000 framework states that, when a material is tested using the ASTM E119 time-temperature curve, the rise in temperature at the unexposed surface must be limited to 130°C after an exposure time of 15 minutes [23, 364]. In this work, certain goals are defined based on the fire behavior of the material for the given fire scenario. It should be noted that these goals can be adjusted by the designer depending on the required performance criteria thereby showing flexibility of the design methodology.

2.) The performance criteria defines the threshold values which indicate that the component is damaged when surpassed. The criteria can be the temperature of the materials, levels of radiative heat flux, gas temperatures etc. Taking the paper of Hidalgo et al. [24] as an example, their perfomance criteria was the onset of pyrolysis defined by a critical pyrolysis temperature on the surface of the comubtible insulation material.

3.) The definition of a fire scenario is an important step because it gives the details on the type of fire and conditions of exposure. In some cases these design fires can be defined by a regulation board. For example, the perfomance of intumescent coating is normally evaluated in a furnace test as stipulated by the standard EN 13381-8:2013 [365]. Even though the precise description of the real fire conditions and scenarios remains a hurdle in the fire community, different methods can be used to define the design fires e.g. simplified empirical expressions using bench-scale data from a cone calorimeter or furnace test based on Eurocodes [307]. Such an expression is applied on the exposed surface as a heat flux boundary condition. In this work, the design fire scenario implemented is based on a novel test bench, shown in Figure 97, that was developed and validated in our lab and is compliant with two different fire tests i.e. ISO2685:1998(E) and FAR25.856(b):2003. The novel test bench is explicitly described by Tranchard et al. [336, 366].

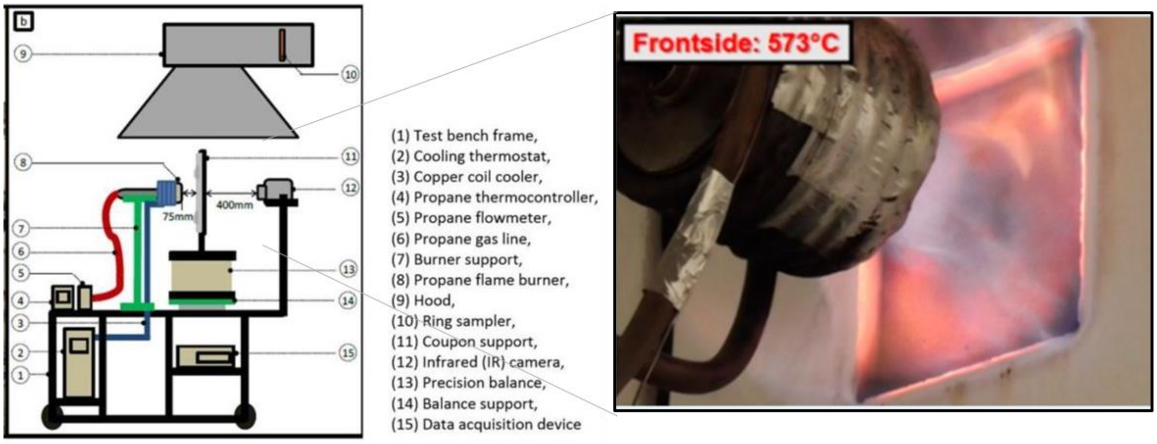

Figure 97. Novel test bench compliant with ISO2685:1998(E) and FAR25.856(b):2003 [336, 366].

The case implemented here is of a propane-air flame that is calibrated at a heat flux of 116 kWm^{-2} and flame temperature 1100°C at a distance of 75 mm between the nose of the burner and a vertically oriented sample. This fire scenario differs from that used in Chapter 3 which is based on a pure radiant heat flux from the ISO 5660 because its heat flux is composed of both radiation and convection contributions as expressed in Equation 1. The first term on the right-hand side represents the radiation from the flame, the second term represents the heat lost by radiation from the surface of the material, and the third term represents the convective heat exchange between the flame and the surface of the material [344]. A simplified boundary condition expression which describes the design fire scenario on the exposed surface based on the one proposed by Tranchard et al. [336] is expressed in Equation 73;

$$q_{net} = \varepsilon q_m - \sigma\varepsilon T^4 + h_{fl}(T_{fl} - T) \qquad \text{Equation 73}$$

where q_{net} is the net flux on the exposed surface and q_m is considered as the measured radiant heat flux which was experimentally determined and is shown in Figure 98. h_{fl} is the coefficient of convective heat transfer between the flame and the material.

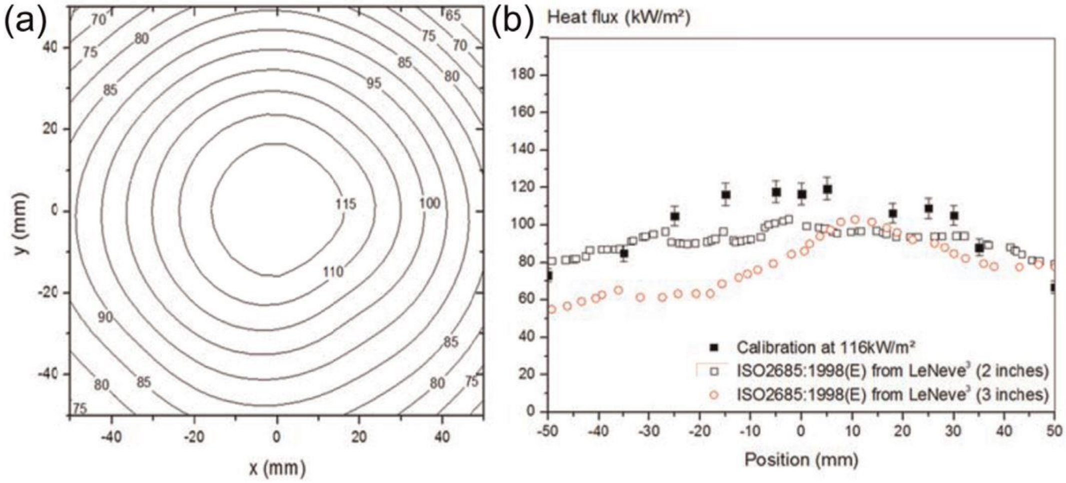

Figure 98. (a) Mapping of heat flux on the surface of a sample, (b) 2D heat flux with comparison to literature [366, 367].

It is assumed as constant throughout the experiment and for simplification, the same value ($h_{fl} = 24\ \mathrm{Wm^{-2}K^{-1}}$) as for the cone experiments in Chapter 3 is implemented. This is a reasonable assumption given that Mouritz and Gibson [344] stated that the values are dependent on the configuration and they may vary from $10\ \mathrm{Wm^{-2}K^{-1}}$ for a flat wall to as high as $50\ \mathrm{Wm^{-2}K^{-1}}$ for a fire impinging a ceiling. T_{fl} the temperature of the gas flame is assumed as constant and a value of 1100°C is applied. In a similar way, all the other boundary conditions i.e. on the sides and the bottom of the copper plate are kept the same as those applied for calsil and CF in Chapter 3.1.

4.) Running trial designs entail testing the proposed design until the achievement of the performance criteria for the given design fire scenario. This is synonymous with conducting an optimization study until the stopping criterion is achieved in numerical modeling. As proposed in the 'SFPE handbook of fire protection engineering [362]', during this step, the designer should 'refer back to the goals of the analysis and decide what types of strategies would best achieve those goals'.

5.) This step comprises of checking the performance and can be grouped together with the previous step on running trial designs. Finally, after accomplishing these steps,

6.) a design is chosen.

In summary, as concluded in Chapter 1.2.1, the design problem for fire safe innovative materials can be considered as an optimization problem. In a general manner, optimization comprises of finding the control variables which minimize the objective function given a certain set of constraints [368]. In this context, the control variables or design parameters are the material properties and the objective can be defined by a failure criterion in such a way to delay the temperature rise at a certain specified point from reaching a failure temperature. In a similar manner to the PBD process, Figure 99, shows the flow chart of the proposed design methodology which will be used for the conceptualization of fire safe fire barriers based on the reference materials used in this study. In Figure 99, the main steps include defining the *fire scenario*. From the numerical models presented in Chapter 3, the boundary conditions on the exposed surface are changed and the fire scenario previously presented in this section is used. The next step is to use the thermophysical properties of the reference materials (*fire barriers*) as initial model input parameters in order to run the numerical models. After running the model using the initial parameters, probe temperatures are evaluated at different locations depending on the material. The probe temperature profiles will show at which time they reach the *fail* zone defined by a failure temperature (T_f). The objective is to obtain optimized material properties that delay the temperature rise meaning that the material is *safe* for longer times i.e. $t_0 > t_i$ [287]. The *performance criterion* is then checked if achieved. The performance criteria will be defined for each material in the next section. If the performance criterion is not met, the input material properties go through optimization until the criterion is achieved. Different optimization techniques can be used in COMSOL Multiphysics® and they will also be described in the next section.

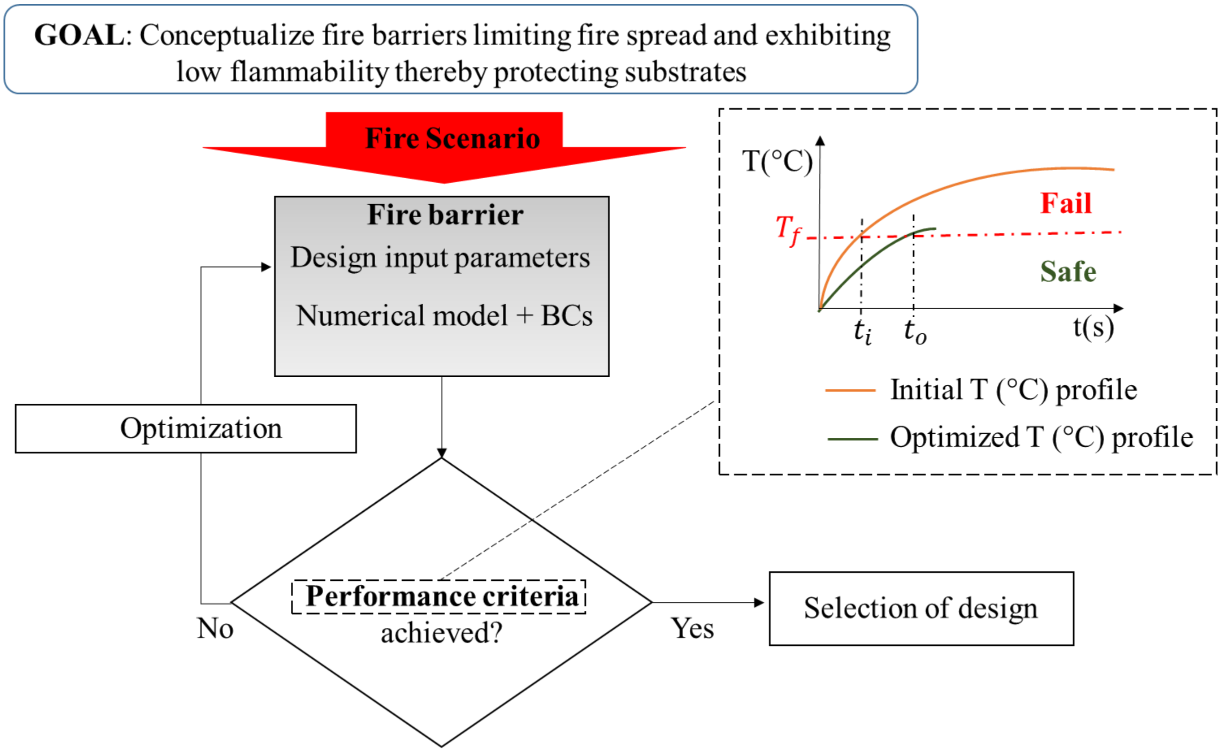

Figure 99. Flowchart for the proposed design methodology

Given that the fire behavior of the reference materials was different, different failure criteria are defined and they are explicitly explained in the next section. In addition, the numerical models developed in Chapter 3 will be implemented for a given fire-safe scenario described in this section.

4.2. Conceptualization

4.2.1. Conceptualization of static non-porous fire barrier

In this part of the section, the conceptualization of static non-porous fire barriers is described. In this case, using the model developed for the calcium silicate (calsil) insulation block and the results from the sensitivity analysis for calsil, the control variables (design parameters) can easily be identified as the thickness, emissivity of the materials and the thermal diffusivity. In addition, Papadopoulos [212] discusses the evolution of insulation thickness that is applied to walls and roofs in Europe over the past years making it also an important design parameter.

Using the fire scenario boundary conditions described in the previous section on the exposed surface and keeping all the other boundary conditions the same as in Chapter 3.1, the temperature profile at the center of the unexposed surface of the calsil block is shown in Figure 100

(TC_initial). It should be noted that the temperature evolution at a distance of 1mm from the interface (calsil block and the copper plate) is considered given that the copper plate is thermally thin (Biot number < 0) and a temperature condition is imposed at its backsurface. TC_optimized represents the temperature profiles obtained by using the optimized parameters.

To explore different ways of conducting the optimization problem in COMSOL Multiphysics® three different methods will be presented. The first one is applicable to the non-combustible insulation materials (calsil and CF) and is presented here. The other two methods are presented in the next sections for PF and SBIC.

The method used for non-combustible materials consists of three steps. Firstly, a temperature profile (TC_initial in Figure 100) is generated from a time dependent heat transfer model using the measured thermophysical parameters of calsil as initial input parameters. This step is used to observe the temperature response of the material under the given fire scenario and boundary conditions. Then, a steady state heat transfer model coupled with an optimization model is then used to minimize the objective function defined as $(T - T_f)^2$ where T is the simulated temperature and T_f is the failure temperature imposed as 50°C. From Figure 100, the maximum temperature that TC_initial reaches is 53°C, therefore the failure temperature was defined at a lower value in order to optimize and improve the material properties. The optimization algorithm used in this case is based on Nelder-Mead. The residual of the objective function is 1.64 x 10^{-6} K^2.

The initial and optimized values of the design parameters used in the design methodology are presented in Table 18. The measured thermal diffusivity is multiplied by a scaling factor α_{cs}^* which is initially set as 1 and then optimized together with the thickness and emissivity (ε_{cs}). From Table 18, it can be concluded that to improve the performance of the fire barrier and to design a static non-porous fire barrier, the thermal diffusivity and emissivity of the material should be reduced while the thickness is increased. The thermal diffusivity of the conceptualized material is $\alpha_{cs}^* * \alpha_{cs}$ = 1.36 x 10^{-7} m^2s^{-1} as compared to that of calsil, α_{cs}= 3.36 x 10^{-7} m^2s^{-1} at room temperature.

Table 18. Initial and optimized values of the design parameters based on calsil.

Parameter	Calsil initial values	Optimized values	Lower bound	Upper bound
α_{cs}^{*}	1	0.404	0.2	0.6
Thickness (m)	0.05	0.063	0.05	0.07
ε_{cs}	0.94	0.804	0.7	1

Finally, to evaluate the optimized parameters, the optimized parameters are then used as input parameters using the previous time dependent calsil heat transfer model and an optimized temperature profile (TC_optimized in Figure 100) is obtained

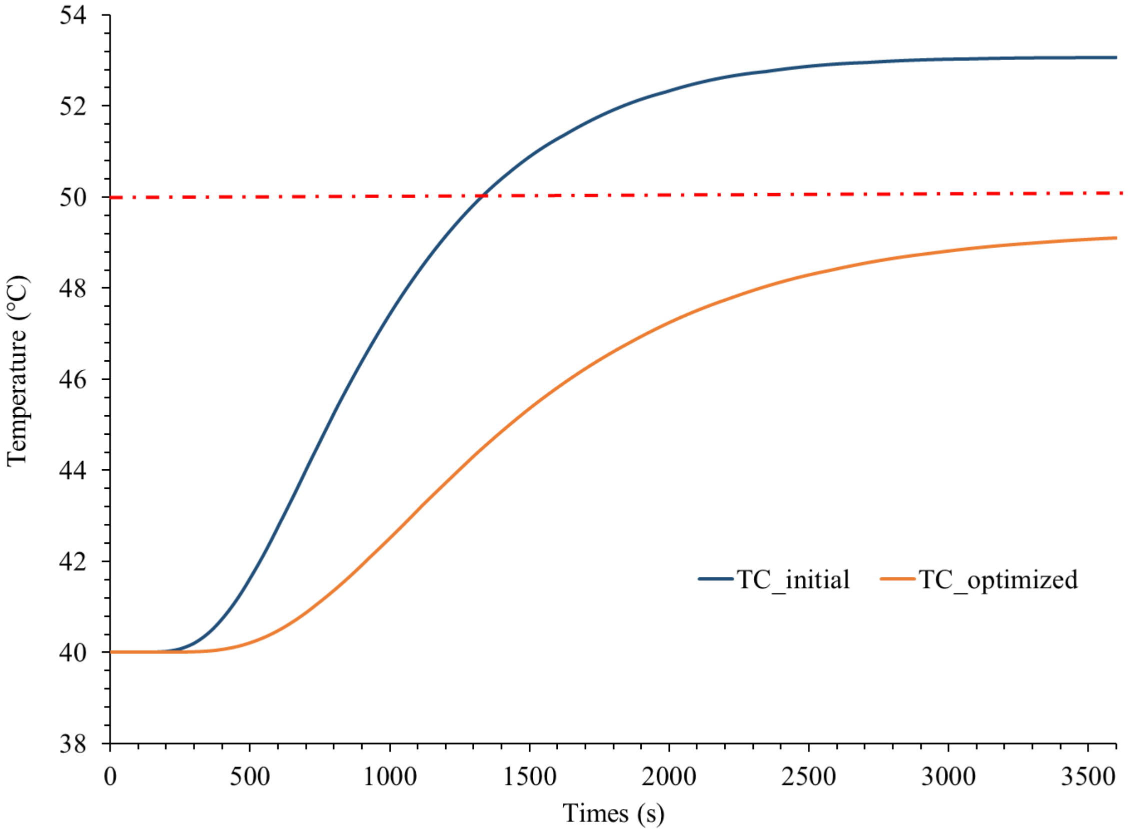

Figure 100. Comparison between the temperature profiles at the center backside of the calsil block using initial values (TC_initial) and optimized values (TC_optimized).

It can be observed that using the optimized parameters, the temperature is delayed from reaching the imposed failure temperature criteria and the maximum temperature reaches 49.1°C after 3500s.

In the next section, the conceptualization of static porous fire barriers is presented. The static porous fire barriers are based on the reference material CF. Indeed, this type of fire barrier takes into account the porosity as well as the properties of the individual components therefore more parameters are considered during optimization.

4.2.2. Conceptualization of static porous fire barriers

In this part of the chapter, the designed fire barrier is based on the reference material ceramic foam (CF). Similarly, as for the previous case for calsil, the design parameters are chosen from the sensitivity analysis results for ceramic foam (CF) i.e. the most influential material properties. However, in this case the gas properties are important in the conceptualization of a static porous fire barrier therefore they are also considered. The design parameters considered include $\delta, \varepsilon_{CF}, C_{ps}, \rho_s, k_g, k_s, C_{pg}, \rho_g$ as well as the thickness of CF. For temperature dependent parameters, a scaling factor which is initially equal to 1 is multiplied with the parameter and then optimized. The scaling factors C_{ps}^*, k_g^*, k_s^*, C_{pg}^*, ρ_g^* where applied for C_{ps}, k_g, k_s, C_{pg}, ρ_g respectively. In addition, the temperature at the center unexposed surface of the CF block was used to evaluate the efficiency of the fire barrier. It should be noted that the temperature evolution considered is at a distance of 1mm from the interface (CF layer and copper plate) due to the same reasons provided for the calsil case. In as similar way to the calsil case, the maximum temperature reached by TC_initial (obtained using the CF values as initial values) is 57.6°C and therefore failure temperature was defined at a lower value. Therefore, the goal was to delay the center backside temperature from reaching 50°C. For the optimization process, the same three-step optimization process explained in the calsil part is implemented.

The initial and optimized parameters implemented in this case are shown in Table 19 and the residual of the objective function is obtained as 3.02×10^{-7} K^2. In Table 19, all the optimized values are not as different as the initial values except for the thickness and the emissivity (ε_{CF}) which requires to be increased and ρ_s slightly reduced in order to improve the efficiency of the fire barrier. The result for ε_{CF} is in contradiction with the one found for the case of calsil in which the emissivity is expected to be decreased in order to make an efficient barrier. This is possibly because optimization problems as explained in Chapter 1.1.3.b and the solution may not be practicable. It would be recommended to further work on the optimization in order to obtain physically realistic values. With these results, it is also noteworthy that the optimization results depend on the bounds that are set for the design parameters and attention should be given when setting them. Moreover, from the sensitivity analysis for CF presented in Chapter 3.3.4, the most influential parameters were concluded as $\delta, C_{ps}, \rho_s, \varepsilon_{CF}$. In this case, depending on the objective of the study, the bounds for thickness can be reduced so that the most influential parameters can be varied more.

Table 19. Initial and optimized values of the design parameters based on CF.

Parameter	**CF values**	**Optimized values**	**Lower bound**	**Upper bound**
δ	0.85	0.85004	0.5	1
ε_{CF}	0.94	1.0000	0.5	1
C_{ps}^*	1	1.0015	0.7	1.5
ρ_s (kgm^{-3})	3647.6	3640.7	2500	4500
k_g^*	1	1.0002	0.8	1.5
k_s^*	1	1.012	0.4	1.5
C_{pg}^*	1	0.99846	0.8	1.5
ρ_g^*	1	0.93263	0.8	1.5
Thickness (m)	0.05	0.07	0.05	0.07

It is noteworthy that to design an efficient static porous fire barrier, the components of the material i.e. the solid matrix and fluid should properly be chosen in order to obtain a material with the best apparent thermophysical properties [329]. This can also be confirmed given that the apparent thermal conductivity is dependent of the properties of these components as well as the porosity as seen in Chapter 3.3.2. Moreover, the apparent diffusivity is also dependent on these parameters. Given that porous fire barriers can be fabricated from different methods; these methods should also be optimized. Gong et al. [228] used foaming and starch consolidation to fabricate porous mullite ceramics of porosity between 73 to 86 vol%. Using this method, they obtained a ceramic foam of 0.09 Wm^{-1}K^{-1}. Moreover, they observed the dependence of porosity on different sintering temperatures.

Finally, Figure 101 shows the comparison between the temperature profiles at the center backside of the CF using initial values (TC_initial) and optimized values (TC_optimized). The initial measured CF parameters yield the temperature profile TC_initial while the optimized parameters yield the temperature profile TC_optimized. Indeed, the optimized temperature profile takes more time to reach the defined failure temperature thereby reaching a maximum temperature of 49°C after 4500s therefore making it efficient.

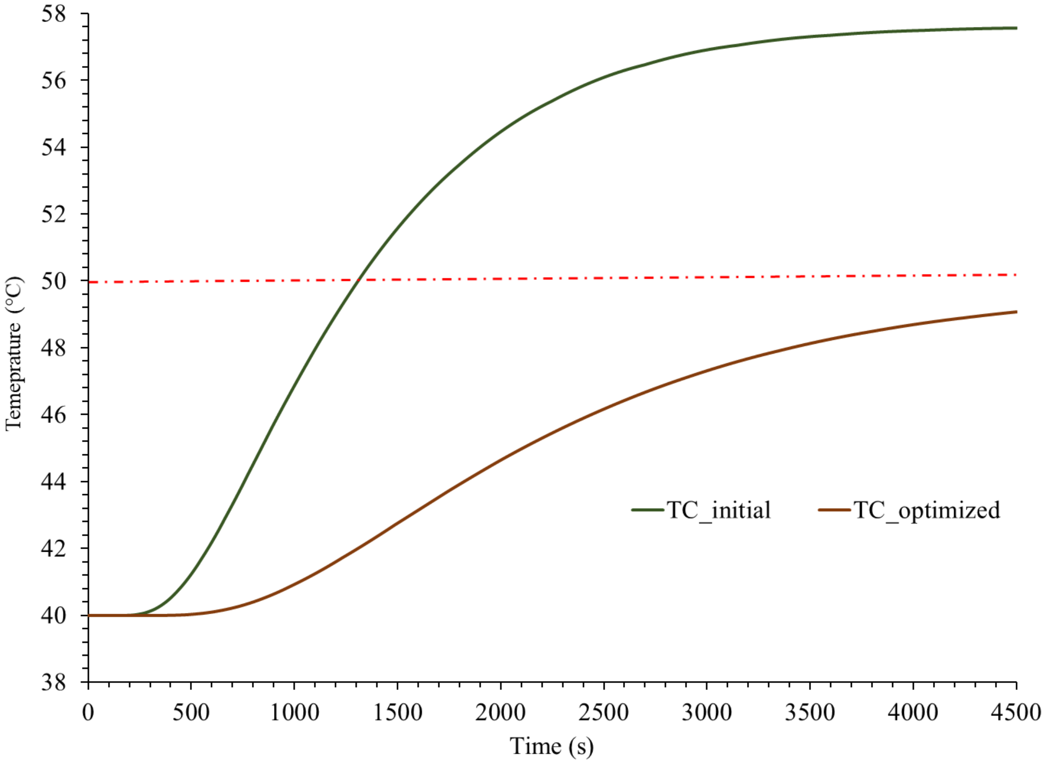

Figure 101. Comparison between the temperature profiles at the center backside of the CF using initial values (TC_initial) and optimized values (TC_optimized).

In the next section, the conceptualization of fire barriers based on PF will be presented. Given that PF is combustible, a different temperature failure criterion is defined.

4.2.3. Conceptualization of fire barriers based on PF

Contrary to the case of non-combustible materials, calsil and CF, the failure criterion considered for combustible phenolic foam (PF) is the onset of pyrolysis on the exposed surface. Using this criterion, the moving surface boundary is therefore neglected in the conceptualization model given that the ablation of the surface is triggered by onset of pyrolysis. Moreover, the deficiencies of the numerical model for PF explained in Chapter 3.4.4 do not influence the conceptualization model given that cracking is also triggered by the onset of pyrolysis and that the failure criterion is considered at the surface. The definition of the 'onset of pyrolysis' is adopted from Hildago et al.

[203] and it is represented by a 'critical temperature'. Figure 102 shows the DTG curves of PF at 2°Cmin^{-1} under an air and nitrogen atmosphere. Assuming that PF does not shrink or melt and using the definition for the 'critical temperature' proposed by Hidalgo et al. [203, 252] stating that the 'temperature of the main peak of pyrolysis obtained from DTG under a nitrogen atmosphere at low heating rates' is the 'critical temperature for materials that do not significantly shrink', in this study, the critical temperature for PF is estimated as 440°C (indicated by the red dashed line in Figure 102). This value corresponds with the value 425°C obtained for a typical phenolic foam by Hidalgo et al. [203].

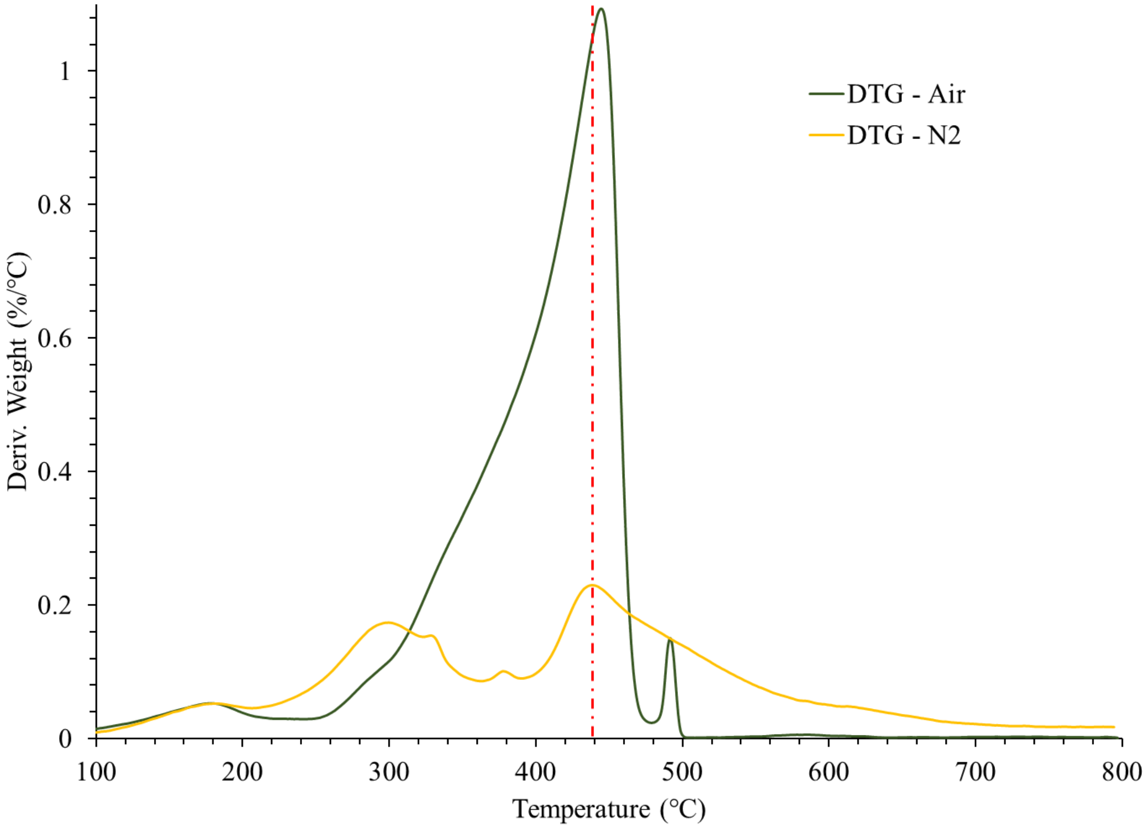

Figure 102. DTG curves of PF at 2°Cmin^{-1} under an air and nitrogen atmosphere.

Having defined the failure criterion for PF, a temperature profiles at the center of the exposed surface is considered. It should be noted that the temperature evolution is considered at 1mm from the exposed surface of the PF because numerically, the exposed surface is a boundary with an imposed heat flux boundary condition (Neumann boundary condition) which results in a constant temperature. In the case of PF, a method implementing the parametric sweep function is implemented in COMSOL Multiphysics®. This method is less time consuming as compared to the one that uses an optimization algorithm as will be discussed for the case of SBIC. Using the parametric sweep function, the idea is to test different parameter combinations and select the one that yields the optimal temperature profile as defined by the designer.

Table 20 shows the initial PF values and the optimized values obtained from the parameter sweep. It should be kept in mind that, the most influential material properties in order of importance from sensitivity studies of PF were ρ_v, C_{pv} k_v, ε_s and E. Therefore, an optimization study with only these control variables is sufficient, however, for conceptualization purposes, char properties are also included and are varied in the same order of magnitude as the virgin properties. It should be noted that for temperature dependent properties, scalar factors multiplied by the respective properties and they are represented by an asterisk. These factors are initially set as 1 and then optimized.

Table 20. Initial and optimized values of the design parameters based on PF

Parameters	**PF values**	**Optimized values**
ρ_v (kgm^{3})	33.68	493.41
k_v^*	1	0.1
C_{pv}^*	1	2
ρ_c (kgm^{-3})	31.63	474
k_c^*	1	0.1
C_{pc}^*	1	2
E(kJmol^{-1})	132.30	350
ε_s	0.94	0.2

Regarding the optimized values of the most influential parameters, ρ_v, C_{pv}^* and E increased while k_v^* *and* ε_s decreased. The emissivity ε_s decreased from 0.94 to 0.2. The optimized values obtained are $k_v^* * k_v$ = 0.00165 Wm^{-1}K^{-1}, $C_{pv}^* * C_{pv} = 2770$ Jkg^{-1}K^{-1} at room temperature. In other terms, the conceptualized material should exhibit a lower thermal diffusivity of 1.2 x 10 $^{-9}$ m^{2}s^{-1} as compared to the thermal diffusivity of PF, 3.4 x 10^{-7} m^{2}s^{-1} at room temperature. An increased activation means that the conceptualized material has a higher thermal stability compared to PF.

Realistically, the optimized thermal conductivity is low as compared to values found in literature which are normally in the order of 0.02 $Wm^{-1}K^{-1}$ at room temperature [244].

Different methods can be used to improve or alter the thermal properties of foams. Chemically, flame retardants can be added to polymers to yield synergistic effects and improve the properties of the material. In this case the activation energy can be altered. Domingeuz et al. [369] phenolic foam with wood flour and they managed to increase the thermal stability of the first degradation step of neat phenolic foam. Physically, inert additives can also be incorporated into the material to modify their thermophysical properties. Roenner et al. [370] incorporated inert additives such as hollow glass spheres and boron nitride platelets in order to change the flammability properties (altering the heat transfer by reducing the thermal diffusivity) of a polymer. Huang et al. [371] incorporated different compositions of hollow glass microspheres (HGM) within syntactic phenolic foams. Using this method, they managed to reduce the thermal conductivity of the syntactic phenolic foams from 0.25 $Wm^{-1}K^{-1}$ to 0.14 $Wm^{-1}K^{-1}$ using 50vol% of HGM thereby improving its thermal insulation properties. In a similar way, Wang et al. [372] used hollow ceramic microspheres to reduce the thermal conductivity of a phenolic-based carbon foam from 0.25 $Wm^{-1}K^{-1}$ to 0.11 $Wm^{-1}K^{-1}$.

As for the surface, given that the conceptualized material requires a low emissivity, low emissivity materials such as aluminium foil can be attached on the surface of the materials, Morgan and Toubia [186] attached an aluminium foil to a phenolic/fiberglass skin balsa composite and studied its fire behavior using a cone calorimeter and ISO 9705 test. They observed that with the aluminium foil attached, the time to ignition of the skin would be increased by almost 250s thereby delaying ignition. The delay in ignition was attributed to infrared reflection caused by the aluminium foil. Schartel et al. [373] proposed sub-micrometer coatings with an absorptivity of less than 0.1 deposited on substrates through physical vapor deposition. These coatings acted as an infrared mirror which would reduce heat absorption and also protect the substrate from oxidation. Moreover, they also increased the time to ignition of the substrate. Zhang et al. (experimental study of fire hazards) tested pure polyurethane and polyurethane with a 0.5 mm thick aluminium paper attached on the exposed surface under a cone calorimeter. The polyurethane had a thermal conductivity of 0.039 $Wm^{-1}K^{-1}$. They observed that the pure polyurethane exhibited a critical heat flux of 6.15 kWm^{-2} that was lower as compared to the modified polyurethane (16.39 kWm^{-2}) show that the later had a better fire performance.

Therefore, the thermophysical properties of foams can be modified in these ways thereby resulting in materials with a better fire performance.

Figure 103. compares the temperature profiles obtained when the initial PF values are implemented and when the optimized values are implemented.

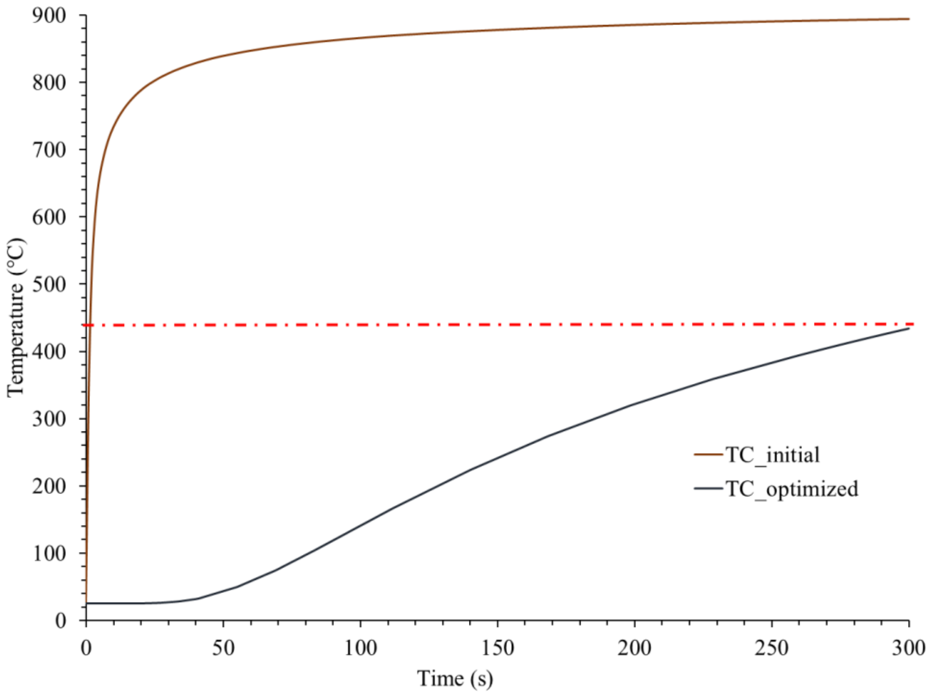

Figure 103. Comparison between the temperature profiles on the center of the exposed surface using PF values (TC_initial) and optimized values (TC_optimized).

In the next section, the conceptualization of fire barriers based on SBIC is presented. A different optimization method is also presented.

4.2.4. Conceptualization of fire barriers based on SBIC

The performance of intumescent coatings is evaluated by considering the temperature evolution at the center backside of the substrate. Temperature at the center backside is therefore used to determine the failure criterion. The temperature limit is defined at 300°C. This temperature limit was chosen given that the maximum temperature for TC_initial (Figure 104) given by the SBIC values was 382°C therefore the failure temperature defined at a lower value in order to optimize the material properties. Moreover, the conceptualized material would be efficient for protecting other substrates that start losing their thermal stability at 300°C for example polymer substrates. The design parameters considered include $E, \varepsilon_s, k, \rho_0, C_p$, the expansion rate ($swell$) and the initial thickness of the coating. In a similar way to the previous optimization studies, a scaling factor which is optimized is multiplied by the temperature or time dependent design parameter. In this case, the scaling factors for k, C_p, and $swell$ are k^*, C_p^* and $swell^*$respectively. The optimization method used in this case was automatic and it was based on the Nelder-Mead algorithm. The objective function was defined as $(T - T_f)^2$, where T is the simulated temperature and T_f is the failure temperature. The simulation time for the whole optimization process was around 13 hours. In addition, the thermal diffusivity should be decreased given that optimized values of ρ_0 and C_p^* are increased and that of k^* is lowered. The optimized value of E is increased.

Table 21 presents the SBIC, initial and optimized parameters. In this study, a parameter sweep was conducted in order to implement reasonable initial values close to the optimized values. The residual objective function was 9.8 x10^{-6} K^2. From Table 21, in order to conceptualize an intumescent coating that limits the temperature to 300°C after 900s when exposed to the given fire scenario it should exhibit the obtained optimized values. Comparing the SBIC values to the optimized values, the materials should have a lower thermal conductivity and emissivity as well as a higher expansion rate and initial thickness. Bourbigot and Duquesne [283] also concluded that to attain the best efficiency of an intumescent coating, it should exhibit a low thermal conductivity and high expansion rate. The conceptualized intumescent material exhibits a thermal conductivity of $k^* * k = 0.22$ $Wm^{-1}K^{-1}$, specific heat capacity of $C_p^* * C_p = 1691$ $Jkg^{-1}K^{-1}$ and a density of $\rho_0 = 1367.5$ kgm^{-3} at room temperature. Lucherini and Maluk [359] observed that the onset of swelling for thin intumescent coatings was influenced by the initial thickness. An intumescent coating with a relatively higher initial thickness had a faster onset of swelling. In a similar manner, Gardelle et al. [374] attributed the excellent fire conditions of a typical silicone-based intumescent coating to its expansion properties and low thermal conductivity. Moreover, to increase the expansion rate, the percentage composition of the expandable graphite (EG) can be increased. Gardelle et al. [56] evaluated the performance of silicone-based coatings by varying the composition of EG from 5% to 25% under a hydrocarbon fire scenario (standard UL1709). The fire performance of the intumescent system was improved with increasing amount of EG added. In addition, the thermal diffusivity should be decreased given that optimized values of ρ_0 and C_p^* are increased and that of k^* is lowered. The optimized value of E is increased.

Table 21. Initial and optimized values of the design parameters based on SBIC.

Parameter	**SBIC values**	**Initial values**	**Optimized values**	**Lower bound**	**Upper bound**
E (kJmol^{-1})	153.17	200	242	150	300
ε_s	0.914	0.914	0.75673	0.6	1
k^*	1	0.49	0.3662	0.2	0.5
ρ_0(kgm^{-3})	1320	1320	1367.5	1000	1500
C_p^*	1	1	1.1949	1	2
$swell^*$	1	1.5	1.57	0.8	2
thickness (m)	0.004	0.005	0.0055548	0.004	0.006

Figure 104 shows the comparison between the temperature profiles obtained at the center backside of the steel plate when using the SBIC values (TC_initial) and the optimized values (TC_optimized).

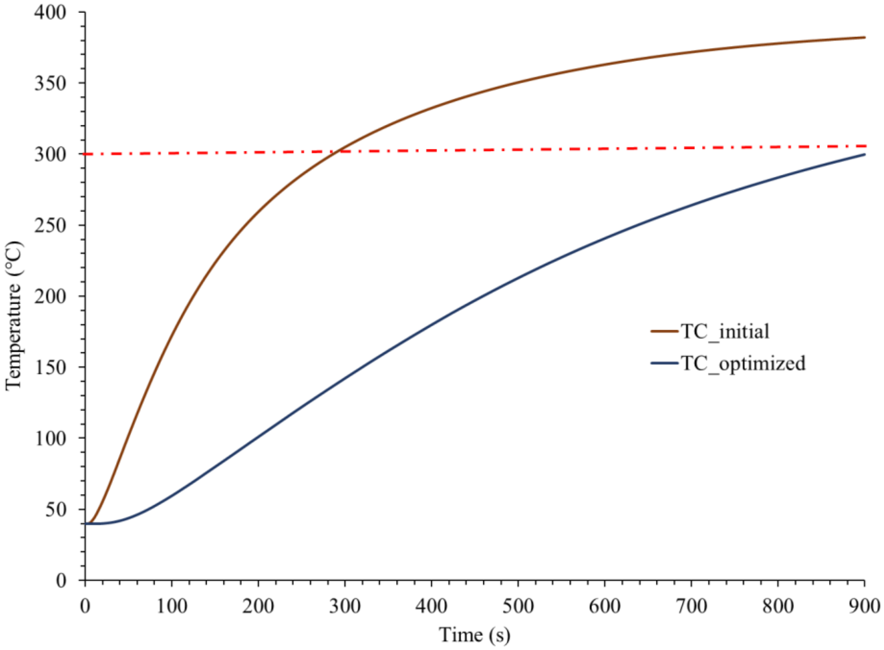

Figure 104. Comparison between the temperature profiles at the center backside of the steel plate using initial values (TC_initial) and optimized values (TC_optimized).

Clearly from Figure 104, the temperature profile obtained by implementing the optimized values is limited to 300°C after 900s.

It should be noted that intumescent systems are based either on ‘conventional bubbling system’ such as epoxy based or ‘self-expanding system’ such as SBIC [352, 375]. For ‘conventional bubbling systems’ based on three components i.e. an acid source (e.g. ammonium phosphate), carbon source (e.g. char forming polymers) and blowing agent (e.g. melamine) [172], optimization of the formulation is required in order to make an efficient intumescent system. For example, a binder can be incorporated into the formulation to control the expansion rate of the char and obtain a uniform alveolar char layer of low conductivity [376]. For ‘self-expanding systems’ based on expandable graphite (EG), different compositions of EG can be optimized in order to increase the expansion rate and lower the thermal conductivity [56].

Puri and Khanna [377] presented an extensive review on the recent advances on intumescent coatings. Their review focused on different types of intumescent coatings depending on their classifications, variations in composition and the effect of different additives. They concluded that the use of appropriate ingredients was essential in obtaining efficient intumescent coatings. In addition, they concluded that the use of nanofillers and nano-clays as well as vitreous fillers were some of the ‘promising approaches in the formulation of high performance coatings’. Alongi et al. [375] also presented an extensive review on intumescence which gives an insight on how to improve intumescent based insulation systems. Given the above ways to optimize the intumescent systems and given design methodology presented in this section, with the help of characterization methods the optimized system can be tested to ensure that the performance criteria have been achieved.

4.3. Conclusion

In this chapter, a design methodology based on the performance-based process was presented. It was then successfully applied for the conceptualization of different fire barriers based on the reference fire retardant materials used in this study using the numerical models developed in

Chapter 3. A fire scenario compliant with ISO2685:1998(E) and FAR25.856(b):2003 was implemented.

When designing fire barriers based on calsil i.e. a static non-porous material, focus should be given to the thermal diffusivity (in other terms, the thermal conductivity, density and specific heat capacity) of the material, thickness and emissivity of the material based on the sensitivity analysis results and design considerations. Based on the results of this work and evaluating its efficiency using the temperature at the unexposed surface, the thermal diffusivity and the emissivity should be reduced while the thickness should be increased in order to design an efficient fire barrier. For the other materials, the fundamental rules are deduced in a same manner.

When designing fire barriers based on closed-cell mullite foam i.e. a static porous material, focus should be given to the porosity, thickness and emissivity of the material as well as the thermophysical properties of the individual components i.e. the matrix and fluid/gas properties. The apparent thermal conductivity is dependent on the porosity and the properties of the individual components.

When designing fire barriers based on phenolic foam i.e. polymeric foams, focus should be given to the density, thermal conductivity and specific heat capacity of the virgin material as well as the activation energy. Based on the results of this work, the objective was to delay the onset of pyrolysis on the exposed surface. To accomplish this, the density, the specific heat capacity of the virgin material and activation energy had to be relatively increased while the thermal conductivity and the emissivity of the virgin material had to be reduced. In other words, the diffusivity of the material was lowered.

When designing fire barriers based on the silicone-based intumescent coating i.e. dynamically evolving fire protection coatings, focus should be given to the emissivity, the thermal conductivity, the specific heat capacity, the density, the expansion rate, initial thickness as well as the activation energy of the material. The efficiency of fire barrier was evaluated by considering the temperature at the backside of the substrate. Based on the results of this work, the thermal conductivity, the emissivity of the material should be decreased. The activation energy, the density, specific heat capacity, initial thickness and the expansion rate should be increased. Similarly, as for the phenolic foam, in general, the thermal diffusivity should be lowered.

The advantages of the methodology are that it can be applied to different fire scenarios and depending on the objectives of the designer, innovative fire-safe materials can be conceptualized. Moreover, through virtual testing, new fire-safe material concepts can be developed without the need to conduct expensive experimental tests. Different optimization methods were implemented in COMSOL Multiphysics® and were also presented. In summary, this chapter provided with the fundamentals on how to design efficient fire barriers.

GENERAL CONCLUSION

This work aimed at providing the fundamentals on how to make an efficient fire barrier based on the experimental and numerical study of the fire behavior of reference fire retardant (FR) materials i.e. calcium silicate, closed-cell mullite foam, phenolic foam and a silicone-based intumescent material containing expandable graphite.

The reference FR materials were subjected to an external radiant heat flux from the cone heating element based on the cone calorimeter ISO 5660. An improved water-cooled sample holder with a well-defined temperature at 40°C was used to avoid the assumption of the adiabatic condition at the unexposed surface of the experimental surface. The fire behavior of the reference FR materials was evaluated by considering the temperature evolution at different in-depth locations using thermocouples. Both the calcium silicate and closed-cell mullite foam did not thermally degrade. For the calcium silicate block, only the heat transfer by pure conduction was considered. Due to the porosity of the closed-cell mullite block, the heat transfer by conduction through the block and radiation in the pores was considered. The phenolic foam exhibited a charring behavior. Moreover, phenomena such as cracking and ablation were observed. The silicone-based intumescent coating exhibited a relatively high expansion rate thanks to the expandable graphite. Cracks were also observed for the intumescent coating.

Based on the results of the experimental studies, model systems were developed in order to numerically predict the fire behavior of the reference FR materials. As a preliminary step to clearly identify and quantify the boundary conditions of the experimental set-up, a study on a steel plate was conducted. This step contributed to the determination of the convection heat transfer coefficients ($h_h = 24\ \mathrm{Wm^{-2}K^{-1}},\ h_v =\ 10\ \mathrm{Wm^{-2}K^{-1}}$). Attention was given in order to develop fundamental and phenomenological numerical models considering the main heat transfer mechanisms involved in the fire behavior of these materials. In order to implement these model systems, material input properties were both extracted from direct measurements and the literature. For the thermally degradable materials i.e. phenolic foam and the silicone-based coating, the thermophysical properties were measured within a given temperature. To use these properties at higher temperatures, certain assumptions were imposed and explained. Moreover, the validity of the measured thermophysical properties were discussed. These thermophysical properties provide a basis as input data for further development of numerical models based on the reference FR materials in the fire safety community. As an important step in numerical modeling, the predicted temperature profiles were confronted with the experimental temperature profiles in order to validate the model systems. For the model systems based on calcium silicate and closed-cell mullite foam, excellent agreement was achieved. However, for the phenolic foam and silicone-based coating, satisfactory agreement was achieved within a given time range. The predicted and experimental results were coherent given that the disagreement was mainly due to the non-inclusion of the thermomechanical behavior of both materials in the model systems. Experimentally, this behavior resulted in surface cracking which propagated into the materials causing rapid rises in the temperature profiles which could not be predicted by the model systems. Modeling the thermomechanical behavior of materials is a complex phenomenon which requires more input parameters. Moreover, given that this was out of the scope of this work, and that the main heat transfer mechanisms were taken considered, it was assumed that the model systems were valid over the entire simulation time. This assumption permitted to conduct sensitivity studies which took into account all the modeled physical phenomena.

The sensitivity studies were conducted for all the reference FR materials. Given that, for the calcium silicate block, the thermal diffusivity and the emissivity were the material properties of interest, the parameters related to the boundary conditions were also considered for the sensitivity study. The influence of these material properties and boundary conditions were clearly identified and quantified. Besides the importance of the thermal diffusivity and the emissivity, it was concluded that the boundary conditions played a major role in the accuracy of the model systems and they need to be well-known and well-defined. As for the other reference FR materials, focus was given only on the material properties during the sensitivity studies. For each of the materials the governing parameters were clearly identified depending on the location of the thermocouples. The influence of the governing parameters was clearly dependent on the location of the thermocouples. For the closed-cell mullite foam, the sensitivity of ΔT_{max} w.r.t. $\delta, \varepsilon_{CF}, C_{ps}, \rho_s, k_g, k_s$ decreased from TC1 to TC3 and $\delta, C_{ps}, \rho_s, \varepsilon_{CF}$ were the most influential parameters. For the phenolic foam, the sensitivity of ΔT_{max} w.r.t. ρ_v, C_{pv}, k_v, ε_s, ρ_c, C_{pc}, k_c and abl decreased from TC1 to TC2 and the most influential parameters were ρ_v, C_{pv}, k_v, and ε_s. For the silicone-based intumescent coating, E was the most influential parameter followed by $k, \varepsilon_s, swell, \rho_0, C_p, Q, A$ and n was the least influential parameter based on their sensitivity to

ΔT_{max}. In a general way, for all the materials, it can be concluded that the thermal diffusivity plays a major role in the fire behavior of a material.

Finally, based on the developed model systems and sensitivity studies, a design methodology that permits the conceptualization of an efficient fire barrier in accordance with specific requirements for a given fire scenario was presented. The design methodology was based on the performance-based process and implemented numerical optimization techniques. The specific requirements were set and a fire scenario compliant with the ISO2685:1998(E) and FAR25.856(b):2003 was implemented. The methodology was explicitly described and applied to all the reference FR materials. The parameters values obtained from the optimization techniques were also discussed. At the end of the study, a certain number of fundamental rules on how to design an efficient fire barrier were clearly stated. For the design of static and non-porous materials; it was concluded that to design an efficient fire barrier, the thermal diffusivity and the emissivity of the material should be reduced while the thickness should be increased. For the design of static and porous fire barriers; generally depending on the thermophysical properties of the individual components i.e. matrix and fluid/gas properties, the porosity and the thickness should be adjusted accordingly in order to conceptualize an efficient fire barrier. For the design of efficient fire barriers based on polymeric foams, the density, specific heat capacity of the virgin material and activation energy should be increased while the thermal conductivity and emissivity of the virgin material should be reduced to obtain an optimized fire barrier. Evidently, the thermal diffusivity of the virgin material should be lowered. Finally, for the design of efficient fire barriers based on dynamically evolving fire protection coatings, the thermal conductivity and the emissivity of the coating should be decreased while the activation energy, the density, the specific heat capacity, initial thickness and expansion rate should be increased. As for the polymeric foams case, the thermal diffusivity should be reduced.

In summary, the first part of this work was oriented towards understanding the fire behavior of the reference FR materials though an experimental and numerical approach. Based on the developed numerical models, the parameters governing the fire performance of the reference FR materials were clearly identified. The knowledge of the governing parameters helped during the conceptualization process during optimization by focusing on these parameters. Finally, the knowledge on how to design innovative fire safe materials was combined and gathered.

OUTLOOK

This study presented an experimental and numerical approach to understand the fire behavior of selected reference fire retardant materials i.e. calcium silicate, closed-cell mullite foam phenolic foam, and a silicon-based coating. A set of computational tools was then developed to predict the fire behavior of the reference materials and a design methodology to conceptualize innovative fire-safe materials for a given fire scenario and constraints was then presented and it was successfully implemented. The set of computational tools can eventually be applied and adapted for different fire scenarios given that the boundary conditions are well-known (virtual testing). An example of application is that of the fire protection of on-board hydrogen storage [378]. In their work, the hydrogen storage tank was exposed to a bonfire test. The hydrogen storage tank is comprised of a liner of high-density polyethylene (HDPE) and a layer of carbon-fiber reinforced polymer (CFRP) which is protected in the case of a fire by an intumescent coating (Figure 105).

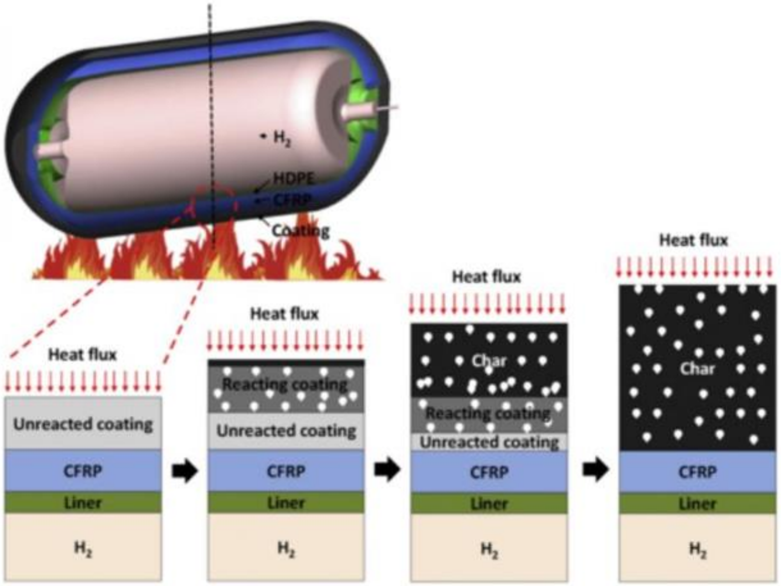

Figure 105. Fire protection of on-board hydrogen storage [378].

This intumescent coating should hence be an efficient fire barrier and delay the substrates (CFRP and HDPE) from reaching their failure temperatures thereby limiting fire spread. Finally, using the design methodology presented in this work, an efficient intumescent coating for the hydrogen storage tank can be proposed.

Moreover, certain issues on how to improve this work can be regarded as perspectives for future work. An optimized experimental set-up including a water-cooled sample holder was used, however it was observed that the temperature readings were very sensitive to the in-depth locations. The method used to place thermocouples into the materials was therefore not efficient enough and to reduce such experimental errors, a better method should be used.

Based on the results of the sensitivity studies, the most influential parameters on the model response are now clearly known therefore they should be precisely measured especially at high temperatures in order to optimize the numerical model systems. Moreover, the major problem with validating the numerical models based on phenolic foam and the silicone-based intumescent coatings due to surface cracking which propagated into the materials causing sudden temperature rises which could not be predicted by the current numerical models. This phenomenon was not considered in the current study and it would be interesting to include a thermo-mechanical sub model.

In this study an assumption of a nth order one step reaction for the numerical model based on phenolic foam was imposed. It would be interesting to implement a more complex kinetic model and understand the effect of this assumption on the model response.

As for the reference fire retardant materials exhibiting a moving boundary i.e. phenolic foam and the silicone-based intumescent coating, it would be interesting to identify the phenomena that control the mechanism and include their coupling in the model in order to obtain the surface recession or expansion profile as an output.

When implementing the design methodology, certain optimization techniques were implemented. In the case that more parameters are added to the problem, genetic algorithms can also be used during the optimization process.

Finally, the proposed fundamental rules and design methodology should then be used for the conceptualization of innovative fire safe materials for any given fire scenario and constraints on a laboratory scale as a proof of concept.

LIST OF TABLES, FIGURES AND REFERENCES

LIST OF FIGURES

LIST OF TABLES

REFERENCES

1. Haynes, H.J.G., *Fire Loss in the United States during 2016*, 2017, National Fire Protection Association.
2. Zuccaro, G., *A Case of Choice of Passive Fire Protection (PFP) in an Oil and Gas EPC project.* Chemical Engineering Transactions, 2012. **26**.
3. Pavel, C.C. and D.T. Blagoeva, *Competitive landscape of the EU's insulation materials industry for energy-efficient buildings*, 2018, European Commission.
4. Drysdale D, D. *Fundamentals of the Fire Behaviour of Cellular Polymers*. in *Fire Cell. Polym.* 1986. Dordrecht: Springer Netherlands.
5. Bourbigot, S. and S. Duquesne, *Fire retardant polymers: recent developments and opportunities.* Journal of Materials Chemistry, 2007. **17**(22): p. 2283.
6. Bourbigot, S., et al., *Recent Advances for Intumescent Polymers.* Macromolecular Materials and Engineering, 2004. **289**(6): p. 499-511.
7. Ghorbani, Z., et al., *Limitations in the predictive capability of pyrolysis models based on a calibrated semi-empirical approach.* Fire Safety Journal, 2013. **61**: p. 274-288.
8. Lautenberger, C. and C. Fernandez-Pello, *Generalized pyrolysis model for combustible solids.* Fire Safety Journal, 2009. **44**(6): p. 819-839.
9. Lautenberger, C., *Gpyro3D: A Three Dimensional Generalized Pyrolysis Model.* Fire Safety Science, 2014. **11**: p. 193-207.
10. Lautenberger, C., *A Generalized Pyrolysis Model for Combustible Solids*, 2007, University of California: Berkeley.
11. Stoliarov, S. and R. Lyon, *Thermo-Kinetic Model of Burning for Pyrolyzing Materials.* Fire Safety Science, 2008. **9**: p. 1141-1152.
12. McGrattan, K., et al. *Fire Dynamics Simulator (Version 5)Technical Reference Guide*. National Institute ofStandards and Technology Special Publication, 2007. **1**.
13. Statler, D.L. and R.K. Gupta, *A Finite Element Analysis on the Modeling of Heat Release Rate*, in *COMSOL Conference*2008: Boston, MA, USA.
14. Girardin, B., et al., *Measurement of kinetics and thermodynamics of the thermal degradation for flame retarded materials: Application to EVA/ATH/NC.* Journal of Analytical and Applied Pyrolysis, 2017. **124**: p. 130-148.

15. Girardin, B., et al., *Characterization of Thermo-Physical Properties of EVA/ATH: Application to Gasification Experiments and Pyrolysis Modeling.* Materials (Basel), 2015. **8**(11): p. 7837-7863.
16. Chaos, M., *Application of sensitivity analyses to condensed-phase pyrolysis modeling.* Fire Safety Journal, 2013. **61**: p. 254-264.
17. Linteris, G.T., R.E. Lyon, and S.I. Stoliarov, *Prediction of the gasification rate of thermoplastic polymers in fire-like environments.* Fire Safety Journal, 2013. **60**: p. 14-24.
18. Stoliarov, S.I., N. Safronava, and R.E. Lyon, *The effect of variation in polymer properties on the rate of burning.* Fire and Materials, 2009. **33**(6): p. 257-271.
19. Ramroth, W.T., P. Krysl, and R.J. Asaro, *Sensitivity and uncertainty analyses for FE thermal model of FRP panel exposed to fire.* Composites Part A: Applied Science and Manufacturing, 2006. **37**(7): p. 1082-1091.
20. Livkiss, K., et al., *Uncertainties in modelling heat transfer in fire resistance tests: A case study of stone wool sandwich panels.* Fire and Materials, 2017. **41**(7): p. 799-807.
21. Staggs, J., *Important Parameter Groups in Thermal Protection of Polymers.* Materials (Basel), 2015. **8**(8): p. 4679-4698.
22. Averill, J.D., *Performance-Based Codes - Economics, Documentation, and Design*, 1998, Worcester Polytechnic Institute.
23. Hidalgo, J.P., S. Welch, and J.L. Torero, *Performance criteria for the fire safe use of thermal insulation in buildings.* Construction and Building Materials, 2015. **100**: p. 285-297.
24. Hidalgo, J.P., S. Welch, and J.L. Torero. *Design tool for the definition of thermal barriers for combustible insulation materials*. in *Proceedings of the 2nd IAFSS European Symposium of Fire Safety Science*. 2015. Nicosia, Cyprus.
25. Sinha, S., et al., *Modelling of Pyrolysis in Wood - A Review.* SESI Journal 2000. **10**: p. 1-17.
26. Kim, M., E. and N.A. Dembsey, *Engineering Guide for Estimating Material Pyrolysis Properties for Fire Modeling*, 2012, Worcester Polytechnic Institute.
27. Valencia, B.L., *Experimental and numerical investigation of the thermal decomposition of materials at three scales: applicatiion to polyether polyurethane foam used in upholstered furniture*, 2009, Ecole Nationale Supérieure de Mécanique et d'Aérotechnique.

28. Guillaume, E., A. Camillo, and T. Rogaume, *Application and Limitations of a Method Based on Pyrolysis Models to Simulate Railway Rolling Stock Fire Scenarios.* Fire Technology, 2013. **50**(2): p. 317-348.
29. Wright, M., et al., *Defining Ablative Thermal Protection System Margins for Planetary Entry Vehicles.* 2011.
30. Staggs, J.E.J., *Population balance models for the thermal degradation of PMMA.* Polymer, 2007. **48**(13): p. 3868-3876.
31. Kim, E., C. Lautenberger, and N. Dembsey, *Property estimation for pyrolysis modeling applied to polyester FRP*, in *11th International Conference and Exhibition*2009: London.
32. Azhakesan, A.M., T.J. Shields, and G.W.H. Silcock. *Developments on the Fire Propagation Test*. in *Fire Safety Science - Proceedings of the fourth international symposium*.
33. Chaos, M., et al., *Evaluation of optimization schemes and determination of solid fuel properties for CFD fire models using bench-scale pyrolysis tests.* Proceedings of the Combustion Institute, 2011. **33**(2): p. 2599-2606.
34. Girods, P., et al., *Comparison of Pyrolysis Behavior Results between the Cone Calorimeter and the Fire Propagation Apparatus Heat Sources.* Fire Safety Science, 2011. **10**: p. 889-901.
35. Quintiere, J.G., *A simplified theory for generalizing results from a radiant panel rate of flame spread apparatus.* Fire and Materials, 1981. **5**(2).
36. Guillaume, E., et al., *Real-scale fire tests of one bedroom apartments with regard to tenability assessment.* Fire Safety Journal, 2014. **70**: p. 81-97.
37. Stoliarov, S.I., et al., *Prediction of the burning rates of charring polymers.* Combustion and Flame, 2010. **157**(11): p. 2024-2034.
38. Stoliarov, S.I., I.T. Leventon, and R.E. Lyon, *Two-dimensional model of burning for pyrolyzable solids.* Fire and Materials, 2014. **38**(3): p. 391-408.
39. Di Blasi C., *Modelling and simulation of combustion processes of charring and non-charring solid fuels.* Progress in Energy and Combustion Science, 1993. **19**: p. 71–104.
40. Di Blasi, C., A. Galgano, and C. Branca, *Modeling the thermal degradation of poly(methyl methacrylate)/carbon nanotube nanocomposites.* Polymer Degradation and Stability, 2013. **98**(1): p. 266-275.

41. Di Blasi, C., *The state of the art of transport models for charrirng solid degradation.* Polymer International, 2000. **49**: p. 1133–1146.
42. Snegirev, A.Y., et al., *A new model to predict pyrolysis, ignition and burning of flammable materials in fire tests.* Fire Safety Journal, 2013. **59**: p. 132-150.
43. Staggs, J., *Simple mathematical models of char-forming polymers.* Polymer International, 2000. **49**: p. 1147±1152.
44. Moghtaderi, B. *Pyrolysis of char forming solid fuels - A critical review of the matematical modelling techniques* in *5th AOSFST*. 2001. Newcastle, Australia.
45. Moghtaderi, B., *The state-of-the-art in pyrolysis modelling of lignocellulosic solid fuels.* Fire and Materials, 2006. **30**(1): p. 1-34.
46. Lautenberger, C. and A.C. Fernandez–Pello, *Pyrolysis modeling, thermal decomposition, and transport processes in combustible solids*, in *Transport Phenomena in Fires*, M.F.a.B. Sunden, Editor. 2008, WIT Press.
47. Vermina Lundström, F., P. van Hees, and É. Guillaume, *A review on prediction models for full-scale fire behaviour of building products.* Fire and Materials, 2017. **41**(3): p. 225-244.
48. Kashiwagi, T. *Polymer combustion and flammability–role of the condensed phase*. in *Proceedings of the Combustion Institute*. 1994.
49. Lyon, R.E. and M.L. Janssens *Polymer Flammability*. DOT/FAA/AR–05/14, 2005.
50. Li, J., J. Gong, and S.I. Stoliarov, *Development of pyrolysis models for charring polymers.* Polymer Degradation and Stability, 2015. **115**: p. 138-152.
51. Shi, L. and M.Y.L. Chew, *A review of fire processes modeling of combustible materials under external heat flux.* Fuel, 2013. **106**: p. 30-50.
52. Ohlemiller, T.J., *Modeling of smoldering combustion propagation.* Progress in Energy and Combustion Science, 1985. **11**: p. 277-310.
53. Mouritz, A.P., et al., *Review of fire structural modelling of polymer composites.* Composites Part A: Applied Science and Manufacturing, 2009. **40**(12): p. 1800-1814.
54. Rein, G., *Smouldering Combustion Phenomena in Science and Technology.* International Review of Chemical Engineering, 2009. **1**: p. 3-18.
55. Rein, G., *Smouldering Combustion*, in *SFPE Handbook of Fire Protection Engineering*. 2016. p. 581-603.

56. Gardelle, B., et al., *Characterization of the carbonization process of expandable graphite/silicone formulations in a simulated fire.* Polymer Degradation and Stability, 2013. **98**(5): p. 1052-1063.
57. Kim, E. and N. Dembsey, *Parameter Estimation for Comprehensive Pyrolysis Modeling: Guidance and Critical Observations.* Fire Technology, 2014. **51**(2): p. 443-477.
58. Staggs, J.E.J., *Thermal conductivity estimates of intumescent chars by direct numerical simulation.* Fire Safety Journal, 2010. **45**(4): p. 228-237.
59. Meunders, A., et al., *Parameter Optimization and Sensitivity Analysis for FDS modelling*, in *10th International Conference on Performance-Based Codes and Fire Safety* 2014: Brisbane, Australia.
60. Lautenberger, C., G. Rein, and C. Fernandez-Pello, *The application of a genetic algorithm to estimate material properties for fire modeling from bench-scale fire test data.* Fire Safety Journal, 2006. **41**(3): p. 204-214.
61. Moghtaderi, B., et al., *An Integral Model for the Transient Pyrolysis of solid materials.* Fire and Materials, 1997. **21**: p. 7-16.
62. Theuns, E., et al., *Critical evaluation of an integral model for the pyrolysis of charring materials.* Fire Safety Journal, 2005. **40**(2): p. 121-140.
63. Theuns, E., et al., *Extension and evaluation of the integral model for transient pyrolysis of charring materials.* Fire and Materials, 2005. **29**(4): p. 195-212.
64. Chen, Y., M.A. Delichatsios, and V. Motvalli, *Material Pyrolysis Properties, Part I: An Integral Model for One-Dimensional Transient Pyrolysis of Charring and Non-Charring Materials.* Combustion Science and Technology, 1993. **88**(5-6): p. 309-328.
65. Weng, W.G. and W.C. Fan, *A pyrolysis model of charring materials considering the effect of ambient oxygen concentration.* Fire and Materials, 2007. **31**(7): p. 463-475.
66. Rhodes, B.T. and J.G. Quintiere, *Burning rate and flame heat flux for PMMA in a cone calorimeter.* Fire Safety Journal, 1996. **26**: p. 221-240.
67. Hopkins, D. and J.G. Quintiere, *Material fire properties and predictions for thermoplastics.* Fire Safety Journal 1996. **26**: p. 221–240.
68. Moghtaderi, B., et al. *An integral model for the pyrolysis of non-charring material*. in *International Association for Fire Safety Science*. 2006.

69. Theuns, E., J. Vierendeels, and P. Vandevelde, *Validation of the integral model for the pyrolysis of charring materials with a moving grid.* Journal of Computational and Applied Mathematics, 2004. **168**(1-2): p. 471-479.
70. Quintiere, J.G., *A Semi-Quantitative Model for the Burning Rate of Solid Materials*, 1992, National Institute of Standards and Technology.
71. Quintiere, J.G. and N. Iqbal, *An approximate Integral Model for the Burning Rate of a Thermoplastic Material.* Fire and Materials, 1994. **18**: p. 89–98.
72. Spearpoint, M.J. and J.G. Quintiere, *Predicting the Burning of Wood Using an Integral Model.* Combustion and Flame, 2000. **123**: p. 308–324.
73. Steckler, K., D., et al. *Analytical model for Transient gasification of Non-charring Thermoplastics materials*. in *Fire Safety Science--Proceedings of the 3rd International Symposium. IAFSS*. 1991. Boston, USA.
74. Bamford, C., J. Crank, and D. Malan, *The combustion of wood. Part I.* Mathematical Proceedings of the Cambridge Philosophical Society, 1946. **42**(2): p. 162–182.
75. Roberts, A.F. and G. Clough, *Thermal decomposition of wood in an inert atmosphere.* Symposium (International) on Combustion, 1963. **9**: p. 158-166.
76. Tinney, E.R., *The combustion of wooden dowels in heated air*, in *10th International Symposium on Combustion*1965: Pittsburgh.
77. Matsumoto, T., T. Fujiwara, and J. Kondo, *Nonsteady thermal decomposition of plastics.* Symposium (International) on Combustion, 1969.
78. Wilson, R.G., *Thermophysical properties of six charring ablators from 140° to 700°K and two chars from 800° to 3000°K*, 1965, NASA: Washington D. C.
79. Kung, H.C., *A mathematical model of wood pyrolysis* Combustion and Flame 1972. **18**: p. 185-195.
80. Kansa, E.J., H.E. Perlee, and R.F. Chaiken, *Mathematical Model of Wood Pyrolysis Including internal forced convection.* Combustion and Flame, 1977. **29**: p. 311-324.
81. Henderson, J.B., J.A. Wiebelt, and M.R. Tant, *A Model for the Thermal Response of Polymer Composite materials with Experimental verification.* Journal of Composite Materials, 1985. **19**: p. 579–595.

82. Henderson, J.B. and T.E. Wiecek, *A Mathematical Model to Predict the Thermal Response of Decomposing, Expanding Polymer Composites.* Journal of Composite Materials, 1987. **21**(4): p. 373-393.
83. Vovelle, C., et al., *Experimental and Numerical Study of the Thermal Degradation of PMMA.* Combustion Science and Technology, 1987. **53**(2-3): p. 187-201.
84. Snegirev, A., et al., *A new model to predict multi-stage pyrolysis of flammable materials in standard fire tests.* Journal of Physics: Conference Series, 2012. **395**: p. 012012.
85. Shi, L., et al., *Modeling the Pyrolysis and Combustion Behaviors of Non-Charring and Intumescent-Protected Polymers Using "FiresCone".* Polymers, 2015. **7**(12): p. 1979-1997.
86. ; Available from: https://github.com/fireFoam-dev.
87. Zeinali, D., et al. *Computational Analysis of Pyrolysis and Flame Spread for MDF Panels Placed in a Corner Configuration*. in *Eighth International Seminar on Fire and Explosion Hazards (ISFEH8).*
88. Nyazika, T., et al., *Modeling heat transfers across a silicone-based intumescent coating.* Journal of Physics: Conference Series, 2018. **1107**: p. 032012.
89. Kempel, F., et al., *Prediction of the mass loss rate of polymer materials: Impact of residue formation.* Combustion and Flame, 2012. **159**(9): p. 2974-2984.
90. Linteris, G.T., *Numerical simulations of polymer pyrolysis rate: Effect of property variations.* Fire and Materials, 2011. **35**(7): p. 463-480.
91. Witkowski, A., et al., *Development of an anaerobic pyrolysis model for fire retardant cable sheathing materials.* Polymer Degradation and Stability, 2015. **113**: p. 208-217.
92. Stoliarov, S.I. and R.N. Walters, *Determination of the heats of gasification of polymers using differential scanning calorimetry*. Polymer Degradation and Stability, 2008. **93**(2): p. 422-427.
93. Lautenberger, C. and A. Fernandez-Pello, *Optimization Algorithms for Material Pyrolysis Property Estimation.* Fire Safety Science, 2011. **10**: p. 751-764.
94. Gustafsson, S.E., *Transient plane source techniques for thermal conductivity and thermal diffusivity measurements of solid materials.* Review of Scientific Instruments, 1991. **62**(3): p. 797-804.

95. Bohac, V., et al., *Parameter estimations for measurements of thermal transport properties with the hot disk thermal constants analyzer.* Review of Scientific Instruments, 2000. **71**(6): p. 2452-2455.

96. Suleiman, B.M., S.E. Gustafsson, and L. Börjesson, *A practical cryogenic resistive sensor for thermal conductivity measurements.* Sensors and Actuators A, 1996. **57**(1): p. 15-19.

97. Parker, W.J., et al., *Flash Method of Determining Thermal Diffusivity, Heat Capacity, and Thermal Conductivity.* Journal of Applied Physics, 1961. **32**(9): p. 1679-1684.

98. Cowan, R.D., *Pulse Method of Measuring Thermal Diffusivity at High Temperatures.* Journal of Applied Physics, 1963. **34**(4): p. 926-927.

99. Cape, J.A. and G.W. Lehman, *Temperature and Finite Pulse-Time Effects in the Flash Method for Measuring Thermal Diffusivity.* Journal of Applied Physics, 1963. **34**(7): p. 1909-1913.

100. Mehling, H., et al., *Thermal difusivity of semitransparent materials determined by the laser -flash method applying a new analytical model.* International Journal of Thermophysics, 1998. **19**: p. 941–949.

101. Li, J. and S.I. Stoliarov, *Measurement of kinetics and thermodynamics of the thermal degradation for non-charring polymers.* Combustion and Flame, 2013. **160**(7): p. 1287-1297.

102. Li, J. and S.I. Stoliarov, *Measurement of kinetics and thermodynamics of the thermal degradation for charring polymers.* Polymer Degradation and Stability, 2014. **106**: p. 2-15.

103. Stoliarov, S.I., et al., *Prediction of the burning rates of non-charring polymers.* Combustion and Flame, 2009. **156**(5): p. 1068-1083.

104. Lobo, H. and C. Cohen, *Measurement of Thermal Conductivity of Polymer Melts by the Line-source Method.* Polymer Engineering & Science, 1990. **30**(2): p. 65-70.

105. Tsilingiris, P.T., *Comparative evaluation of the infrared transmission of polymer films.* Energy Conversion and Management, 2003. **44**(18): p. 2839-2856.

106. Hallman, J.R. and J.R. Welker, *Polymer Surface Reflectance-Absorptance Characteristics.* Polymer Engineering & Science, 1974. **14**(10): p. 717-723.

107. Muller, M., *Systematic approach of the synergism in flame retarded intumescent polyurethanes*, 2012, University of Lille 1: France.

108. Tranchard, P., et al., *Modelling Behaviour of a Carbon Epoxy Composite Exposed to Fire: Part I-Characterisation of Thermophysical Properties.* Materials (Basel), 2017. **10**(5).

109. De Ris, J.L. and M.M. Khan, *A Sample Holder for Determining Material Properties.* Fire and Materials, 2000. **24**: p. 219-226.

110. Calabrese, L., et al., *Parameter estimation approach to the thermal characterization of intumescent fire retardant paints.* Journal of Physics: Conference Series, 2015. **655**: p. 012048.

111. Kim, E., *Parameter Estimation Methods for Comprehensive Pyrolysis Modeling*, 2014, Worcester Polytechnic Institute.

112. Stoliarov, S.I. and J. Li, *Parameterization and Validation of Pyrolysis Models for Polymeric Materials.* Fire Technology, 2015. **52**(1): p. 79-91.

113. Bruns, M.C., *Inferring and Propagating Kinetic Parameter Uncertainty for Condensed Phase Burning Models.* Fire Technology, 2015. **52**(1): p. 93-120.

114. Levenberg, K., *A method for the solution of certain non-linear problems in least squares.* Quarterly of Applied Mathematics, 1944. **2**: p. 164–168.

115. Marquardt, D.W., *An algorithm for least-squares estimation of non linear parameters.* Journal of the Society for Industrial and Applied Mathematics, 1963. **11**: p. 431–441.

116. Ferriol, M., et al., *Thermal degradation of PMMA : Modelling of DTG and TG curves.* Polymer Degradation and Stability. **79**: p. 271-181.

117. Mamleev, V. and S. Bourbigot, *Modulated thermogravimetry in analysis of decomposition kinetics.* Chemical Engineering Science, 2005. **60**(3): p. 747-766.

118. Griffin, G.J., *The Modeling of Heat Transfer across Intumescent Polymer Coatings.* Journal of Fire Sciences, 2009. **28**(3): p. 249-277.

119. Reverte, C., J.-L. Dirion, and M. Cabassud, *Kinetic model identification and parameters estimation from TGA experiments.* Journal of Analytical and Applied Pyrolysis, 2007. **79**: p. 297-305.

120. Loulou, T., S. Salvador, and J.L. Dirion, *Determination of Reaction Parameters for Cardboard Thermal Degradation Using Experimental Data.* Chemical Engineering Research and Design, 2003. **81**(9): p. 1265-1270.

121. Calabrese, L., et al., *Thermal characterization of intumescent fire retardant paints.* Journal of Physics: Conference Series, 2014. **547**: p. 012005.

122. Bozzoli, F., et al., *Inverse heat transfer modeling applied to the estimation of the apparent thermal conductivity of an intumescent fire retardant paint.* Experimental Thermal and Fluid Science, 2018. **90**: p. 143-152.
123. Scott, E.P. and J.V. Beck, *Estimation of Thermal Properties in Carbon-Epoxy Composite Materials during Curing.* Journal of Composite Materials, 1992. **26**.
124. Pau, D., et al., *Sensitivity of Heat of Reaction for Polyurethane Foams.* Fire Safety Science, 2014. **11**: p. 179-192.
125. Marquis, D.M., et al., *Influence of reaction mechanism accuracy on the chemical reactivity prediction of complex charring material in fire condition.* Journal of Analytical and Applied Pyrolysis, 2016. **118**: p. 231-248.
126. Richter, F. and G. Rein, *Pyrolysis kinetics and multi-objective inverse modelling of cellulose at the microscale.* Fire Safety Journal, 2017. **91**: p. 191-199.
127. Bal, N., *Uncertainty and complexity in pyrolysis modelling*, 2012, University of Edinburgh.
128. Bal, N. and G. Rein, *Relevant model complexity for non-charring polymer pyrolysis.* Fire Safety Journal, 2013. **61**: p. 36-44.
129. Bal, N. and G. Rein, *On the effect of inverse modelling and compensation effects in computational pyrolysis for fire scenarios.* Fire Safety Journal, 2015. **72**: p. 68-76.
130. Rein, G., A. Carlos Fernandez-Pello, and D.L. Urban, *Computational model of forward and opposed smoldering combustion in microgravity.* Proceedings of the Combustion Institute, 2007. **31**(2): p. 2677-2684.
131. Ohlemiller, T.J. *Modeling of Smoldering Combustion Propagation*. NBSIR 84-2895, 1984.
132. Vyazovkin, S. and C. Wight, A., *Isothermal and non-isothermal kinetics of thermally stimulated reaction of solids.* International Reviews in Physical Chemistry, 1998. **17**(3): p. 407-433.
133. E698-11, A., *Standard Test Method for Kinetic Parameters for Thermally Unstable Materials by Differential Scanning Calorimetry Using the Kissinger Method*, A. International, Editor 2012: West Conshohocken, PA,.
134. Vyazovkin, S., et al., *ICTAC Kinetics Committee recommendations for collecting experimental thermal analysis data for kinetic computations.* Thermochimica Acta, 2014. **590**: p. 1-23.

135. Jain, A.A., A. Mehra, and V.V. Ranade, *Processing of TGA data: Analysis of isoconversional and model fitting methods.* Fuel, 2016. **165**: p. 490-498.

136. Opfermann, J.R., E. Kaisersberger, and H.J. Flammersheim, *Model-free analysis of thermoanalytical data-advantages and limitations.* Thermochim Acta 2002. **391**: p. 119-27.

137. Khawam, A. and D.R. Flanagan, *Basics and applications of solid-state kinetics: a pharmaceutical perspective.* J Pharm Sci, 2006. **95**(3): p. 472-98.

138. Brown, M.E., et al., *Computational aspects of kinetic analysis - Part A The ICTAC kinetics project-data, methods and results.* Thermochimica Acta, 2000. **355**: p. 125-143.

139. Roduit, B., *Computational aspects of kinetic analysis. Part E - The ICTAC Kinetics Project—numerical techniques and kinetics of solid state processes.* Thermochimica Acta, 2000. **355**: p. 171–180.

140. Ozawa, T., *A New Method of Analyzing Thermogravimetric Data.* Bull. Chem. Soc. Jpn., 1965. **38**: p. 1881-1886.

141. Coats, A.W. and J.P. Redfern, *Kinetic Parameters from Thermogravimetric Data.* Nature, 1964. **201**: p. 68-69.

142. Vyazovkin, S. and C. Wight, A., *Kinetics of solids.* Annu Rev Phys Chem., 1997. **48**: p. 125-49.

143. Vyazovkin, S., et al., *ICTAC Kinetics Committee recommendations for performing kinetic computations on thermal analysis data.* Thermochimica Acta, 2011. **520**(1-2): p. 1-19.

144. Mani, T., P. Murugan, and N. Mahinpey, *Determination of Distributed Activation Energy Model Kinetic Parameters Using Simulated Annealing Optimization Method for Nonisothermal Pyrolysis of Lignin.* Ind. Eng. Chem. Res. , 2009. **48**: p. 1464–1467.

145. Rein, G., et al., *Application of genetic algorithms and thermogravimetry to determine the kinetics of polyurethane foam in smoldering combustion.* Combustion and Flame, 2006. **146**(1-2): p. 95-108.

146. Li, K.-Y., et al., *Pyrolysis of Medium-Density Fiberboard: Optimized Search for Kinetics Scheme and Parameters via a Genetic Algorithm Driven by Kissinger's Method.* Energy & Fuels, 2014. **28**(9): p. 6130-6139.

147. Song, C., *Parameter estimation of the pyrolysis model for fir based on particle swarm algorithm*, in *Second International Conference on Mechanic Automation and Control Engineering*2011.

148. Park, W.-H. and K.-B. Yoon, *Optimization of pyrolysis properties using TGA and cone calorimeter test.* Journal of Thermal Science, 2013. **22**(2): p. 168-173.

149. Park, W.-H., et al., *Estimation of pyrolysis-related properties using repulsive particle swarm optimization.* Journal of Mechanical Science and Technology, 2012. **26**(7): p. 2129-2132.

150. Khawam, A. and D.R. Flanagan, *Solid-state kinetic models: basics and mathematical fundamentals.* J Phys Chem B, 2006. **110**(35): p. 17315-28.

151. Burnham, A.K. and B.R. L., *Global Kinetic Analysis of Complex Materials.* Energy and Fuels, 1999. **13**(1).

152. Tranchard, P., et al., *Kinetic analysis of the thermal decomposition of a carbon fibre-reinforced epoxy resin laminate.* Journal of Analytical and Applied Pyrolysis, 2017. **126**: p. 14-21.

153. Bourbigot, S., J.W. Gilman, and C.A. Wilkie, *Kinetic analysis of the thermal degradation of polystyrene–montmorillonite nanocomposite.* Polymer Degradation and Stability, 2004. **84**(3): p. 483-492.

154. Rogaume, T., *Thermal decomposition of solid fuels. Objectives, challenges and modelling.* Journal of Physics: Conference Series, 2018. **1107**: p. 022001.

155. Opfermann, J., *Kinetic Analysis Using Multivariate Non-linear Regression. I. Basic concepts.* Journal of Thermal Analysis and Calorimetry, 2000. **60** p. 641–658.

156. Anderson, H.L., A. Kemmler, and R. Strey, *Comparison of different non-linear evaluation methods in thermal analysis.* Thermochimica Acta, 1996. **271**: p. 23-29.

157. Bruns, M.C., J.H. Koo, and O.A. Ezekoye, *Population-based models of thermoplastic degradation: Using optimization to determine model parameters.* Polymer Degradation and Stability, 2009. **94**(6): p. 1013-1022.

158. Ceamanos, J., et al., *Kinetics of pyrolysis of high density polyethylene. Comparison of isothermal and dynamic experiments.* Journal of Analytical and Applied Pyrolysis, 2002. **65**: p. 93–110.

159. Koga, N., *A review of the mutual dependence of Arrhenius parameters evaluated by the thermoanalytical study of solid reactions_the kinetic compensation effect.* Thermochimica Acta, 1994. **244** p. 1-20

160. Di Blasi, C. and C. Branca, *Mathematical Model for the Nonsteady Decomposition of Intumescent Coatings.* AIChE J., 2001. **47**: p. 2359–2370.

161. Rozycki, C., *Comparison of methods of determining Arrhenius evaluation of parameters by Least Squares Method* Journal of Thermal Analysis and Calorimetry, 1984. **29** p. 959-963.

162. Lyon, R.E., *Heat Release Kinetics.* Fire and Materials, 2000. **24**: p. 179–186.

163. Stoliarov, S.I. and R.E. Lyon, *Thermo-Kinetic Model of Burning*, 2008, U.S. Department of Transportation, Federal Aviation Administration.

164. Li, J., J. Gong, and S.I. Stoliarov, *Gasification experiments for pyrolysis model parameterization and validation.* International Journal of Heat and Mass Transfer, 2014. **77**: p. 738-744.

165. Oztekin, E.S., et al., *Sources of variability in fire test data: A case study on poly(aryl ether ether ketone) (PEEK).* Combustion and Flame, 2012. **159**(4): p. 1720-1731.

166. McKinnon, M.B., S.I. Stoliarov, and A. Witkowski, *Development of a pyrolysis model for corrugated cardboard.* Combustion and Flame, 2013. **160**(11): p. 2595-2607.

167. Salvador, S., M. Quintard, and C. David, *Combustion of a substitution fuel made of cardboard and polyethylene: influence of the mix characteristics-modeling.* Fire and Materials, 2008. **32**(7): p. 417-444.

168. Webster, R., *Pyrolysis model parameter optimization using a customized stochastic hill-climber algorithm and bench scale fire test data*, 2009, University of Maryland.

169. Duan, Q.Y., V.K. Gupta, and S. Sorooshian, *Shuffled Complex Evolution Approach for Effective and Efficient Global Minimization.* Journal of Optimization Theory and Application, 1993. **76**: p. 501-521.

170. Houck, C., J.A. Joines, and M.G. Kay, *A Genetic Algorithm for Function Optimization - A Matlab Implementation*, 1995.

171. Şahin, Ö., et al., *Calcination Kinetics of Ammonium Pentaborate Using the Coats-Redfern and Genetic Algorithm Method by thermal Analysis.* Ind. Eng. Chem. Res., 2001. **40**: p. 1465-1470.

172. Jimenez, M., S. Duquesne, and S. Bourbigot, *Characterization of the performance of an intumescent fire protective coating.* Surface and Coatings Technology, 2006. **201**(3-4): p. 979-987.

173. Matala, A., S. Hostikka, and J. Mangs, *Estimation of pyrolysis model parameters for solid materials using thermogravimetric data.* Fire Safety Science, 2008. **9**: p. 1213-1223.

174. Lefebvre, J., et al., *Study of the kinetics of pyrolysis of a rigid polyurethane foam: use of the invariant kinetics parameters method.* Polymers for Advanced Technologies, 2003. **14**(11-12): p. 796-801.

175. Lautenberger, C. and A. Fernandez-Pello. *Optimization Algorithms for Material Pyrolysis Property Estimation*. in *Fire Safety Science - Proceedings of the Tenth International symposium*. 2011.

176. Chen, Y., V. Motevalli, and M.A. Delichatsios, *Material Pyrolysis Properties, Part II: Methodology for the Derivation of Pyrolysis Properties for Charring Materials.* Combustion Science and Technology, 1995. **104**(4-6): p. 401-425.

177. Ding, Y., C. Wang, and S. Lu, *Modeling the pyrolysis of wet wood using FireFOAM.* Energy Conversion and Management, 2015. **98**: p. 500-506.

178. Chaos, M., et al. *Experiments and modeling of single- and triple-wall corrugated cardboard: Effective material properties and fire behavior*. in *Fire and Materials*. 2011. San Francisco, California USA: Interscience Communications.

179. Ghorbani, Z., et al., *Critical evaluation of parameter estimation techniques for pyrolysis of charring materials*, in *8th U. S. National Combustion Meeting*2013: University of Utah.

180. Capote, J., et al., *Pyrolysis Characterization of a Lineal Low Density Polyethylene.* Fire Safety Science, 2011. **10**: p. 877-888.

181. Marquis, D.M., et al., *Existence and uniqueness of solutions of a differential equation system modeling the thermal decomposition of polymer materials.* Combustion and Flame, 2013. **160**(4): p. 818-829.

182. Marquis, D.M. and É. Guillaume, *Modelling Reaction-to-fire of Polymer-based Composite Laminate.* 2011.

183. Lauer, P., C. Trettin, and F.W. Wittbecker *Performance of optimization algorithms for deriving material data from bench scale tests*.

184. Iraa, J., L. Hasalováa, and M. Jahodaa. *The use of optimization techniques for estimation of pyrolysis model input*. in *Application of Structural Fire Engineering*. 2013. Prague, Czech Republic

185. Saha, B., P.K. Reddy, and A.K. Ghoshal, *Hybrid genetic algorithm to find the best model and the globally optimized overall kinetics parameters for thermal decomposition of plastics.* Chemical Engineering Journal, 2008. **138**(1-3): p. 20-29.

186. Morgan, A.B. and E. Toubia, *Cone calorimeter and room corner fire testing of balsa wood core/phenolic composite skin sandwich panels.* Journal of Fire Sciences, 2013. **32**(4): p. 328-345.

187. Ding, Y., et al., *Determination of kinetics and thermodynamics of thermal decomposition for polymers containing reactive flame retardants: Application to poly(lactic acid) blended with melamine and ammonium polyphosphate.* Polymer Degradation and Stability, 2016. **129**: p. 347-362.

188. Rabitz, H., *Chemical sensitivity analysis theory with applications to molecular dynamics and kinetics.* Computers & Chemirlry 1981. **5**(4): p. 167-180.

189. Rabitz, H., M. Kramer, and D. Dacol, *Sensitivity analysis in chemical kinetics.* Ann. Rev. Phys. Chern., 1983. **34**: p. 419-61.

190. Hamby, D.M., *A review of techniques for parameter sensitivity analysis of environmental models.* Environmental Monitoring and Assessment, 1994. **32**: p. 135–154.

191. Batiot, B., et al., *Sensitivity and uncertainty analysis of Arrhenius parameters in order to describe the kinetic of solid thermal degradation during fire phenomena.* Fire Safety Journal, 2016. **82**: p. 76-90.

192. Saltelli, A., et al., *Sensitivity Analysis - A Guide to assessing scientific models*. 2004: John Wiley & Sons.

193. Galgano, A., et al., *Numerical simulation of the glowing combustion of moist wood by means of a front-based model.* Fire and Materials, 2014. **38**(6): p. 639-658.

194. Stoliarov, S., S. Crowley, and R. Lyon, *Prediction of the burning rates of noncharring polymers*, 2009, U.S. Department of Transportation, Federal Aviation Administration.

195. Linteris, G., et al., *Absorption and reflection of infrared radiation by polymers in fire-like environments.* Fire and Materials, 2012. **36**(7): p. 537-553.

196. Dong, Z., et al., *Local Sensitivity Analysis of Kinetic Models for Cellulose Pyrolysis.* Waste and Biomass Valorization, 2017. **10**(4): p. 975-984.

197. Ashby, M.F., *Multi-objective optimization in material design and selection.* Acta Materialia, 2000. **48**(1): p. 359-369.

198. Daryabeigi, K. *Thermal Analysis and design of multilayer insulation for re-entry aerodynamic heating*. in *35th AIAA Thermophysics Conference*. 2001. Anaheim, CA.

199. Kumar, S. and S.P. Mahulikar, *Selection of Materials and Design of Multilayer Lightweight Passive Thermal Protection System.* Journal of Thermal Science and Engineering Applications, 2015. **8**(2): p. 021003.

200. Meacham, B. and R.L.P. Custer, *Perfomance-based fire safety engineering : An introduction of basic concepts.* Journal of Fire Protection Engineering, 1995. **7**(2): p. 35-53.

201. P., H.J., *Performance-based methodology for the fire safe design of insulation materials in energy efficient buildings*, 2015, University of Edinburg.

202. Vacca, P., *Optimized fire safe and energy efficient design of insulated assemblies using a multi-criteria approach*, 2017, The University of Edinburgh – The University of Queensland.

203. Hidalgo, J.P., J.L. Torero, and S. Welch, *Experimental Characterisation of the Fire Behaviour of Thermal Insulation Materials for a Performance-Based Design Methodology.* Fire Technology, 2016. **53**(3): p. 1201-1232.

204. Hurley, M.J. and E.R. Rosenbaum, *Performance-Based Fire Safety Design*. 2015: CRC Press.

205. Duthinh, D., *Structural Design for Fire: A Survey of Building Codes and Standards*, 2014, National Institute of Standards and Technology.

206. Duthinh, D., *Structural Design for Fire: A Survey of Building Codes and Standards*, 2014, National Institute of Standards and Technology. p. 120.

207. Calbraith, C., *The European Market for Thermal Insulation products*, 2015, IAL Consultants.

208. Johnson, C., *Numerical Solution of Partial Differential Equations by the Finite Element Method*. 1987: Cambridge University Press.

209. Lazar, S., et al., *Extreme Heat Shielding of Clay/Chitosan Nanobrick Wall on Flexible Foam.* ACS Appl Mater Interfaces, 2018. **10**(37): p. 31686-31696.

210. Mathieu, R.D., *Mechanical spallation of charring ablators in hyperthermal environments.* AIAA Journal, 1964. **2**(9): p. 1621-1627.

211. Zeitler, M., *Thermal insulation material for building equipment*, in *Materials for Energy Efficiency and Thermal Comfort in Buildings*, M.R. Hall, Editor. 2010, Woodhead Publishing.

212. Papadopoulos, A.M., *State of the art in thermal insulation materials and aims for future developments.* Energy and Buildings, 2005. **37**(1): p. 77-86.

213. Aditya, L., et al., *A review on insulation materials for energy conservation in buildings.* Renewable and Sustainable Energy Reviews, 2017. **73**: p. 1352-1365.

214. Stec, A.A. and T.R. Hull, *Assessment of the fire toxicity of building insulation materials.* Energy and Buildings, 2011. **43**(2-3): p. 498-506.

215. Zhang, M., et al., *Experimental Study of the Heat Flux Effect on Combustion Characteristics of Commonly Exterior Thermal Insulation Materials.* Procedia Engineering, 2014. **84**: p. 578-585.

216. LU, G., et al. *Study on modified phenolic foam for Insulation of building's exterior wall*. in *3rd International Conference on Mechatronics, Robotics and Automation*. 2015. Atlantis Press.

217. Sabarilal, S. and A. Kumar, *Effect of Back Boundary Condition on Pyrolysis of Charring and Non-charring Materials.* Journal of Physics: Conference Series, 2018. **1107**: p. 032024.

218. Ebert, H.-P. and F. Hemberger, *Intercomparison of thermal conductivity measurements on a calcium silicate insulation material.* International Journal of Thermal Sciences, 2011. **50**(10): p. 1838-1844.

219. Geoffroy, L., et al., *Intumescent Polymer Metal Laminates for Fire Protection.* Polymers (Basel), 2018. **10**(9).

220. Croy, D.E. and D.A. Dougherty, *Handbook of thermal insulation applications*, 1983, Naval Civil Engineering Laboratory.

221. Wulf, R., G. Barth, and U. Gross, *Intercomparison of Insulation Thermal Conductivities Measured by Various Methods.* International Journal of Thermophysics, 2007. **28**(5): p. 1679-1692.
222. Van Belleghem, M., et al., *Drying behaviour of calcium silicate.* Construction and Building Materials, 2014. **65**: p. 507-517.
223. Cao, W., et al., *Thermal conductivity of highly porous ceramic foams with different agar concentrations.* Materials Letters, 2015. **139**: p. 66-69.
224. Coquard, R., D. Rochais, and D. Baillis, *Conductive and Radiative Heat Transfer in Ceramic and Metal Foams at Fire Temperatures.* Fire Technology, 2010. **48**(3): p. 699-732.
225. Huo, W.-L., et al., *Highly Porous Zirconia Ceramic Foams with Low Thermal Conductivity from Particle-Stabilized Foams.* Journal of the American Ceramic Society, 2016. **99**(11): p. 3512-3515.
226. Dréan, V., et al., *Numerical simulation of the fire behaviour of façade equipped with aluminium composite material-based claddings—Model validation at intermediate scale.* Fire and Materials, 2019.
227. McKenna, S.T., et al., *Fire behaviour of modern facade materials - Understanding the Grenfell Tower fire.* J Hazard Mater, 2019. **368**: p. 115-123.
228. Gong, L., et al., *Porous mullite ceramics with low thermal conductivity prepared by foaming and starch consolidation.* Journal of Porous Materials, 2013. **21**(1): p. 15-21.
229. Boetes, R., *Heat transfer reduction in closed cell polyurethane foams*, 1986, Technische Universiteit Delft
230. Hilyard, N.C. and A. Cunningham, *Low density cellular plastics*. 1994: Springer Science.
231. Hildmann, B. and H. Schneider, *Heat capacity of mullite.* Journal of the American Ceramic Society, 2004. **87**: p. 227–34.
232. Barea, R., et al., *Thermal conductivity of highly porous mullite material.* Acta Materialia, 2005. **53**(11): p. 3313-3318.
233. Clayton, W.A., et al., *Thermal properties of ablative chars*, 1967, The Boeing Company.
234. Gong, L., et al., *Thermal conductivity of highly porous mullite materials.* International Journal of Heat and Mass Transfer, 2013. **67**: p. 253-259.

235. Guo, H., W. Li, and F. Ye, *Preparation of microporous mullite ceramics by foaming for high temperature thermal isolation.* Ceramics International, 2016. **42**(15): p. 17332-17338.

236. Wang, J., et al., *A new approach to modelling the effective thermal conductivity of heterogeneous materials.* International Journal of Heat and Mass Transfer, 2006. **49**(17-18): p. 3075-3083.

237. Han, Y., et al., *Porous anorthite ceramics with ultra-low thermal conductivity.* Journal of the European Ceramic Society, 2013. **33**(13-14): p. 2573-2578.

238. Guo, H., et al., *Preparation and characterization of foamed microporous mullite ceramics based on kyanite.* Ceramics International, 2015. **41**(10): p. 14645-14651.

239. Loeb, A., *A theory of thermal conductivity of porous materials.* Journal of The American Ceramic Society, 1954. **37**(2).

240. Bourret, J., et al., *Thermal Conductivity of Very Porous Kaolin-Based Ceramics.* Journal of the American Ceramic Society, 2014. **97**(3): p. 938-944.

241. Siegel, R. and J.R. Howell, *Thermal Radiation Heat transfer*. 1992, London: Taylor & Francis.

242. Bourbigot, S., et al., *Nonwoven as heat barrier: Modeling of the efficiency of Carbtex fibers.* Journal of Applied Polymer Science, 2008. **108**(5): p. 3245-3255.

243. Coquard, R., D. Rochais, and D. Baillis, *Experimental investigations of the coupled conductive and radiative heat transfer in metallic/ceramic foams.* International Journal of Heat and Mass Transfer, 2009. **52**(21-22): p. 4907-4918.

244. Tseng, C.J. and K.T. Kuo, *Thermal properties of phenolic foam insulation.* Journal of the Chinese Institute of Engineers, 2002. **25**(6): p. 753-758.

245. Kandola, B.K. and E. Kandare, *Composites having improved fire resistance.* 2008: p. 398-442.

246. Buist, J.M., S.J. Grayson, and W.D. Woolley, *Fire and cellular polymers*. 1986: Elsevier.

247. Johnson, A. and A. Gibson, *The Tools of the Design Process and Management of Design.* 2014: p. 113-180.

248. Guillaume, E., *Effects of under-ventilated conditions on the reaction to fire of a PIR foam*, in *International Conference Fire and Materials*2013.

249. Shi, S., et al., *Modeling of one-dimensional thermal response of silica-phenolic composites with volume ablation.* Journal of Composite Materials, 2012. **47**(18): p. 2219-2235.

250. Schiavoni, S., et al., *Insulation materials for the building sector: A review and comparative analysis.* Renewable and Sustainable Energy Reviews, 2016. **62**: p. 988-1011.

251. Carvalho, G.d. and E. Frollini, *Lignin in Phenolic Closed Cell Foams: Thermal Stability and Apparent Density.* Journal of Macromolecular Science, Part A, 2002. **39**(7): p. 643-656.

252. Hidalgo, J.P., J.L. Torero, and S. Welch, *Fire performance of charring closed-cell polymeric insulation materials: Polyisocyanurate and phenolic foam.* Fire and Materials, 2018.

253. Branca, C., et al., *Reaction kinetics and morphological changes of a rigid polyurethane foam during combustion.* Thermochimica Acta, 2003. **399**(1-2): p. 127-137.

254. Wang, Y.C. and A. Foster, *Experimental and numerical study of temperature developments in PIR core sandwich panels with joint.* Fire Safety Journal, 2017. **90**: p. 1-14.

255. Glicksman, L., M. Schuetz, and M. Sinofsky, *Radiation heat transfer in foam insulation.* International Journal of Heat and Mass Transfer, 1987. **30**: p. 187-197.

256. Rostami, A., J. Murthy, and M. Hajaligol, *Modeling of a smouldering cigarette.* Journal of Analytical and Applied Pyrolysis, 2002. **66**: p. 281-301.

257. GHABI, C., et al. *Bidimensionnal numerical model for polyurethane smoldering in a fixed bed*. in *4th International Conference on Computational Heat and Mass Transfer*. 2005.

258. Bar-Ilan, A., et al., *Forced forward smoldering experiments in microgravity.* Experimental Thermal and Fluid Science, 2004. **28**: p. 743-751.

259. Rein, G., et al., *Modeling of one-dimensional smoldering of polyurethane in microgravity conditions.* Proceedings of the Combustion Institute, 2005. **30**(2): p. 2327-2334.

260. Di Blasi, C., *Mechanisms of Two-Dimensional Smoldering Propagation Through Packed Fuel Beds.* Combustion Science and Technology, 1995. **106**(1-3): p. 103-124.

261. Chen, Y.-K. and F.S. Milos, *Multidimensional Finite Volume Fully Implicit Ablation and Thermal Response Code.* Journal of Spacecraft and Rockets, 2018. **55**(4): p. 914-927.

262. Bahramian, A.R., et al., *Ablation and thermal degradation behaviour of a composite based on resol type phenolic resin: Process modeling and experimental.* Polymer, 2006. **47**(10): p. 3661-3673.

263. Moyer, C.B. and R.A. Rindal, *Finite Difference Solution for the In-Depth Response of charring materials considering surface chemical & energy balances*.

264. Chen, Y.K. and F.S. Milos, *Ablation and Thermal Response Program for Spacecraft Heatshield Analysis.* Journal of Spacecraft and Rockets, 1999. **36**(3): p. 475-483.

265. Milos, F.S., Y.-K. Chen, and T.H. Squire. *Updated ablation and thermal response program for spacecraft heatshield analysis*. in *17th Thermal and Fluids Analysis Workshop*. 2016. University of Maryland.

266. Duquesne, S., et al., *Intumescent paints: fire protective coatings for metallic substrates.* Surface and Coatings Technology, 2004. **180-181**: p. 302-307.

267. Gardelle, B., et al., *Thermal degradation and fire performance of intumescent silicone-based coatings.* Polymers for Advanced Technologies, 2013. **24**(1): p. 62-69.

268. Bourbigot, S., B. Gardelle, and S. Duquesne. *Intumescent silicone-based coatings for the fire protection of carbon fiber reinforced composites*. in *Fire Safety Science -- Proceedings of Eleventh International Symposium*. 2014. International Association for Fire Safety Science.

269. Gardelle, B., et al., *Resistance to fire of intumescent silicone based coating: The role of organoclay*. Progress in Organic Coatings, 2013. **76**(11): p. 1633-1641.

270. Gardelle, B., et al., *Resistance to fire of curable silicone/expandable graphite based coating: Effect of the catalyst.* European Polymer Journal, 2013. **49**(8): p. 2031-2041.

271. Bourbigot, S., B. Gardelle, and S. Duquesne, *Intumescent silicone-based coatings for the fire protection of carbon fiber reinforced composites.* Fire Safety Science, 2014. **11**: p. 781-793.

272. Jimenez, M., S. Duquesne, and S. Bourbigot, *Multiscale Experimental Approach for developing High-Performance Intumescent Coatings.* Ind. Eng. Chem. Res., 2006. **45**(13): p. 4500-4508.

273. Anderson, C.E. and D.K. Wauters, *A thermodynamic heat transfer model for intumescent systems.* International Journal of Engineering Science, 1984. **22**(7): p. 881-889.

274. Gillet, M., L. Autrique, and L. Perez, *Mathematical model for intumescent coatings growth: application to fire retardant systems evaluation.* Journal of Physics D: Applied Physics, 2007. **40**(3): p. 883-899.

275. Staggs, J.E.J., R.J. Crewe, and R. Butler, *A theoretical and experimental investigation of intumescent behaviour in protective coatings for structural steel.* Chemical Engineering Science, 2012. **71**: p. 239-251.

276. Di Blasi, C., *Modeling the effects of high radiative heat fluxes on intumescent material decomposition.* Journal of Analytical and Applied Pyrolysis, 2004. **71**(2): p. 721-737.

277. Shih, Y.C., F.B. Cheung, and J.H. Koo, *Theoretical Modeling of Intumescent Fire-Retardant Materials.* Journal of Fire Sciences, 2016. **16**(1): p. 46-71.

278. Bourbigot, S., S. Duquesne, and J.-M. Leroy, *Modeling of Heat Transfer of a Polypropylene-Based Intumescent System during Combustion.* Journal of Fire Sciences, 1999. **17**(1): p. 42-56.

279. Cirpici, B.K., Y.C. Wang, and B. Rogers, *Assessment of the thermal conductivity of intumescent coatings in fire.* Fire Safety Journal, 2016. **81**: p. 74-84.

280. Cirpici, B.K., *Simulating the expansion process of intumescent coating*, in *Faculty of Engineering and Physical Sciences*2015, University of Manchester.

281. Zhang, Y., et al., *Global modelling of fire protection performance of intumescent coating under different cone calorimeter heating conditions.* Fire Safety Journal, 2012. **50**: p. 51-62.

282. Bhargava, A. and G.J. Griffin, *A Two Dimensional Model of Heat Transfer Across a Fire Retardant Epoxy Coating Subjected to an Impinging Flame.* Journal of Fire Sciences, 2016. **17**(3): p. 188-208.

283. Bourbigot, S. and S. Dusquene. *Quantitative approach of intumescence by numerical simulation*. in *243 rd American Chemical Society National meeting*. 2012. San Diego.

284. Ye, F., C.G. Zhu, and Z.H. Zhang, *Study on the Growth Model of Expandable Graphite.* Advanced Materials Research, 2014. **989-994**: p. 814-819.

285. Longo, A., S. De Nicola, and G. Carotenuto, *Thermal expansion of graphite intercalation compounds*, in *Trends in Nanotechnology Conference*2008: Italy.

286. Mysyk, R.D., et al., *Theoretical model and experimental study of pore growth during thermal expansion of graphite intercalation compounds.* Journal of Thermal Analysis and Calorimetry, 2005. **79**: p. 515–519.

287. Franssen, J.-M., V. Kodur, and R. Zaharia, *Designing Steel Structures for Fire Safety*. 2009: CRC Press/Balkema.

288. (CEN), C.E.d.N., *EN 1993-1-1:2005 Eurocode 3: Design of steel structures - Part 1-1: General rules and rules for buildings*, 2005: Brussels.

289. (CEN), C.E.d.N., *EN 1993-1-2:2005 Eurocode 3: Design of Steel Structures - Part 1-2: General Rules - Structural Fire Design*, 2005: Brussels, Belgium.

290. Băetu, G., T.-F. Gălățanu, and S.-A. Băetu, *Behavior of Steel Structures under Elevated Temperature.* Procedia Engineering, 2017. **181**: p. 265-272.

291. (ISO), I.O.f.S., *Reaction to fire tests - Heat release, smoke production and mass loss rate*, 2015.

292. Lucherini, A., J. Torero, and C. Maluk, *Effects of thermal conditions of steel on the fire performance of thin intumescent coatings*, in *15th International Conference and Exhibition on Fire Science and Engineering* 2019: Royal Holloway College, London, UK.

293. Schartel, B., M. Bartholmai, and U. Knoll, *Some comments on the use of cone calorimeter data.* Polymer Degradation and Stability, 2005. **88**(3): p. 540-547.

294. Beck, J.V., *Thermocouple Temperature disturbances in low conductivity materials.* Journal of Heat Transfer, 1962. **84**(2).

295. Reszka, P., *In-Depth Temperature Profiles in Pyrolyzing Wood*, 2008, University of Edinburgh.

296. Lindemann, A., F. Beckstein, and M. Brunner, *Penetration Model in the NETZSCH LFA Software - Porous Materials Finally Handled Properly!*, NETZSCH-Gerätebau GmbH.

297. Lian, T.-W., et al., *Rapid thermal conductivity measurement of porous thermal insulation material by laser flash method.* Advanced Powder Technology, 2016. **27**(3): p. 882-885.

298. Kövér, M., et al., *Determination of the specific heat using laser flash apparatus.* Journal of Thermal Analysis and Calorimetry, 2015. **122**(1): p. 151-156.

299. Brunner, M., et al., *Only an Excellent Model Yields Great Results! New Approach in Proteus® 7.1 for LFA Analysis*, NETZSCH-Gerätebau GmbH.

300. Zajas, J. and P. Heiselberg, *Measurements of thermal diffusivity specific heat capacity and thermal conductivity with LFA 447 apparatus*, 2013, Department of Civil Engineering - Aalborg University.

301. Seifter, A., K. Boboridis, and A.W. Obst, *Emissivity Measurements on Metallic surfaces with various degrees of roughness: A Comparison of Laser Polarimetry and Integrating Sphere Reflectometry.* International Journal of Thermophysics, 2004. **25**(2): p. 547–560.

302. Seifter, A., K. Boboridis, and A.W. Obst. *Comparison of emissivity measurement using an integrating sphere reflectrometer and a laser polarimeter on surfaces with various degrees of roughness*. in *XVII IMEKO World Congress*. 2003. Dubrovnik, Croatia.
303. King, J.L., et al., *Computation of total hemispherical emissivity from directional spectral models.* International Journal of Heat and Mass Transfer, 2017. **109**: p. 894-906.
304. Del Pino, C.B., M.V. Eesbeek, and T. Rohr. *Hemispherical emissivity by infrared reflectance*. in *European Conference on Spacecraft Strucutures, Materials & Mechanical Testing ESA SP-581*. 2005. Noordwijk, The Netherlands.
305. Pryor, R.W., *Multiphysics modeling using COMSOL : a first principles approach*. 2011, Sudbury, Massachusetts: Jones and Bartlett Publishers.
306. Multiphysics®, C. *COMSOL Multiphysics Reference Manual* 2017.
307. Wickström, U., *Heat transfer by radiation and convection in fire testing.* Fire and Materials, 2004. **28**(5): p. 411-415.
308. Wickstrom, U., D. Duthinh, and K. McGrattan, *Adiabatic surface temperature for calculating heat transfer to fire exposed structures*, in *Interflam 2007 (Interflam '07) International Interflam Conference 11th Proceedings*2007, Interscience Communications: London, England.
309. Wilson, M.T., B.Z. Dlugogorski, and K.E. M., *Uniformity of radiant heat fluxes in cone calorimeter.* Fire Safety Science -- Proceedings of the Seventh International Symposium, 2003(International Association for Fire Safety Science): p. 815-827.
310. 5660-1:2015, I., *Reaction to fire tests - Heat release, smoke production and mass loss rate*, 2015.
311. Blumm, J., et al., *Measurement of Selected Thermophysical Properties of the NPL Certified Reference Material Stainless Steel 310.* International Journal of Thermophysics, 2007. **28**(2): p. 674-682.
312. Wei, G., et al., *Thermal Diffusivity Measurements on Insulation Materials with the Laser Flash Method.* International Journal of Thermophysics, 2006. **27**(1): p. 235-243.
313. Yoon, K.-B., W.-H. Park, and T.-K. Kim, *Estimation of convection heat transfer coefficient and surface emissivity of a nonreacting specimen in cone calorimeter using RPSO method.* Journal of Mechanical Science and Technology, 2013. **27**(6): p. 1575-1580.

314. Staggs, J.E.J., *A reappraisal of convection heat transfer in the cone calorimeter.* Fire Safety Journal, 2011. **46**(3): p. 125-131.
315. Staggs, J.E.J., *Convection heat transfer in the cone calorimeter.* Fire Safety Journal, 2009. **44**(4): p. 469-474.
316. Vermesi, I., et al., *Pyrolysis and spontaneous ignition of wood under transient irradiation: Experiments and a-priori predictions.* Fire Safety Journal, 2017. **91**: p. 218-225.
317. Ryder, N.L. and E.J. Weckman, *Effects on Convective Heat Transfer Coefficient In Predictions of Materials Properties from Cone Calorimeter Testing*, in *Fire & Materials Conference*2013: San Francisco, CA.
318. Jacob, V., M. Bhasi, and R. Gopikakumari, *Impact of Human Factors on Measurement Errors.* International Journal of Measurement Technologies and Instrumentation Engineering, 2011. **1**(4): p. 28-44.
319. de Oliveira, J.T., J.V. Beck, and K.J. Arnold, *Parameter Estimation in Engineering and Science.* International Statistical Review / Revue Internationale de Statistique, 1979. **47**(1): p. 85.
320. García, E., M.I. Osendi, and P. Miranzo, *Thermal diffusivity of porous cordierite ceramic burners.* Journal of Applied Physics, 2002. **92**(5): p. 2346-2349.
321. Geoffroy, L., et al., *Additive manufacturing of fire-retardant ethylene-vinyl acetate.* Polymers for Advanced Technologies, 2019.
322. Nield, A.D. and A. Bejan, *Convection in Porous Media*. 3rd ed. 2006: Springer.
323. Van Keulen, J., *Density of porous solids.* Journal of Materials and Construction, 1973. **6**: p. 181.
324. Song, S.A., Y.S. Chung, and S.S. Kim, *The mechanical and thermal characteristics of phenolic foams reinforced with carbon nanoparticles.* Composites Science and Technology, 2014. **103**: p. 85-93.
325. Schneider, H., J. Schreuer, and B. Hildmann, *Structure and properties of mullite—A review.* Journal of the European Ceramic Society, 2008. **28**(2): p. 329-344.
326. Shackelford, J.F. and W. Alexander, *Thermal properties of materials*, in *Materials Science and Engineering Handbook*. 2001, CRC Press.
327. Hildmann, B. and H. Schneider, *Thermal Conductivity of 2/1-Mullite Single Crystals.* Journal of the American Ceramic Society, 2005. **88**(10): p. 2879-2882.

328. Francl, J. and W.D. Kingery, *ExperimentaI Investigation of Effect of Porosity on Thermal Conductivity.* Journal of The American Ceramic Society, 1954. **37**(2).

329. Salazar, A., *On thermal diffusivity.* European Journal of Physics, 2003. **24**(4): p. 351-358.

330. Feih, S., et al., *Influence of water content on failure of phenolic composites in fire.* Polymer Degradation and Stability, 2008. **93**(2): p. 376-382.

331. Bousah, M., et al., *Effect of microsphere content on fire perfomance and thermomechanical properties of phenolic resole syntactic foam composites*, in *The 19th International Conference on Composite Materials - ICCM19*2013: Montreal Canada.

332. Roberts, A.F., *Problems associated with the theoretical analysis of the burning of wood*, in *Symposium (International) on Combustion*1971.

333. Boonmee, N. and J.G. Quintiere, *Glowing ignition of wood: the onset of surface combustion.* Proceedings of the Combustion Institute, 2005. **30**(2): p. 2303-2310.

334. Ewing, M.E., T.S. Laker, and D.T. Walker, *Numerical Modeling of Ablation Heat Transfer.* Journal of Thermophysics and Heat Transfer, 2013. **27**(4): p. 615-632.

335. Moyer, C.B., *User's manual - Aerotherm charring material thermal response and ablation program - version 3*, 1970, Air Force Rocket Propulsion Laboratory.

336. Tranchard, P., et al., *Modelling Behaviour of a Carbon Epoxy Composite Exposed to Fire: Part II-Comparison with Experimental Results.* Materials (Basel), 2017. **10**(5).

337. Wang, X.-M., et al., *Estimation of temperature-dependent thermal conductivity and specific heat capacity for charring ablators.* International Journal of Heat and Mass Transfer, 2019. **129**: p. 894-902.

338. Mazzaracchio, A., *One-Dimensional Thermal Analysis Model for Charring Ablative Materials.* Journal of Aerospace Technology and Management, 2018. **10**.

339. Russell, G.W. and F. Strobel, *Modeling Approach for Intumescing Charring Heatshield Materials.* Journal of Spacecraft and Rockets, 2006. **43**: p. 739-749.

340. Polifke, W., W. Geng, and K. Döbbeling, *Optimization of Rate Coefficients for Simplified Reaction Mechanisms with Genetic Algorithms.* Combustion and Flame, 1998. **113**: p. 119-134.

341. Milos, F.S. and D.J. Rasky, *Review of numerical procedures for computational surface thermochemistry.* Journal of Thermophysics and Heat Transfer, 1994. **8**(1): p. 24-34.

342. Galgano, A., C. Branca, and C. Di Blasi, *Development of a front-based model for the glowing combustion of wood*, in *XXXIX Meeting of the Italian Section of the Combustion Institute*.

343. Li, K.Y., X. Cheng, and H. Zhang, *A simplified model on vertical density profile and shrinkage ratio of virgin and charred medium density fibreboard.* Fire and Materials, 2014. **38**(6): p. 659-672.

344. Mouritz, A.P. and A.G. Gibson, *Fire Properties of Polymer Composite Materials*. Solid Mechanics and its Applications. Vol. 143. 1999: Springer.

345. Bouslah, M., et al. *Effect of microsphere content on fire performance and thermomechanical properties of phenolic resole syntactic*. in *The 19th International Conference on Composite Materials*. 2013.

346. Wilson, R., G., *Thermophysical properties of six charring ablators from 140° to 700°K and two chars from 800° to 3000°K*, 1965, NASA.

347. Lachaud, J., et al., *TACOT v3.0*, A.W.C.C. 4., Editor 2014.

348. Alonso, M.V., et al., *Thermal degradation of lignin–phenol–formaldehyde and phenol–formaldehyde resol resins.* Journal of Thermal Analysis and Calorimetry, 2011. **105**(1): p. 349-356.

349. Shen, D.K., S. Gu, and K.H. Luo, *Analysis of Wood Structural Changes under Thermal Radiation.* Energy & Fuels, 2009. **23**: p. 1081-1088.

350. Sullivan R. M. and Stokes E. H., *Porous Media and mixture models for hygrothermal behaviour of phenolic composites.* NASA Report TM-1999-209444, 1999.

351. Potts, R.L., *Application of integral methods to ablation charring erosion - A review.* Journal of Spacecraft and Rockets, 1995. **32**(2): p. 200-209.

352. Okyay, G., et al., *Fractal conceptualization of intumescent fire barriers, toward simulations of virtual morphologies.* Sci Rep, 2019. **9**(1): p. 1872.

353. Mesquita, L.M.R., et al., *Decomposition of Intumescent Coatings comparison between a numerical method and experimental results.* Acta Polytechnica 2009. **49**(1).

354. Nørgaard, K.P., et al., *Engineering model for intumescent coating behavior in a pilot-scale gas-fired furnace.* AIChE Journal, 2016. **62**(11): p. 3947-3962.

355. Quintiere, J.G., R.E. Lyon, and S.B. Crowley, *An exercise in obtaining flame radiation fraction from the cone calorimeter.* Fire and Materials, 2016. **40**(6): p. 861-872.

356. Girardin, B., *Numerical modelling and small scale testing of fire perfomances for halogen-free cable*, 2016, University of Lille: Lille, France.

357. Tewarson, A., *Combustion efficiency and its radiative component.* Fire Safety Journal, 2004. **39**(2): p. 131-141.

358. Hostikka, S. and J. Axelsson, <*Modelling of the radiative feedback from the flames in cone calorimeter.pdf*>, 2003, VTT Building and Transport & SP Swedish National Testing and Research Institute.

359. Lucherini, A. and C. Maluk, *Assessing the onset of swelling for thin intumescent coatings under a range of heating conditions.* Fire Safety Journal, 2019. **106**: p. 1-12.

360. Koo, J.H., *Thermal Characteristics Comparison of Two Fire Resistant Materials.* Journal of Fire Sciences, 1997. **15**(3): p. 203-221.

361. Gardner, L. and K.T. Ng, *Temperature development in structural stainless steel sections exposed to fire.* Fire Safety Journal, 2006. **41**(3): p. 185-203.

362. SPFE, *SFPE handbook of fire protection engineering*. 5th ed. 2016, New York, United States: Springer New York.

363. SFPE, *SFPE Engineering Guide to Performance-Based Fire Protection*. 2006, MA: Quincy.

364. *Building Construction and Safety Code*, in *5000*, NFPA, Editor 2015.

365. (CEN), C.E.d.N., *EN 13381-8:2013 Test Methods for determining the contribution to the fire resistance of structural memebers - Part 8: Applied reactive protection to steel members*, 2013: Brussels, Belgium.

366. Tranchard, P., et al., *Fire behaviour of carbon fibre epoxy composite for aircraft: Novel test bench and experimental study.* Journal of Fire Sciences, 2015. **33**(3): p. 247-266.

367. Le Nevé, S., *Fire tests on components used in fire zones. Comparison of gas burner to oil burner*, 2010, International aircraft materials fire test working group: Atlantic City, NJ.

368. COMSOL. *Introduction to Design Optimization in COMSOL Multiphysics®*. 2019 [cited 2019 18 June]; Available from: https://www.comsol.fr/video/introduction-to-design-optimization-in-comsol-multiphysics.

369. Dominguez, J., et al., *Thermal properties and thermal degradation kinetics of phenolic and wood flour-reinforced phenolic foams.* Journal of Composite Materials, 2017. **51**(1): p. 125–138.

370. Roenner, N., et al., *Computational study of how inert additives affect the flammability of a polymer.* Fire Safety Journal, 2019. **106**: p. 189-196.
371. Huang, C., Z. Huang, and Q. Wang, *Effect of high-temperature treatment on the mechanical and thermal properties of phenolic syntactic foams.* Polymer Engineering & Science, 2018. **58**(12): p. 2200-2209.
372. Wang, S., R. Luo, and Y. Ni, *Preparation and characterization of resin-derived carbon foams reinforced by hollow ceramic microspheres.* Materials Science and Engineering: A, 2010. **527**(15): p. 3392-3395.
373. Schartel, B., et al., *Sub-micrometre coatings as an infrared mirror: A new route to flame retardancy.* Fire and Materials, 2012. **36**(8): p. 671-677.
374. Gardelle, B., *Development and resistance to fire of intumescnt silicone-based coating- fire protection of steel in simulated fire*, 2013, Université de Lille.
375. Alongi, J., Z. Han, and S. Bourbigot, *Intumescence: Tradition versus novelty. A comprehensive review.* Progress in Polymer Science, 2015. **51**: p. 28-73.
376. Duquesne, S., et al., *Thermoplastic resins for thin film intumescent coatings – towards a better understanding of their effect on intumescence efficiency.* Polymer Degradation and Stability, 2005. **88**(1): p. 63-69.
377. Puri, R.G. and A.S. Khanna, *Intumescent coatings: A review on recent progress.* Journal of Coatings Technology and Research, 2016. **14**(1): p. 1-20.
378. Kim, Y., et al., *Modelling heat transfer in an intumescent paint and its effect on fire resistance of on-board hydrogen storage.* International Journal of Hydrogen Energy, 2017. **42**(11): p. 7297-7303.

APPENDIX 1. TECHNICAL SHEETS

- **Calcium silicate properties (DISTRISOL)**

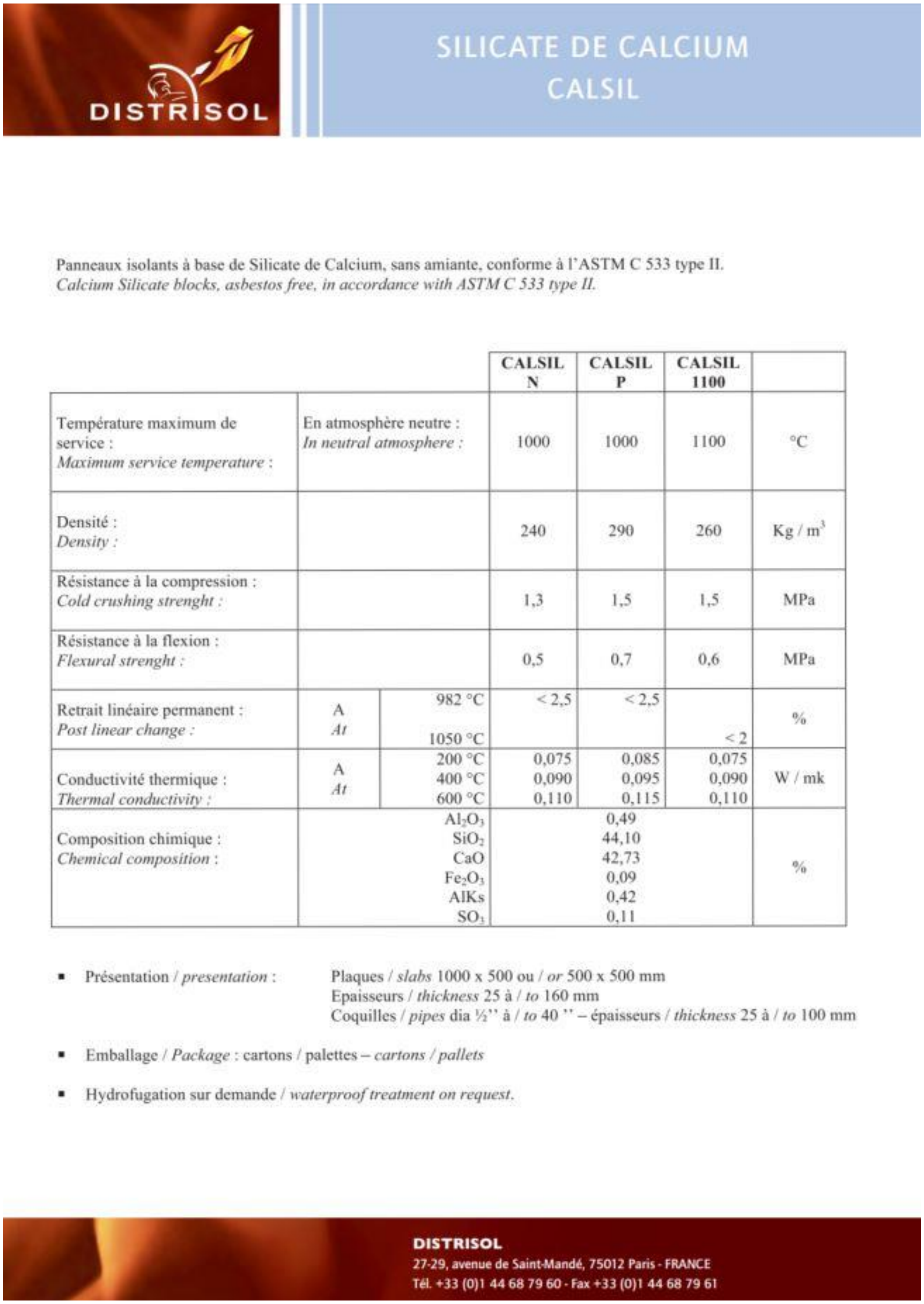

DISTRISOL

SILICATE DE CALCIUM
CALSIL

Panneaux isolants à base de Silicate de Calcium, sans amiante, conforme à l'ASTM C 533 type II.
Calcium Silicate blocks, asbestos free, in accordance with ASTM C 533 type II.

			CALSIL N	CALSIL P	CALSIL 1100	
Température maximum de service : *Maximum service temperature :*	En atmosphère neutre : *In neutral atmosphere :*		1000	1000	1100	°C
Densité : *Density :*			240	290	260	Kg / m^3
Résistance à la compression : *Cold crushing strenght :*			1,3	1,5	1,5	MPa
Résistance à la flexion : *Flexural strenght :*			0,5	0,7	0,6	MPa
Retrait linéaire permanent : *Post linear change :*	A *At*	982 °C	< 2,5	< 2,5		%
		1050 °C			< 2	
Conductivité thermique : *Thermal conductivity :*	A *At*	200 °C	0,075	0,085	0,075	W / mk
		400 °C	0,090	0,095	0,090	
		600 °C	0,110	0,115	0,110	
Composition chimique : *Chemical composition :*		Al_2O_3	0,49			%
		SiO_2	44,10			
		CaO	42,73			
		Fe_2O_3	0,09			
		AlKs	0,42			
		SO_3	0,11			

- Présentation / *presentation* : Plaques / *slabs* 1000 x 500 ou / *or* 500 x 500 mm
  Epaisseurs / *thickness* 25 à / *to* 160 mm
  Coquilles / *pipes* dia ½'' à / *to* 40 '' – épaisseurs / *thickness* 25 à / *to* 100 mm
- Emballage / *Package* : cartons / palettes – *cartons / pallets*
- Hydrofugation sur demande / *waterproof treatment on request.*

DISTRISOL
27-29, avenue de Saint-Mandé, 75012 Paris - FRANCE
Tél. +33 (0)1 44 68 79 60 - Fax +33 (0)1 44 68 79 61

- **Closed-cell mullite foam properties (BYLIM)**

Closed-cell Mullite foam block

Specifications

Characteristics		**QN - 23**	**Units**
Safety application temperature		1260	°C
Bulk density		500	$kg.m^{-3}$
Crushing strength		≥1.0	MPa
Reheat linear change		1230 °C x 24h	**%**
		≤-0.3	
Reversible thermal expansion 1090°C		≤0.5	**%**
Thermal conductivity	at 400°C	0.15	$W.m^{-1}.K^{-1}$
	600°C	0.17	
	800°C	0.19	
	1000°C	0.35	
Chemical composition	Al_2O_3	≥ 37	%
	Fe_2O_3	≤ 1.0	%
	SiO_2	≤ 55%	%
Porosity		85	%
Average pore size		100	µm

Bylim Special Products, Bogaartsborg 6, 6228 AM Maastricht, The Netherlands
Tel: +31 43 3110764 Fax: +31 842274893
ING Bank: 68.21.91.965 NCC nr.: 14105923 VAT nr.: NL2100.11.580B01

- **Phenolic foam properties (KINGSPAN)**

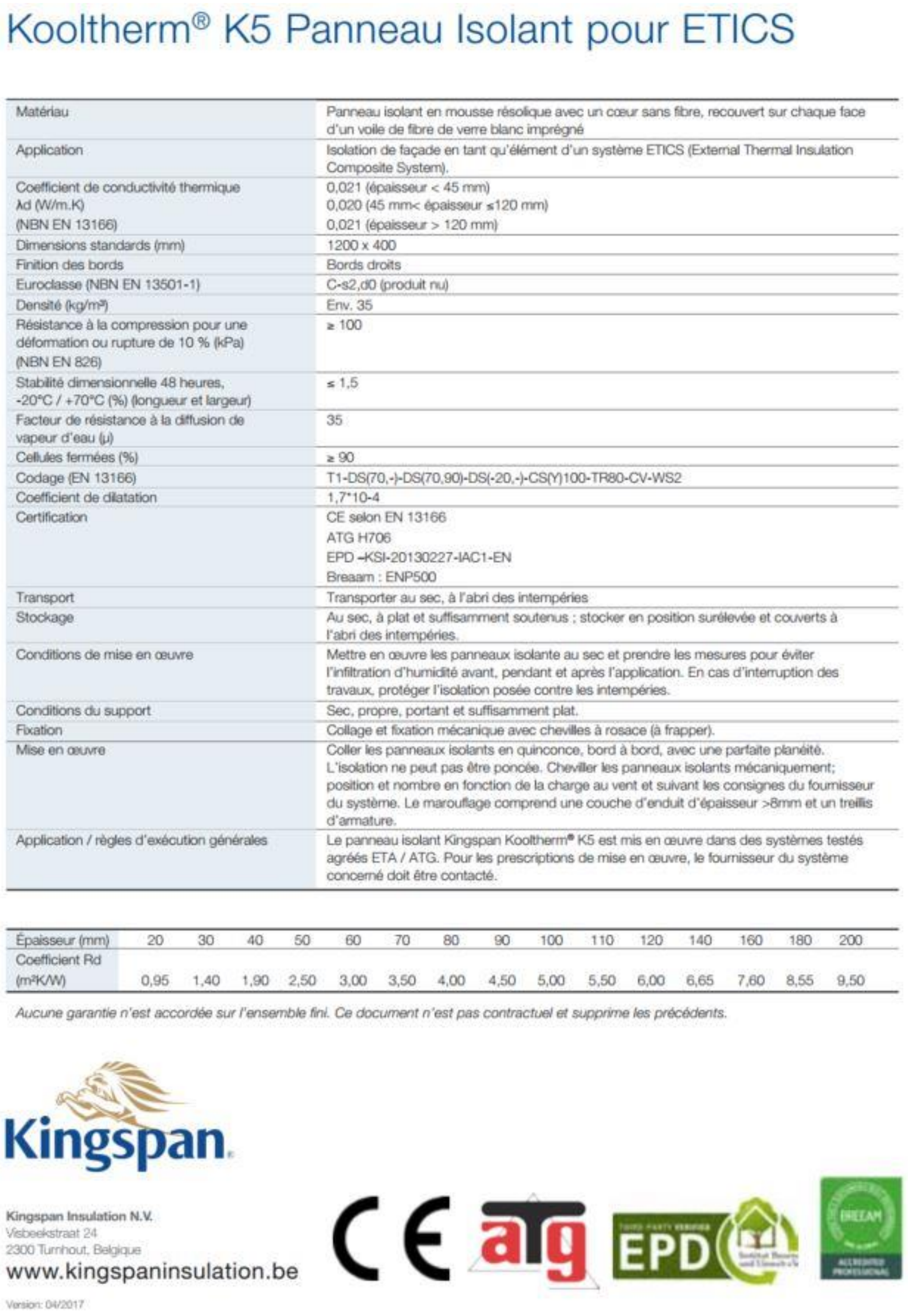

Kooltherm® K5 Panneau Isolant pour ETICS

Matériau	Panneau isolant en mousse résolique avec un cœur sans fibre, recouvert sur chaque face d'un voile de fibre de verre blanc imprégné
Application	Isolation de façade en tant qu'élément d'un système ETICS (External Thermal Insulation Composite System).
Coefficient de conductivité thermique λd (W/m.K) (NBN EN 13166)	0,021 (épaisseur < 45 mm) 0,020 (45 mm< épaisseur ≤120 mm) 0,021 (épaisseur > 120 mm)
Dimensions standards (mm)	1200 x 400
Finition des bords	Bords droits
Euroclasse (NBN EN 13501-1)	C-s2,d0 (produit nu)
Densité (kg/m^3)	Env. 35
Résistance à la compression pour une déformation ou rupture de 10 % (kPa) (NBN EN 826)	≥ 100
Stabilité dimensionnelle 48 heures, -20°C / +70°C (%) (longueur et largeur)	≤ 1,5
Facteur de résistance à la diffusion de vapeur d'eau (µ)	35
Cellules fermées (%)	≥ 90
Codage (EN 13166)	T1-DS(70,-)-DS(70,90)-DS(-20,-)-CS(Y)100-TR80-CV-WS2
Coefficient de dilatation	1,7*10-4
Certification	CE selon EN 13166 ATG H706 EPD –KSI-20130227-IAC1-EN Breaam : ENP500
Transport	Transporter au sec, à l'abri des intempéries
Stockage	Au sec, à plat et suffisamment soutenus ; stocker en position surélevée et couverts à l'abri des intempéries.
Conditions de mise en œuvre	Mettre en œuvre les panneaux isolante au sec et prendre les mesures pour éviter l'infiltration d'humidité avant, pendant et après l'application. En cas d'interruption des travaux, protéger l'isolation posée contre les intempéries.
Conditions du support	Sec, propre, portant et suffisamment plat.
Fixation	Collage et fixation mécanique avec chevilles à rosace (à frapper).
Mise en œuvre	Coller les panneaux isolants en quinconce, bord à bord, avec une parfaite planéité. L'isolation ne peut pas être poncée. Cheviller les panneaux isolants mécaniquement; position et nombre en fonction de la charge au vent et suivant les consignes du fournisseur du système. Le marouflage comprend une couche d'enduit d'épaisseur >8mm et un treillis d'armature.
Application / règles d'exécution générales	Le panneau isolant Kingspan Kooltherm® K5 est mis en œuvre dans des systèmes testés agréés ETA / ATG. Pour les prescriptions de mise en œuvre, le fournisseur du système concerné doit être contacté.

Épaisseur (mm)	20	30	40	50	60	70	80	90	100	110	120	140	160	180	200
Coefficient Rd (m^{2}K/W)	0,95	1,40	1,90	2,50	3,00	3,50	4,00	4,50	5,00	5,50	6,00	6,65	7,60	8,55	9,50

Aucune garantie n'est accordée sur l'ensemble fini. Ce document n'est pas contractuel et supprime les précédents.

Kingspan

Kingspan Insulation N.V.
Visbeekstraat 24
2300 Turnhout, Belgique
www.kingspaninsulation.be

Version: 04/2017

APPENDIX 2. RESULTS AT OTHER HEAT FLUXES

Figure 106 shows the comparison between numerical and experimental temperatures at the center back side of the steel plate for an external heat flux of 25kWm^{-2}.

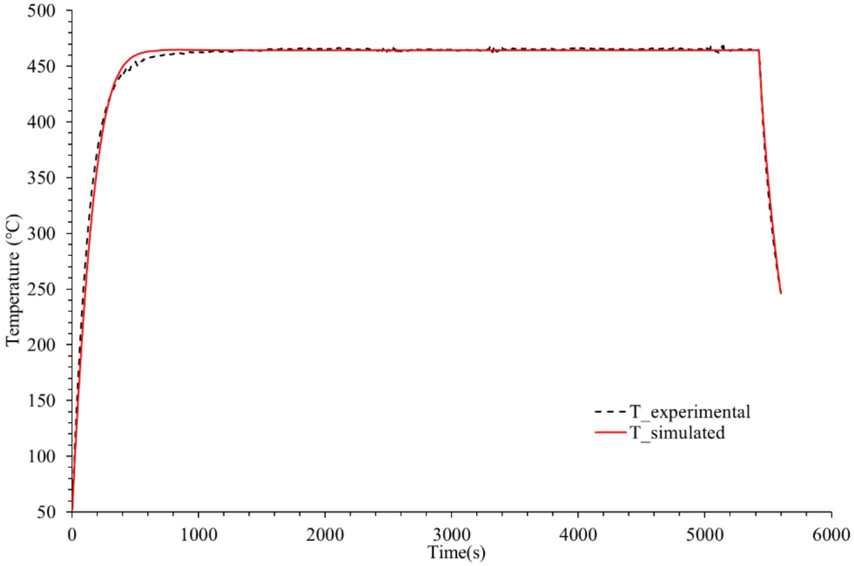

Figure 106. Comparison between numerical and experimental temperatures at the center back side of the steel plate for an external heat flux of 25kWm^{-2}.

Figure 107. shows the experimental temperature profiles for calsil when exposed to an external heat flux of 50 kWm^{-2}.

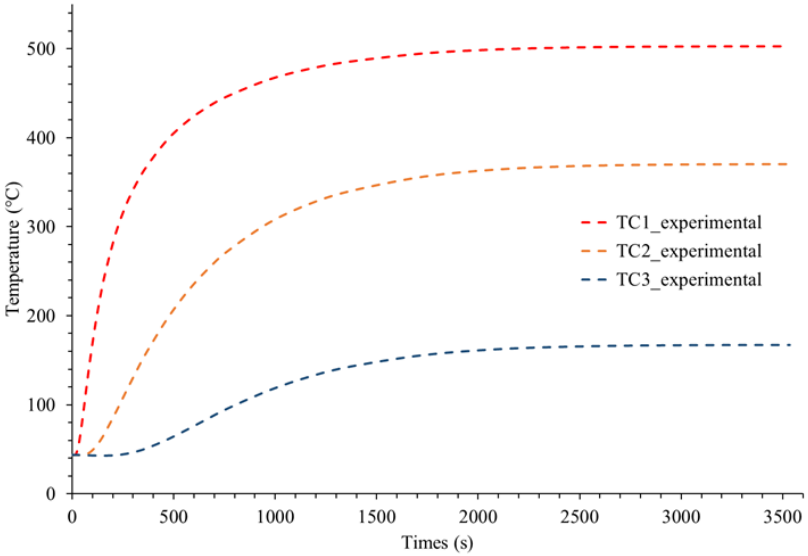

Figure 107. Experimental temperature profiles for calsil when exposed to an external heat flux of 50 kWm^{-2}.

Figure 108. shows the experimental temperature profiles for CF when exposed to an external heat flux of 50 kWm-2.

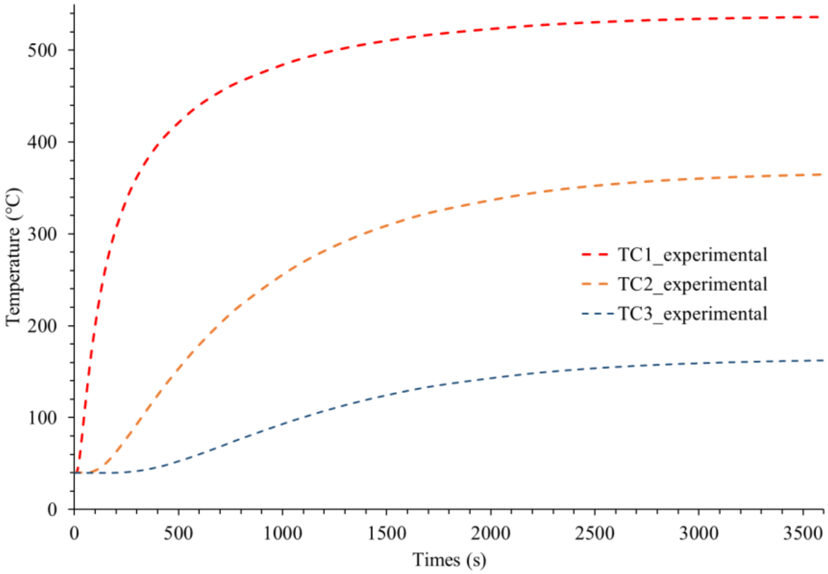

Figure 108. Experimental temperature profiles for CF when exposed to an external heat flux of 50 kWm^{-2}.

Table 22. shows the cross-section of PF at 600s for external radiative heat fluxes of 25kWm^{-2} and 50kWm^{-2}. It can be observed that at 50kWm^{-2}, the cracks are deeper into the material as compared to 25kWm^{-2}.

Table 22. Cross-section of PF at 600s for different heat fluxes.

	25kWm^{-2}	50kWm^{-2}
Cross-section		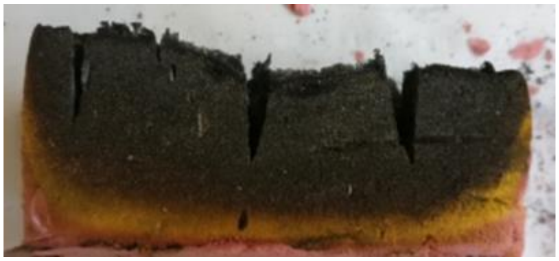

Conceptualisation physique de barrières de protection au feu : approche numérique et expérimentale

Résumé: Le feu est à la cause des pertes en vies humaines et des dégâts matériels considérables. En cas d'incendie dans un système fermé tel que les bâtiments, navires, ou avions, un feu doit être compartimenté et sa propagation restreinte afin de sauver des vies et des biens en laissant le temps aux personnes d'évacuer. Afin d'y arriver, une barrière de feu ayant une très faible inflammabilité qui limiterait la propagation du feu doit être conçu et assemblé. L'objective de ce travail de thèse est de fournir les bases fondamentales pour la conception de barrières feu efficace quand ils subissent une contrainte thermique. En se basant sur la compréhension du comportement au feu de matériaux de référence c.-à-d. le silicate de calcium, la mousse de mullite à cellules fermées, la mousse phénolique, et un revêtement intumescent à base de silicone, des tests feux avec un flux radiant externe basé sur la norme ISO 5660 du cône calorimètre sont effectués. En parallèle, des modèles numériques sont développés afin de prédire le comportement au feu de ces barrières feu. Leurs domaines d'application ainsi que leurs limites sont expliqués. Les propriétés physiques d'entrées requises pour alimenter les modèles sont obtenus soit par mesure directe par analyse thermique, soit de la littérature. Par ailleurs, des études de sensibilité sont effectués afin d'identifier les paramètres essentiels qui contrôlent le comportement au feu des matériaux de référence. Les modèles numériques sont ensuite appliqués à la conceptualisation de nouvelles barrières feu grâce à la méthodologie basée sur le 'performance-based design' ainsi que l'optimisation. Enfin, après les étapes de conception et les études de sensibilité, les règles fondamentales sur la conceptualisation de barrières de feu pour un scenario feu précis en accord avec des normes définies sont énoncées.

Mots-clés : Comportement au feu des matériaux, modèles de pyrolyse, analyse de sensibilité, optimisation numérique, modélisation et simulation

Conceptualization of fire barriers: fundamentals and experimental approach

Abstract: Fire causes injuries, the loss of lives and property. In the case of a fire in an enclosed system such as buildings, naval ships or aircraft, the fire should be compartmentalized and restricted from spreading from one point to another in order to save lives and property as well as give people enough time to evacuate. To accomplish this, fire barriers exhibiting low flammability and limiting fire spread need to be designed and assembled. The aim of this PhD is to provide with the fundamentals on how to design efficient fire barriers when subjected to a thermal stress. Based on understanding the fire behavior of selected reference fire retardant materials i.e. calcium silicate, closed-cell mullite foam, phenolic foam and a silicone-based intumescent coating, fire tests using the external radiant heat flux from the ISO 5660 cone calorimeter are conducted. At the same time, numerical models are developed to predict the fire behavior of these fire barriers and their applicability as well as limitations are explained. The input materials properties to run the numerical models are obtained from both direct measurements and from the literature. In addition, sensitivity studies are conducted in order to identify the governing parameters that control the fire behavior of the reference fire resistant materials. The numerical models are then used for the conceptualization of innovative fire safe materials based on the performance-based design process and optimization. Finally, based on the sensitivity studies and the conceptualization process, fundamental rules on how to make an efficient fire barrier in order to meet certain requirements in a given fire scenario are clearly stated.

Key words: Fire behavior of materials, pyrolysis modeling, sensitivity analysis, optimization, virtual testing